

A COMPUTER SIMULATION OF STIRLING
CYCLE MACHINES

Israel Urieli

A COMPUTER SIMULATION OF STIRLING CYCLE MACHINES

Israel Urieli

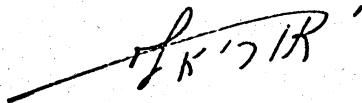
A Thesis Submitted to the Faculty of Engineering,
University of the Witwatersrand, Johannesburg, for
the Degree of Doctor of Philosophy.

Johannesburg, February 1977



DECLARATION

I, Israel Urieli, hereby declare that this thesis is my own work and that the material herein has not been submitted by me for degree purposes at any other University.



ABSTRACT

This thesis describes the development of a computer program to accurately simulate the performance and detailed behaviour of Stirling cycle machines. The program can be used both as a development tool to predict the performance characteristics of particular machines, as well as a research tool to study the inter-related gas dynamic, thermodynamic and heat transfer behaviour of such machines.

Other simulation methods published to date are based on oversimplified pressure drop, friction and heat transfer relationships.

The approach adopted in the present study was to subdivide the machine into a finite number of one-dimensional cells. Complete differential equations of continuity, momentum and energy of the working gas, as well as energy of the regenerator matrix and heat exchanger walls, are developed. In particular the energy equation of the working gas also includes kinetic energy terms whilst the momentum equation includes the effects of working gas acceleration.

The resulting set of non-linear partial differential equations is solved numerically by the 'method of lines', due regard being taken of the local instantaneous values of dynamic viscosity, Reynolds number, friction factor and heat transfer coefficient, which are all non-linear empirical functions of the system geometry and fluid properties.

A unique method of accelerating convergence of the solution to cyclic steady state is used. The effect of the number of cells of the system subdivision on the accuracy and consistency of the results has also been investigated.

Simulation results of a hypothetical test engine are presented. These include, inter alia, efficiency and indicated power versus rotational speed using air, helium and hydrogen as the working gas. Three-dimensional plots showing incremental temperature, flow and pressure profiles through a complete cycle are presented. The results show the detailed behaviour of the working fluid as influenced by the various machine parameters and working fluid properties, and as such help to provide a new insight into the complex behaviour of Stirling cycle machines.

ACKNOWLEDGEMENTS

I would like to express my particular appreciation to the following:

Costa J Rallis, my supervisor, for his unfailing encouragement and active support throughout all phases of the project. His spontaneous assistance and guidance has contributed substantially to the successful conclusion of this work, for which I am deeply grateful.

Dave M Berkowitz, a postgraduate student in Mechanical Engineering who has worked with me on this research topic and who many times has helped me to clarify various salient topics.

Jim Archbold, of the NITR, who continually provided the important liaison with the CSIR computing center. The staff of the CSIR Computer Centre, without whose help I could not have been able to do the quite considerable computer runs required in this work. In particular I wish to thank Francois van der Merwe, Norma Whiteley, and Ann Hulme for their cheerful assistance.

The members of staff of the NITR, who encouraged me throughout this study.

Fernanda Andrade, who had the unenviable task of typing this Thesis.

Finally, to Nili - Thank you.

TABLE OF CONTENTS

DECLARATION	(i)
ABSTRACT	(ii)
ACKNOWLEDGEMENTS	(iv)
TABLE OF CONTENTS	(v)
LIST OF FIGURES	(ix)
LIST OF TABLES	(xii)
NOTATION	(xiii)
1. <u>INTRODUCTION</u>	1
1.1 General	1
1.2 The Stirling Cycle	2
1.3 Problem Areas	6
1.4 Computer Simulation	7
1.5 Purpose of this Study	8
1.6 Equations	10
1.7 References	10
2. <u>REVIEW OF STIRLING CYCLE MACHINE ANALYSIS</u>	12
2.1 Introduction	12
2.2 Schmidt Cycle Analysis	12
2.3 Basic Analysis	16
2.4 Non-Isothermal Compression and Expansion Processes	17
2.5 Comprehensive Analysis including Pressure Drop	18
2.6 Discussion	30
2.7 Statement of the problem	34

3.	<u>SYSTEM MODEL</u>	
3.1	General	39
3.2	The In-Line Configuration	39
3.3	The Fundamental Equations	42
3.4	The Cellular Model	44
3.5	The Variable Volume Working Spaces	48
3.6	System Algorithms	53
3.7	Method of Solution	57
3.8	Conclusion	58
4.	<u>AN APPLICATION EXAMPLE</u>	60
4.1	Introduction	60
4.2	Description of the Engine	62
4.3	Organization of the Computer Experiments	67
5.	<u>DISCUSSION OF THE MODEL</u>	71
5.1	Introduction	71
5.2	Definition of the Model	72
5.3	Accuracy of the Model	85
5.3.1	General	85
5.3.2	Time discretization	85
5.3.3	Space discretization	88
5.4	Summary and Conclusions	91
6.	<u>DISCUSSION OF THE RESULTS</u>	94
6.1	Introduction	94
6.2	Performance Characteristics	94
6.3	Incremental Characteristics	101
6.4	Summary and Conclusions	118
7.	<u>CONCLUSIONS AND RECOMMENDATIONS</u>	119
7.1	General	119
7.2	Major Advances Attained in the Present Investigation	119

7.3	Recommendations for Future Work	123
<u>APPENDICES</u>		126
A.	<u>PARAMETERS AND SYMBOLS</u>	127
A.1	General	127
A.2	Normalized Parameters	128
A.3	Prefix Set	133
A.4	Suffix Set	134
A.5	Subscript Set	137
A.6	Dimensionless groups	139
B.	<u>SCHMIDT CYCLE ANALYSIS</u>	140
C.	<u>BASIC IDEAL CYCLE ANALYSIS</u>	147
C.1	Introduction	147
C.2	The Ideal Stirling Cycle	147
C.3	The Ideal Pseudo-Stirling Cycle	152
C.4	The Ideal Ported Regenerative Constant Volume Cycle	155
C.5	Conclusions	158
D.	<u>THE FUNDAMENTAL EQUATIONS - CONTINUITY, MOMENTUM, ENERGY</u>	160
D.1	Introduction	160
D.2	Continuity	162
D.3	Momentum	163
D.4	Energy	165
D.5	The Fundamental Systems of Equations	170
E.	<u>TRANSPORT PROPERTIES - VISTOSITY, THERMAL CONDUCTIVITY</u>	172
E.1	Introduction	172
E.2	Dynamic Viscosity	172
E.3	Thermal Conductivity	174

F.	<u>FRICTION FACTOR AND HEAT TRANSFER COEFFICIENT</u>	176
F.1	Introduction	176
F.2	The Reynolds Friction Factor	176
F.3	Friction Factor for Circular Pipes	179
F.4	Heat Transfer Coefficient for Circular Pipes	184
F.5	Regenerator Matrices	186
F.6	Conclusions	192
G.	<u>METHOD OF SOLUTION</u>	193
G.1	The Method of Lines	193
G.2	Approach to Solution	194
G.3	The Algorithm of Solution	196
H.	<u>SYSTEM ALGORITHMS</u>	199
H.1	General	199
H.2	Continuity	201
H.3	Momentum	203
H.4	Energy Balance of the Working Gas	214
H.5	Energy Balance of the Cooler (Heater) Wall	220
H.6	Energy Balance of the Regenerator Matrix	224
H.7	Viscosity	227
H.8	Reynolds Friction Factor and Flow Tag	228
H.9	The Heat Transfer Coefficient	231
H.10	Volume Variation	232
I.	<u>COMPUTER PROGRAM</u>	234
I.1	General	234
I.2	Subroutine DERIV	235
I.3	Main Program	238
J.	<u>SELECTED COMPUTER OUTPUT AND RESULTS</u>	245
J.1	General	245
	REFERENCES	273

LIST OF FIGURES

<u>FIGURE</u>	<u>TITLE</u>	<u>PAGE</u>
1.1	Carnot and Stirling cycles	5
1.2	The Stirling cycle	4
2.1	Schmidt cycle	14
2.2	Equivalent flow system (After Ki63)	18
2.3	Temperature profile for heat transfer calculations (After Ki63)	20
2.4	Stirling engine model (After Fi62)	21
2.5	Stirling engine model (After Fi64)	23
2.6	Stirling engine model (After Fi67.1)	24
2.7	Generalized working fluid node (After Fi75)	27
2.8	Basic ideal system (After QS68)	28
2.9	The ported regenerative engine (After Fi53)	32
3.1	Classification of Stirling cycle engines	40
3.2	Generalized elemental control volume	44
3.3	The <i>nc</i> -cell model	48
3.4	The generalized <i>i</i> 'th elemental cell	49
3.5	The generalized compression space	54
4.1	The test engine	62
5.1	The <i>i</i> 'th cell	73
5.2	A hypothetical pressure distribution	74
5.3	The <i>i</i> 'th cell	75
5.4	The Stirling cycle engine cellular model	76
5.5	Temperature profiles (mean node temperatures)	79
5.6	Temperature profiles (conditional node temperatures)	81
5.7	The <i>i</i> 'th node	82
5.8	Efficiency versus number of cells	84
5.9	Energy error factor versus operating frequency	88
5.10	Thermal efficiency and power output versus operating frequency	90

<u>FIGURE</u>	<u>TITLE</u>	<u>PAGE</u>
5.11	Thermal efficiency and power output versus operating frequency	92
6.1	Thermal efficiency versus power output	95
6.2	Comparative performance using different working fluids (After Meijer Me70)	96
6.3	Efficiency and power versus speed (After Meijer Me70)	100
6.4	Temperature and flow profiles versus crank-angle	102
6.5	Turbulent flow from the expansion space to the compression space	103
6.6	Turbulent flow from the compression space to the expansion space	104
6.7	Flow reversal transition	106
6.8	Flow reversal transition	107
6.9	Pressure profiles versus crankangle	109
6.10	Pressure profiles versus crankangle	110
6.11	Pressure profiles versus crankangle	111
6.12	Pressure versus crankangle diagrams	113
6.13	Pressure versus crankangle diagrams	114
6.14	Farnboro indicator diagrams of a Stirling engine (After Meijer Me61)	115
6.15	Experimental pressure versus crankangle diagrams (After Kirkley Ki63)	116
6.16	Experimental $p\theta$ diagrams of a Stirling cycle cooling machine (After Walker Wa62.1)	117
C.1	The ideal Stirling cycle	148
C.2	The pseudo-Stirling cycle	153
C.3	The ported regenerative constant volume cycle	156
D.1	Control volume V	160
F.1	Fanning friction factor diagram (After Pipe Friction Manual, 3rd Edition, Hydraulic Institute, 1961)	180

<u>FIGURE</u>	<u>TITLE</u>	<u>PAGE</u>
F.2	Approximate friction factor diagram	182
F.3	Approximate Reynolds friction factor diagram	184
F.4	Flow Friction and heat transfer characteristics for flow through stacked sphere matrices (After Kays and London KL64)	189
F.5	Flow Friction and heat transfer characteristics for flow through infinite randomly stacked woven screen matrix (After Kays and London KL64)	191
G.1	The algorithm of solution	197
H.1	The generalized i 'th elemental cell	199
H.2	The generalized compression space	200
H.3	The i 'th cell	201
H.4	The compression space	202
H.5	The i 'th node	204
H.6	The i 'th node - unequal adjacent cells	207
H.7	Node 1	209
H.8	Abrupt expansion and contraction pressure coefficients (After Kays and London KL64)	210
H.9	The i 'th cell	216
H.10	The compression space	217
H.11	The cooler (heater) wall	220
H.12	The regenerator matrix and enclosing wall	224

LIST OF TABLES

<u>TABLE</u>	<u>TITLE</u>	<u>PAGE</u>
4.1	Properties of air, helium and hydrogen	69
A.1	Normalized and actual parameters	131
A.2	Dimensionless groups	139
E.1	Values of the viscosities of gases (Br71)	174
J.1	Power and efficiency for air	246
J.2	Power and efficiency for air	247
J.3	Energy error factor and number of increments per cycle for air	248
J.4	Power and efficiency for helium	249
J.5	Energy error factor and number increments per cycle for helium	251
J.6	Power and efficiency for hydrogen	253
J.7	Energy error factor and number of increments per cycle for hydrogen	255

NOTATION

The parameter notation is made up of the basic parameter symbols augmented by prefixes, suffices and subscripts. The philosophy behind the choice of the notation is given in Appendix A. In the notation which follows the different types of parentheses have different usage. Normal curved parentheses () have either normal usage or enclose the equivalent computer program symbol to a text symbol. Square parentheses enclose the dimensions of a parameter in SI units, where applicable. Various dummy variables used in the computer program in order to avoid repeated evaluation of factors have not been defined in this section, eg, $GTN(I) = G(I) * TN(I)$.

Latin symbols denoting parameters in the text are italicized, however the computer program equivalent forms are typed in regular format. All operators and Greek symbols are typed in regular format. In general dimensioned parameters in the text are supercripted by a *tilda* (~). Exceptions to this rule are the base parameters *M*, *Vs*, *Tk*, *R* (Refer to Appendix A). In the computer program, all dimensioned parameters are prefixed by E.

- A (A) area:
 free flow area;
 control surface area.
- A_i (A(I)) free flow area at node i .
- A_f frontal area.
- A_{m_i} effective cross section area of regenerator matrix
 for longitudinal heat conduction calculations at
 node i .
- A_{mg_i} (AMG(I)) matrix surface area in cell i wetted by
 the working gas.
- A_{w_i} (AW(I)) cross section area of heat exchanger wall
 for longitudinal heat conduction calculations
 at node i .
- A_{wg_i} (AWG(I)) heat exchanger wall surface area in cell
 i wetted by the working gas.
- A_{wm_i} effective area of contact between regenerator matrix
 in cell i and enclosing wall for axial heat con-
 duction calculations.
- A_{wo_i} external wall surface area of cell i wetted by the
 external heat exchange medium.
- B_0 constant term of a Fourier series expansion (Appendix B).
- B_{ci} i 'th cosine term of a Fourier series expansion
 (Appendix B).

B_{si} i 'th sine term of a Fourier series expansion
(Appendix B).

B_1, B_2, B are constants defined and used only in
Appendix B.

B prefix used in the computer program only in order to
denote a term made up of a combination of various
constants and parameters. It is used exclusively
to avoid repeated evaluation of the same term.

c defines the compression space location - usually as
a suffix to a parameter.

C_{m_i} heat capacity of the matrix material in the i 'th cell.

c_v (CVS) specific heat capacity at constant volume.

c_p (CPS) specific heat capacity at constant pressure.

\tilde{c}_w (ECSW) [J/kg.K] actual specific heat capacity of the
heat exchanger wall material.

c_w (CSW) specific heat capacity of the heat exchanger
wall material.

C_w (CW) heat capacity of the heat exchanger wall material
contained in a single cell.

d (D) hydraulic diameter of the heat exchanger pipes.

d_i (D(I)) minimum hydraulic diameter of the two cells
adjacent to the i 'th node.

dia (DIA) external to internal heat exchanger pipe
diameter ratio.

d_m matrix mesh wire diameter

\tilde{d} (ED) [m] actual internal diameter of heat exchanger pipes.

d_o (DO) external diameter of heat exchanger pipes.

\tilde{d}_o (EDO) [m] actual external diameter of heat exchanger pipes.

D (D) prefix used to denote the total time derivative differential operator d/dt .

DTIME time increment for numerical integration (Appendix I).

DYDT dummy variable increment (Appendix I).

e specific enthalpy;
defines expansion space location - usually as a suffix to a parameter

E prefix used in the computer program only in order to denote an actual (dimensioned) parameter or a normalizing factor (Appendix A).

EX[m] length normalizing factor.

EA[m²] area normalizing factor.

EU[m/s] velocity normalizing factor.

ETIME[s] time normalizing factor.

EMU[kg/m.s] dynamic viscosity normalizing factor.

$EK [J/m \cdot s \cdot K]$ thermal conductivity normalizing factor.

$ENERGY [J]$ energy normalizing factor.

$ERO [kg/m^3]$ density normalizing factor.

$EVS [m^3]$ volume normalizing factor.

$ETK [K]$ temperature normalizing factor.

$EM [kg]$ mass normalizing factor.

$ER [J/kg \cdot K]$ specific heat capacity normalizing factor.

\tilde{f} (EFREQ) [Hz] cyclic operating frequency.

F_i frictional drag force at node i .

Ff Fanning friction factor (Table A.2, Appendix A).

Fr (FR) Reynolds friction factor (Table A.2, Appendix A).

\bar{g} momentum per unit volume or mass flux density
(superscripted bar indicates a vector quantity).

g_i (G(I)) mass flux density at node i .

Gi mass flux at defined location i .

G_i mass flux at node i .

h denotes the heater location - usually as a suffix
to a parameter

h_i (H(I)) heat transfer coefficient at node i .

$Iflo_i$ (IFLO(I)) signed integer indicating the direction and condition of flow (ie laminar, turbulent, sonic, etc) at node i .

JCYCL two valued integer {1,2} specifying if the cycle is an initial cycle or a continuation cycle, used in the computer program only.

JPRNT two valued integer {0,1} specifying if a partial or full printout is required, used in the computer program only.

\tilde{k}_w (EKW) [J/m.s.K] actual thermal conductivity of the wall material.

k_w (RKW) thermal conductivity of the wall material.

k_m (RKM) thermal conductivity of the regenerator matrix material.

k denotes the cooler location - usually as a suffix to a parameter;
working gas thermal conductivity.

k_i flow resistance constant at defined location i .

K_c (RKC) contraction pressure loss coefficient.

K_e (RKE) expansion pressure loss coefficient.

M (EM) [kg] actual total mass of working gas in the system.

mm matrix material mass
m working gas mass.
mc (RMC) mass of working gas in the compression space.
me (RME) mass of working gas in the expansion space.
mi mass of working gas at defined location *i*.
m_i (RM(I)) mass of working gas in cell *i*.
nc (NC) total number of cells in the system model.
nk (NK) number of cells in the cooler section.
nh (NH) number of cells in the heater section.
nr (NR) number of cells in the regenerator section.
ninc (NINC) number of integration time increments per cycle.
NPRNT number of increments per printout, computer program only.
nkr (NKR) $\Delta nk+nr$.
np (NP) number of heat exchanger pipes
Nu Nusselt number (Table A.2, Appendix A).
o denotes the external environment - usually as a suffix to a parameter.
p working gas pressure.

p_i working gas pressure at defined location or state i .

p_i (P(I)) working gas pressure in cell i .

p_c (PC) working gas pressure in the compression space.

p_e (PE) working gas pressure in the expansion space.

\tilde{p}_k (EPK) Pa nominal actual charge pressure.

Pr (PR) Prandtl number (Table A.1, Appendix A).

\tilde{P} [W] actual power.

p_h working gas pressure in the heater space.

p_k working gas pressure in the cooler space.

p_r working gas pressure in the regenerator space.

p_o pressure of the surrounding environment.

p_{n_i} working gas pressure at node i .

Q heat transferred to working gas by convection; heat generation or absorption.

${}^i Q_j$ heat transferred to working gas during process from state i to state j .

Q_i (Q(I)) heat transferred to working gas by convection in cell i .

Q_w axial conductive heat flow.

- Q_m axial conductive heat flow in the regenerator matrix
- Q_{w_i} (QW(I)) axial conductive heat flow in the wall across the i 'th node.
- Q_{m_i} axial conductive heat flow in the regenerator matrix across the i 'th node.
- Q_{wm_i} radial conductive heat flow between the enclosing wall and the regenerator matrix of the i 'th regenerator cell.
- Q_{wo_i} heat flow from the external environment to the wall at the i 'th cell.
- Q_k (QK) heat flow from the external environment to the cooler wall in order to maintain it at a constant temperature.
- Q_h (QH) heat flow from the external environment to the heater wall in order to maintain it at a constant temperature.
- Q_{r_i} (QR(I)) heat flow from the regenerator matrix to the working gas in the i 'th regenerator cell.
- Q_{wr_i} (QWR(I)) axial conductive heat flow in the wall of the i 'th regenerator node.
- r volume compression ratio (Appendix C);
defines the regenerator space - usually as a suffix to a parameter.
- R a prefix to a real mode parameter having an integer mode symbol, used in the computer program only,

where a distinction between real and integer parameters exists (Appendix A).

k (ER) [J/kg.K] the gas constant.

\bar{Re} (RE) Reynolds number (Table A.2, Appendix A).

Ro (RO) relative roughness factor (Table A.2, Appendix A).

RMSQR root mean square net regenerator heat.

s specific entropy.

St Stanton number (Table A.2, Appendix A).

t (TIME) time.

T absolute temperature.

Tk (ETK) [K] actual cold sink temperature.

Tk cold sink temperature ($Tk = 1$);
temperature of the working gas in the cooler space.

$\tilde{T}h$ (ETH) [K] actual hot source temperature.

Th hot source temperature;
temperature of the working gas in the heater space.

Twk (TWK) temperature of the cooler wall.

Twh (TWH) temperature of the heater wall.

Tr temperature of the working gas in the regenerator space.

T_c temperature of the working gas in the compression space.

T_e temperature of the working gas in the expansion space.

T_{wc} temperature of the compression cylinder wall.

T_{we} temperature of the expansion cylinder wall.

T_i temperature of the working gas at defined location or state i .

T_i (T(I)) temperature of the working gas in cell i .

T_{n_i} (TN(I)) temperature of the working gas at node i .

T_{w_i} (TW(I)) temperature of the wall enclosing cell i .

T_{wr_i} (TWR(I)) temperature of the wall enclosing regenerator cell i .

T_{m_i} (TM(I)) temperature of the matrix in regenerator cell i .

\tilde{T}_{su} (ETSU) [K] actual Sutherland constant (Appendix E).

T_{su} (TSU) Sutherland constant.

\tilde{T}_0 (ETO) [K] temperature at which the dynamic viscosity of the working gas is defined.

U velocity.

u specific internal energy

v specific volume of the working gas
 v_i (VS(I)) specific volume of the working gas in cell i .
 vn_i (VSN(I)) specific volume of the working gas at node i .
 v_c (VSC) specific volume of the working gas in the
compression space.
 v_e (VSE) specific volume of the working gas in the
expansion space.
 V control volume;
volume of the cell void space.
 V_m volume of the matrix material.
 V_d (VD) dead volume.
 V_{cl} (VCL) clearance volume of the compression or expansion
space.
 V_s (EVS) [m³] total power stroke volume.
 V_i volume at defined location or state i .
 V_i (V(I)) void volume of cell i .
 V_c (VC) compression space volume.
 V_e (VE) expansion space volume.
 V_T total working gas volume.
 W (W) mechanical work done.
 W_c (WC) mechanical work done in the compression space.

W_e (WE) mechanical work done in the expansion space.

x (X) length;
longitudinal heat exchanger length variable.

\tilde{x}_p (EXP)[m] actual length of heat exchanger pipe bundle.

x_p (XP) length of heat exchanger pipe bundle.

x_m total effective length of the wire in the regenerator matrix (number of wires times the length of each wire), where applicable.

$Y(I)$ variable vector, used in the computer program only.

z transverse or radial length variable;
height of protrusions on the inside surface of the heat exchanger pipes, in order to define the relative roughness factor R_o .

α (ALPHA) phase angle advance of the expansion space to the compression space volume variations.

β angle defined and used in Appendix B only.

γ (GAMMA) ratio of specific heat capacities of the working gas ($\gamma \triangleq c_p/c_v$).

δ difference operator;
phase shift of the pressure peak of the expansion space with respect to the compression space, in degrees of crankangle.

Δ (DEL, DL) difference operator. DEL denotes a spacial difference and DL (used only in the Runge-Kutta integration routine) denotes a time incremental difference.

Δp_e (DELPC) pressure drop across the entrance to the compression space due to contraction or expansion entrance effects.

Δp_e (DELPE) pressure drop across the entrance to the expansion space due to contraction or expansion entrance effects.

Δp pressure drop across cell length Δx .

Δx (DELX) longitudinal cell length.

Δx_i (DELX(I)) length of the i 'th cell.

ϵ regenerator effectiveness (Appendix C).

ζ energy error factor (Chapter 5).

η (EFF) thermal efficiency.

θ crankangle.

κ swept volume ratio (Appendix B).

$\tilde{\mu}_0$ (EMUO) [kg/m.s] actual dynamic viscosity of the working gas at defined temperature \tilde{T}_0 .

μ_k (RMUK) dynamic viscosity of the working gas at base temperature T_k .

μ (RMU) dynamic viscosity of the working gas at the local operating node temperature T_{n_i} .

$\tilde{\rho}_w$ (EROW) [kg/m³] actual density of the wall material.

ρ_w (ROW) density of the wall material.

ρ_m density of the matrix material.

ρ density of the working gas.

σ shear stress (Appendices E, F).

ϕ angle defined and used in Appendix B only.

ψ porosity of the matrix (Appendix F);
ratio of free flow to total cross-sectional area.

ω (OMEGA) angular cyclic operating frequency.

I. INTRODUCTION

1.1 GENERAL

"Economy of fuel" is the cry of the day. The sudden rise in the price of coal seems to have done at once what scientific engineers have been trying for years - only with moderate success - to do; - awakened users of steam power to a consciousness of the terribly wasteful manner in which they are so often working, and of the value of the fuel which they are persistently throwing away.'

The above paragraph forms the opening statement in a series of articles on air engines in *Engineering* of March 12, 1875.

The world oil crisis of October 1973 was the main trigger which stimulated this research.

Significantly, the word research can be resolved into its components 're-search' -- another way of expressing the well known adage -- that history repeats itself.

Each time a subject is 're-searched', however, it is done so with the advantage of an updated technological development. The Stirling cycle engine is no exception. It has in the past given way to other forms of prime mover, even those that are theoretically inferior to it, mainly because its peak performance was restricted by technological limitations.

This is aptly stated in the words of Robert Stirling, in 1876, shortly before his death (Zi71):

'These imperfections have been in great measure removed by time, and especially by the genius of the distinguished Bessemer. If Bessemer iron or steel had been known 35 or 40 years ago, there is scarce a doubt that the air engine would have been a great success. It remains for some skilled and ambitious mechanist in a future age to repeat it under more favourable circumstances and with complete success.'

1.2 THE STIRLING CYCLE

The well-known Carnot theorem in thermodynamics states that no heat engine can be more efficient than a reversible heat engine which is operating between the same temperature limits. Reversible cycles are defined by two isothermal processes bounded by any two processes which taken together are externally adiabatic. This class of cycle was analysed by Reitlinger in 1873 (Ko68). The Carnot cycle is a particular case of a reversible cycle in which the two isothermals are joined by two reversible adiabatics. It is generally recognized that the Carnot cycle is impractical, giving an extremely low value of specific work done per cycle.

Under imposed constraints of pressure, volume and temperature limits, the reversible cycle yielding maximum work done per cycle is the Stirling cycle, which is defined by two isotherms bounded by two isochors (figure 1.1).

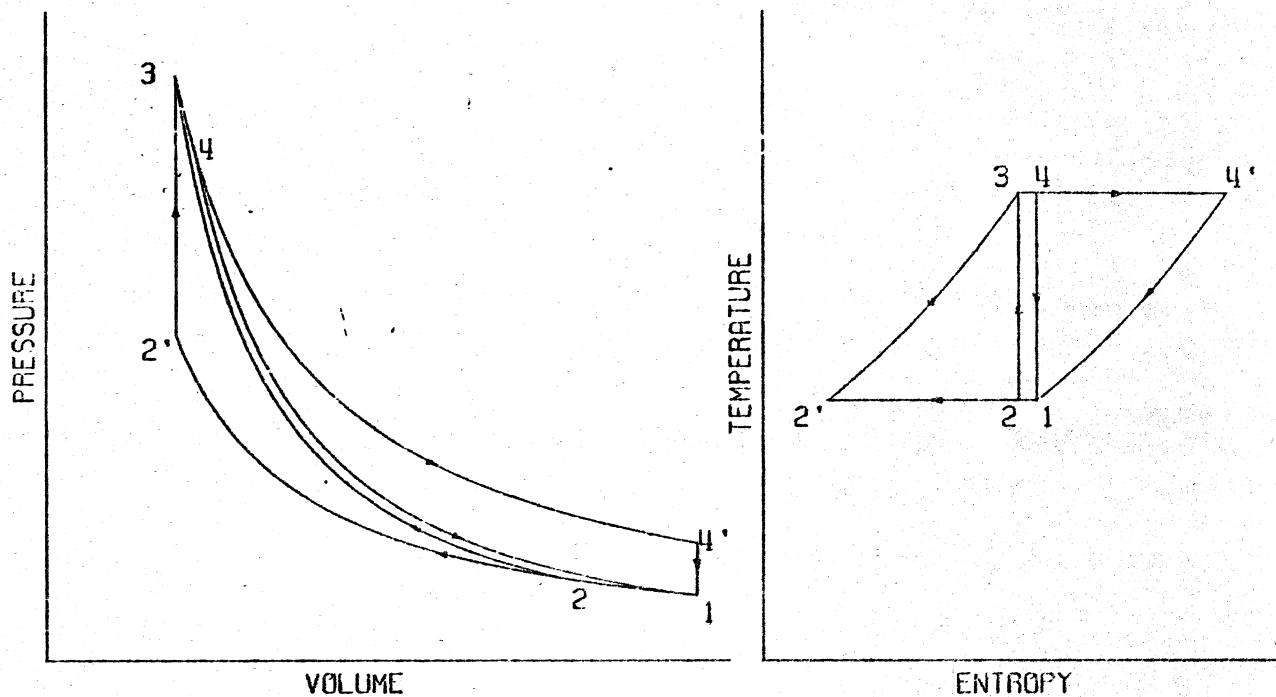


Figure 1.1 CARNOT AND STIRLING CYCLES

Figure 1.1 depicts the Carnot and Stirling cycles on pV and Ts coordinates respectively. Here the Carnot cycle is comprised of the processes linking the state points 1-2-3-4-1 and the Stirling cycle 1-2'-3-4'-1. A necessary condition for reversibility is that all the heat is transferred to the surroundings during isothermal processes at the hot source and cold sink temperatures respectively. In the Stirling cycle however, the isochoric processes require the transfer of heat for their execution at varying temperatures -- as is apparent from the Ts diagram of figure 1.1. However, since in each case the quantities of heat

rejected and supplied are equal, ie, $4'Q_1 = -2'Q_3$ then provided such heat is reversibly transferred internally the cycle is reversible.

This internal transfer of heat is done by means of a reversible regenerator in which the heat rejected during the process 4'-1 is stored, and subsequently recovered during the process 2'-3.

Mechanically there are two main classes of configuration which yield practical Stirling cycle machines. These are referred to as the dual-piston and piston-displacer arrangements.

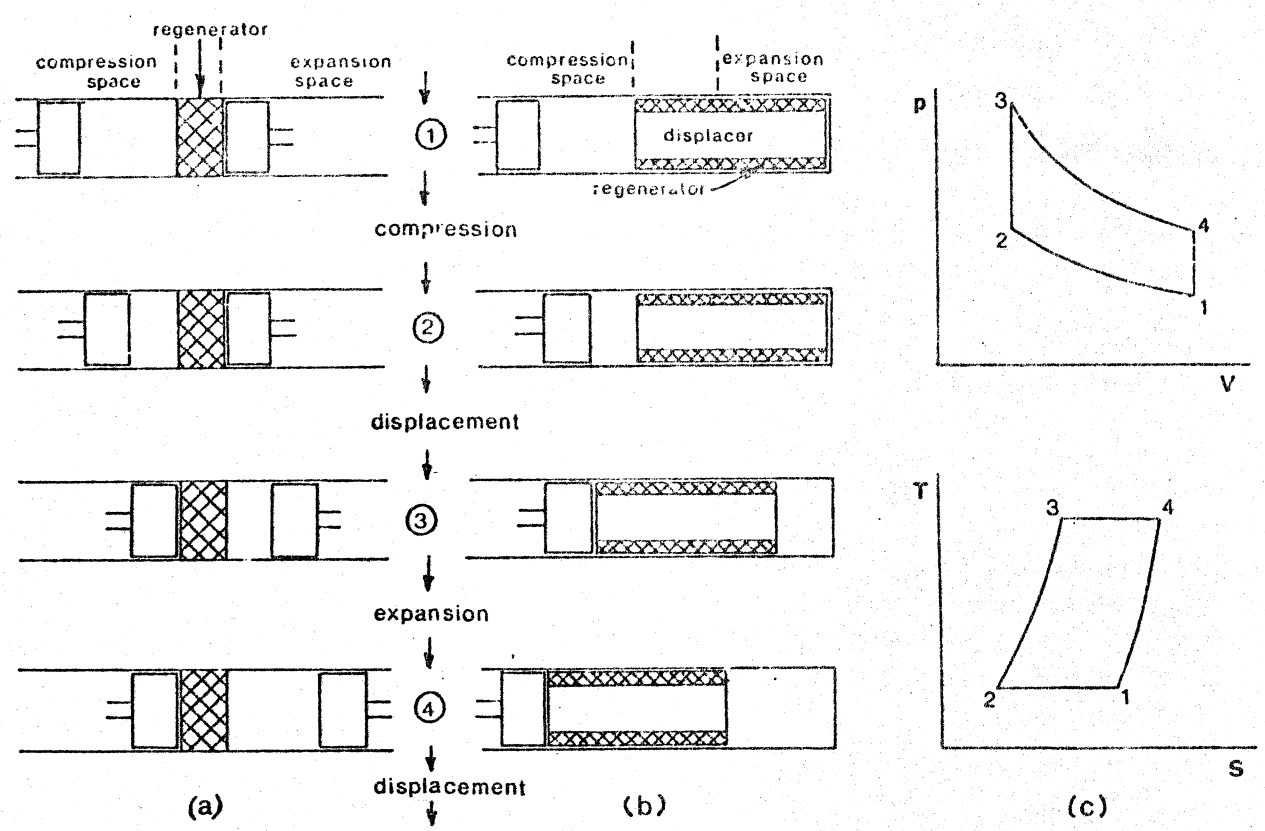


Figure 1.2 THE STIRLING CYCLE

Figure 1.2(a) and 1.2(b) show the positions of the pistons for these two configurations at each state point of the cycle. The dual-piston arrangement (figure 1.2(a)) consists of separate compression and expansion pistons operating (in this case) in the same cylinder. The regenerator, usually consisting of a matrix of fine wires which allows free passage of the working fluid, is interposed between the cooled compression space and the heated expansion space. Constant volume displacements (2-3 and 4-1, figure 1.2(c)) of the working fluid are achieved by synchronously moving the two pistons, thus transferring the fluid through the regenerator.

In the piston displacer arrangement (figure 1.2(b)) both the compression and expansion processes are brought about by the same piston. The displacer, as its name implies, simply shuttles the working fluid, at the appropriate points in the cycle, between the compression and expansion spaces. As shown in figure 1.2(b) the regenerator forms part of the displacer, however it could form part of the stationary cylinder wall.

The ideal constant volume transfer processes required in figure 1.2 are incapable of practical realization by any mechanisms operating at finite accelerations. At best, crank and connecting rod devices coupled to a rotating output shaft can be expected to produce volume variations in both hot and cold spaces which vary in a sinusoidal fashion with crank angle, rather than in a discontinuous fashion as called for in these ideal cycles. With such mechanical limitations it is then no longer possible to clearly distinguish the

various separate processes since they tend to overlap.

1.3 PROBLEM AREAS

The Stirling engine, although available since 1816, is still in the process of research and development. The ambitious research program of the Philips Company, Holland, since the late 1930's, has pulled Stirling engines out of obsolcsence and developed them to a stage where they have impressive characteristics and performance. What is surprising is that although reports of many of these developments have been available in the literature for over thirty years, no engines are currently being built for purposes other than research and development.

The problem areas in the development of Stirling engines may be divided into practical and theoretical branches. On the practical side, it is found that in order to obtain a high specific performance, the working fluid (usually helium or hydrogen) must be operated at high mean pressure and at large differences in temperature. This poses formidable problems in heat transfer and sealing. Heat exchangers are required to operate continuously at high pressures close to their metallurgical temperature limits. The closed cycle nature of the engine requires a high cooling effectiveness and precludes the use of large heat exchangers.

On the theoretical side it is found that practical machines cannot be analysed by ideal cycle analysis. Not only must the practical effects of fluid friction and heat transfer be considered, but also the fact that not all the particles of working gas in the system

undergo the same cycle (Wa73, Or75, Or76). The temperature variation of the working gas is so large that the nonlinear variation of its properties with temperature must be considered. The complexity and nonlinear nature of the behaviour of the working fluid has thus precluded any form of mathematical analysis.

1.4 COMPUTER SIMULATION

The advent of high speed digital computers has introduced a new dimension into the 're-search' of Stirling cycle engines. It allows numerical simulation of the complex behaviour of such machines to a controllable degree of accuracy, the limitations being only the size, speed and availability of the computer. This is important since unlike other prime movers, which can rely on a history of experimental experience upon which to guide their development, the Stirling engine presents unique requirements for the cooperation of computational analysis and design in its development (Za73).

Prior to the advent of the computer, analysis could be divided into theoretical and experimental branches. The question now arises, where does computational analysis fit into these branches? The answer is that it is separate from each, although it has aspects of both, and that it supplements rather than replaces them (Ro72).

Computational analysis does not have the rigour of mathematical analysis; however it relies upon fundamental mathematical analysis in order to set up the equations for solution. It is much closer to experimental analysis

and retains many of its disadvantages. The analyst 'turns on' the computer and waits to see what happens, just as the experimenter does. He can run the 'experiment' with a particular configuration of the machine and can only determine the effect of variation of the various parameters on the performance after an exhaustive set of experiments. He has the advantage over the experimenter that he can vary the configuration of the system without recourse to the workshop (a trying experience); he can test the effects of replacing the working gas, say air, with helium or hydrogen without involving additional expensive equipment and safety measures; he can even define some hypothetical working gas (Section 6.2), and test the sensitivity of the performance to independent theoretical approximations; he is not concerned with the accuracy of various test instruments, or whether or not they interfere with or modify the parameter that he is measuring; he has continuous access to all the parameters at even the most inaccessible locations in the machine. The list is extensive.

On the other hand his model will always be an approximation of reality, and in no sense can computer experimentation ever replace physical experimentation, or, for that matter theoretical analysis. At some stage or another the computer model must be validated against experimental experience.

1.5 PURPOSE OF THIS STUDY

It was the purpose of this study to develop a comprehensive computer model for the thermodynamic, fluid dynamic

and heat transfer behaviour of Stirling cycle type machines, and to validate it against current knowledge in the field. It is hoped that this work will serve as reference material for a continuing program of Stirling cycle machine development, and as such it has been presented in a tutorial type of format. In particular it has been attempted to make the computer techniques and programs as readable unified parts of this work. Wherever possible, the computer program symbols have been made identical to the text symbols. An algorithmic approach has been used in order to define specific parameters so as to render it unnecessary to continually cross reference the text (Appendix A).

Rather than intersperse comments throughout the computer program, it has been considered preferable to introduce the computer program with the text. Thus each algorithm developed is followed by its FORTRAN equivalent statement (Appendix H). In consequence an approach and technique for modelling this class of systems has been provided rather than a program which is installed in some computer center. As new interconnections of the basic components are devised, or new experimental back up data becomes available, so the program can be easily modified and, hopefully, saved from obsolescence.

It is noted that although this whole study has been directed towards prime movers, this has been done mainly for the sake of clarity, and it can be applied to Stirling cycle type refrigerators or heat pumps as well.

1.6 EQUATIONS

In order to render the equations in the text less cumbersome, in particular with respect to the use of brackets, the following rules of usage are defined:

- (i) Multiplication and division are done before addition and subtraction, eg, $x+y/z \equiv x+(y/z)$.
- (ii) Factors are evaluated from right to left. Thus all parameters to the right of a division sign are evaluated before division takes place, eg, $x/y.z \equiv x/(y.z)$.
- (iii) Functions of a variable operate only on the variable immediately following, unless the group of variables following are enclosed by brackets, eg, $\sin\theta/4Th \equiv \sin(\theta)/(4Th)$.

1.7 REFERENCES

The system of reference designation has been proposed by Rallis, and is considered to provide a better means of information retrieval than the usual numerical sequencing of articles. Hence each publication is referred to by two letters followed by two numerals. The latter refer to the year of publication. Where the publication has a single author the first two letters of the surname appear, the second in lower case. Where there is more than one author the initial letters of the surnames of the first two, both in upper case, are used. Exceptions to this is that if the reference is prior to 1900, then four numerals denoting the year appear, and if the name of the author is unknown, then

three letters denoting the name of the journal are used instead. The references are listed in alphabetical order according to the names of the authors.

2. REVIEW OF STIRLING CYCLE MACHINE ANALYSIS

2.1 INTRODUCTION

In this chapter an attempt is made to review the various forms of Stirling cycle machine analysis that have appeared in the literature, rather than the historical development of such machines. Excellent reviews of the historical development of Stirling cycle engines have been given in Finkelstein (Fi59) and Flynn et al (FP60). In the concluding section a 'statement of the problem' is also presented.

Patents for the first Stirling engine were taken out by Robert Stirling in 1816. This is undoubtedly one of the most amazing inventions of its kind, being well in advance of all pertinent scientific knowledge of the time. In this connection it is worth recalling that Sadi Carnot published his 'Reflections on the motive power of fire' in 1824, whilst Joule established the mechanical equivalent of heat, and thus laid the foundations for the first law of thermodynamics, in 1849. Like many others of his time, Stirling (and likewise Ericsson) firmly believed in perpetual motion of the second kind. One could not expect therefore, that any rational analysis of the Stirling cycle machine would be produced until some considerable time thereafter.

2.2 SCHMIDT CYCLE ANALYSIS

In conventional, mechanically realizable Stirling cycle machines the volumes of the hot and cold spaces

vary in an approximately sinusoidal fashion with crank angle. With such mechanical limitations the various separate processes cannot be clearly distinguished. In particular expansion does not take place completely in the hot space, nor compression completely in the cold space. However with suitably selected phasing of the volume variations, such that the volume variation of the hot space leads that of the cold space by about 90° , it is possible to arrange that expansion takes place mainly in the hot space and compression mainly in the cold space, with a net positive work output per cycle. The analysis of such a cycle with sinusoidal piston displacements and isothermal compression and expansion was first carried out by Schmidt in 1871 (Sci1871). Most published Stirling cycle analyses to date essentially follow Schmidt's original analysis, and it has generally become known as the Schmidt cycle analysis. The ideal nature of the cycle is still retained in that perfect heat transfer and regeneration is assumed to occur, and the pressure throughout the system is assumed constant at any instant. However the system is now a multicomponent one, and finite spaces account for the heat exchanger, clearance and regenerator volumes. The Schmidt cycle analysis has been generally accepted as an ideal standard against which to compare actual Stirling cycle machine performance. It has a closed form solution giving the variation of pressure with crank angle, and the work done and heat transferred externally per cycle as functions of the geometric and operating parameters of the machine.

The original paper by Schmidt is not generally available, however his analysis has been reproduced in many available publications (RD46, Fi53, De53, KJ54, Fi60.1, Kö60, Ki62, Wa62.1, Ki63, Me68, UR76). It is presented in non-dimensional form in Appendix B, for convenience. Typical pV diagrams obtained using the Schmidt cycle analysis are shown in figure 2.1.

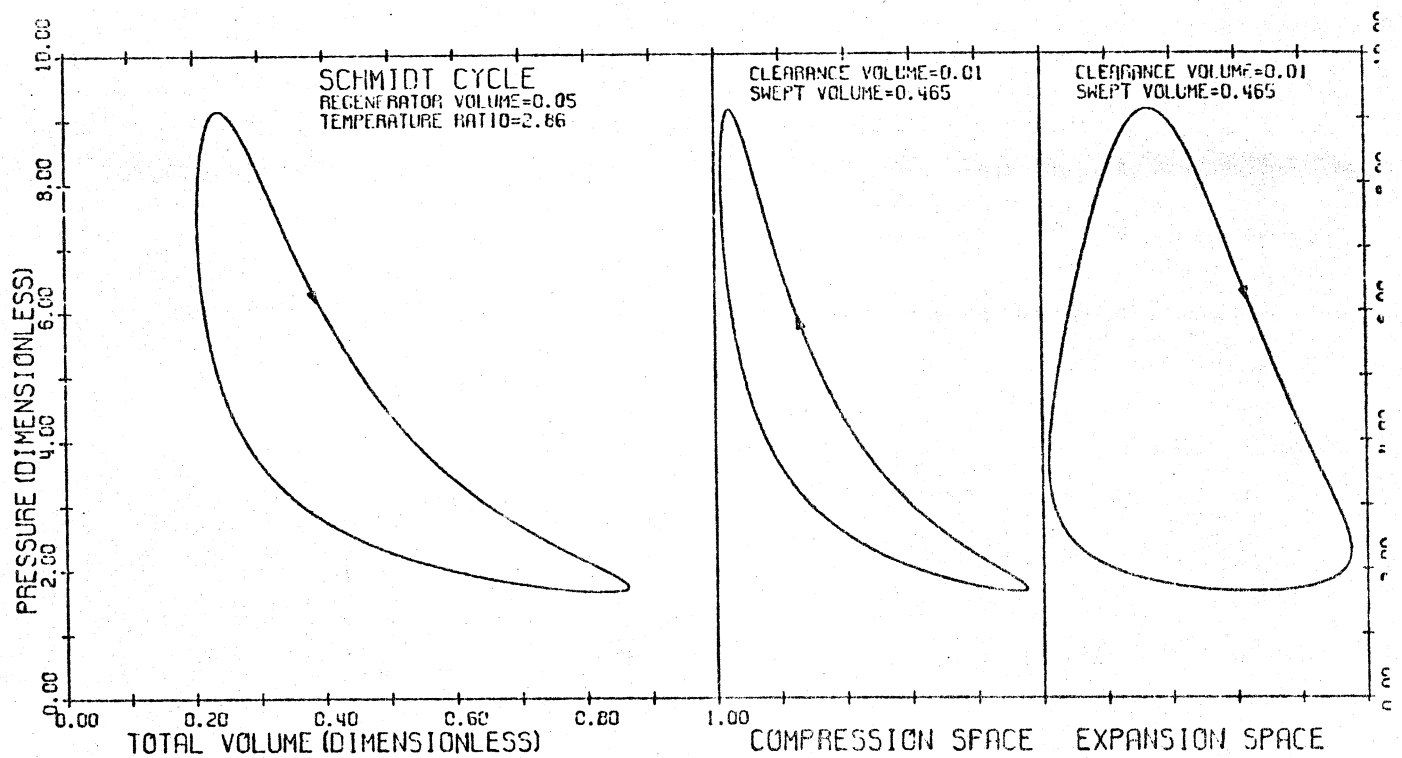


Figure 2.1 SCHMIDT CYCLE

The Schmidt cycle analysis involves four independently chosen dimensionless design parameters:

- (i) The temperature ratio T_h (refer to the section entitled 'NOTATION' in the frontispiece).

- (ii) The ratio of the expansion space to the compression space swept volumes. (This ratio is usually chosen to be unity).
- (iii) The dead volume ratio V_d
- (iv) The phase angle α by which the volume variations in the expansion space lead those in the compression space.

Various papers have been presented in which the Schmidt cycle analysis has been extended to include optimization with respect to variations in the above design parameters. (Fi60.1, Wa62.1, Wa62.2, Ki62, Wa73).

Walker and Agbi (WA73) have extended the Schmidt cycle analysis to include the use of two-phase two-component working fluids.

Walker has stated 'It cannot be over-emphasized that the predictions of Schmidt-cycle calculations are highly optimistic. Experience suggests that it is unwise to expect from a practical engine more than 30 to 40 per cent of the power and efficiency predicted by Schmidt-type analyses' (Wa73). Unfortunately, if an attempt is made to depart from any of the idealizations imposed by Schmidt, then the closed form equations break down and the system can only be solved by means of a differential equation analysis. If Schmidt's restrictive assumptions are retained then the results of analysis (in particular in optimisation studies) may result in misleading conclusions.

2.3 BASIC ANALYSIS

Rallis and Urieli (RU76, Appendix C), in an attempt to establish basic trends, presented a simplified closed form analysis based on idealized cycles but without the mechanical or thermodynamic restrictions imposed by Schmidt. In particular they examined the effects of non-isothermal compression and expansion as well as imperfect regeneration. The major assumption made was that all particles of working fluid undergo the same processes throughout the cycle. The results of this analysis are summarized in figures C.1 and C.2 (Appendix C). From figure C.1 for the ideal Stirling cycle it appears advantageous to operate such cycles at as high a value of volume compression ratio as possible, from both power output and efficiency points of view, independent of the value of regenerator effectiveness. Apparently, however, actual machines are restricted to compression ratios not exceeding 2.5 to 1, suggesting a discrepancy between the theoretical ideal Stirling cycle and its practical realization. This leads to the postulation of the ideal pseudo-Stirling cycle, as defined in figure C.2, having non-isothermal expansion and compression processes. From figure C.2 it is seen that both the thermal efficiency and specific work curves exhibit maxima at finite, and low, values of volume compression ratio. Thus, in contradistinction to the ideal Stirling cycle, it appears detrimental to operate the pseudo-Stirling cycle at large volume compression ratios. As far as is known, no other publication provides guidance of the criteria leading to an optimum choice of volume compression ratio.

Various papers have been written on the differential equation approach to ideal Schmidt cycle analysis. Karavanski and Meltzer (KM59) examined the 'per second' rates of heat flow throughout the cycle. Creswick (Cr65) presented a differential equation analysis of the Schmidt cycle in order to determine heat transfer coefficients from the resultant differential mass flow rates, and thus undertake a thermal design of the heat exchanger components. Urieli and Rallis (UR76) presented a differential equation analysis of the Schmidt cycle in order to validate the differential equation solution technique for more complex models.

Simplified Stirling cycle analysis methods have been presented by Cooke-Yarborough (Co74) and Martini (MJ68). Kolin (Ko68) illustrated a graphical procedure for analysing the Schmidt cycle.

2.4 NON-ISOTHERMAL COMPRESSION AND EXPANSION PROCESSES

Finkelstein (Fi60.2) presented a differential equation analysis of the ideal Schmidt type cycle having non-isothermal compression and expansion processes. In this paper he first introduced the concept of a 'conditional enthalpy', in which working fluid flowing in or out of the heat exchanger spaces always took on their upstream values of temperature. He presented a procedure for numerically integrating the equations noting that 'One single solution corresponds to about six weeks work on an electric desk machine, which warrants the use of an electronic computer'.

The theory presented by Finkelstein was explored by

Walker and Kahn (WK65) with particular emphasis on the limiting case of adiabatic compression and expansion processes. A study of the effect of the four principal design parameters (temperature ratio, phase angle, swept volume ratio, and dead volume ratio) on the performance of the engine was made. Some design charts and three-dimensional performance diagrams were presented, however the theory has not yet been fully exploited.

2.5 COMPREHENSIVE ANALYSES INCLUDING PRESSURE DROP

Kirkley (Ki63, Ki66) analysed the Stirling cycle engine in which allowance was made for non-isothermal processes in the compression and expansion spaces, pressure drop due to aerodynamic friction, and imperfect regeneration. He evaluated the work done and the heat supplied externally per cycle in an uncoupled manner using two different models:

- a) Work done per cycle - he defined an 'equivalent flow system', as in figure 2.2.

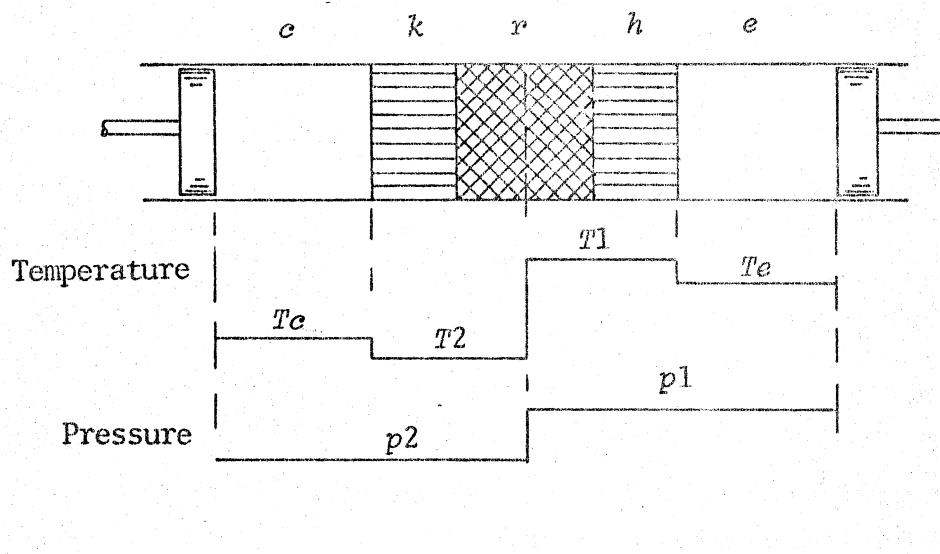


Figure 2.2 EQUIVALENT FLOW SYSTEM (After Ki63)

In the equivalent flow system there is a single pressure discontinuity in the middle of the regenerator space. The temperature of the cooler and its adjacent half of the regenerator is at a constant value T_2 , and that of the heater and its adjacent half of the regenerator at a constant value T_1 . The compression and expansion space temperatures vary due to the non-isothermal processes.

This system is described in terms of differential equations governing the mass accumulation in the compression space (Dm_c), the expansion space (Dm_e), the cooler plus half of the regenerator (Dm_2) and the heater plus half of the regenerator (Dm_1). The pressure drop $\Delta p = p_1 - p_2$ is described by the conditional equation.

$$\Delta p = K(Dm)^n / p \quad (2.1)$$

where

$$Dm_1 + Dm_e > 0 \Rightarrow Dm \leftarrow Dm_1 + Dm_e, p \leftarrow p_2$$

$$Dm_1 + Dm_e \leq 0 \Rightarrow Dm \leftarrow Dm_2 + Dm_e, p \leftarrow p_1$$

K is a flow resistance constant

n is an index greater than 1

Eight sets of differential equations in Dm_1 , Dm_2 , Dm_e and Dm_c are integrated in a conditional manner, using successive approximation techniques until cyclic steady state conditions are attained.

b) Heat supplied externally per cycle - the effect of imperfect regeneration is included by defining a 'rege-

erator effectiveness' as in figure 2.3.

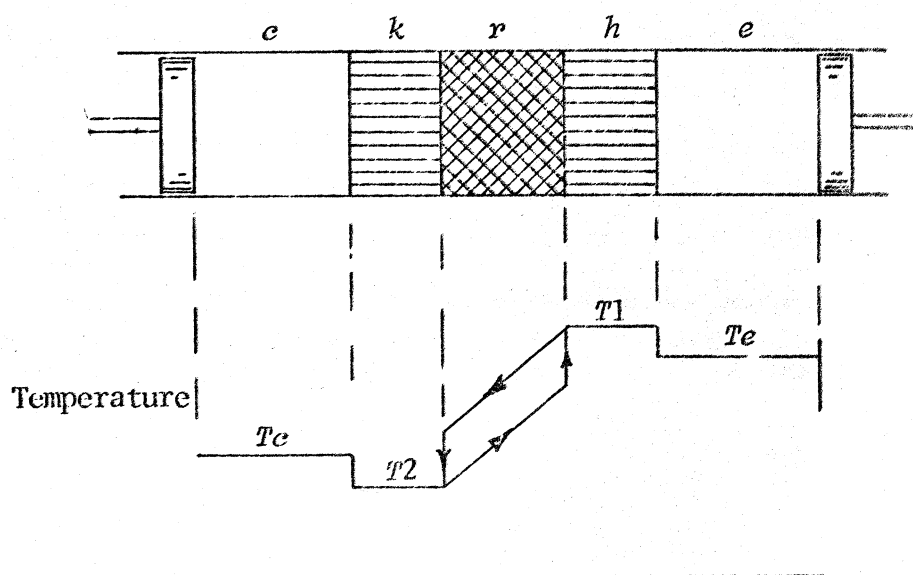


Figure 2.3 TEMPERATURE PROFILE FOR HEAT TRANSFER CALCULATIONS (After Ki63)

Thus when flow is from the compression space to the expansion space then the working gas leaves the regenerator at a temperature which is lower than that of the heater T_1 , and when the flow is from the expansion space to the compression space, then the working gas leaves the regenerator at temperature which is higher than that of the cooler T_2 .

Using experimentally determined values of K and n the performance of the theoretical model was far more optimistic than that of the equivalent experimental engine

performance. Improved correlation was attained after allowance was made for an increase of friction factor which apparently occurs in fluctuating flow conditions.

Finkelstein (Fi62, Fi64, Fi67.1, Fi67.2, Fi75) has presented five papers on the analysis of Stirling cycle machines in which allowance was made for non-isothermal processes in the expansion and compression spaces, pressure drop due to flow friction, and imperfect heat transfer and regeneration.

In his first paper (Fi62) Finkelstein proposed a model as in figure 2.4.

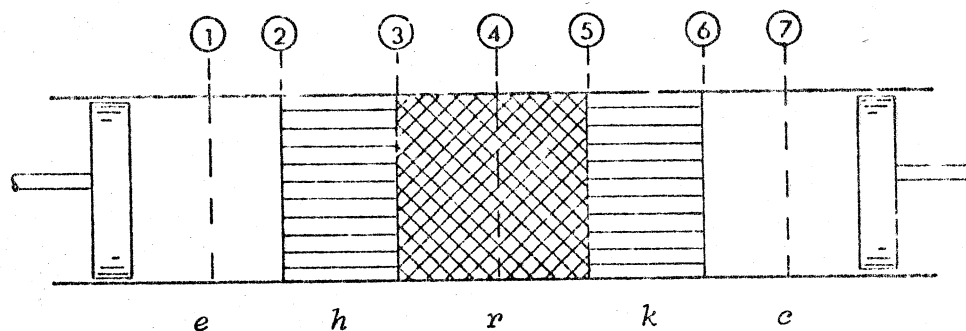


Figure 2.4 STIRLING ENGINE MODEL (After Fi62)

The system was represented by seven reference points in which:

- 1 refers to conditions in the expansion space
- 2 refers to conditions at the expansion space/heater interface
- 3 refers to conditions at the heater/regenerator interface

- 4 refers to conditions at the central cross section of the regenerator
- 5 refers to conditions at the regenerator/cooler interface
- 6 refers to conditions at the cooler/compression space interface
- 7 refers to conditions in the compression space.

The fundamental equations derived for analysis were energy equations at the expansion and compression spaces, heat transfer equations in the heater, cooler, and regenerator, flow loss in the heat exchanger ducts, and continuity of mass flow. The following major assumptions were made:

- (i) In determining heat transfer in the heat exchanger ducts, the net enthalpy was equated to the net heat transferred.
- (ii) Pressure was defined only at stations 1, 4 and 7. The pressure drops were determined by the following:

$$p_4 - p_1 = K_1 \cdot Dm_1 / p_4 \quad (2.2)$$

$$p_4 - p_7 = K_2 \cdot Dm_7 / p_4 \quad (2.3)$$

where K_1 is the combined friction factor between stations 1 and 4 and K_2 is that between stations 4 and 7.

- (iii) Conditional temperatures were defined for enthalpy flow across stations 2, 3, 5 and 6.

Thus the temperatures crossing these stations always took on their upstream values.

The system of eleven simultaneous equations derived was programmed on a digital computer simulating a digital differential analyser and one theoretical example was evaluated.

In his second paper (Fi64) Finkelstein proposed a model as in figure 2.5.

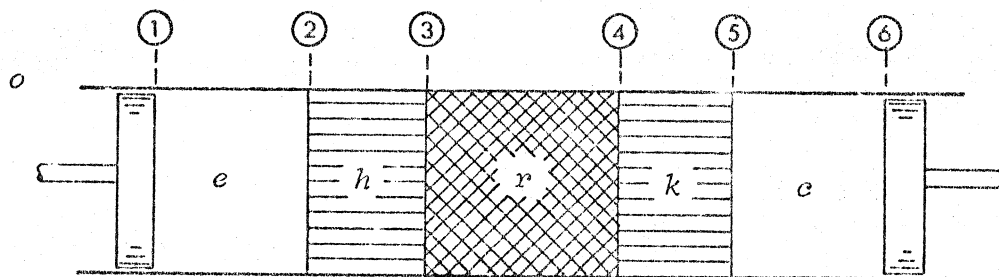


Figure 2.5 STIRLING ENGINE MODEL (After Fi64)

In this model the station numbers referred to the end planes of the five main spaces. Energy balance equations were derived for all five spaces, and heat transfer to the environment was considered, the major assumptions being as follows:

- (i) The resistances to flow were treated as lumped resistances, or leakage factors K , placed at the dividing planes between the main spaces. Thus we have the following:

$$G1 = K1(p_o - p_e) \quad (2.5)$$

where $G1$ is the leakage mass flux past the piston in the expansion space.

$$G2 = K2(p_e - p_h)$$

where $G2$ is the mass flux across station 2 etc.

- (ii) In determining the heat transferred to the main spaces, mixed mean temperatures were assumed in each space. Thus conditional temperatures were defined for enthalpy flow across the stations such that the upstream values of temperature were used.

Twenty eight simultaneous equations were developed for solution. It was stated that computation results were in excellent agreement with experimental results, however no results were presented.

In his third paper (Fi67.1), Finkelstein proposed a model as in figure 2.6.

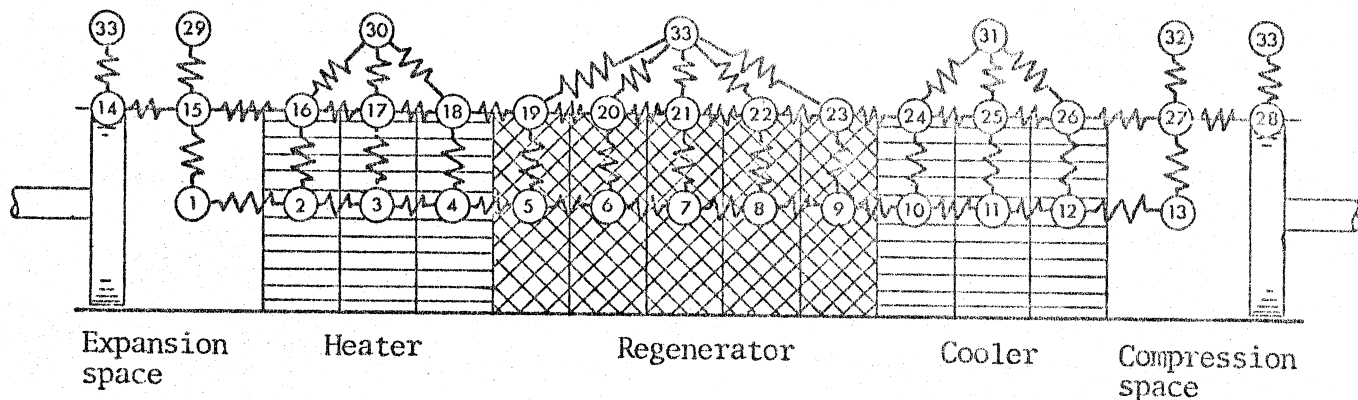


Figure 2.6 STIRLING ENGINE MODEL (After Fi67.1)

The machine was subdivided into thirteen spaces in series: one expansion space, three heater sections, five regenerator sections, three cooler sections and one compression space. This was an arbitrary subdivision, and any other subdivision could have been chosen. Significant temperatures were shown in the form of nodes of a thermal network, with identifying subscripts and connecting admittances. Nodes 1 to 13 corresponded to the respective mixed mean working fluid temperatures, nodes 14 to 28 to the metal surface temperatures in contact with the working fluid, and nodes 29 to 33 to the environmental temperatures. Thus the whole system was reduced to the time variable thermal nodal network. As in the previous model (figure 2.5), working gas flow resistance was accounted for by lumped leakage factors K at the dividing planes between the main stations. Results for an isothermal machine only were presented in a parametric manner.

In his fourth paper (Fi67.2), Finkelstein presented the same model as previously (figure 2.6), however the relation between mass flux and pressure drop was changed to the following:

$$G_{i,i+1} = K_{i,i+1} (p_i - p_{i-1}) \sqrt{(p_{i+1} + p_{i-1}) / (p_{i+1} - p_{i-1})} \quad (2.7)$$

where the subscript $i, i+1$ refers to the plane interfacing node space i and node space $i+1$.

Results were given for an isothermal analysis only.

In his fifth paper (Fi75), Finkelstein presented a sophisticated generalization of his nodal type thermal

analysis program. He retained a rather simplistic approach on the pressure drop by restricting flow resistances at the inlet to the expansion space and the inlet to the compression space only. However, this was not a fundamental limitation of the method. All of the system equations at the various nodes were reduced to the equivalent form given by the following:

$$C \cdot DT = \Sigma h(T_w - T) + Q$$

where

C is thermal capacity

h is thermal conductance

Q is heat generation or absorption

The equations of mass distribution and wall heat balance could be directly reduced to the equivalent form, however the energy equations for the working fluid required additional nonlinear terms in order to account for the conditional enthalpy terms. A generalized working gas node was thus proposed, as in figure 2.7.

From figure 2.7 it is seen that the gas nodes are linked by unidirectional conditional enthalpy conductances, conditional on the direction of working gas flow.

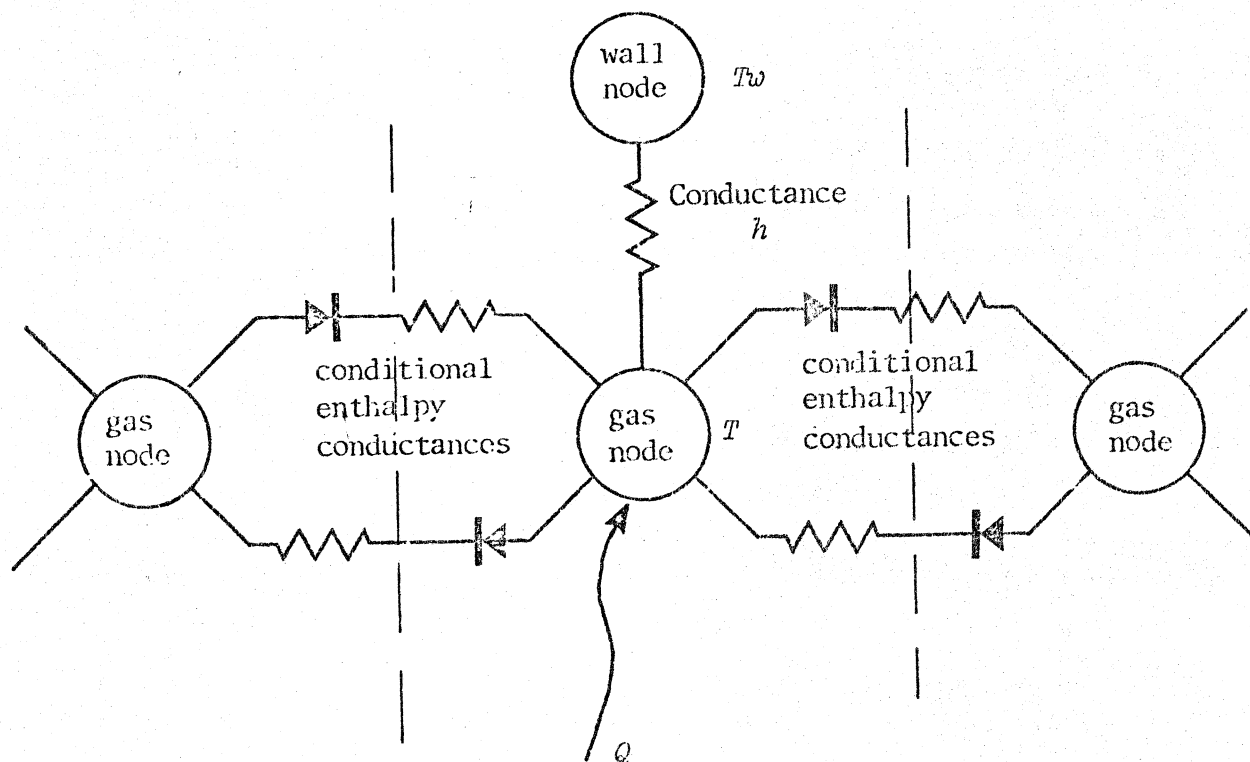


Figure 2.7 GENERALIZED WORKING FLUID NODE (After Fi75)

The computer program developed was used to simulate a cryogenic cooler and results of this simulation were presented. Being a close analog of the actual machine the program solution went through the same process of 'warm-up' requiring some several hundred crankshaft revolutions. In order to speed up the attainment of cyclic steady state a method was proposed whereby the large wall thermal capacitances were reduced to zero for a partial cycle, and then reinstated.

Qvale and Smith (QS68) analysed the Stirling cycle engine in a manner which allowed decoupling of the irreversibilities from the basic performance of the system. The basic system considered was one having^a adiabatic compression and expansion processes, ideal heat exchange,

and no pressure drop (figure 2.8).

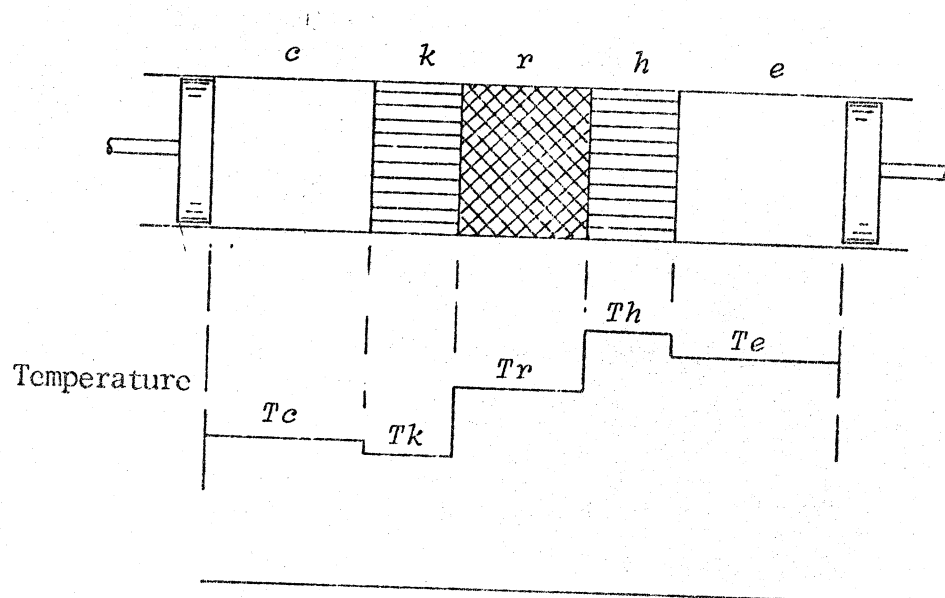


Figure 2.8 BASIC IDEAL SYSTEM (After QS68)

The heat exchanger gas temperatures were considered constant at T_k , T_r and T_h respectively. Working space temperature T_c and T_e varied according to the adiabatic processes in these spaces. Conditional temperatures were defined for enthalpy flux across the working space/heat exchanger interfaces such that the temperatures crossing these interfaces always took on their upstream values. Sinusoidal variation in system pressure and the mass of gas in the expansion and compression spaces was assumed. The system equations were integrated numerically in order to

obtain the work done per cycle as well as determine the volume variations, which were not sinusoidal. The equivalent sinusoidal volume variations were determined to give the same work done per cycle. It is noted that the work done per cycle for each working space must equal the heat transferred to each of their respective adjacent heat exchangers.

The various loss terms were then considered and their effect on the basic work done and heat transferred per cycle evaluated, as follows:

- (i) Frictional flow losses -- the momentum equation was reduced to equating the pressure drop to the frictional drag, and the effect of this pressure drop on the cyclic work done evaluated.
- (ii) Heat transfer -- the effect of imperfect heat transfer in the heater and cooler was considered to require a correction on the average temperature entering the adjacent respective working cylinder only. However, in order to examine the effect of imperfect heat transfer in the regenerator the concept of net enthalpy flux was introduced. The temperature of the gas moving towards the warm end is lower than that of the gas moving towards the cold end. The effect of this is to induce a net enthalpy flux per cycle in which heat is removed at the heater and added at the cooler.

A method of computing this net enthalpy flux was presented in a companion paper by Qvale and Smith

(QS69). In this paper approximate closed form solutions to the net enthalpy flux were derived, the major assumption being that there is no pressure drop across the regenerator. Sinusoidal mass flux and pressure variation, with a phase angle difference between them was used.

Rios and Smith (RS70) extended and refined the approach adopted by Qvale and Smith. The relative effects of decoupling the system from the various component irreversibilities were examined in depth, in particular the losses due to pressure drop. The results were verified by experiment and found to be in excellent agreement.

Kim (Ki70) developed the concept of enthalpy flux introduced by Qvale and Smith (QS68) in order to experimentally determine the heat transfer and friction factor correlations for reversing flow. He evaluated these for a regenerator consisting of a randomly packed sphere matrix and obtained results which were about 20% higher than the steady flow correlations given by Kays and London (KL64, Appendix F).

2.6 DISCUSSION

The advanced analyses of Stirling cycle machines have developed into two main streams. Qvale, Rios, Smith, and others at MIT and Purdue University have attempted to decouple the Stirling engine into its major components; separating out the regenerator, heater and cooler from the working spaces. In this way the various components can be independantly analysed and optimised. Thus the

concept of net enthalpy flux, being a measure of the regenerator effectiveness, has been developed.

This approach has obvious advantages, however, the important question to ask is 'to what extent can the system be decoupled without departing from reality?' One can only validate the theory against experiment. Unfortunately, the only existing documented experimental results are those of the General Motors PD-67 engine (ASD63). These results are for a single specific engine prototype developed for space applications, and leave much to be desired. Qvale and Smith have validated their theory against the PD-67 results and have obtained reasonable agreement as to work output and thermal efficiency. However, these are gross parameters and the agreement may be fortuitously close because of 'fudge factors' both in experimental error and in the model limitations.

The concept of net enthalpy flux is also limited to the particular configuration of a series connection of the various elements. However, this may not necessarily be the optimum or even the most practical configuration of Stirling cycle engine. As early as 1953, Finkelstein (Fi53) proposed an engine in which the heater and cooler were respectively bypassed in the two flow directions by means of simple flap valves, and heuristically proposed that the performance of this engine would be superior to the standard series connected system (figure 2.9).

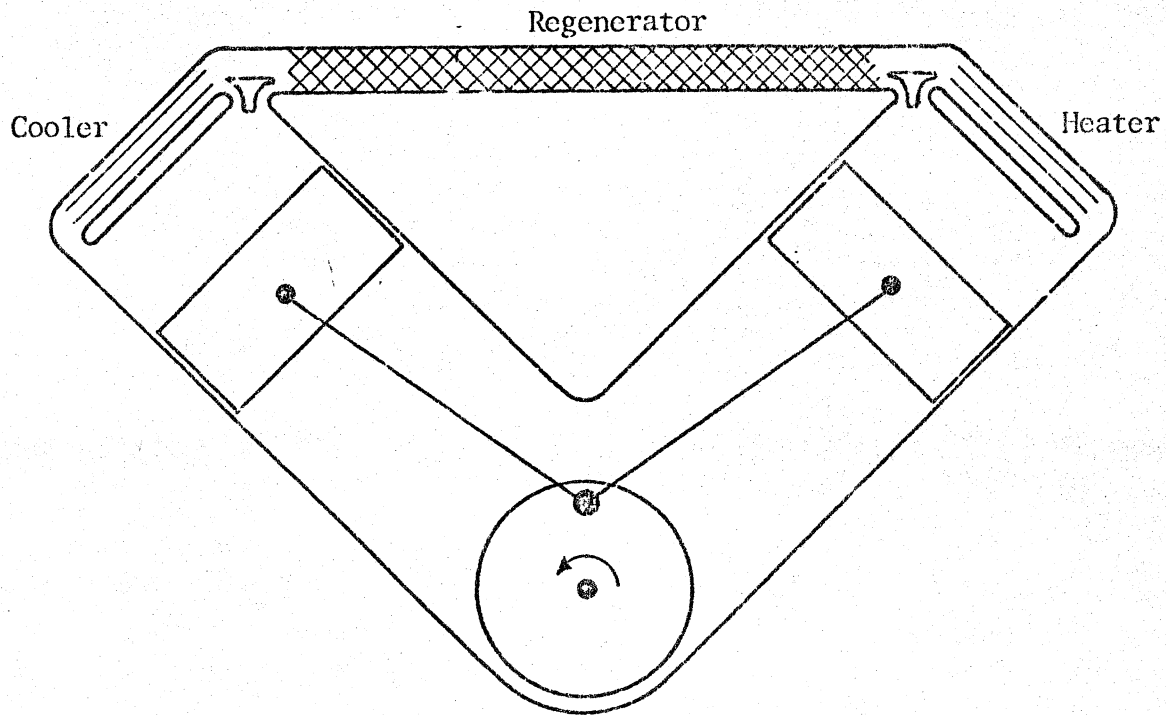


Figure 2.9 THE PORTED REGENERATIVE ENGINE (After Fi53)

As far as is known the potential of this simple modification to the basic Stirling cycle machine was never exploited or analysed in the open press. Rallis and Urieli analysed such a system using simplified ideal cycle analysis (to be published, refer Appendix C). Their results are shown in figure C.3 and should be compared with the pseudo-Stirling cycle of figure C.2. It is seen that under all conditions of regenerator effectiveness and volume compression ratio the so-called 'ported regenerative constant volume cycle' gives higher

thermal efficiency than the pseudo-Stirling cycle. In bypassing the heater it is noted that the working fluid is cooled by adiabatic expansion before entering the regenerator in the one flow direction, and heated by adiabatic compression before entering the regenerator in the other flow direction. Thus from figure C.3 it is seen that the same regenerator can be extremely beneficial at low values of volume compression ratio, and alternatively it can be extremely detrimental at high values of volume compression ratio. The regenerator thus cannot be treated as a separate entity in this system configuration and the concept of net enthalpy flux is not relevant.

The other stream has been successively developed by Finkelstein. The Stirling cycle machine has been retained as a unified complex entity, in which the describing mathematical model has evolved in a progressive attempt to simulate this entity. The main disadvantage of this technique is that as the model becomes more sophisticated, so it requires more computer time for solution. The principal simplification of Finkelstein's models has been his method of accounting for working fluid momentum losses. Leach and Fryer (LF68) in attempting to develop a comprehensive model for the Stirling engine using the method of characteristics have stated: 'The large scale digital computer is not yet ready for this problem in conjunction with the complicated thermodynamics of the irreversible Stirling cycle'. However, computer power is a relative term, and it is found that order of magnitude changes are possible in

less than a decade. During the course of this study, three very different computers were compared on the identical Stirling cycle simulation problem: an IBM 1130 (which came out in about 1960), a HP 2100 minicomputer and an IBM 370/158. It was found that the IBM 1130 is ten times slower than the HP 2100, which in turn is ten times slower than the IBM 370/158! Also, minicomputers are relatively inexpensive, extremely powerful and sophisticated devices, and it is not uncommon for a minicomputer to be dedicated to a specific problem.

2.7 STATEMENT OF THE PROBLEM

It is seen from the above review that in the open literature there does not exist a complete unsimplified model for the computer simulation of Stirling cycle type machines. In assessing the requirement of such a model, Walker has stated (Wa73): 'The principal difficulty is that much of the information on heat transfer and fluid flow, required for the data input, is not known. Thus it is not possible to assess the accuracy of the simulation without experimental results, and when the experimental machine is available the need for computer simulation largely disappears. Of course, it can be argued that, once the program is validated by comparison and adjustment of the predicted values to close agreement with the experimental values, it can be used to optimize the design of the experimental unit. This is partially true, but the order of uncertainty increases as conditions depart from those of the experimental machine, because the "fudge" factors used to validate the model do not remain constant.'

However, the computer model is not necessarily required in order to replace the need for experimentation, but rather to supplement it. One cannot in the real world, for example, arbitrarily define properties of a working fluid in order to determine the relative effect of the various properties on the performance of a machine. It is impractical to measure the instantaneous values of *all* the variables in all locations of the machine, or arbitrarily vary the operating conditions and geometry of a machine required in an optimization study. The effect of the so-called 'fudge' factors depends upon the sophistication of the model, and the accuracy of the experimental results, and cannot be determined a priori. Experimental effort can be directed in order to obtain the required heat transfer and fluid flow information, as for example the initial work by Kim (Ki70) for packed spherical beds.

In the most sophisticated models that have been presented the following is noted:

- (i) The momentum equation has been reduced to the steady flow momentum equation, ie, equating the pressure drop to friction forces, either by implied assumption or by order of magnitude analysis.
- (ii) Kinetic energy terms have been discarded from the energy equation, either by assumption or order of magnitude analysis.

- (iii) In the cellular approach, no guidance has been given as to the minimum number of cells required for accurate representation.

Order of magnitude analyses in order to reduce the complexity of the governing equations should be treated warily. They are based on intuitive reasoning as to the order of magnitude of the parameters and their first derivatives. This intuitive reasoning can be subjective, influenced by the degree of simplification which can be attained, and may thus be prone to error. A better approach would be to develop and solve the complete governing equations, thereby laying a basis with respect to which the simplified approaches can be compared.

The problem formulation is thus as follows:

- (i) Develop from first principles the comprehensive governing equations of the working gas, ie, continuity, momentum and energy. Because of axial symmetry normally found in Stirling cycle type machines, the one dimensional formulation of these equations is considered.
- (ii) Develop a model which can apply the above equations to the simulation of Stirling cycle type machines. The model should be adaptive in that it can be reduced or increased in complexity in accordance with experience; that any realistic system configuration and interconnection of the basic components can be simulated; and that the algorithms for evaluating the empirical correlations of fluid friction and heat transfer coefficients can be updated, in accordance with current knowledge in the field.

- iii) Validate the model. This validation can be divided into consistency requirements and experimental verification. Consistency requirements include the non-violation of the fundamental laws of nature, numerical stability and accuracy, and determining if the performance trends indicated by the model on specific configurations of machine are in accordance with current knowledge in the field.

As far as experimental verification is concerned, the only documented experimental results available in the open press are those of the General Motors Allison Division PD-67 engine (ASD63). The report in which they are published is not widely available, and a copy was obtained only recently -- too late to include it in this work. The PD-67 engine was not designed as a research tool in order to make available fundamental experimental information, but rather as a prototype machine in order to assess its applicability to a specific single-purpose space application. As such the results relate to some tens of hours of running experience on the prototype machine and leave much to be desired. The development and testing of research machines is currently being undertaken by a number of institutions specifically for the purpose of providing fundamental data. The effort required is at least as large as this work, and as such no experimental validation of the model developed in this study has been possible. Rallis, et al, of the University of the Witwatersrand, have begun an experimental program based on the

two-piston configuration. Buckingham, Rice and Dunn of Reading University in England are involved in an experimental program based on a piston-displacer type engine. Vote, Hoehn and Finegold of the Jet Propulsion Laboratory in California are developing an opposed dual-piston engine specifically in order to produce fundamental data. It is hoped that these efforts will begin to produce results within the next year and enable validation of this work.

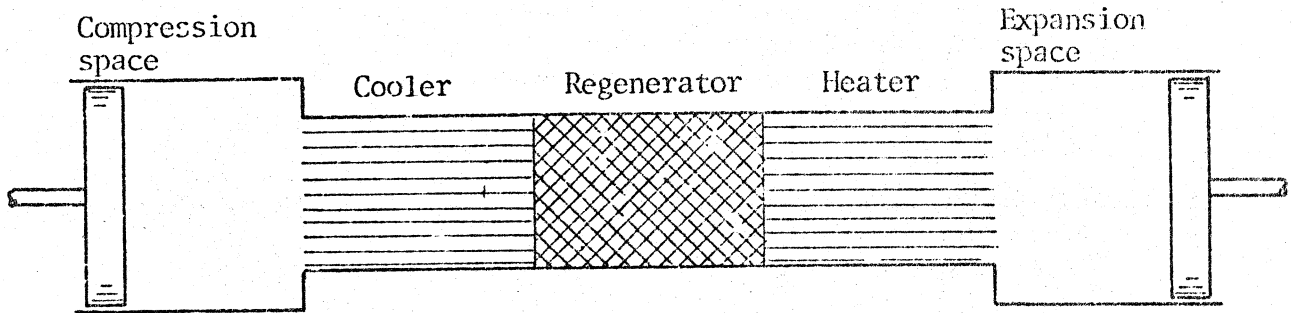
3. SYSTEM MODEL

3.1 GENERAL

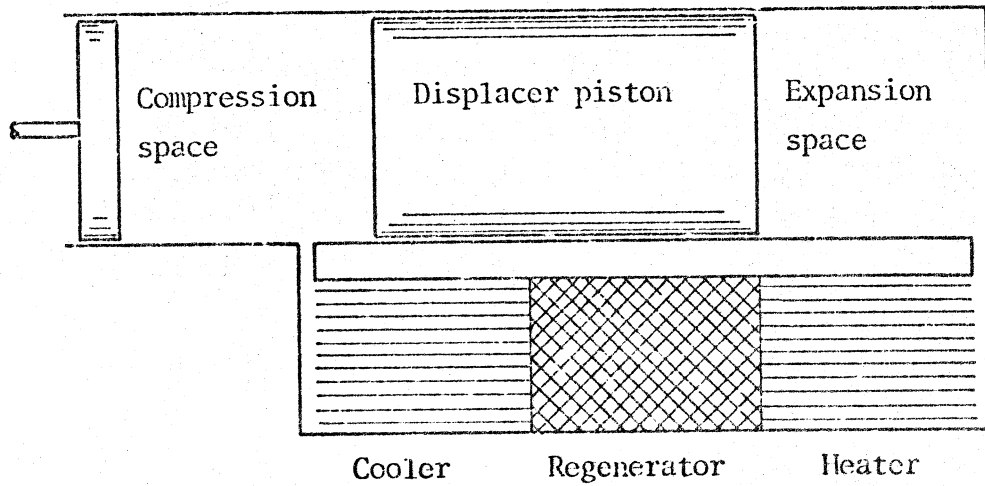
In this chapter the fundamental equations, system model and method of solution are treated. The system is basically divided into so-called variable working spaces, heat exchanger spaces and interconnecting spaces. These spaces are not necessarily mutually exclusive and it may be found that working gas in a working space may be undergoing heat exchange with the bounding surfaces. Most practical machines, however, have separate heaters, regenerators and coolers, and the model will be restricted to systems having adiabatic working spaces. The fundamental analysis is however sufficiently flexible to allow the inclusion of heat exchange in the working spaces should it be found necessary. The three configurations into which it is possible to classify all known designs of reciprocating Stirling engines are now considered, after Kirkley (Ki62).

Alpha engines (figure 3.1a) are the dual piston engines and include V-engines (CL75, We47), Swash plate or Rider type engines (Ba1885, We47), and opposed piston engines (We47, Wa62.1). The working spaces are the swept compression and expansion spaces, and their respective clearance spaces. The two working spaces are separated by the series connection of the heat exchange spaces -- being the cooler, regenerator and heater respectively.

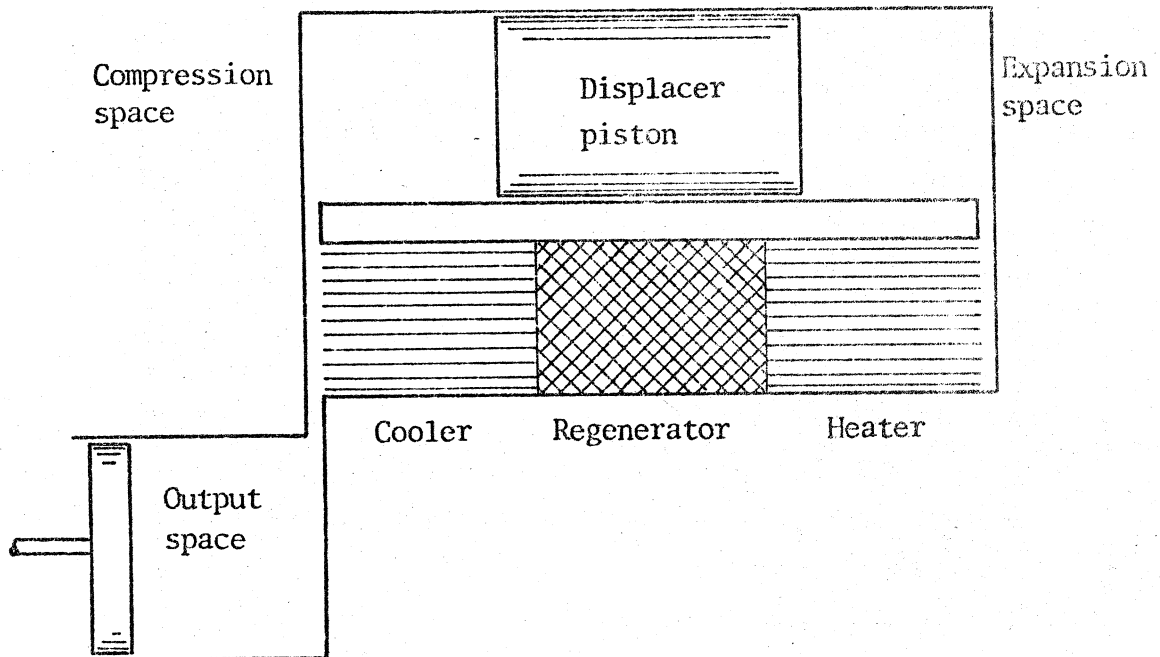
Beta engines (figure 3.1b) are single cylinder piston-displacer engines and include rhombic drive engines (Me59), Beale type free piston Stirling engines (Be69)



3.1a Alpha engine



3.1b Beta engine



3.1c Gamma engine

Figure 3.1 CLASSIFICATION OF STIRLING CYCLE ENGINES

and the Harwell thermomechanical generator (CF74). The working spaces are the swept spaces on either side of the displacer piston, including their respective clearance spaces. The compression space volume variation is controlled by the combined movement of the displacer and power pistons, and the two working spaces are separated by the series connection of the heat exchanger spaces.

Gamma engines (figure 3.1c) have a power piston and a displacer piston as in Beta engines, however they are housed in different cylinders, thus defining the so-called 'output' space, being a third working space. These engines include Robinson and Heinrich engines (Wa73) and Martini type free piston Stirling engines (MW74). The compression and expansion spaces are separated by the series connection of the heat exchanger spaces.

Finkelstein (Fi76) has stated that he does not agree with the separate classification of the Gamma engine, and that it is just a subclass of Beta type engines. However, the output space need not be connected directly to the compression space, as is normally done, but may be advantageously connected to (say) the interface between the regenerator and the cooler, or the regenerator and the heater. As far as is known, these non-standard configurations have never been exploited or analysed.

Thus it is seen that the Alpha and Beta engines are thermodynamically equivalent, however, the Gamma engine can operate on a different thermodynamic cycle. More complete classifications of the various known configurations are given in Walker (Wa73) and Kolin (Ko68).

The ensuing analysis is restricted to Alpha type machines, however the analysis can be adapted to include standard or non-standard Gamma type engines, or in fact any conceivable valved or unvalved configuration and inter-connection of the basic components, provided that the working fluid operates in a single phase throughout the cycle.

3.2 THE IN-LINE CONFIGURATION

The in-line Alpha configuration shown in figure 3.1a is considered. The compression and expansion spaces are treated as adiabatic spaces having respectively uniformly distributed thermodynamic properties. The heat exchanger space consists of the heater, cooler and regenerator. The heater and cooler normally consists of banks of pipes containing the working gas and immersed within the heating medium and cooling fluid respectively.

The regenerator usually consists of a porous solid, called the matrix, the void volume of which is open to flow of the working gas. The matrix is made of heat storage material and is usually in the form of wire wool, wire gauze screens, a packed bed of particles such as spheres, or ceramics. However in some instances the regenerator matrix reduces to the walls of an annular space or simple pipes.

The interconnecting spaces are usually included in the clearance volume of one of the working spaces, however they can be included in the analysis as separate entities if required.

The analysis of the heat exchanger spaces in a Stirling cycle machine is extremely complex, even though the geometric structure of these spaces are usually simply defined, for the following reasons:

- (i) The thermodynamic state varies continuously both in time during the cycle and with position along the heat exchanger spaces.
- (ii) The temperature of the gas varies with position and temperature dependencies of the physical properties have to be considered.
- (iii) The mass flow rate along the heat exchangers varies considerably with time and position. At some instances of time simultaneous laminar and turbulent flow can occur in both directions through the heat exchanger spaces. Thus the heat transfer and flow friction parameters which are nonlinear functions of thermodynamic state, physical properties and mass flow rate of the working gas will not be constant.
- (iv) The heater and cooler walls are usually maintained at a constant temperature, however the matrix temperature (and enclosing walls) fluctuate both in time during the cycle and with position. The matrix heat capacity is much higher than that of the gas, however, and the time fluctuations of the matrix temperature is usually relatively small.

The complexity and nonlinear nature of the behaviour of the working gas in the heat exchanger spaces precludes

any closed form analytical solution, thus the system can only be described by partial differential equations.

3.3 THE FUNDAMENTAL EQUATIONS

In Appendix D the fundamental equations of continuity, momentum and energy are derived for fluid flowing through a generalized elemental control volume V (figure 3.2)

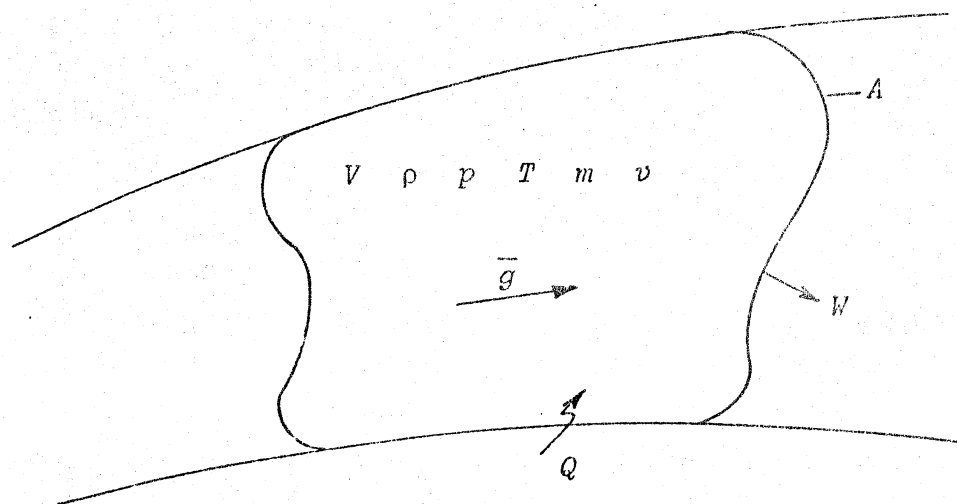


Figure 3.2 GENERALIZED ELEMENTAL CONTROL VOLUME

It is assumed that the control volume is chosen such that either all the fluid properties are uniform and constant in space throughout the control volume, or that it is small enough such that all the fluid properties can be adequately represented throughout the control volume by their mean values. The fluid properties are represented by the specific volume v

(or density ρ), pressure p , temperature T , and momentum per unit volume \bar{g} (refer to Appendix A and the section entitled 'NOTATION' in the frontispiece). The control volume is in an Eulerian framework, but may vary in magnitude with time. Thus the momentum per unit volume \bar{g} assumes the role of a mass flux density while it is crossing the bounding control surface A , transporting matter, energy and momentum flux into and out of the control volume V . Energy in the form of heat Q crosses the control surface A , and mechanical work W is done by the control volume V on the surrounding environment by virtue of its volume variation with time. Shaft work done by virtue of a rotating shaft crossing the bounding control surface A is ignored. The fluid is Newtonian, and the nonlinear variation of its dynamic viscosity with temperature is considered. It is assumed that the fluid behaves as a perfect gas, and that its dynamic viscosity does not vary with pressure. This is not, however, a fundamental limitation of the method of analysis or solution, and the nonlinear behaviour of any of the parameters can be included if required.

Because of the axial symmetry normally found in Stirling engine heat exchangers, the equations developed in Appendix D are reduced to the one-dimensional case. In order to include the strictly three-dimensional effects of turbulence in the one-dimensional system empirical correlations are invoked to determine the heat transfer and friction behaviour of the working gas with respect to its surroundings.

In the momentum equation the effects of momentum flux and the acceleration of the working gas are taken into account. In the energy equation, the stored working gas energy is assumed to consist of internal energy and kinetic energy. All other forms of stored energy have been ignored as being irrelevant to the class of systems that will be considered.

The fundamental equations derived in Appendix D for the above arguments and assumptions are given in equations (D.5), (D.9) and (D.18) below:

Continuity:

$$\frac{\partial m}{\partial t} + V \frac{\partial g}{\partial x} = 0 \quad (\text{D.5})$$

Momentum:

$$\frac{\partial}{\partial t}(g \cdot V) + V \frac{\partial}{\partial x}(g^2 v) + V \frac{\partial p}{\partial x} + F = 0 \quad (\text{D.9})$$

Energy:

$$\frac{dQ}{dt} = \frac{\partial}{\partial t} \left(\frac{m \cdot T}{\gamma - 1} \right) + V \frac{\partial}{\partial x} \left(\frac{\gamma T \cdot g}{\gamma - 1} \right) + \frac{dW}{dt} - g \cdot v \left(V \frac{\partial p}{\partial x} + F \right) \quad (\text{D.18})$$

The perfect gas equation of state is given by:

$$p \cdot V = m \cdot T \quad (\text{H.20})$$

The mechanical work W is considered to be done reversibly, thus, since shaft work is ignored, it can be related directly to the volume variation with time of the control volume.

$$dW/dt = p dV/dt$$

In order to complete the basic system of equations, the various heat flows, by convection between the working gas and the matrix or the heat exchanger wall, and by conduction within the wall, are considered.

$$dQ/dt = h \cdot A_{wg} (T_w - T^*) \quad (3.1)$$

$$\partial Q_w / \partial t = k_w \cdot A_w \cdot \partial T_w / \partial x \quad (3.2)$$

where

T_w is the temperature of the wall forming one of the bounding surfaces of the control volume V

A_{wg} is the wall area wetted by the working gas in V

Q_w is the axial conductive heat flow in the wall

A_w is the wall cross sectional area

h and k_w are respectively the heat transfer coefficient and thermal conductivity of the wall.

Finally the energy balance of the wall is considered:

$$C_w dT_w/dt = \sum_i (dQ_{w_i}/dt) \quad (3.3)$$

where

C_w is the heat capacity of the wall

Q_{w_i} are all the heat flows into the wall

It is noted that equations (3.1) through (3.3) apply to the matrix as well, by replacing the suffix w by the suffix m .

Equations (D.5) through (3.3) above form the complete system of basic equations which apply to the elemental control volume V . In the following section the system is subdivided into elemental control volumes in order to apply the basic equations.

3.4 THE CELLULAR MODEL

The usual method of solving partial differential equations on a digital computer consists of approximating the partial derivatives with respect to all the independent variables by finite difference expressions. The resulting algebraic relationships are then solved at the grid points of the discretized region of interest. The approach that has been adopted here is to convert the partial differential equations to a system of ordinary differential equations by discretizing the spacial coordinate only (Appendix G). This is done by subdividing the machine into a finite number of thermodynamic entities, or cells (figure 3.3).

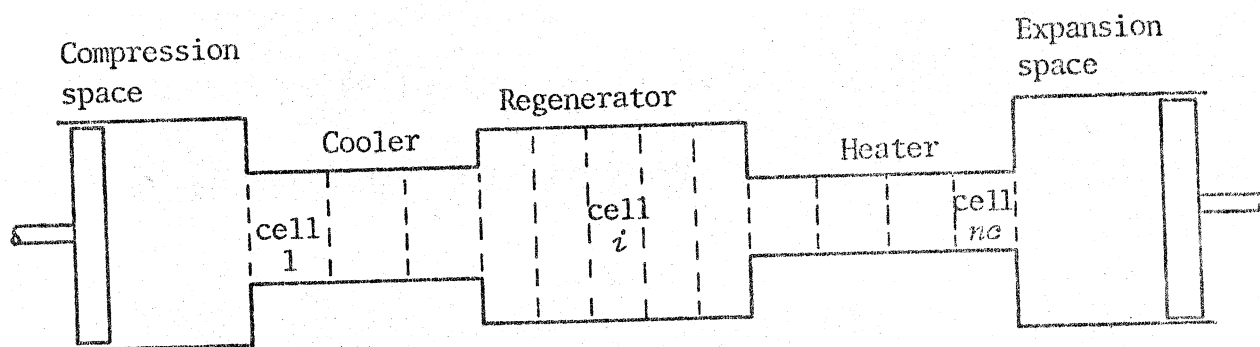


Figure 3.3 THE nc -CELL MODEL

The elemental cells are interconnected by interfaces, or nodes, having zero volume. Each cell has uniform, time varying properties, and thus can be represented by a system of total differential equations.

A detailed description of the most general i 'th elemental cell (figure 3.4) is now considered. The i 'th elemental cell consists of a void space having a void volume V_i and containing working gas of mass m_i , temperature T_i , pressure p_i and specific volume v_i (or density ρ_i).

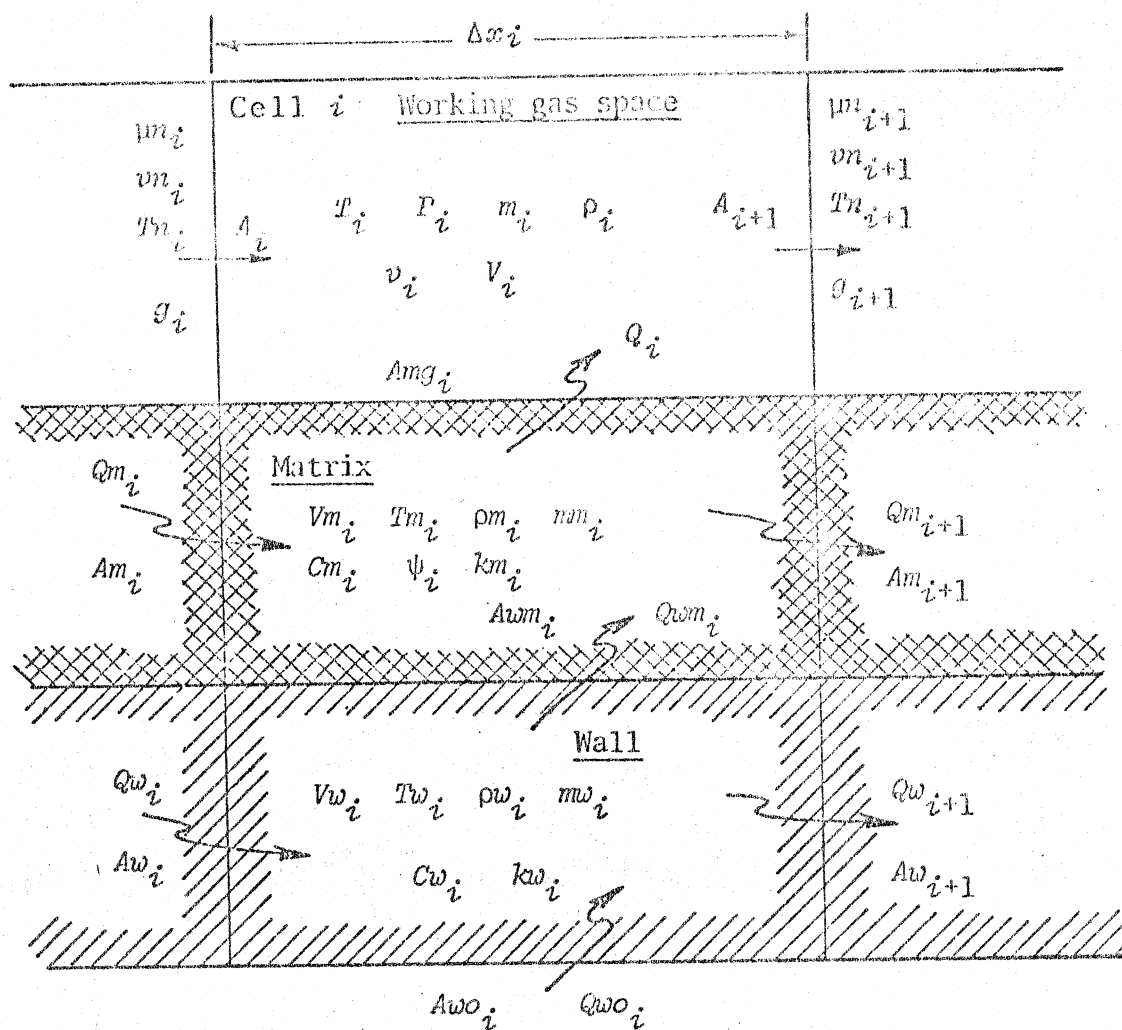


Figure 3.4 THE GENERALIZED i 'TH ELEMENTAL CELL

The working gas in this void space is in intimate open communication with the porous cell matrix. The matrix presents a wetted area $A_m g_i$ to the working gas, allowing heat Q_i to be transferred by convection from the matrix to the working gas. The cell axial length is Δx_i . Cell i is bounded by node i being the interface to adjacent cell $i-1$, and node $i+1$ being the interface to adjacent cell $i+1$. Mass flux density g_i flows across node i through the free flow area A_i giving a total mass flux G_i . The various working gas properties are defined as being constant throughout the cell and discontinuous at the nodes. Thus the node temperature T_{n_i} and the node specific volume v_{n_i} are conditional variables, taking on their respective upstream adjacent cell values, conditional on the direction of mass flux density g_i . Thus referring to the arbitrarily defined positive direction of flow given in figure 3.4 (which has been adhered to throughout) one obtains:

$$\begin{aligned}
 g_i \geq 0 &\Rightarrow T_{n_i} \leftarrow T_{i-1}, \quad v_{n_i} \leftarrow v_{i-1} \\
 g_i < 0 &\Rightarrow T_{n_i} \leftarrow T_i, \quad v_{n_i} \leftarrow v_i
 \end{aligned}
 \tag{3.4}$$

where the symbols \Rightarrow and \leftarrow take on their usual mathematical connotations of 'leads to' and 'is replaced by' respectively.

The above definition of conditional node temperatures has been introduced by Finkelstein (Fi60.2). The cell model having mixed mean properties (in particular temperature) in the cell and conditional upstream properties at the nodes has been criticized during private

communications by many researchers in the field, for two reasons. Fokker of Philips, Holland; Bratt and Sjöholm of United Stirling, Sweden; and Gedeon of Sunpower, USA have stated that in the real system the temperature distribution is continuous; thus the model may lead to pessimistic system performance owing to thermodynamic irreversibilities associated with finite temperature discontinuities. Organ of London University and Van Eekelen of Philips, Holland have stated that mixed mean properties in a cell having a finite axial length implies instantaneous propagation of information, being in violation of the laws of nature. Variants of the above system model were thus considered in which the various properties are continuously distributed axially across the system in a piecewise linear manner. In this case the node properties were defined as the arithmetic means of the adjacent cell properties, and invariant with the direction of mass flux density. The results of analysis using these variants are discussed in Chapter 5 in the light of the above criticisms.

The cell matrix properties are defined in terms of its overall volume (being the void volume V_i plus the volume occupied by the matrix material V_{m_i}), porosity ψ_i , density of the matrix material ρ_{m_i} , mass m_{m_i} , heat capacity C_{m_i} , thermal conductivity k_{m_i} and temperature T_{m_i} . (Refer to figure 3.4). Heat transfer by conduction between adjacent cell matrices Q_{m_i} takes place at node i through the matrix effective cross sectional area A_{m_i} . Heat transfer by conduction Q_{wm_i}

takes place between the matrix and containing wall through the effective area of contact Awm_i .

The containing wall associated with the i 'th cell has its properties defined in terms of its volume Vw_i , density ρw_i , mass mw_i , heat capacity Cw_i , thermal conductivity kw_i and temperature Tw_i . Heat transfer by conduction between adjacent cell walls Qw_i occurs at node i through the wall cross sectional area Aw_i . Heat transfer with the external environment adjacent to the wall of the i 'th cell, Qwo_i , takes place through the external wall area Awo_i .

In the case of a regenerator cell it is usually assumed that the regenerator is externally adiabatic (no heat transfer takes place between the containing wall and the surrounding environment, ie, $Qwo_i = 0$). It is also usually assumed that the axial thermal conduction leakage path is predominantly in the containing wall ($Qm_i = 0$) and that there is no thermal conduction between the containing wall and the regenerator matrix ($Qwm_i = 0$). These are not fundamental limitations of the model, however, and all of the above heat flows can easily be included if necessary. It is also noticed from figure 3.4 that no heat transfer occurs between the containing wall and the working gas. In the special case in which there is no regenerator matrix, ie, that the wall acts as the regenerator (for example the application example in Chapter 4) then the heat transfer to the working gas Q_i takes place between the working gas and the cell wall.

In the case of a heater or cooler cell no matrix is present, and convective heat transfer Q_i takes place between the working gas and the cell wall. It is usually assumed that the wall temperature T_{w_i} is constant, and heat flow $Q_{w_o_i}$ is exactly metered out in order to maintain this constant value of wall temperature. The model can easily be adapted to allow a varying wall temperature T_{w_i} if it is found necessary.

3.5 THE VARIABLE VOLUME WORKING SPACES

The boundary conditions for the series connected heat exchanger cells are the compression and expansion spaces respectively. The compression space is adjacent to the first cell (figure 3.5) and the expansion space is adjacent to the n 'th cell.

The compression space consists of variable volume V_c containing working gas of mass m_c having temperature T_c , pressure p_c and specific volume v_c (or density ρ_c). The working fluid is contained in a wall having a temperature T_{w_c} . The actual value of T_{w_c} cannot be determined theoretically and depends inter alia upon the nature of the environment, the cylinder configuration, the mechanical friction heat generated by the piston seals and the heat transfer to the working fluid. Heat conduction Q_{w_1} takes place between the cylinder wall and the wall of cell 1. It is usually assumed that the cylinder wall is adiabatic ($Q_{w_1} = 0$) unless experimental values of T_{w_c} are available, which can then be included in the model. Heat transfer between

the cylinder wall and the working fluid is not normally considered, but can be included in the model if found necessary.

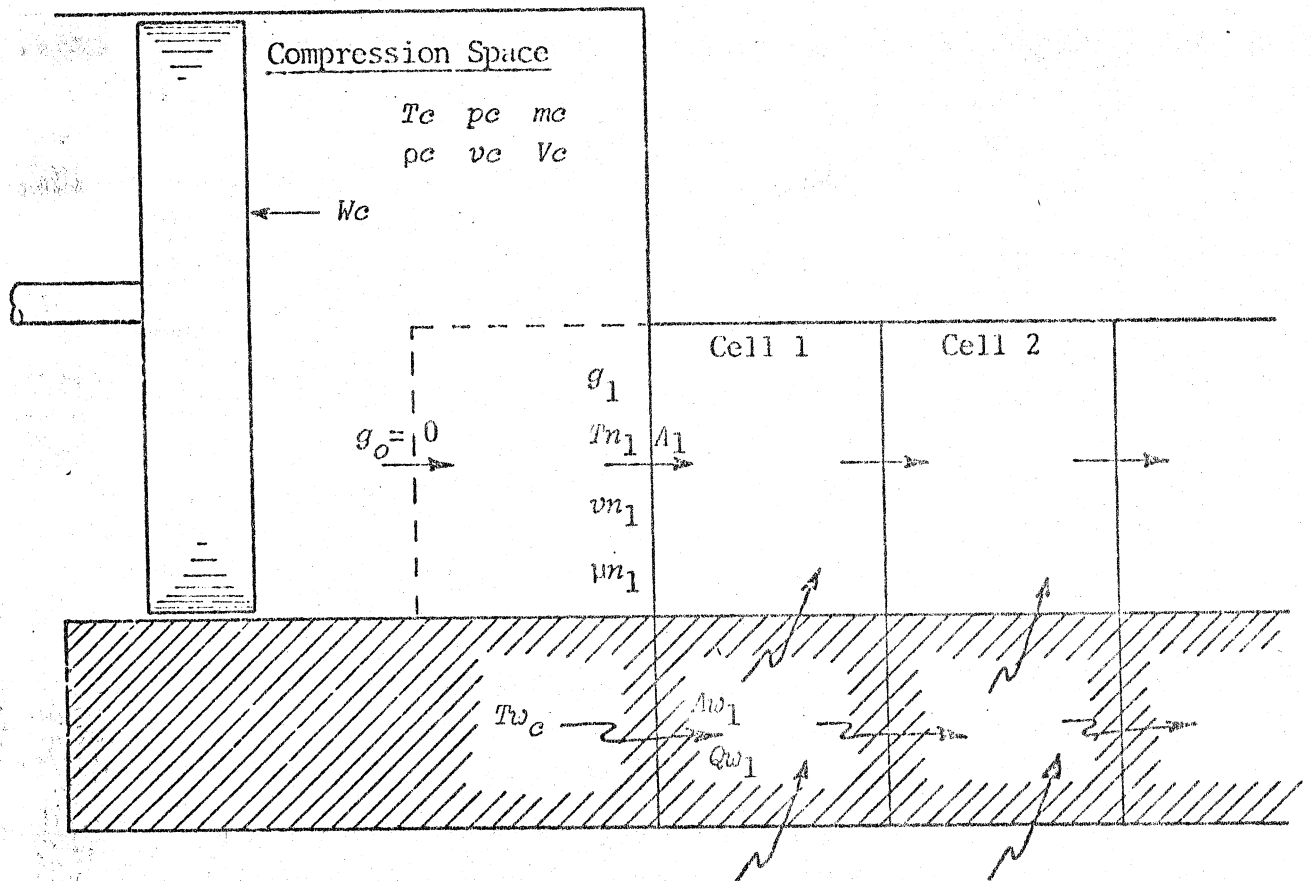


Figure 3.5 THE GENERALIZED COMPRESSION SPACE

The compression space interfaces with the first cell via node 1. Mass flux density g_1 flows across node 1 through free flow area A_1 giving a total mass flux G_1 . Conditional node temperature T_{n_1} and specific volume vn_1 are defined at node 1 as in equation (3.4). A pressure drop Δp_c due to contraction (expansion) loss exists across node 1. In determining the momentum balance it is assumed that a zeroth cell is projected into the compression space, in which the working fluid has the same properties as that in the compression space. It is assumed that the working fluid in the compression space is stationary and thus has no momentum.

Mechanical work W_c is done on the external environment by virtue of the change in volume of the compression space. It is assumed that this work is done reversibly.

All the above arguments and assumptions for the compression space apply to the expansion space as well.

3.6 SYSTEM ALGORITHMS

The fundamental equations of section 3.3 are applied to the system model defined in sections 3.4 and 3.5 in order to obtain the system of simultaneous first order ordinary differential equations for solution. It is found that a distinction is made between cell parameters and node parameters. The working gas energy equation (D.18), work done equation (H.19), convection heat transfer equation (3.1), and wall (or matrix) heat balance equation (3.3) are applied to the cells and variable working spaces only. However, it is seen that

the mass flux density is defined only at the nodes, thus the momentum equation (D.9) is applied at the nodes. Also, since the wall temperature T_w is constant throughout the cell wall, the heat conduction equation (3.2) can only apply to heat flow across the nodes between adjacent cell walls. The continuity equation (D.5) relates the mass accumulation of working gas in the cells to the mass flux density across the adjacent nodes.

In Appendix H the fundamental equations are applied to the complete system model in order to obtain the system algorithms suitable for solution. Together with every derived algorithm the FORTRAN equivalent statements are given, in keeping with the aim not to divorce the computer program from the text. It is found that in order to obtain the frictional drag force F in equation (D.9) and the heat transfer coefficient h in equation (3.1) it is necessary to determine the local value of dynamic viscosity μ and thermal conductivity k of the working gas, as well as invoke the empirical correlations for the specific system configuration.

The determination of μ and k is given in Appendix E, and the empirical correlations for F and h are given in Appendix F. It is found from Appendix F that very little experimentally validated information on the matrix surfaces used in Stirling cycle type machines is available to date. However, the nature of the modelling approach is such as to allow updating of the various algorithms in keeping with current knowledge.

3.7 METHOD OF SOLUTION

At this stage, the complete system of algorithms has been derived, taking the form of a system of first order total differential equations which are required to be integrated simultaneously. The method of solution of the system of equations is given in Appendix G.

Systems of total differential equations can be solved as initial value problems using well established numerical methods, eg, Runge-Kutta methods. However, in the case of a Stirling cycle machine the initial conditions of all the relevant parameters at some arbitrary initial reference point in the cycle are not known. The system is thus converted into an initial value problem by starting the engine at a stationary initial condition with the working gas in temperature equilibrium with the surroundings. Thus since the engine is stationary, all the values of mass flux density are zero, and there is no pressure drop axially along the machine. This is sufficient information to enable a consistent set of initial conditions to be defined in order to begin the integration routine.

The system then goes through a 'warmup' period by integrating the equations through several complete cycles until cyclic steady state has been attained. This is the equivalent of the 'warmup' operation of an actual machine in which the machine starts from some initial state and goes through successive transient cycles until the values of all the variables at the end of each cycle are equal to those at the beginning of

that cycle. The time needed until cyclic steady state is reached is dependant mainly upon the thermal capacitance of the system -- in particular that of the regenerator matrix and wall -- and can require some several hundred crankshaft revolutions (Fi75).

A technique for accelerating convergence to cyclic steady state was developed, and is presented in Appendix G. It is based upon the principle that when cyclic steady state has been attained then through each cycle the net transfer of heat between the working fluid and the regenerator matrix is zero. Thus the a posteriori value of residual regenerator heat is used in a simple feedback loop in order to alter the regenerator matrix temperature distribution. The root mean square of the residual regenerator heat is used as a measure of the degree of departure of the machine from cyclic steady state.

3.8 CONCLUSION

The actual form of the cellular model given above was arrived at after quite considerable trial and error, some of which is discussed in Chapter 5. The evaluation of this model was mainly influenced by the threefold requirement of solubility, numerical stability, and accuracy.

The solubility requirement was met by reducing the set of partial differential fundamental equations to a set of first order total differential equations. This is done by discretizing the partial differential equations in the spacial coordinate only and retaining the time

derivative. This approach of discretizing a partial differential equation in all but one coordinate is known as the 'method of lines', and is discussed in Appendix G. Rather than discretize the continuous equations, it was decided to discretize the continuous model and convert it to a finite cellular form.

The requirement of numerical stability governs not only the time increment for integration, but also the form of the model and the method of integration.

The requirement of accuracy governs the choice of the number of cells as well as the time increment for integration.

Both of these latter requirements will be discussed more fully in Chapter 5.

4. AN APPLICATION EXAMPLE

4.1 INTRODUCTION

The major aim of this work is to present a technique of modelling and solution such as to enable any configuration of single component single phase thermal machine to be evaluated. As such the model needs to be validated against current knowledge in the field. This validation can be resolved into streams, as follows:

- (i) The model must be numerically stable. In this context it was found necessary in this study to differentiate between so-called dynamic and static instability. Dynamic instability is a positive feedback effect which manifests itself in the solution variables tending to infinity. As such it is easily detected and overcome by simply decreasing the integration time interval. Static instability is much more difficult to detect since it can have a limiting restraining effect and can pass completely unnoticed if only the gross computational parameters, such as efficiency or work done per cycle, are presented. It manifests itself in introducing spacial oscillations in the parameters, where such oscillations do not exist in the actual machine. Thus in validating the model for numerical stability both static and dynamic instability must be considered.
- (ii) The model must be consistent. The consistency conditions require that the fundamental laws of continuity, momentum and energy must not be

violated, from the basic defining equations through to the system algorithms and numerical solution. Thus for example, if leakage is not allowed for then the total mass of working gas must always be a constant.

- (iii) The model must be accurate. The real machine parameters vary continuously in both time and space, however, the model is discretized in both time and space. This discretization is necessary in order to make the model soluble on a digital computer in a finite time. It is obviously advantageous that this solution time be minimized. This can be done by reducing the number of cells (spacewise discretization) or increasing the integration time interval. However, the effect of these on the accuracy of the solution must be evaluated, and either corrected for, or contained within reasonable limits.
- (iv) The model must be realistic - it must reflect the behaviour of the real machine, preferably in accordance with actual experimental observation on a prototype machine, or if a prototype machine is not available, then in accordance with current experience and knowledge in the field.

In this chapter an application example test engine which is used in order to validate the model is defined. In validating the model, a considerable computational effort is required in order to obtain an exhaustive set of results. The test engine configuration has been chosen to be both a practically feasible system, as well as to minimize the computational effort.

4.2 DESCRIPTION OF THE ENGINE

The hypothetical test engine is shown in figure 4.1. It consists of an adiabatic expansion space and an adiabatic compression space interconnected by a homogeneous bundle of heat exchanger pipes.

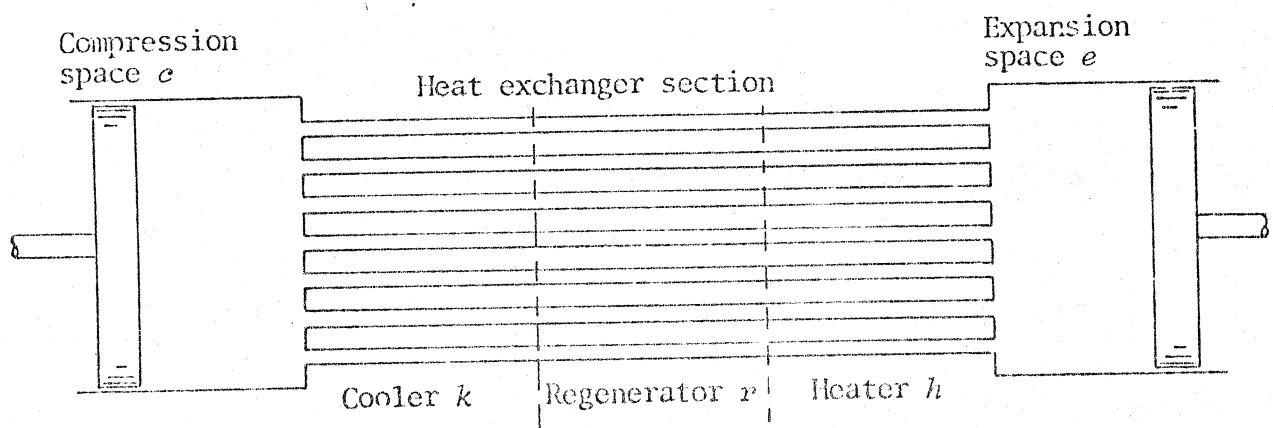


Figure 4.1 THE TEST ENGINE

The bundle of pipes are divided into three sections, the cooler, regenerator, and heater respectively. The pipes in the cooler section are maintained at a constant wall temperature T_{wk} , and the pipes in the heater section are maintained at a constant wall temperature T_{wh} . The pipes in the regenerator section attain their own specific temperature distribution in accordance with the governing heat flow equations and

the requirements for cyclic steady state.

There is no regenerator matrix in the pipes of the regenerator section, regenerative action taking place in the walls of the pipes.

The reasons for the choice of a bundle of pipes for the heat exchanger section are as follows:

- (i) The flow friction and heat transfer behaviour of circular pipes has been well documented over the past three decades (Appendix F). True, this documentation is valid for steady flow only, and there is evidence to show that the fluctuating flow conditions encountered in Stirling cycle type machines give rise to higher values of friction factor and Nusselt number for the same conditions of Reynolds number (Ki70). However, it has been found that the flow conditions in the test engines that have been examined are mainly turbulent with laminar flow reversal being propagated through the system over only a small fraction of the cycle. Thus it is believed that steady flow data in this case is realistic.
- (ii) The homogeneous geometry of the pipes allows for extremely simplified programming, and corresponding computer run time reduction. The only difference between the three heat exchanger sections is the wall temperature. The form of regenerator section chosen is considered quite practical, and is reminiscent of the annular gap type regenerators of the Harwell thermomechanical generator (CF74)

or the Beale free piston Stirling engine (Be69). The homogeneous pipe regenerator has a larger wall/gas wetted surface area than the equivalent annular gap and would thus be applicable to higher performance machines, with the advantage of being less complicated to manufacture than systems having standard porous regenerator matrices.

The volume variation of the adiabatic compression and expansion spaces are sinusoidal, in accordance with the Schmidt cycle analysis (Appendix B).

A specific system within the framework of the above test engine is defined by five sets of parameters (the square brackets enclose parameter dimensions in SI units, wherever applicable).

(i) Size and configuration

V_s [m³] - The total stroke volume, being the sum of the swept volumes of the compression and expansion spaces.

V_d - The fractional dead volume, defined as the sum of the void volume in the bundle of pipes, the clearance volume of the compression space and the clearance volume of the expansion space, normalized with respect to the stroke volume V_s .

$V_{c/l}$ - The fractional clearance volume of either the expansion space or the compression space (both are assumed identical) normalized with respect to the total stroke volume V_s .

\tilde{x}_p [m] - The length of heat exchanger bundle of pipes.

n_p - The number of heat exchanger pipes in the bundle.

dia - The ratio of external to internal diameter of the heat exchanger pipes.

Ro - The relative roughness factor on the internal surface of the pipes.

(ii) Working gas properties

γ - The ratio of specific heat capacities c_p/c_v .

R [J/kg.K] - The gas constant.

$\tilde{\mu}_0$ [kg/m.s] - The dynamic viscosity at temperature \tilde{T}_0 .

\tilde{T}_0 [K] - The temperature at which $\tilde{\mu}_0$ is defined.

\tilde{T}_{su} [K] - The Sutherland constant for the gas (refer to Appendix E).

Pr - The Prandtl number of the gas.

(iii) Pipe wall material properties

\tilde{k}_w [J/m.s.K] - The thermal conductivity of the wall material.

\tilde{c}_w [J/kg.K] - The specific heat capacity of the wall material.

$\tilde{\rho}_w$ [kg/m³] - The density of the wall material.

(iv) Operational parameters

T_k [K] - The cold sink temperature.

\tilde{T}_h [K] - The hot source temperature.

\tilde{p}_k [Pa] - The equivalent charge pressure when the whole system is at a constant (cold sink) temperature T_k , is stationary, and at a volume V_s .

\tilde{f} [Hz] - The system cyclic operating frequency.

α [rad] - The angular phase lead of the expansion space volume variation to the compression space volume variation. The volume variations are assumed to be sinusoidal.

(v) Numerical parameters

n_k - The number of cooler cells.

n_r - The number of regenerator cells.

n_h - The number of heater cells.

n_{inc} - The number of integration increments per cycle.

The size of all the cells are assumed to be identical, thus the relative size of the cooler, regenerator and heater sections are determined by the number of cells in each section.

4.3 ORGANIZATION OF THE COMPUTER EXPERIMENTS

In section 4.2 above it is noted that there are twenty four parameters that define a specific system. Some of these parameters are, however, interrelated, ie, the six gas properties and the three heat exchanger pipe wall material properties. Thus given a choice of gas and heat exchanger pipe material there are fifteen main parameters that can be independantly varied. An attempt was made to reduce the number of parameters by introducing dimensionless parameter groups. Unfortunately the physical nature of the system does not allow of this approach, mainly because of the nonlinear nature of the dynamic viscosity of the working gas. A form of normalization of all the parameters has been done with respect to a base parameter set which does allow of a restricted form of dimensionless extension of the results (Refer to Appendix A). From table A.1 it is seen that the normalizing factor for dynamic viscosity is $M\sqrt{R.T\bar{K}}/(Vs)^{2/3}$. Thus machines having the same value of this normalizing factor will behave in a similar manner. Because of the restricted nature of this extension this approach has not been exploited.

No attempt has been made to optimize the system based on a variation of the parameters. Rather a specific system has been chosen and the intimate behaviour of the various variables over a cycle has been examined in order to validate conditions (i) and (ii) of section 4.1. The number of cells in the heat exchanger space has been varied in order to validate condition (iii) of section 4.1. The frequency \tilde{f} , gas properties and diameter ratio d/α has been varied in order to validate condition (iv) of section 4.1.

The specific configuration chosen as well as the range of parameters varied are given as follows (the computer equivalent symbol to the parameter is given in curved brackets - refer to Appendix A):

(i) Specific configuration of test engine

Stroke volume $v_s(\text{EVS}) = 0,000216 \text{ [m}^3\text{]}$
 Fractional dead volume $v_d(\text{VD}) = 0,32$
 Fractional clearance volume $v_{c\ell}(\text{VCL}) = 0,01$
 Length of pipes $\tilde{x}_p(\text{EXP}) = 0,5 \text{ [m]}$
 Pipe diameter ratio $dia(\text{DIA}) = 1,5$
 Number of pipes $n_p(\text{NP}) = 100$
 Relative roughness factor $R_o(\text{RO}) = 0,01$
 Expansion space volume phase advance $\alpha(\text{ALPHA})$
 $= \pi/2 \text{ [rad]}$

(ii) Operating conditions

Charge pressure $\tilde{p}_k(\text{EPK}) = 200\ 000 \text{ [Pa]}$
 Cold sink temperature $T_k(\text{ETK}) = 350 \text{ [K]}$
 Hot source temperature $\tilde{T}_h(\text{ETH}) = 1000 \text{ [K]}$

(iii) Heat exchanger wall properties

The properties chosen are those of stainless steel.
 Specific heat capacity $\tilde{c}_w(\text{ECSW}) = 461,0 \text{ [J/kg.K]}$
 Thermal conductivity $k_w(\text{EKW}) = 25,0 \text{ [W/m.K]}$
 Density $\tilde{\rho}_w(\text{EROW}) = 7690 \text{ [kg/m}^3\text{]}$

(iv) Working fluid properties

Air, helium and hydrogen have been chosen as alternative choices of working fluid, in accordance with

current practice. Their respective properties are given in table 4.1.

Table 4.1 PROPERTIES OF AIR, HELIUM AND HYDROGEN

	Ratio of specific heat capacities γ (GAMMA)	Gas constant [J/kg.K] R (ER)	Prandtl Number Pr (PR)	Sutherland constant [K] \tilde{T}_{su} (ETSU)	Dynamic Viscosity at $T_0 = 350$ K [kg/m.s] μ_0 (EMU)
1004.5 5-22.99 16.5 2.7 Air	1,4	287,0	0,71	112,0	$20,66 \times 10^{-6}$
Helium	1,67	2078,6	0,71	80,0	$22,66 \times 10^{-6}$
Hydrogen	1,4	4157,2	0,71	84,4	$9,97 \times 10^{-6}$

(v) Variation of paramaters

The heat exchanger is divided equally in length between the heater, regenerator, and cooler ($nk = nr = nh$). The total number of cells used in the experiments vary between $nc = 3$ and $nc = 45$.

The frequency of operation f used in the experiments depends on the working fluid, varying between 1 Hz for air and 140 Hz for hydrogen.

The diameter ratio dia affects the heat loss due to axial thermal conductivity along the heat exchanger pipes, and is varied in some experiments between 1,5 and 5,0.

In all the experiments the number of time increments per cycle $ninc$ has been chosen such as to ensure dynamic stability of the numerical solution.

The results of experiments are tabulated in Appendix J.

5. DISCUSSION OF THE MODEL

5.1 INTRODUCTION

In this chapter the cellular model is discussed from the point of view of stability and accuracy. Variants on the model are considered, but it is found that all such variants lead to some form of static instability.

Roache (Ro72) gives an extremely good overview of computational fluid dynamics and includes stability criteria. He finds that even in linear incompressible fluid dynamics problems the various stability criteria are not defined with universal applicability. The source of perturbation originates from machine round-off error, and is propagated advectively through the system. If the numerical scheme is unstable, then two forms of error growth having a spacial period equivalent to the mesh size are seen. The first is an oscillating error growth in which the error at each mesh node changes sign after each time increment. This is the so-called 'dynamic instability' and can generally be completely eliminated by decreasing the solution time increment. The second is a monotonic error growth and is unaffected by the magnitude of the solution time increment. This is the so-called 'static instability', and Roache attributes it to the centered advective differencing technique.

In this study the system partial differential equations have been reduced to ordinary differential equations via a finite element type technique, rather than to difference equations via some specific differencing

technique. Thus the phenomenon of static stability is due to the specific definition of the cellular model. It has been one of the most important criteria in defining the model, resulting in quite considerable 'trial and error' until the current definition of the model was decided upon. Unfortunately, the complexity and nonlinear nature of the system precluded the application of any form of stability criteria and the various models were evaluated on a trial and error basis.

5.2 DEFINITION OF THE MODEL

In Chapter 3 a model of the i 'th elemental cell (figure 3.4) is presented in which a distinction is made between cell parameters and node parameters. The fundamental equations of continuity, momentum, and energy of the working gas have, however, been derived for parameters within the control volume, or cell. (Refer to Appendix D). Why then has it been found necessary to distinguish between cell and node variables? Why for example is the mass flux density g defined exclusively as a node parameter, whereas pressure is defined exclusively as a cell parameter?

Consider the momentum equation (D.9) as applied to a constant volume cell:

$$\frac{\partial g}{\partial t} + \frac{\partial}{\partial x}(g^2 v) + \frac{\partial p}{\partial x} + \frac{F}{V} = 0 \quad (5.1)$$

One method of modelling equation (5.1) would be to define node and cell values of each parameter as in figure (5.1).

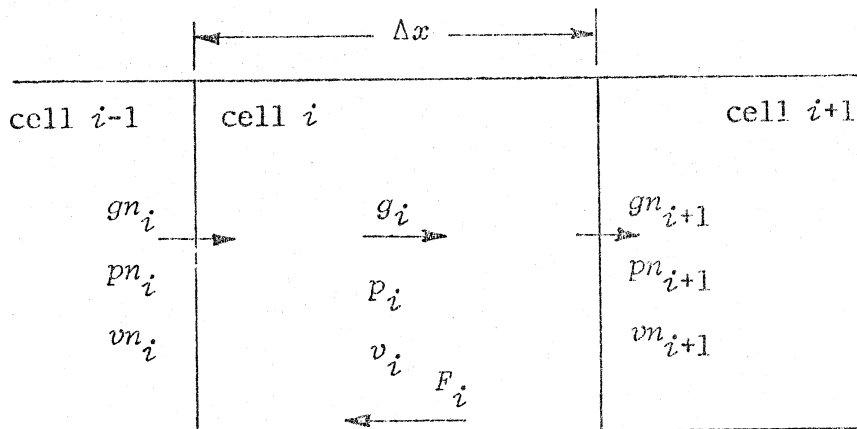


Figure 5.1 THE i 'TH CELL

The node parameters are used to discretize the spacial partial derivatives and are defined as the arithmetic mean values of the adjacent cell parameters. Thus if only the term $\partial p/\partial x$ in equation (5.1) is considered, one obtains:

$$pn_i = (p_{i-1} + p_i)/2 \quad (5.2)$$

$$pn_{i+1} = (p_i + p_{i+1})/2 \quad (5.3)$$

$$(\partial p/\partial x)_i = (pn_{i+1} - pn_i)/\Delta x \quad (5.4)$$

The purpose of the momentum equation is to sense a pressure difference between adjacent cells (or nodes), compare it to the frictional drag force F_i and momentum flux $\partial(g^2 v)/\partial x$, and allow any unbalance of forces to accelerate working gas, finally causing a redistribution of the working gas.

A possible hypothetical cellular pressure distribution is considered in figure 5.2.

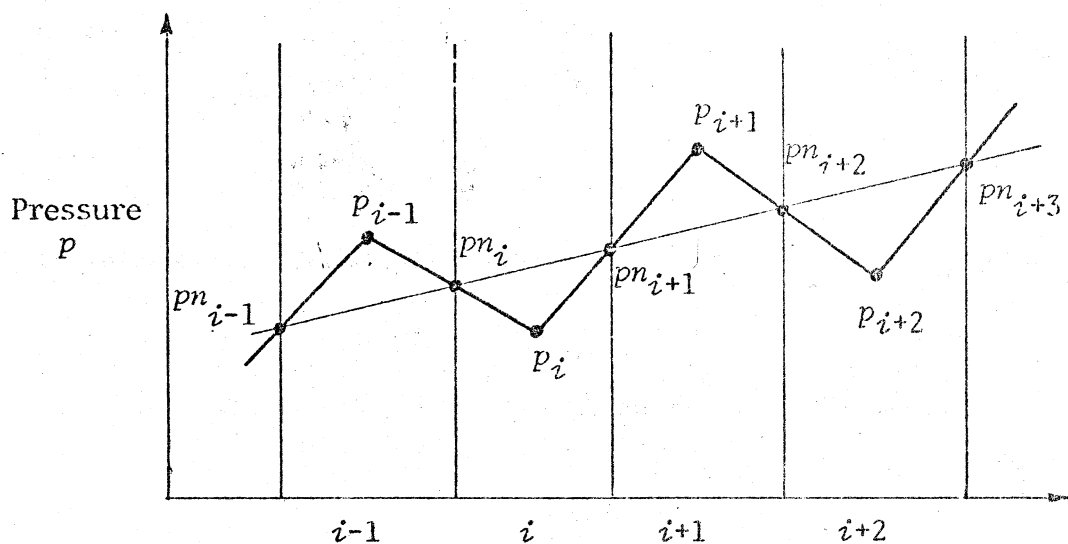


Figure 5.2 A HYPOTHETICAL PRESSURE DISTRIBUTION

It is seen that equations (5.2) and (5.3) are satisfied, in that the node pressures are in fact the arithmetic means of the adjacent cell pressures. From equation (5.4) it is noted that only the node pressure distribution determines the change of momentum of the working gas. Figure 5.2 shows a linear monotonic increasing node pressure distribution - typical of flow from right to left in figure 5.2, even though the cell pressure has an oscillatory spacewise distribution. Furthermore the model does not have any compensating means by which it can affect the cell pressure distribution, and the system can achieve steady state, independent of the integration time interval, with an oscillatory spacewise pressure distribution.

This is the phenomenon that has been referred to as 'static instability'. It is caused entirely by the use of equations (5.2) and (5.3) in defining a node pressure as the arithmetic mean of the adjacent cell pressures.

(5.2), (5.3) + (5.4):

$$(\partial p / \partial x)_i = (P_{i+1} - P_{i-1}) / 2\Delta x \quad (5.5)$$

From equation (5.5) it is seen that the above model is in fact equivalent to the central difference technique, to which Roach attributes the cause of static instability.

Another method of modelling equation (5.1) which is equivalent to a backward difference technique is shown in figure 5.3.

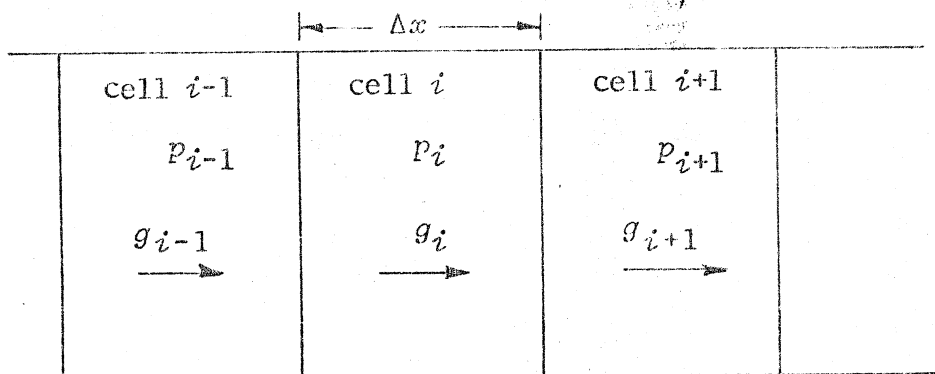


Figure 5.3 THE i 'TH CELL

In figure 5.3 no node parameters have been defined and the term $\partial p / \partial x$ in equation (5.1) is defined by

the backward difference technique as follows:

$$(\partial p / \partial x)_i \leftarrow (p_i - p_{i-1}) / \Delta x \quad (5.6)$$

This method is stable as long as the direction of flow is constant. However, the Stirling cycle engine is a reversing flow type system, and when g_i becomes negative then the technique reverts to a forward differencing type technique which is unstable. In order to maintain stability in the reversing flow situation, a so-called 'upstream difference' technique can be used, in which the parameters chosen for differencing are conditional on the direction of flow as follows:

$$g_i \geq 0 \Rightarrow (\partial p / \partial x)_i \leftarrow (p_i - p_{i-1}) / \Delta x \quad (5.7)$$

$$g_i < 0 \Rightarrow (\partial p / \partial x)_i \leftarrow (p_{i+1} - p_i) / \Delta x$$

Thus in equation (5.7) only upstream and local values of pressure are used, and the system should be stable. Consider, however, the situation when applying this model to the Stirling cycle machine in figure 5.4.

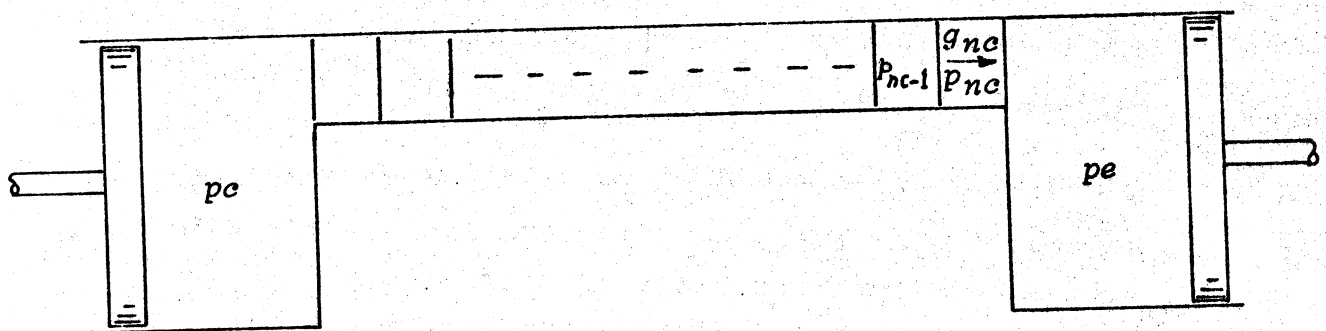


Figure 5.4 THE STIRLING CYCLE ENGINE CELLULAR MODEL

In figure 5.4, cell nc is considered. The flow in cell nc is positive and from equation (5.7) it is seen that $(\partial p/\partial x)_{nc}$ is given in terms of p_{nc} and p_{nc-1} . However, at some stage during the cycle, the volume variations are such that both the compression space pressure p_c and the expansion space pressure p_e are increasing. As long as the system senses an increase in p_e it will continue to show a negative pressure gradient in cell nc given by $p_{nc} - p_{nc-1}$ even if p_e becomes much greater than p_{nc} ! Thus the model breaks down, not because of stability problems, but because it is unrealistic.

A plethora of variants of models of the above forms were attempted during this study all of them displaying their own specific pitfalls.

The problem was solved by defining the model shown in Chapter 3, in which the mass flux density, and hence the momentum equation is defined to apply exclusively at the nodes (interfaces between adjacent cells) of the system model. Thus discretizing the term $\partial p/\partial x$ in equation (5.1) at the i 'th node, one obtains:

$$(\partial p/\partial x)_i \leftarrow (p_i - p_{i-1})/\Delta x \quad (5.8)$$

where the pressures p_i , p_{i-1} are exclusively cell pressures of the cells adjacent to the i 'th node.

Since only cell pressures are defined as applying to both the momentum equation and the working gas energy equation, the situation cannot exist as in figure 5.2 where two different pressure distributions exist simultaneously.

From equation (5.1) it is noted that the derivative $\partial g/\partial x$ is required to be evaluated as well. Since only nodal values of g have been defined, the upstream difference technique is used in order to evaluate $\partial g/\partial x$, always in terms of upstream and local values of g .

The node temperatures Tn_i are now considered. The node temperatures define the enthalpy transport through adjacent cells, being the predominant energy carrier through the system. In view of the various criticisms of the use of the conditional temperature definition of node temperature referred to in Chapter 3, a variant on the model was analysed in which a continuous, piecewise linear, working gas temperature profile was defined through the system. Thus the node temperatures were defined as the arithmetic means of their respective adjacent cell temperatures.

$$Tn_i = (T_{i-1} + T_i)/2 \quad (5.9)$$

Results of a computer experiment using air as the working gas at a cyclic operating frequency of 20 Hz are shown in figure 5.5. The temperature profile of the working gas through the system is shown at every ten degrees of crank angle through a complete cycle, after cyclic steady state has been attained. For clarity of presentation, the temperature ordinate has been offset by a fixed amount for each successive profile, so as not to allow overlap of the profiles. Superimposed on the temperature profiles are arrows indicating the direction of flow, with short vertical lines indicating the flow reversal point. The solid lines indicate turbulent flow and the dotted lines indicate laminar flow.

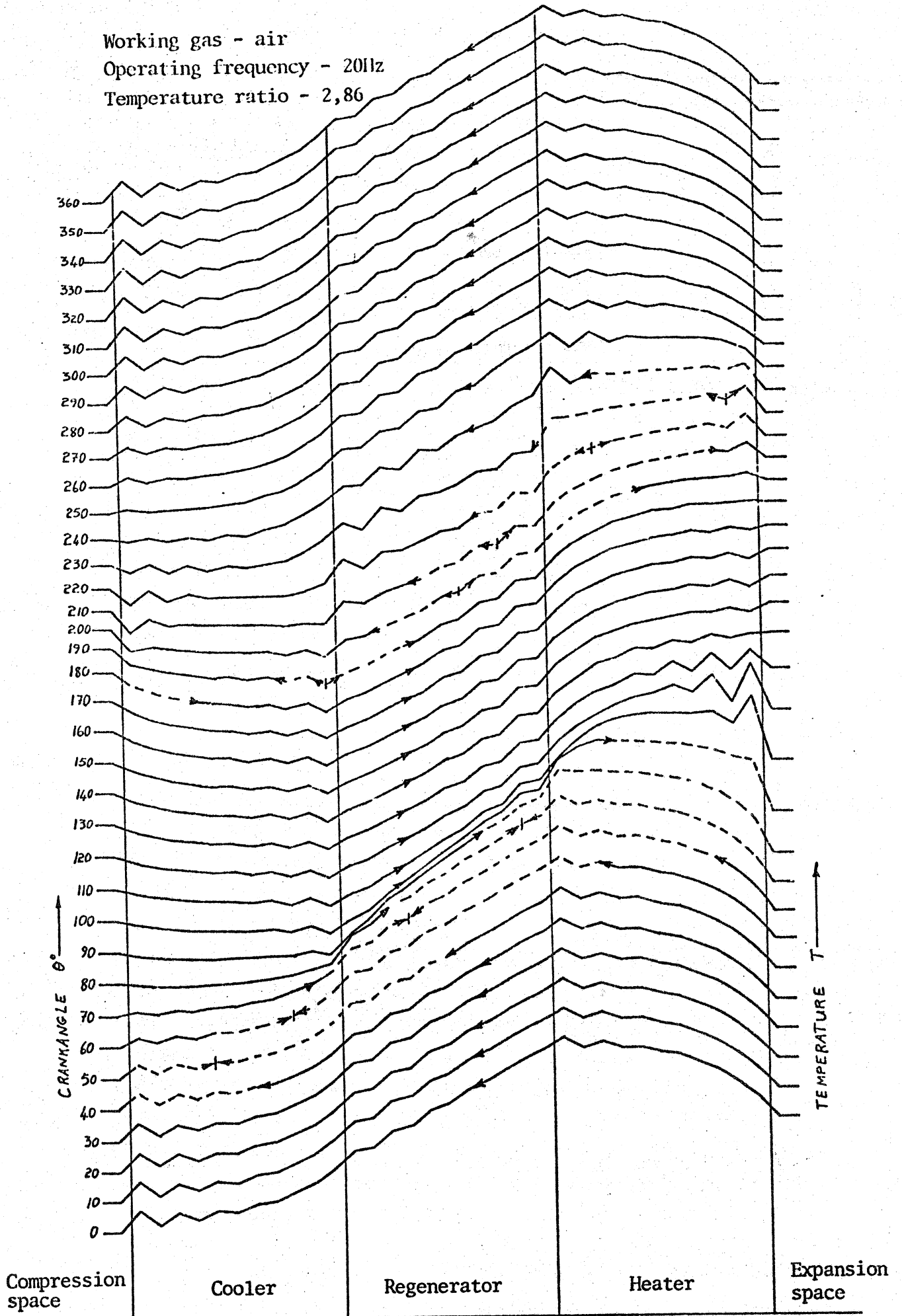


Figure 5.5

TEMPERATURE PROFILES (MEAN NODE TEMPERATURES)

It is seen from figure 5.5 that the temperature profiles tend to be oscillatory, with a spacewise period of oscillation equal to the cell length -- another typical example of static instability. Significantly it is seen that this instability is of an advective form in that it builds up in the direction of flow. At each change of boundary condition (eg, at the exit from the heater and entrance to the regenerator, the direction of heat flow is reversed) then the oscillation is completely damped out and begins to build up again advectively. As with the pressure type of static instability, the temperature profiles are unaffected by the integration time interval. In the experiment shown in figure 5.5, reducing the integration time interval by a factor of five produced no observable change.

Without examining the temperature profiles, this static instability can go completely unnoticed, since all the gross parameters -- being work done per cycle, heat supplied and rejected per cycle, and net regenerator heat flow -- are perfectly feasible, but nevertheless wrong.

The various forms of static instability can exist independantly. In the experiment shown in figure 5.5 the equivalent pressure profiles gave no indication of static instability, since the momentum equation was evaluated at the nodes. In an experiment in which the momentum equation was evaluated at the cells, as in figure 5.1, and the node temperatures were defined by the conditional temperature method, then static instability was indicated in the pressure profiles,

Working gas - air
 Operating frequency - 20Hz
 Temperature ratio - 2,86

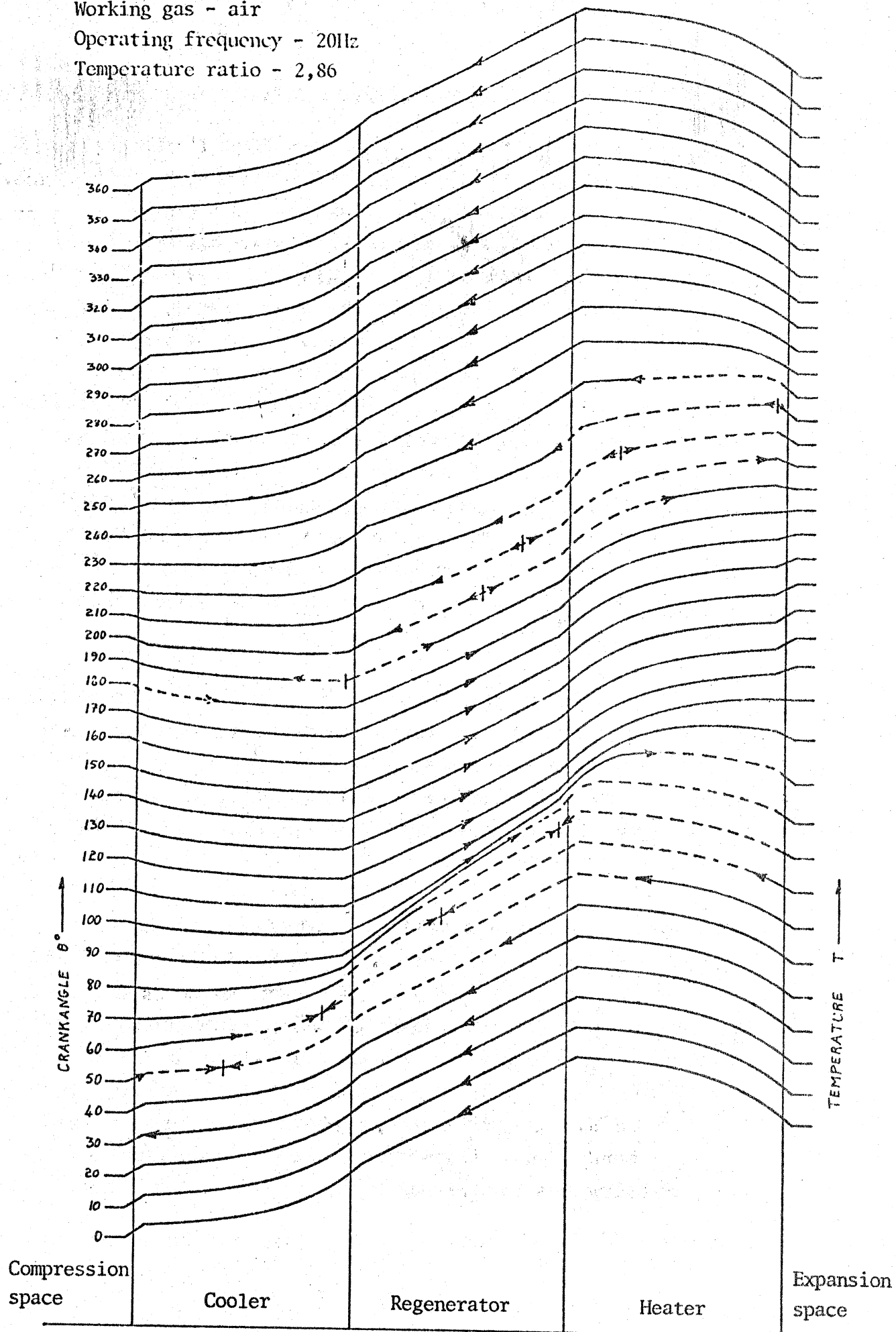


Figure 5.6 TEMPERATURE PROFILES (CONDITIONAL NODE TEMPERATURES)

but not in the temperature profiles.

In figure 5.6 the temperature profiles are shown resulting from a computer experiment on the identical example as in figure 5.5, however using the node temperatures defined as conditional temperatures, as in equation (3.4). It is seen in figure 5.6 that the temperature profiles are devoid of all oscillatory tendencies, and that the shape of the profiles are as expected.

The cellular model implying mixed mean properties within each cell has been criticized on a fundamental basis by Organ of London University, and Van Eckelen of the Philips Co, Holland, during separate private communications. Their criticism can be summarized with reference to figure 5.7 as follows.

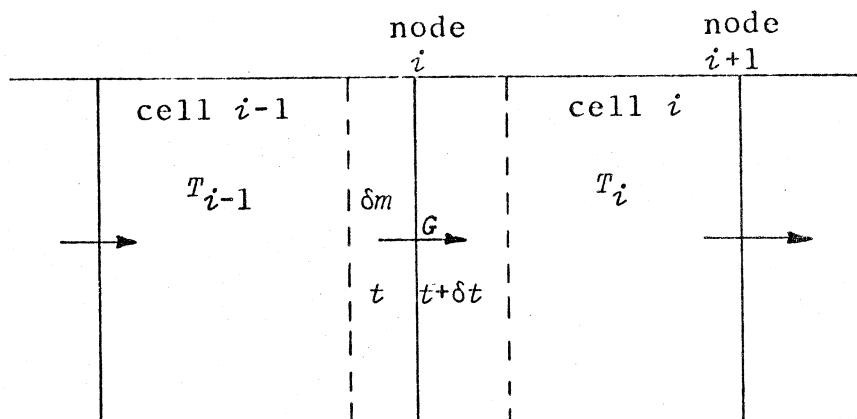


Figure 5.7 THE i 'TH NODE

The adjacent cells ($i-1$) and i are considered. Because of the mass flux G an elemental mass δm is transported

across node i during the time interval δt , along with its associated temperature T_{i-1} . Since perfect mixing has been assumed it is found that this enthalpy input has affected the internal energy of the entire cell i in a uniform manner, by changing the cell temperature T_i . Thus it is found that close to the next node ($i+1$) the effect of this enthalpy input has been felt *before* the element of gas δm which is transporting that enthalpy has physically been able to cross the finite cell length. Information on the energy transport has been anticipated at the far end of the cell before it has had the time to arrive there.

This is a gross approximation of reality which cannot be rationalized by the statement that in the limiting case of a vanishing cell size and time increment the approximation falls away, since that limit is never attained. However, whenever a continuous system is discretized in order to perform numerical integration, then this form of gross approximation is made. The only rationalization of this method is that as the mesh size is decreased, a limiting performance index is usually asymptoted on well behaved phenomena, which experience has shown tends to agree with the theoretical continuum. In the case of the model defined in Chapter 3, the number of cells was varied from $n_c = 3$ (one cell each for the cooler, regenerator and heater respectively) to $n_c = 45$. The performance index chosen was thermal efficiency, being a gross parameter which includes all of the work done (pressure, flow friction) and heat transfer (temperature, enthalpy) effects. The

results using air as the working gas are shown in figure 5.8, for varying cyclic operating frequencies.

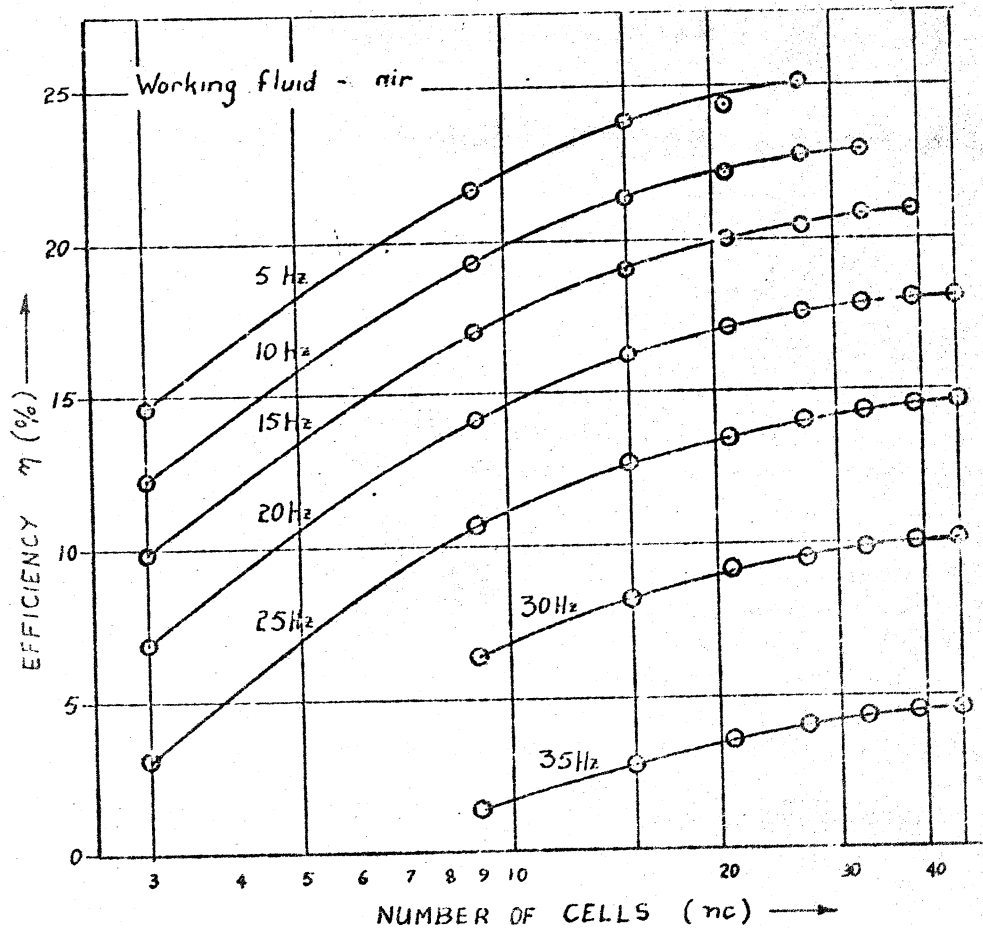


Figure 5.8 EFFICIENCY VERSUS NUMBER OF CELLS

From figure 5.8 it is seen that the model seems extremely well behaved, all the thermal efficiency curves monotonically tending to an asymptote as the number of cells is increased. Computer time limitations did not allow more than 45 cells to be tested, however it is seen that in all cases the difference in thermal efficiency for $nc = 39$ and $nc = 45$ is only 0,1%.

5.3 ACCURACY OF THE MODEL

5.3.1 General

Both the space (cellular) and time discretization impose inaccuracies of different types on the model which can be examined separately. Because of the quite considerable computer time required in analysing the complete model it is obviously required to reduce both the number of cells and the number of time intervals per cycle to a minimum.

5.3.2 Time discretization

The Runge-Kutta integrating routine is the most widely used mainly because of its ease of programming and good stability properties. Opponents of the technique emphasize its inability to indicate the extent of the errors arising from discretization and thus that it does not allow the adaptive time interval variation that is available in the predictor - corrector type techniques. However, there are two modifying factors which lead to the choice of the Runge-Kutta routine for the Stirling cycle model.

- (i) There is a maximum time increment which cannot be exceeded.

This limit is imposed by the use of the momentum equation in its complete form, allowing acceleration of the working gas. Acceleration introduces a second order type differential equation which is oscillatory in nature. If a time increment is chosen which is larger than this maximum, then dynamic instability results and the solution breaks down. It was found that not much could be gained from an adaptive time interval variation in reducing computer

time because of this stability imposed limit.

- (ii) The cyclic nature of the system allows of a posteriori error evaluation.

This evaluation is done via the first law of thermodynamics which states that if the system has attained cyclic steady state then the net heat supplied externally per cycle must be equal to the net work done per cycle. Cyclic steady state is determined by examining the root mean squared net heat transferred in the regenerator at the end of the cycle, which must be zero. Thus the 'energy error factor', ζ , is defined as follows:

$$\zeta \triangleq \frac{\left(\text{Net heat supplied externally per cycle} \right) - \left(\text{Net work done per cycle} \right)}{\left(\text{Heat supplied externally at the heater per cycle} \right)}$$

$$\zeta = (Q_h + Q_r + Q_k - W) / Q_h$$

(5.10)

where all the energy quantities are taken at the end of the cycle, after cyclic steady state has been attained.

The use of the energy error factor ζ is extremely representative of all the accumulated errors in the system, since both heat and work terms are involved.

Thus in a typical computer experiment, the procedure adopted is to choose the integration time interval empirically to ensure dynamic stability, then, on attainment of cyclic steady state the resultant energy error factor is evaluated.

In figure 5.9 a plot of the energy error factor ζ versus the cyclic operating frequency \tilde{f} is shown for all experiments using air as the working gas. It is seen that the curve is exponential in form. From $\tilde{f} = 1$ Hz to $\tilde{f} = 20$ Hz (peak power), the energy error factor ζ is less than 1,8%. Thereafter ζ rises exponentially until at $\tilde{f} = 35$ Hz (cut off power), ζ becomes 4,5%. It was found that the energy error factor ζ is almost independent of the number of cells used, and does not seem to be affected by the number of time increments chosen per cycle. A possible reason for this behaviour of the energy error factor ζ is as follows. The criterion for attaining cyclic steady state is when the root mean square net regenerator heat transferred is less than a certain value, nominally chosen to be 0,01 normalized energy units. However, at operating frequencies above that of peak power, less heat is transferred between the working gas and the regenerator matrix than at operating frequencies below that of peak power. Thus using the same criterion of net root mean square regenerator heat would result in differing degrees of attainment of cyclic steady state, as a function of the operating frequency. The energy error factor ζ can be considered as a measure of the system net stored energy per cycle, and should asymptotically tend to zero as the system reaches cyclic steady state.

The fact that varying the number of time increments per cycle does not seem to affect the value of the energy error factor ζ indicates that the stability imposed maximum time interval limit satisfies the accuracy requirements of the solution as well.

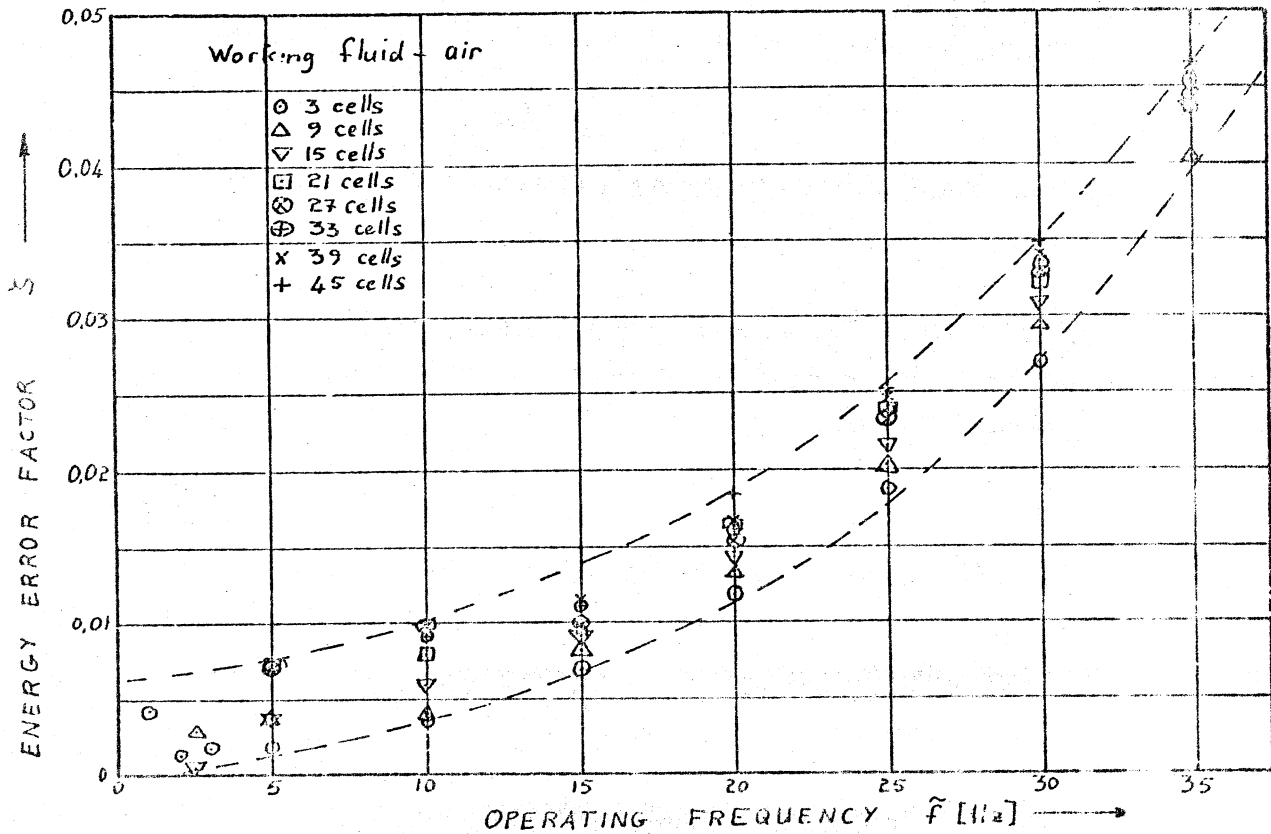


Figure 5.9 ENERGY ERROR FACTOR VERSUS OPERATING FREQUENCY

5.3.3 Space discretization

One of the most important parameters contributing to the amount of computer time used is the number of cells in the system model. Each additional regenerator cell adds five differential equations to the system, and each additional heater or cooler cell adds three differential equations to the system. However, not only are there additional differential equations, but adding more cells requires an increase in the number of time

intervals per cycle for stability. Thus, for example, with air as the working gas, at peak power ($\tilde{f} \approx 20$ Hz) for $nc = 3$, 360 time increments were required per cycle, and for $nc = 45$, 1980 time increments were required per cycle to ensure stability. Thus it is important to know what the effect of the number of cells is on the system.

Figure 5.10 shows a plot of thermal efficiency and power output versus operating frequency for varying number of cells between $nc = 3$ to $nc = 45$, using air as the working gas.

It is seen that at $nc = 33$ the system has essentially converged. The power error at $\tilde{f} = 20$ Hz between $nc = 33$ and $nc = 45$ is 0,47%. It is also noted that for all values of nc , the efficiency curves are essentially parallel. This surprising result can be used in order to predict the performance curves at (say) $nc = 33$ with high accuracy, even with only one experiment at $nc = 33$.

A set of experiments covering the frequency range through to cutoff power is plotted using (say) $nc = 15$ (or even $nc = 3$). A single experimental point using $nc = 33$ is then plotted. The efficiency curve is drawn through this point parallel to the efficiency curve for $nc = 15$. Enough information is now available to plot the entire power versus frequency curve for $nc = 33$.

On figure 5.10 the performance curves for $nc = 3$ have been extended down to $\tilde{f} = 1$ Hz, in order to examine the effect of varying heat leakage due to conduction

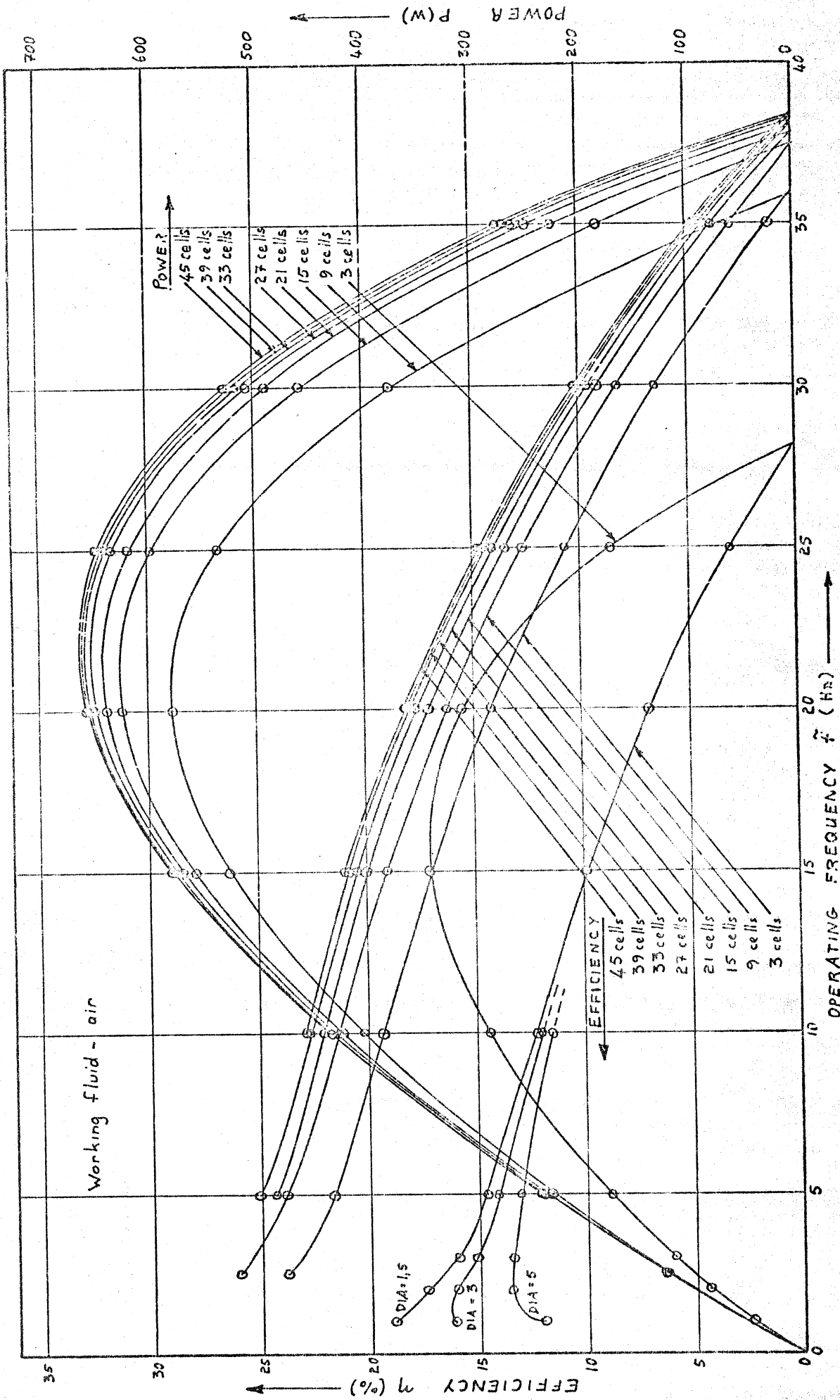


Figure 5.10 THERMAL EFFICIENCY AND POWER OUTPUT VERSUS OPERATING FREQUENCY

directly through the walls of the heat exchanger pipes. External to internal pipe diameter ratios of 1,5, 3,0 and 5,0 were chosen and the results are as expected. Because of the well behaved nature of the performance curves, these three efficiency curves could be directly translated onto the $nc = 33$ efficiency curve -- resulting in a considerable saving of computer time.

Figure 5.11 shows a plot of thermal efficiency and power output versus operating frequency for $nc = 15$ and $nc = 33$, using air, helium and hydrogen as the working gases. It is found that for each of the three working gases the efficiency curve for $nc = 15$ is parallel to that for $nc = 33$. Another interesting observation is that the difference of efficiency between the curves for $nc = 15$ and $nc = 33$ is approximately constant at 1.8%, independent of the working gas used.

It is thus found that using the model defined in Chapter 3, it is feasible with as few as 3 cells to do a large number of computer experiments required in a parameter optimisation study. Thereafter, on obtaining a single result using (say) thirty three cells it is possible to predict with high accuracy the entire performance characteristics of the prototype machine.

5.4 SUMMARY AND CONCLUSIONS

In this chapter the concepts of dynamic and static instability were introduced. Various cellular models were evaluated and only the present model defined in Chapter 3 was found to be free of all forms of static

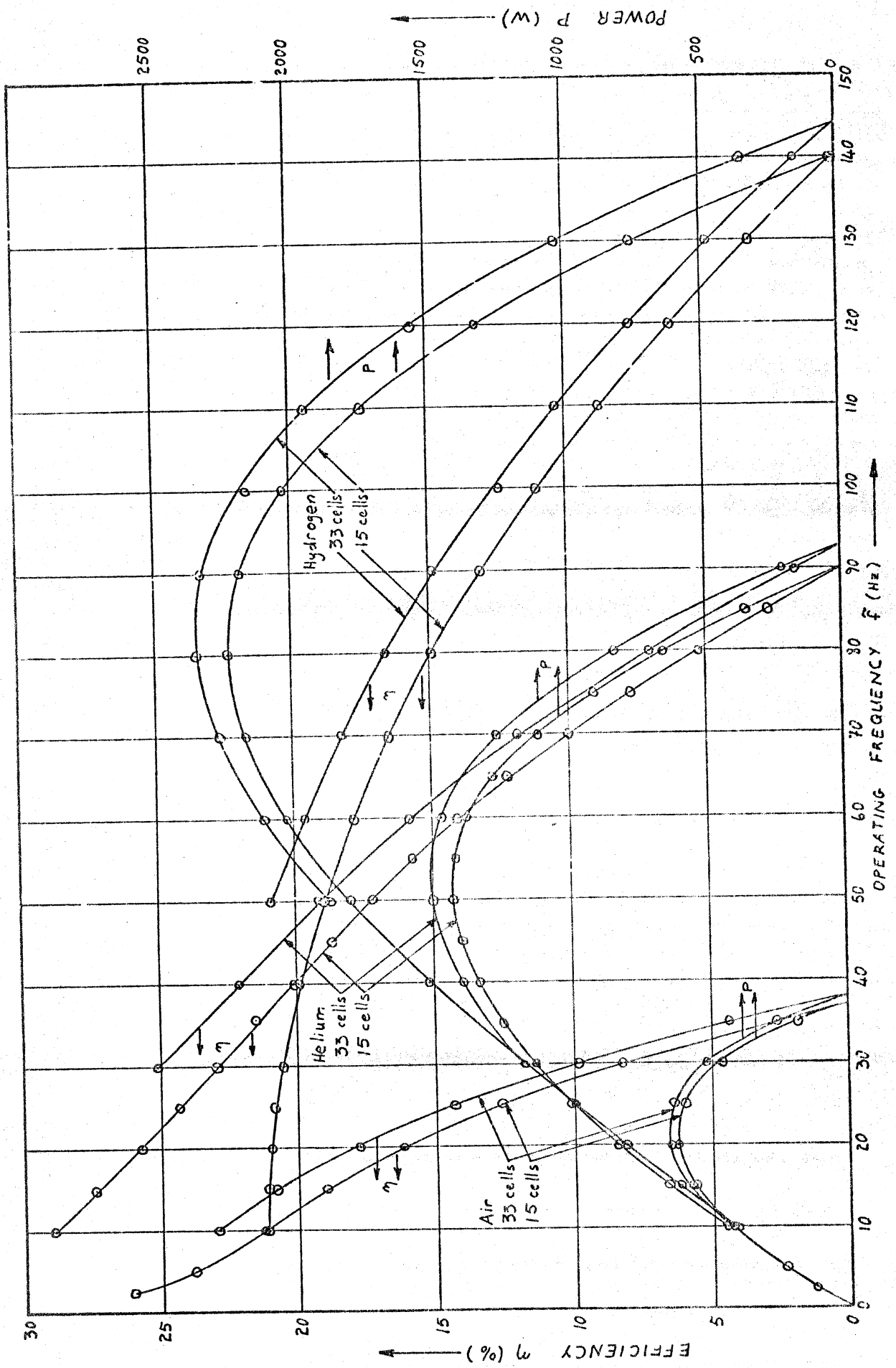


Figure 5.11 THERMAL EFFICIENCY AND POWER OUTPUT VERSUS OPERATING FREQUENCY

instability. This required that all the working gas variables be considered as constant throughout each cell and discontinuous at the nodes excepting for the mass flux density g , which is defined and continuous across the nodes and undefined within the cells. Node temperatures and specific volumes are defined as conditional variables, taking on their upstream adjacent cell values.

Dynamic stability was eliminated semi-empirically by simply reducing the integration time interval.

The accuracy of the model was considered with respect to time and space discretization. It was found that the dynamic stability imposed time interval limit is sufficiently small to ensure accuracy with respect to time discretization. The energy error factor ζ was defined, and it was seen that the method of convergence to cyclic steady state based upon the net residual regenerator cell heat transfer gave finite values of ζ which were functions of the cyclic operating frequency.

Spacewise discretization effects were such that as the number of cells was increased, the performance characteristics tended to asymptote to a limit. It was found that about 33 cells gave results sufficiently close to that asymptote, but required excessive computer time for solution. Fortunately it was noted that all the efficiency versus operating frequency profiles were parallel, independent of the number of cells used, thus allowing an accurate extension of the results using as few as 3 cells to those using (say) 33 cells, with only one result at 33 cells.

6. DISCUSSION OF THE RESULTS

6.1 INTRODUCTION

In this chapter the results obtained using the application example test engine defined in Chapter 4 are discussed, from the viewpoint of Stirling cycle engine performance, in the light of openly available current knowledge in the field. Two types of results are presented; gross performance characteristics which are available a posteriori and include net work and heat flows per cycle, and the intimate incremental behaviour of the various variables throughout the cycle. Typical detailed printouts are presented in Appendix J using air as the working fluid at an operating frequency of 20 Hz (peak power).

6.2 PERFORMANCE CHARACTERISTICS

Figure 6.1 shows a plot of thermal efficiency versus power for the test engine using three different working gases; air, helium and hydrogen. These curves have been based on the experimental results for $nc = 15$ and $nc = 33$ given in figure 5.11, and represent actual and predicted performance for $nc = 33$. On each curve various discrete values of operating frequency \tilde{f} [Hz] are indicated. This method of presenting the performance characteristics was introduced by researchers at the Philips Co, Holland, as exemplified in the much quoted performance curves shown in figure 6.2 (Me70). Comparing figures 6.1 and 6.2 it is seen that the curves are similar in that for all three working gases peak power is attained at approximately the same efficiency, and the curves

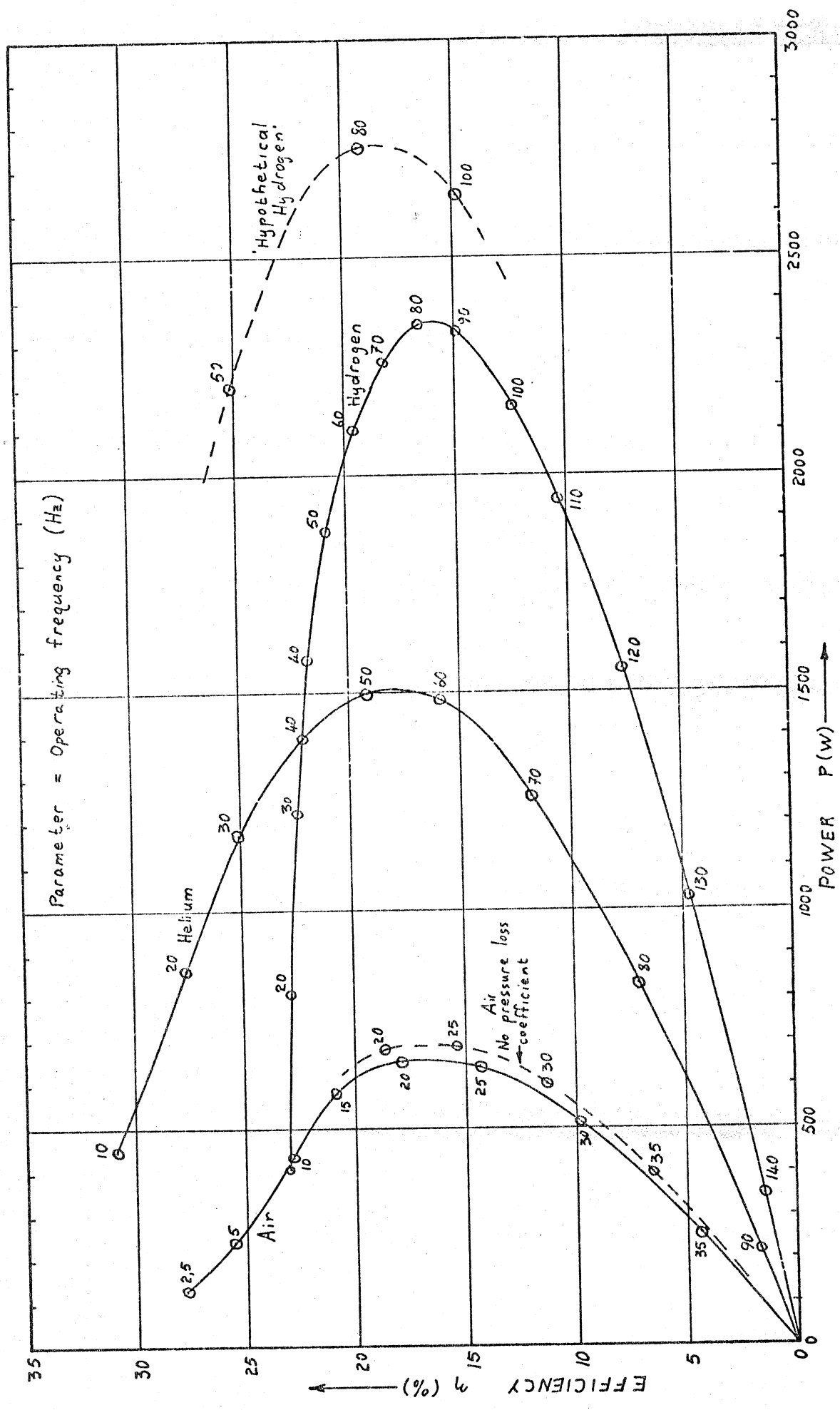


Figure 6.1 THERMAL EFFICIENCY VERSUS POWER OUTPUT

for air and helium are of similar scaled form.

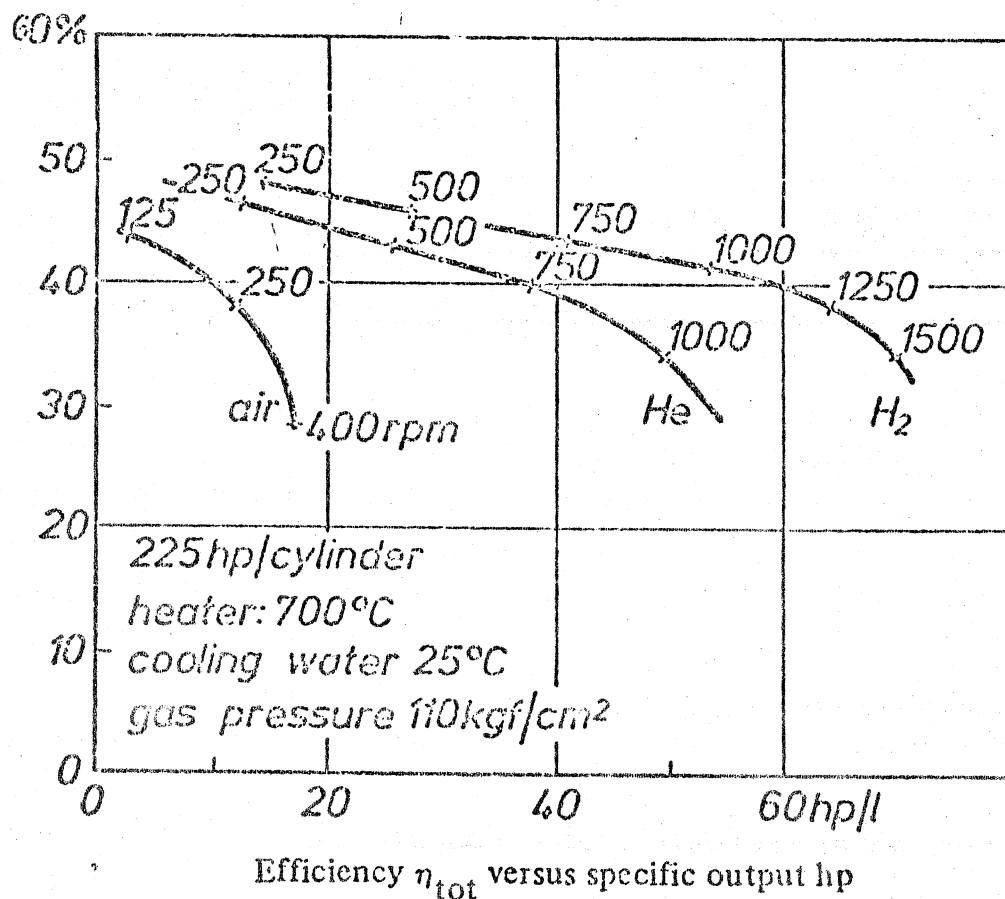


Figure 6.2 COMPARATIVE PERFORMANCE USING DIFFERENT WORKING FLUIDS (After Meijer Me70)

However, at operating frequencies below that of peak power the relative performance using hydrogen is completely different in the two figures. Very little information is available from the Philips Co, Holland, who maintain much of their research as closely guarded secrets. It has been stated that the performance characteristics (figure 6.2) are the results of

advanced simulation calculations (Wa73, Mi76), however the basic assumptions and model upon which these calculations are based have never been disclosed.

In attempting to explain both the nature of the curves, and the discrepancy between their form in figures 6.1 and 6.2, it is postulated here that two of the most important characteristics defining a working gas in the context of its suitability for use in Stirling cycle machines are the gas constant R and the dynamic viscosity $\tilde{\mu}$.

The speed of propagation of pressure information in the working gas is proportional to the square root of the gas constant R , and this defines the operating frequency at which a specific performance level can be attained. It is a well known experimentally observed fact that the peaks of the pressure waveforms in the expansion and compression spaces of a Stirling cycle machine are separated by a phase difference δ with respect to the cycle (Wa73). The value of δ depends upon the operating frequency.

Berchowitz et al (BR77) calculated the phase angle δ on a simplified Schmidt cycle, with no friction, based purely on the velocity of propagation of pressure information between the compression and expansion space along the length of the heat exchanger pipes. Using the application example test engine specifications of Chapter 4 with air as the working gas at an operating frequency of 20 Hz, they obtained a value of $\delta = 7,1^\circ$. The actual value of δ obtained from the computer simu-

lation (refer to Appendix J) is $\delta = 6^0$. The closeness of these results suggests that the major contribution to the phase angle δ is the finite time required for pressure information to propagate between the two working spaces.

If this is in fact correct, then if in a hypothetical situation, the only parameter differentiating between the various working gases was the gas constant R , and if there were no heat leakage paths due to conduction, then it should be possible to scale the performance curves for different working gases at (say) peak power in the ratio of the square roots of the respective gas constants. The ratio of the square roots of the gas constants for air, helium and hydrogen are respectively 1:2,69:3,81. From figure 6.1, it is found that the ratios of the operating frequencies at peak power (which all occur at approximately the same thermal efficiency) are 20:55:80, ie, 1:2,75:4,0. Thus even though all the actual gas properties have been used in each case, and heat leakage paths exist in the test engine, the results are remarkably close.

The same comparison could not be made on the curves of figure 6.2 because of lack of background information. However it is noted that the forms of the curves are similar, as the above simplified theory predicts.

Why then, the discrepancy in the form of the hydrogen curve of figure 6.1? It is postulated here that this is due to the effect of the second important working gas characteristic, ie, the dynamic viscosity $\tilde{\mu}$. The reason for its importance is that both the friction factor and the heat transfer coefficient are functions of $\tilde{\mu}$. From table E.1 in Appendix E it is seen that

at a temperature of 273 K, the values of dynamic viscosity $\tilde{\mu}$ for air and helium are respectively $17,08 \times 10^{-6}$ [kg/m.s] and $18,85 \times 10^{-6}$ [kg/m.s], ie, almost identical. Also, notwithstanding the difference in Sutherland constant \tilde{T}_{su} , the normalized variation of $\tilde{\mu}$ with temperature is approximately the same for both gases. The equivalent value of dynamic viscosity $\tilde{\mu}$ for hydrogen is, however, $8,35 \times 10^{-6}$ [kg/m.s]. In order to validate the above hypothesis three experiments were run using a 'hypothetical hydrogen' working gas, having the gas constant R of hydrogen, and the dynamic viscosity $\tilde{\mu}$ of helium. The results of these three experiments are plotted on figure 6.1. It is observed that the 'hypothetical hydrogen' points do in fact lie on a scaled up curve, similar in form to both the helium and air curves, and similar in form to the curves of figure 6.2.

In another graph from the Philips Co, Holland, (Me70) curves of efficiency and power output versus operating frequency have been plotted for a heat pipe operated swashplate type Stirling cycle engine (figure 6.3).

In comparing figures 6.3 and 5.11, it is seen that in both figures the efficiency curve for hydrogen crosses the efficiency curve for helium. The conditions of operation are similar in that the walls of the test engine heater are at a constant temperature -- typical of heat pipe operation.

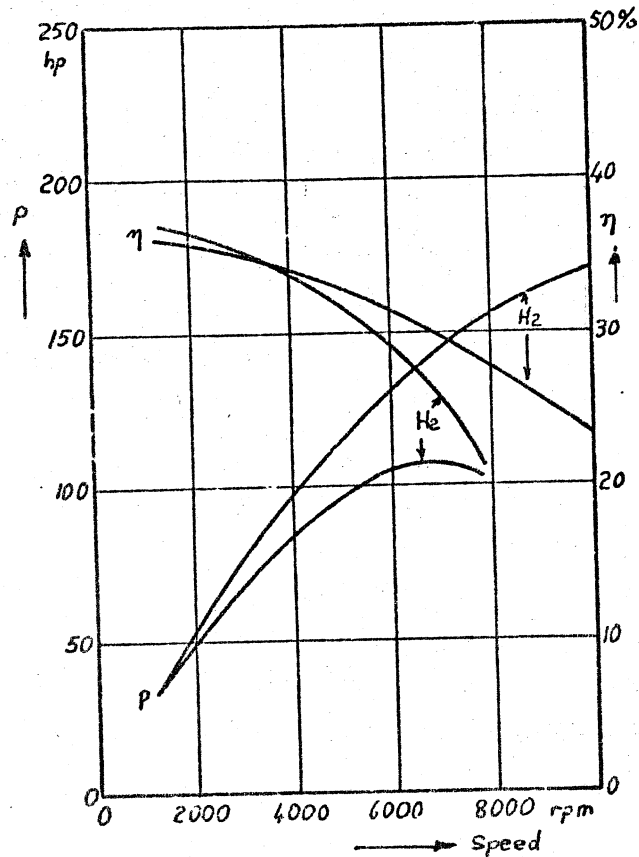


Figure 6.3 EFFICIENCY AND POWER VS SPEED (After Meijer Me70)

All the performance curves from the Philips Co, Holland (figures 6.2 and 6.3) show a higher thermal efficiency than has been obtained on the test engine (figure 6.1). However, no attempt has been made in this study to optimise on thermal efficiency, the test engine being chosen mainly on the basis of computational ease and simplicity.

In the test engine defined in Chapter 4, abrupt expansion and contraction pressure drop losses are assumed to occur at the working space/heat exchanger interfaces

(Refer to Appendix H). Experiments were done using air as the working gas in which the heat exchanger pipes were well rounded -- exhibiting no entrance or exit pressure drop losses. The results are plotted on figure 6.1, and it is seen that both the power output and efficiency are increased. Significantly, peak power occurs at the same thermal efficiency as in the case of abrupt expansion and contraction losses, however at a higher operating frequency.

6.3 INCREMENTAL CHARACTERISTICS

Each computer experimental run at cyclic steady state results in a wealth of information, and it is extremely difficult to decide in which way to present this information. Quantitative information is available from the computer output (Refer to Appendix J), however a qualitative overview as to the behaviour of the various parameters can only be obtained graphically. Figure 6.4 is a three-dimensional plot of the temperature profiles shown in figure 5.6. Superimposed on the temperature profiles are arrows showing the direction of fluid flow, the solid lines indicating turbulent flow and the dotted lines indicating laminar flow. It is not possible on the three-dimensional plot to show the wall temperature as well, since that would make the plot totally unreadable. However, several of the profiles, including the wall temperature, are shown singly in figures 6.5 through to 6.8.

In figure 6.4 it is seen that the working gas spends a larger part of the cycle flowing from the expansion space to the compression space than it does in the reverse direction. A little reflection shows why this must be so, since during the time when flow is from the

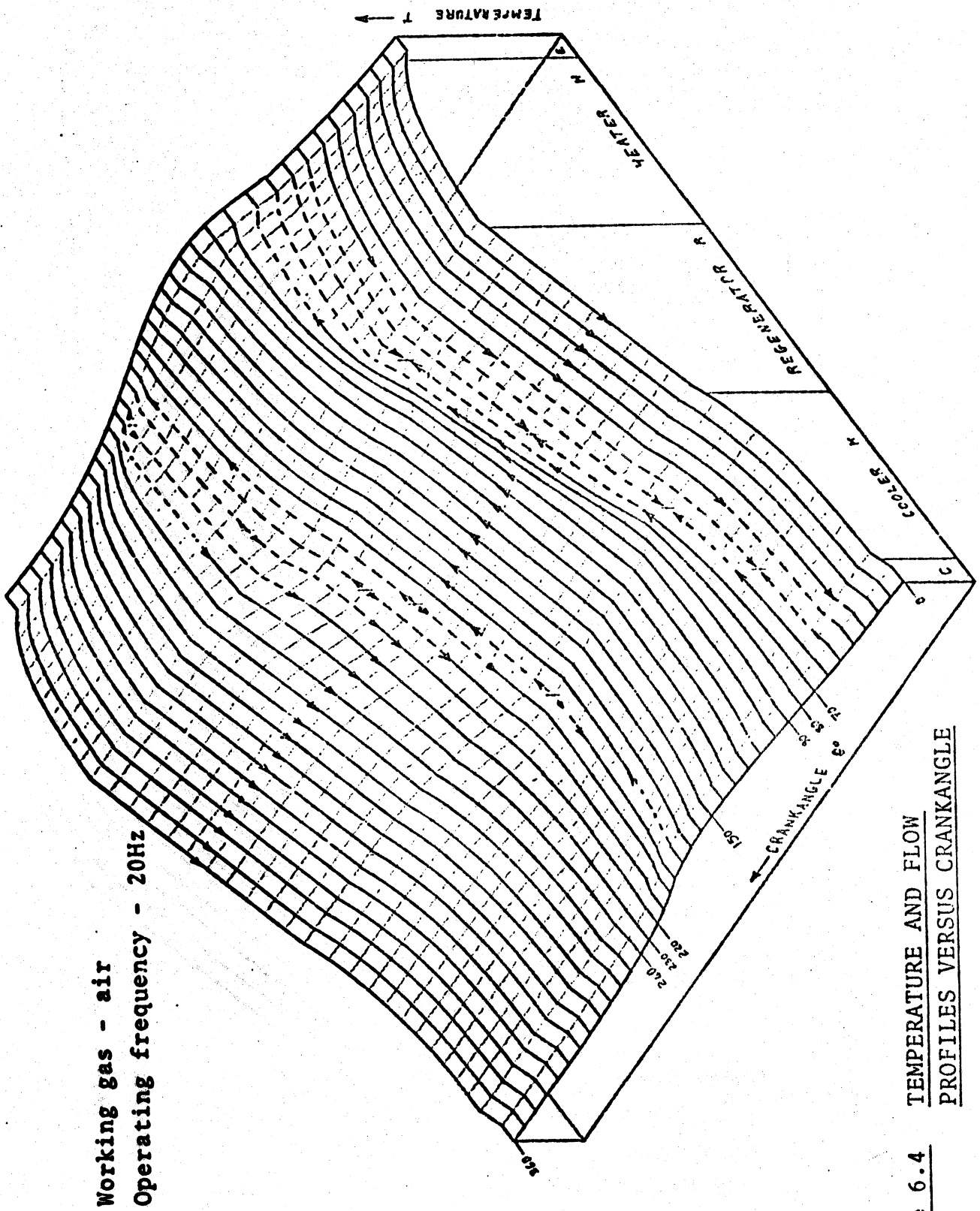


Figure 6.4 TEMPERATURE AND FLOW PROFILES VERSUS CRANK ANGLE

expansion space to the compression space the pressure, and thus the density of the working fluid is lower. This flow is typified by the temperature profile at 0° crank angle, given in figure 6.5.

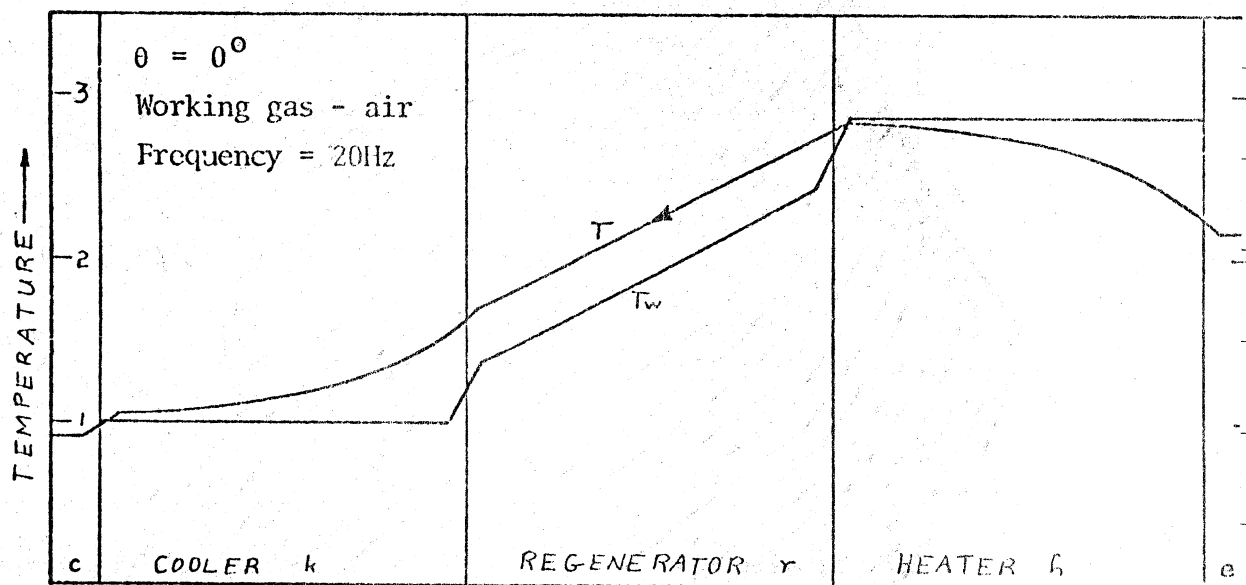


Figure 6.5 TURBULENT FLOW FROM THE EXPANSION SPACE TO THE COMPRESSION SPACE

From figure 6.5 it is seen that in the regenerator section the temperature of the working fluid T is higher than the temperature of the heat exchanger wall T_w . In this section the gas and wall temperature profiles are essentially parallel resulting in a large wall temperature difference at the regenerator/cooler and regenerator/heater inter-

faces. This is because the heater and cooler walls are maintained at a constant temperature, and the convective heat flow in the regenerator is apparently predominantly greater than the conductive heat leakage axially along the heat exchanger walls. There has been a tendency in the past to choose much fewer cells in the heater and cooler sections than in the regenerator section (Fi67). However, in figure 6.5 it is seen that in the heater and cooler sections the variation in working gas temperature and likewise in the working gas/wall temperature difference is significant, warranting the choice in this study of equal size cells throughout the heat exchanger section.

The portion of the cycle in which the working gas flows from the compression space to the expansion space is typified by the temperature profile at 150° crank angle given in figure 6.6.

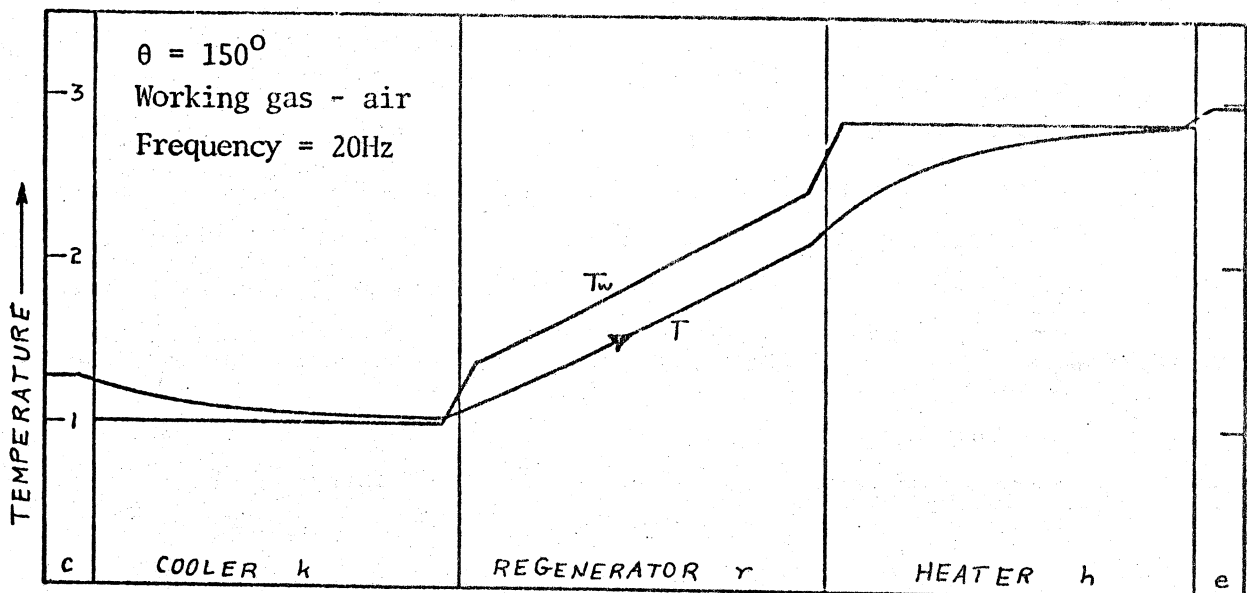


Figure 6.6 TURBULENT FLOW FROM THE COMPRESSION SPACE TO THE EXPANSION SPACE

A comparison of figures 6.6 and 6.5 shows that the regenerator wall temperature profile remains essentially constant throughout the cycle due to the large thermal capacitance of the wall material. It is seen that for flow from the compression space to the expansion space the working gas temperature is lower than the wall temperature in the regenerator section (figure 6.6), and for flow in the reverse direction the working gas temperature is higher than the wall temperature (figure 6.5). In both flow directions the regenerator section acts as a contra-flow type heat exchanger, the temperature difference between the working gas and the wall remaining approximately constant throughout.

It is of interest to examine the transition region, where the flow reverses, as typified by the temperature profiles at 70° , 80° and 90° crank angle (figure 6.7) and at 220° , 230° and 240° crank angle (figure 6.8). Figure 6.7 shows the transition when flow from the expansion space to the compression space reverses direction, and figure 6.8 when flow from the compression space to the expansion space reverses direction. In figure 6.7, the profile at 70° crank angle shows that at some instants during the cycle the flow can be both turbulent (solid line) and laminar (dotted line) in both directions! The flow transition occurs during a significant portion of the cycle beginning at crank angle $\theta = 50^\circ$ and ending at $\theta = 90^\circ$. During this transition the turbulent flow relaminarizes, the flow reverses, there is buildup of the laminar boundary layer, and finally the flow becomes turbulent. The complex processes occurring during this period are not fully understood

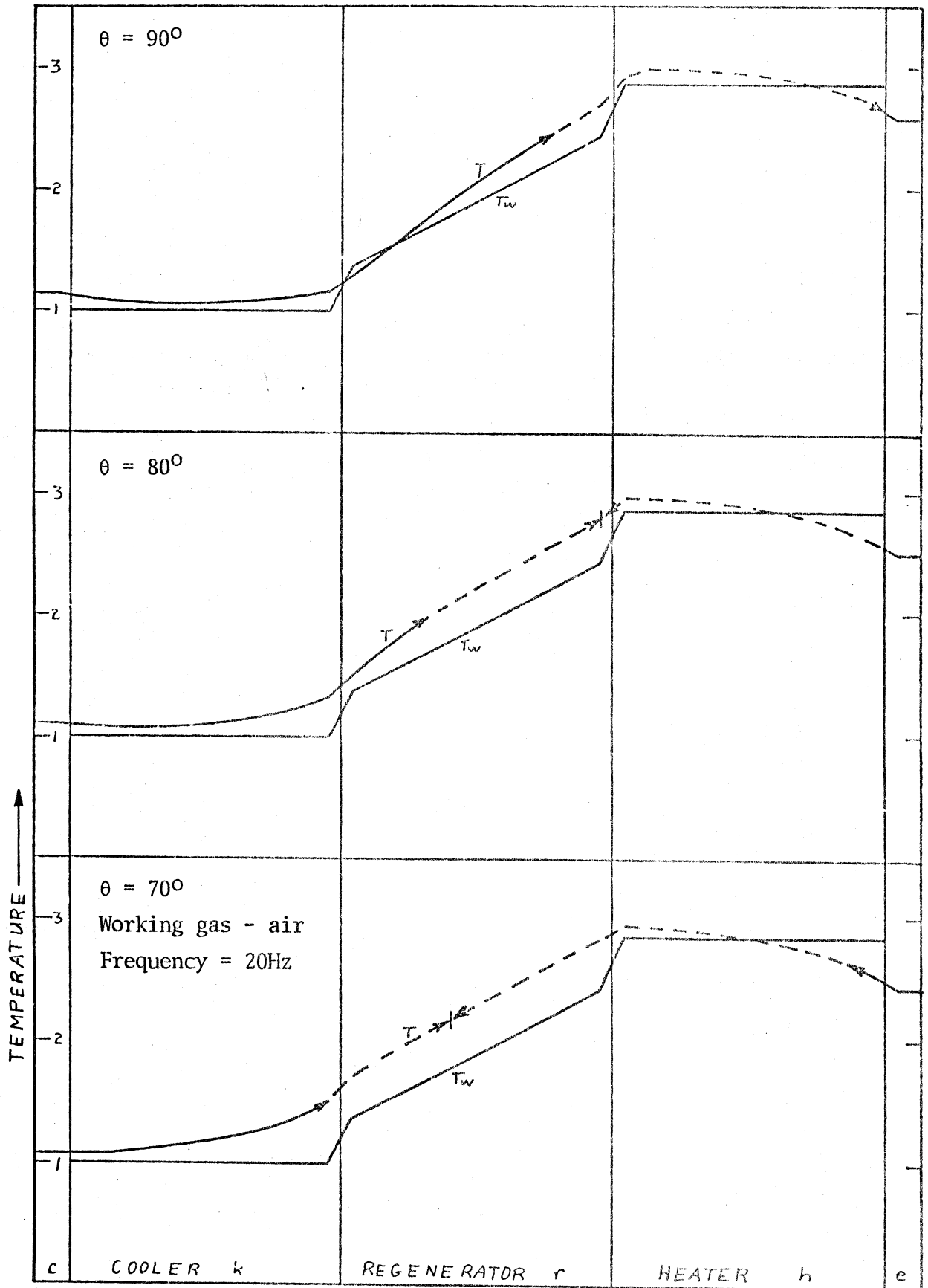


Figure 6.7 FLOW REVERSAL TRANSITION

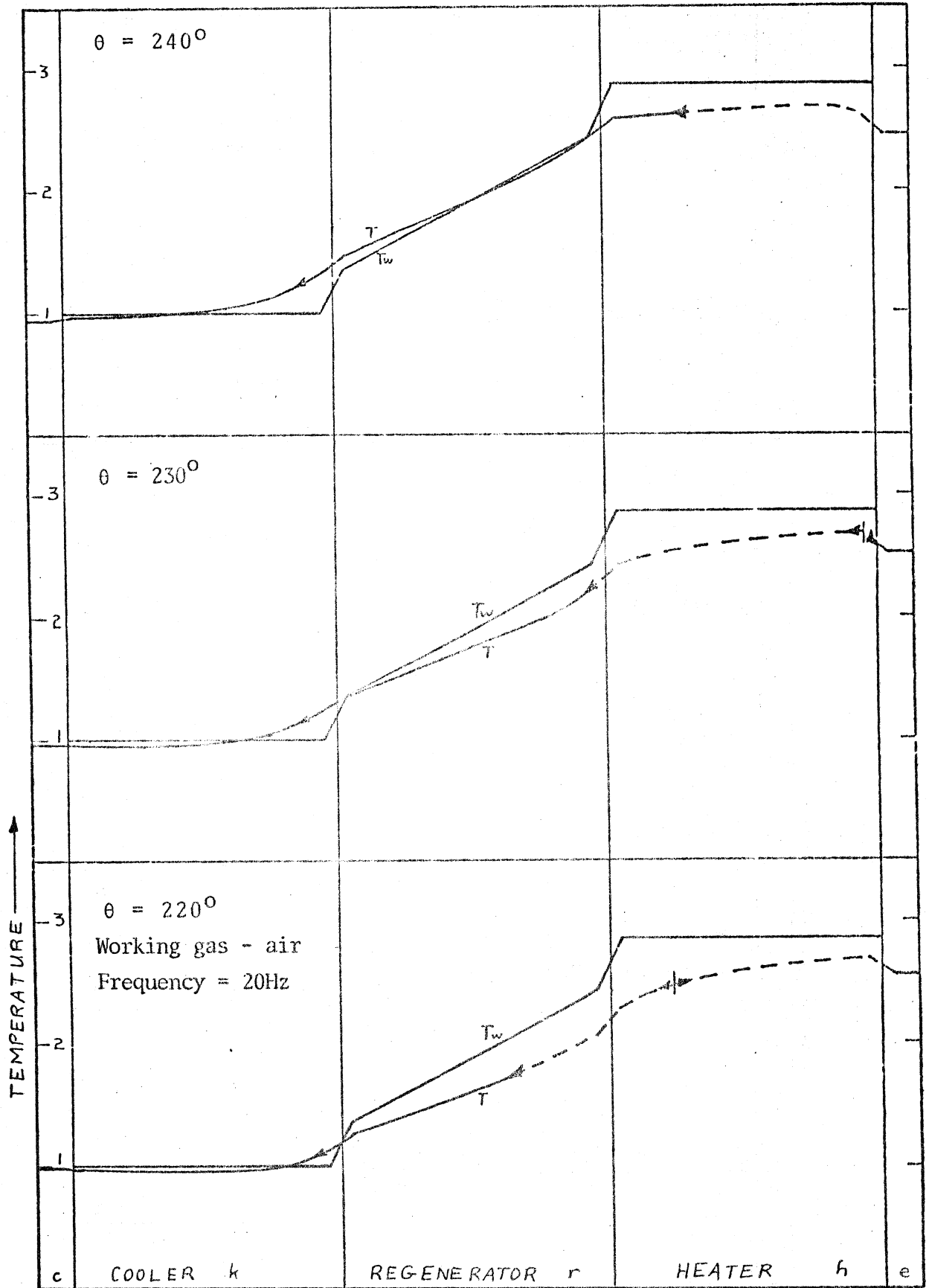


Figure 6.8 FLOW REVERSAL TRANSITION

and the use of the steady flow friction factor and heat transfer characteristics may be in error.

Fortunately, the important effects of heat transfer and flow friction occur during those portions of the cycle when the flow is unidirectional and fully turbulent, thus the error involved may not be significant.

In figure 6.7 it is seen that the temperature of the working gas in the heater section rises above that of the heater wall. This is due to the compression of the working gas and poor heat transfer in the heater section. Similarly in figure 6.8 it is seen that the temperature of the working gas in the cooler section falls below that of the cooler wall. The flow transition in this case occurs between crank angle $\theta = 190^\circ$ through to $\theta = 240^\circ$.

Figures 6.9, 6.10 and 6.11 show three-dimensional plots of the pressure profiles using air as the working gas at operating frequencies of 20 Hz (peak power), 35 Hz (cutoff power) and 60 Hz (excessive overdrive) respectively. In figure 6.9 it is seen that apart from a pressure drop at the entrance to the working spaces over portion of the cycle, the pressure profiles are essentially linear throughout the cycle. This would tend to suggest that a simplified momentum equation could be used for operation up to peak power. Detailed examination of the pressure distribution and mass flow rate given in the complete printout of Appendix J reveals, however, that over a significant portion of the cycle the fluid flow is in the same direction as the positive pressure gradient over parts of the heat exchanger section. This can only be accounted for by the complete momentum equation in

Working gas - air
 Operating frequency - 20Hz

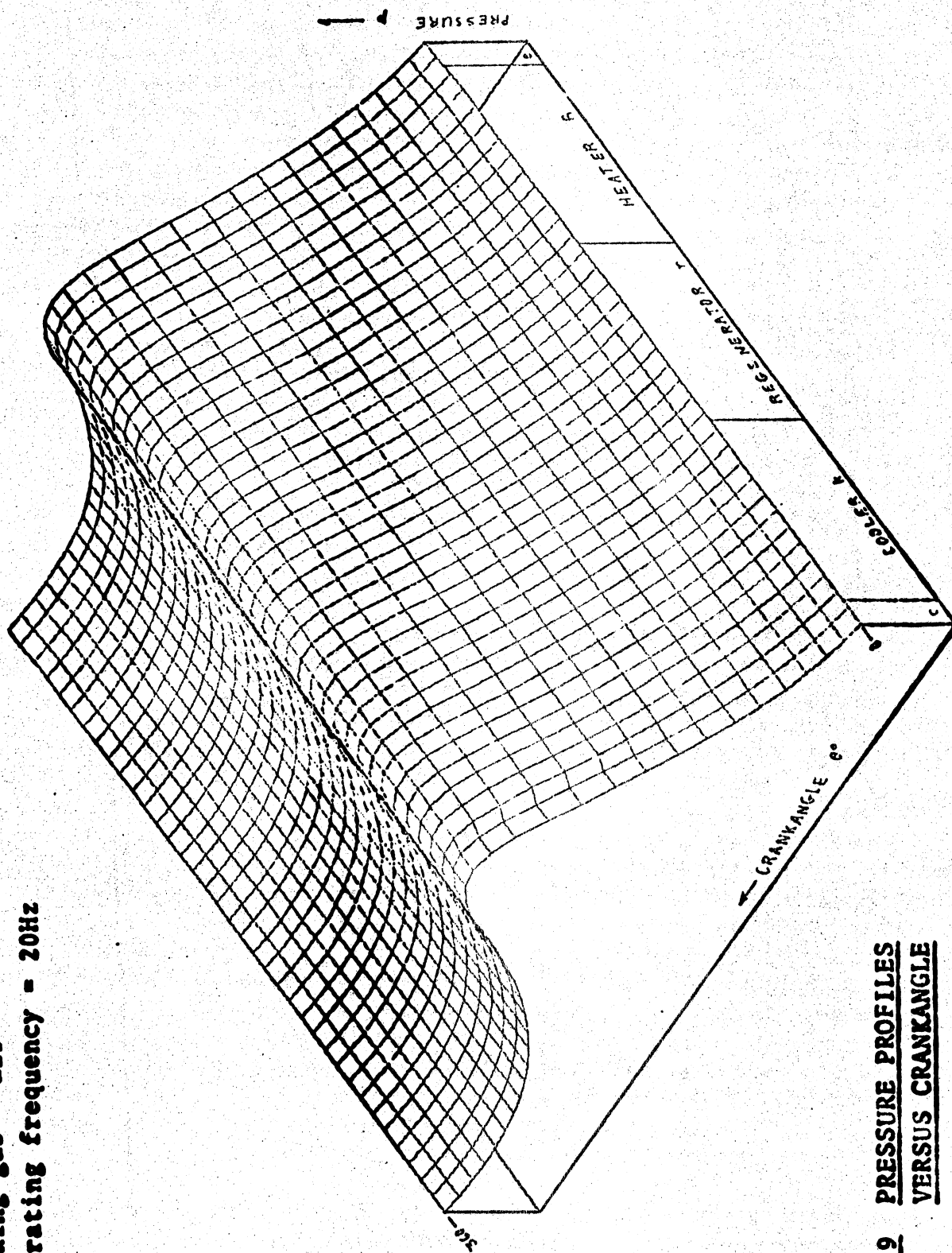


Figure 6.9 PRESSURE PROFILES
VERSUS CRANK ANGLE

Working gas - air
 Operating frequency = 35Hz

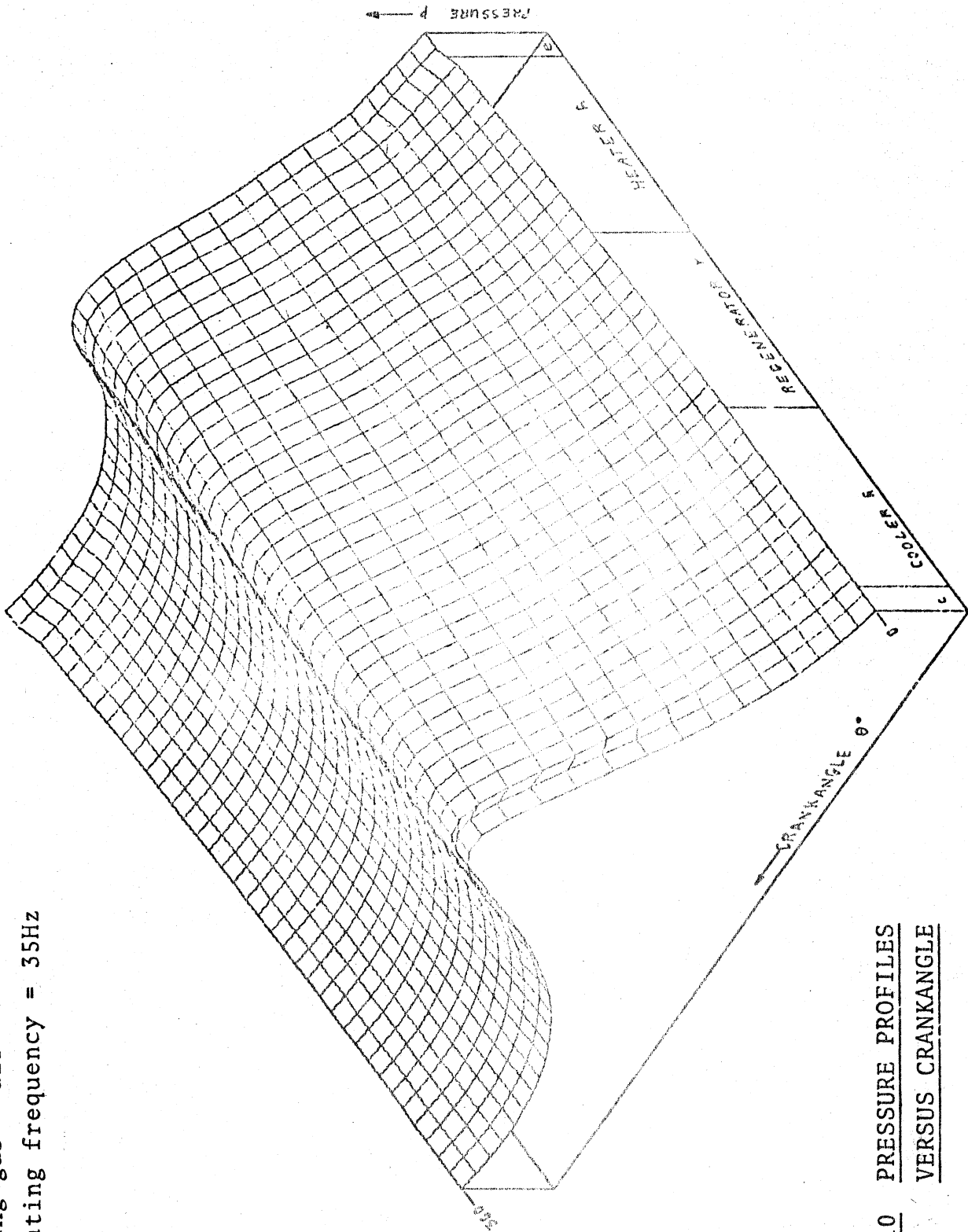


Figure 6.10 PRESSURE PROFILES
VERSUS CRANK ANGLE

Working gas - air
Operating frequency = 60Hz

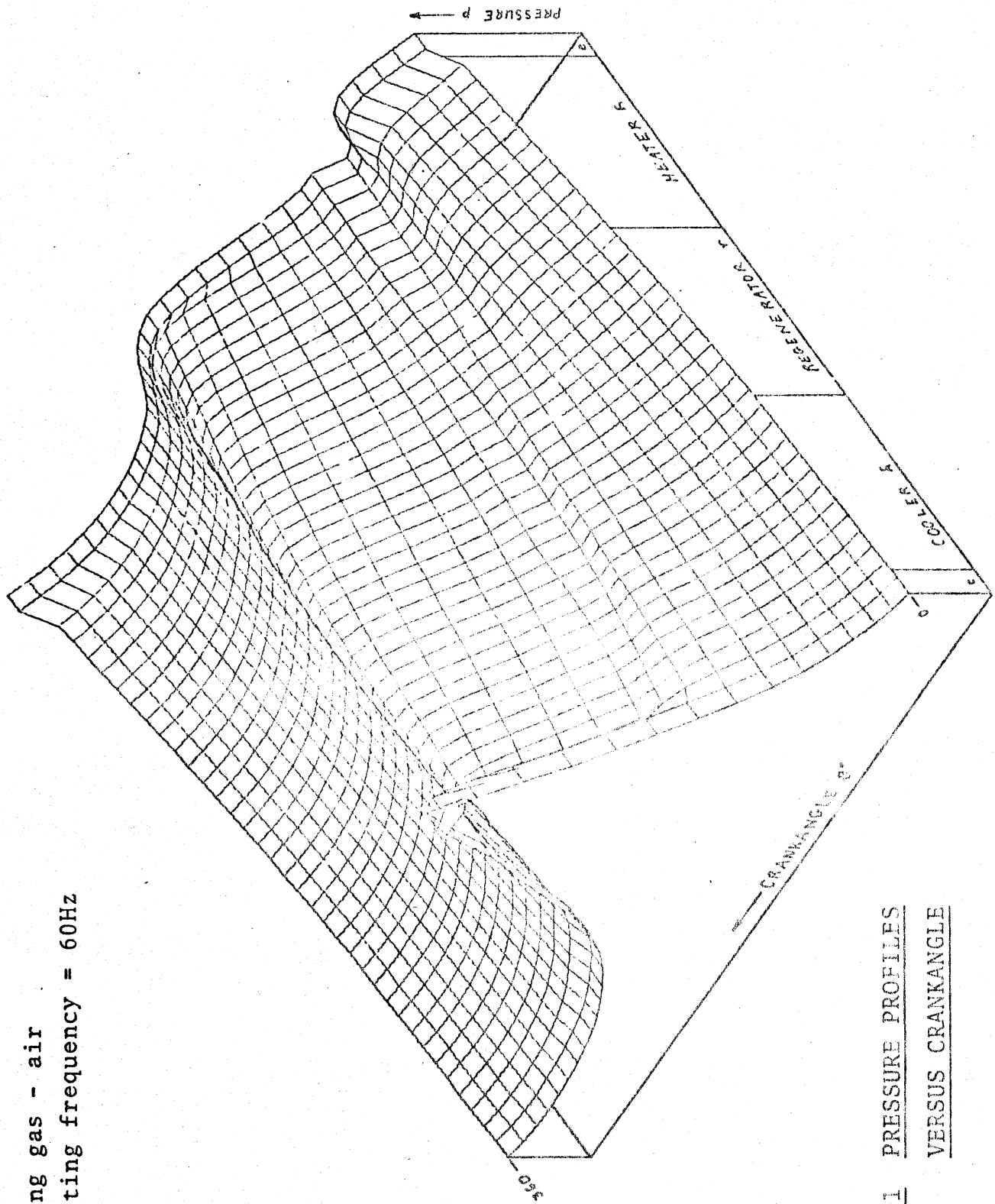


Figure 6.11 PRESSURE PROFILES
VERSUS CRANKANGLE

which both momentum flux and gas acceleration is considered.

In figure 6.10 it is seen that the entrance pressure drop is accentuated somewhat, and that an irregularity is beginning to appear in the expansion space section of the profile at a crank angle θ of between 60° and 100° . This is in phase with the minimum volume condition of the expansion space. In figure 6.11 an excessive overdrive condition has been chosen in order to accentuate these characteristics. The irregularity in the expansion space has produced a local pressure peak probably due to choking flow. However, this pressure peak has not propagated to the compression space. The entrance pressure drop at the entrance to the working space is also highly accentuated.

Figures 6.12 and 6.13 are cross sections of figures 6.9, 6.10 and 6.11 respectively in which the pressure variation with crank angle θ for the compression and expansion space are shown. It is noted that the phase angle of the compression space pressure peak remains relatively constant with respect to the volume variation with increase in operating frequency. However the phase lag of the pressure peak in the expansion space increases with operating frequency. Also, the difference in pressure between the compression space and the expansion space increases with frequency, culminating with the choking type local expansion space pressure peak which is not propagated through to the compression space.

Only three experimental pressure p versus crank angle

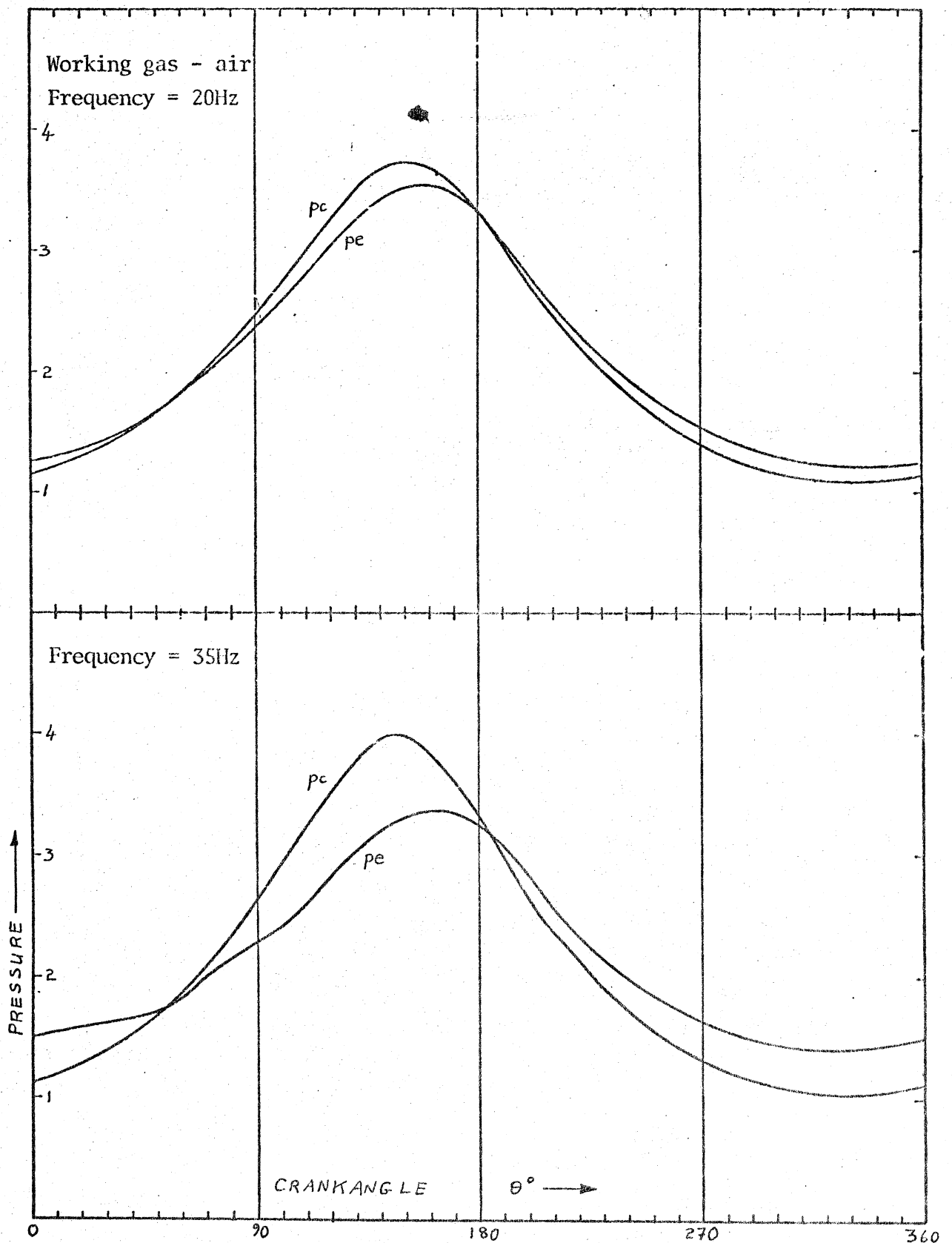


Figure 6.12 PRESSURE VERSUS CRANK ANGLE DIAGRAMS

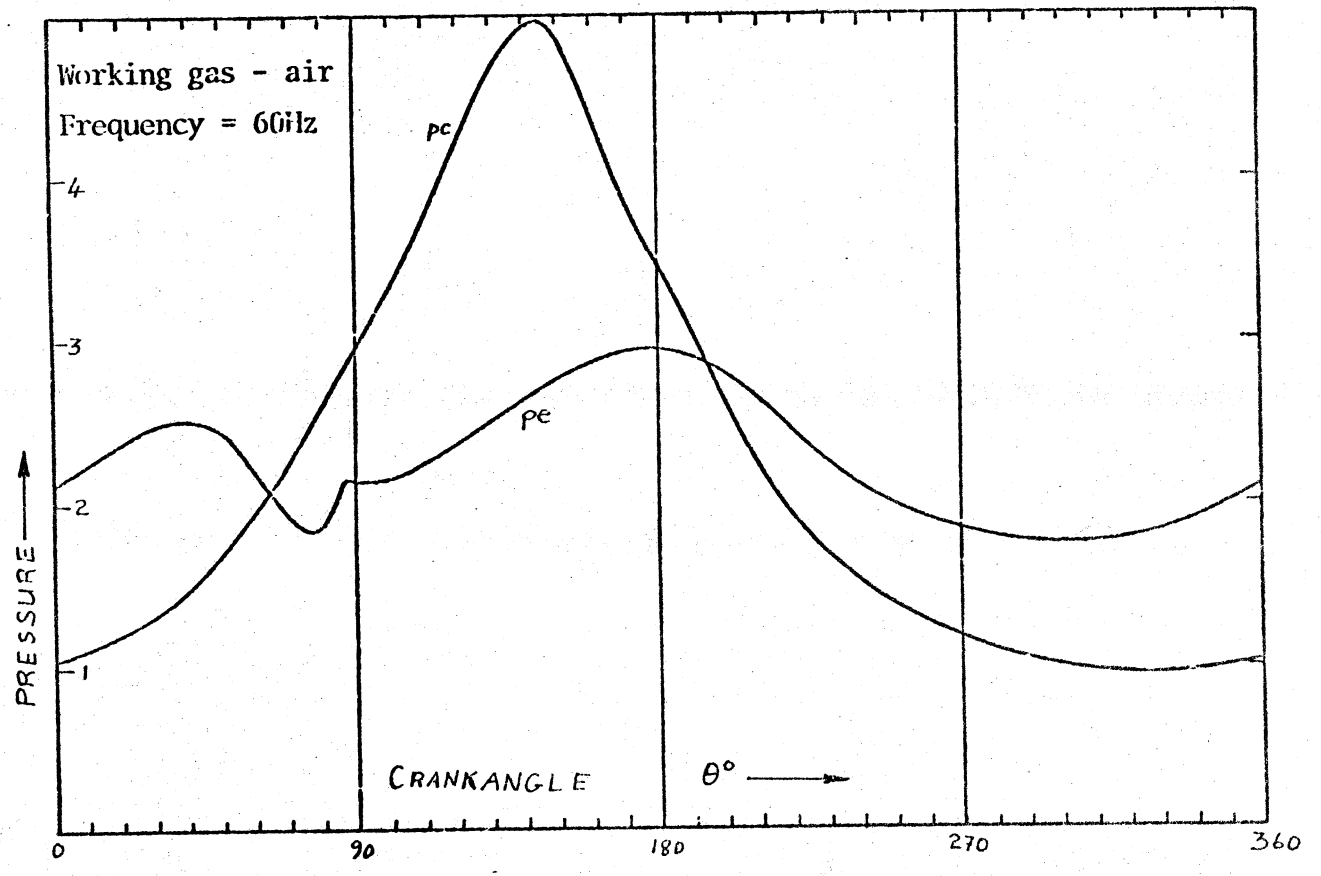


Figure 6.13 PRESSURE VERSUS CRANKANGLE DIAGRAMS

0 plots are available in the open literature. Meijer (Me61) presented a single figure giving simultaneous Farnboro indicator $p\theta$ diagrams of the compression and expansion space. This figure has been reproduced in figure 6.14 and has similar form to that of figure 6.12 for $\dot{f} = 20$ Hz.

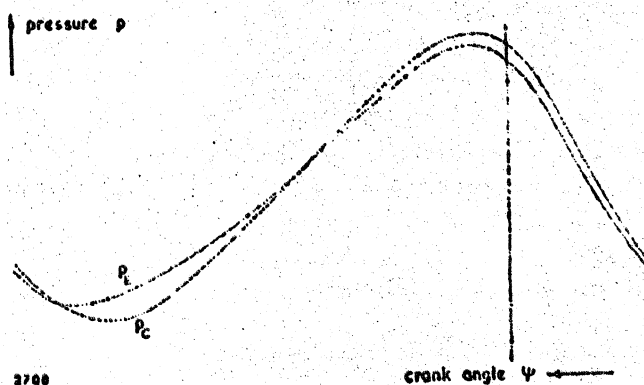


Figure 6.14 FARNBORO INDICATOR DIAGRAMS OF A STIRLING ENGINE (After Meijer Me61)

It is noted particularly that the peak expansion space pressure is less than, and lags, the peak compression space pressure. Kirkley (Ki63) presented experimental $p\theta$ diagrams over a range of operating speeds. These diagrams have been reproduced in figure 6.15, and show the same choking type phenomenon in the expansion space as in figure 6.13. Significantly it is seen in both figures 6.13 and 6.15 that the local pressure peak in

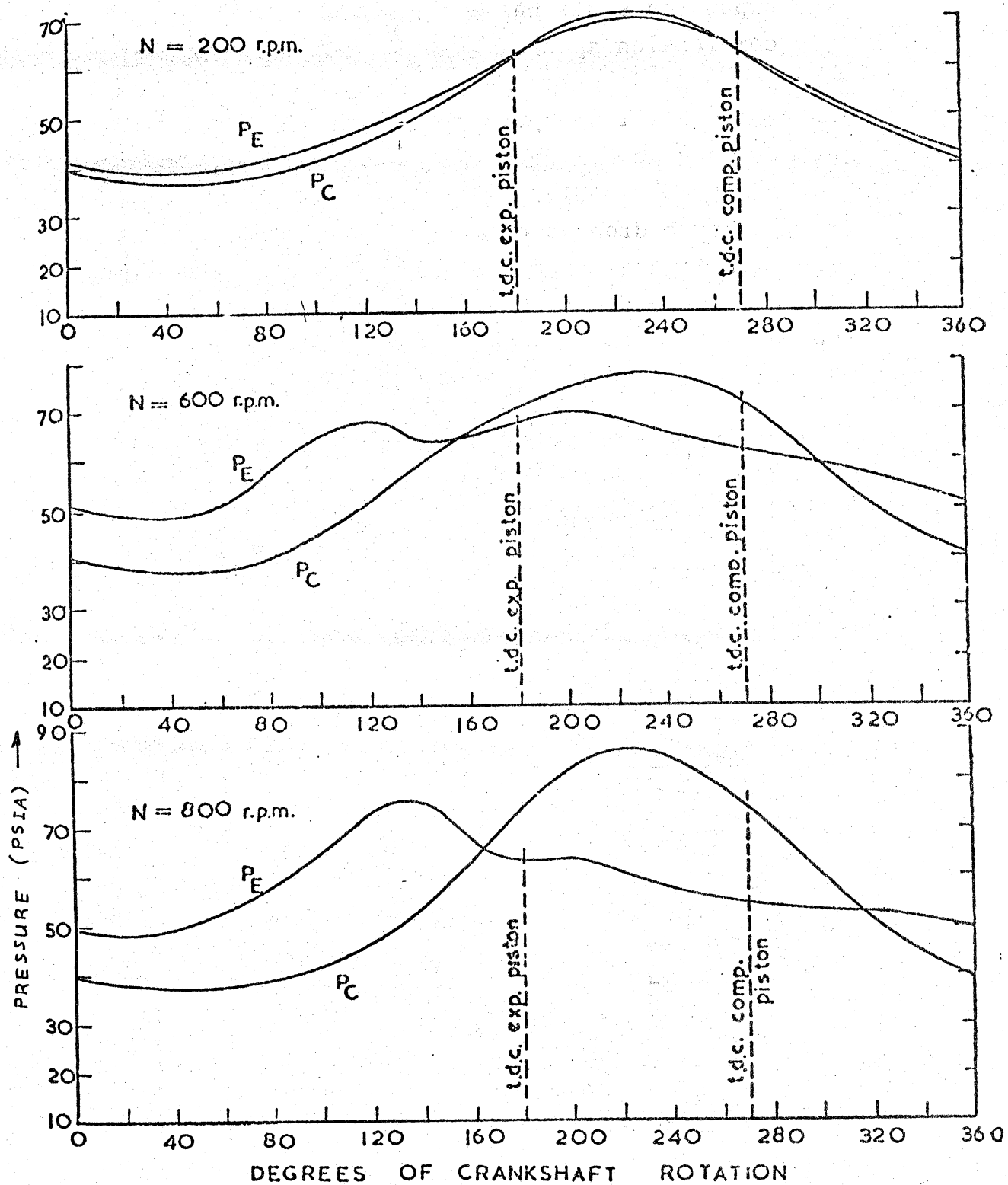


Figure 6.15 EXPERIMENTAL PRESSURE VERSUS CRANKANGLE DIAGRAMS (After Kirkley Ki63)

the expansion space has not propagated through to the compression space. Walker (Wa62.1) has presented experimental $p\theta$ diagrams at two operating speeds for a Philips Stirling cycle refrigerating machine. These curves have been reproduced in figure 6.16, and show no pressure irregularity at high speed, even though the pressure drop is extremely large. In contradistinction to figures 6.12, 6.13 and 6.14, figures 6.15 and 6.16 show the pressure peak of the expansion space leading that of the compression space. This discrepancy is not understood.

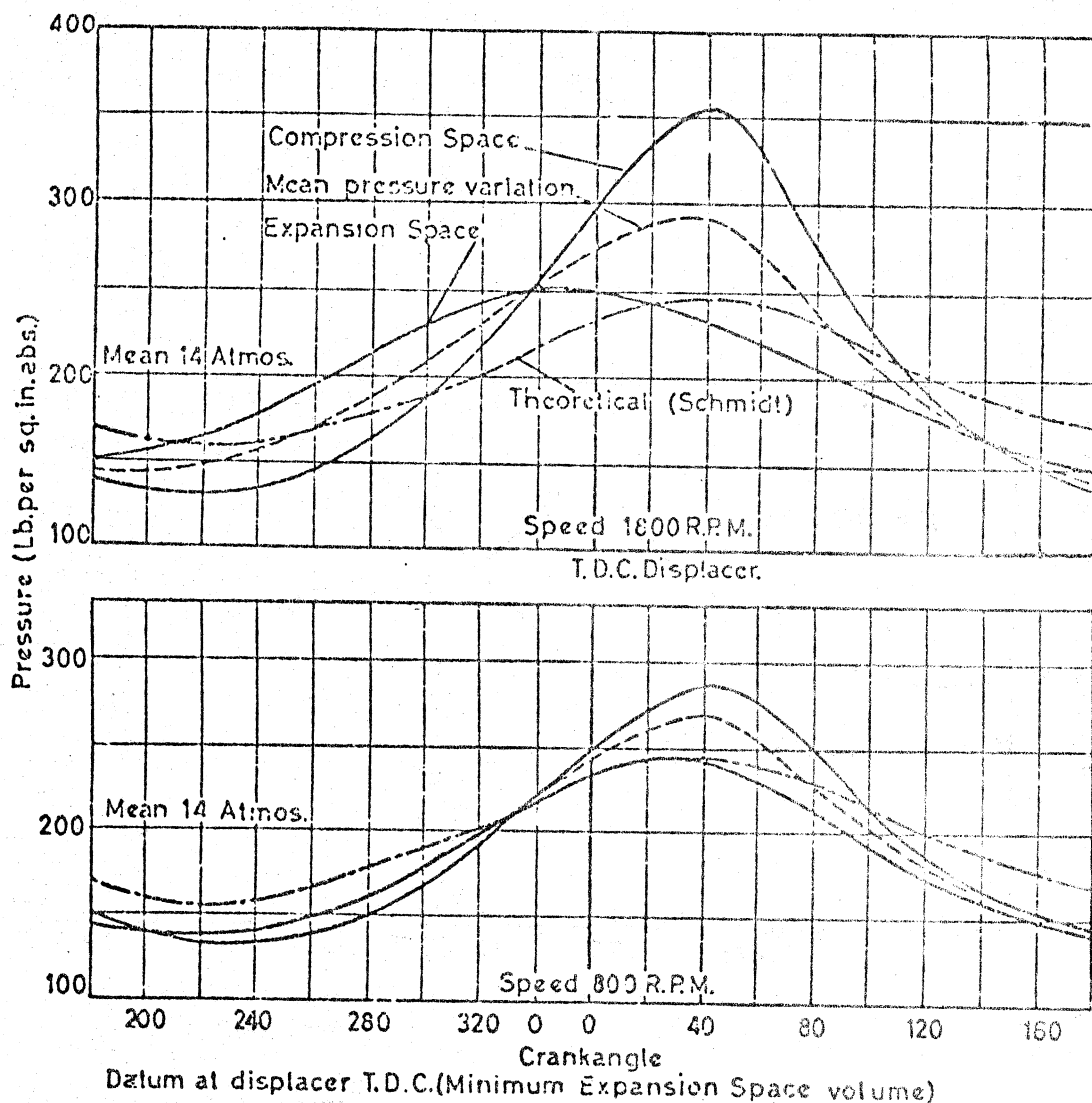


Figure 6.16 EXPERIMENTAL $p\theta$ DIAGRAMS OF A STIRLING
CYCLE COOLING MACHINE (After Walker Wa62.1)

6.4 SUMMARY AND CONCLUSIONS

Two types of results were presented in this chapter; gross performance characteristics including thermal efficiency η and power P , and the intimate incremental behaviour of the various variables throughout the cycle and throughout the machine. The gross performance results are as expected. It was postulated that the two most important properties which define the applicability of a working gas to Stirling cycle type machines are its gas constant R and dynamic viscosity $\bar{\mu}$. It was seen that R affects mainly the maximum attainable power, whereas $\bar{\mu}$ mainly affects the form of the performance characteristic at varying operating frequencies.

The intimate incremental behaviour was shown in the form of three-dimensional plots, and various cross sections through these plots. The information presented here has been previously unavailable, hence cannot be compared to current knowledge in the field, however the results are consistent, well behaved and as expected. In particular it was seen that over a significant portion of the cycle the fluid flow direction was the same as the positive pressure gradient over parts of the heat exchanger section. This indicates the importance of using the complete momentum equation including the momentum flux and acceleration terms.

7. CONCLUSIONS AND RECOMMENDATIONS

7.1 GENERAL

The model that has been developed and analysed in this study gives results that are well behaved, consistent, and in general agree with current available knowledge in the field. It is realized that a model is not validated until it is compared with results of experimental experience, however an extensive search has shown that no sufficiently documented experimental results are available in the open press. Notwithstanding the lack of experimental data available the computer results contain a wealth of information much of which has not been available previously. It has not been the purpose of this study to exploit the technique fully, which is not restricted to Stirling cycle machine type applications. For example, a research program has been started at the University of the Witwatersrand, using the modelling technique of this study in order to determine fundamental friction factor and heat transfer data for regenerator matrices.

7.2 MAJOR ADVANCES ATTAINED IN THE PRESENT INVESTIGATION

The initial objective of this study was to develop a comprehensive model for the simulation of Stirling cycle type machines, and to validate the model against current knowledge in the field. The work of Finkelstein served as a starting point for the study. The major advances attained in the present investigation are summarized below.

a) In the course of the theoretical study the following results were obtained:

- (i) The complete one-dimensional momentum and energy equations were derived from first principles. It was shown theoretically that the inclusion of the kinetic energy term in the energy equation is consistent with and equivalent to the inclusion of the momentum flux and acceleration terms in the momentum equation (Appendix D). As far as is known this result has not been available previously. The importance of the kinetic energy term was demonstrated in that for peak power using air as the working fluid, it was seen that for a significant portion of the cycle the fluid flow direction is the same as that of the positive pressure gradient over parts of the heat exchanger section. The use of the simplified momentum equation (D.20) implies a priori that the fluid flow direction will always be the same as that of the negative pressure gradient over all of the cycle, in contradistinction to the observed results (Chapter 6).
- (ii) The limitations of using the conventional Fanning friction factor in reversing flow problems were determined. A new form of friction factor, the so-called Reynolds friction factor was defined which overcomes these limitations, apart from being intuitively more logical to apply (Appendix F). For example, during the flow reversal the Reynolds number becomes zero, the equivalent Fanning friction factor becomes infinite, and the frictional drag force becomes indeterminate. The Reynolds friction factor, however, maintains a constant value throughout the laminar flow regime,

including the point at which the Reynolds number becomes zero.

- (iii) A cellular model of the Stirling cycle machine was defined and a system of first order differential equations developed for this model. The concept of static instability was introduced and it was shown that the model was completely free of all forms of static instability (Chapter 5). A variant of the model, advocated by researchers who have criticized the present model, was analysed and found to be subject to static instability when used in conjunction with the complete momentum and energy equations.
 - (iv) A unique method of accelerating convergence of the solution to cyclic steady state was presented which reduced the time to convergence by some orders of magnitude (Appendix G).
 - (v) A unique base parameter set $\{M, Tk, Vs, R\}$ was proposed in order to normalize all the system dimensioned parameters (Appendix A). In particular, the choice of the gas constant R as a base parameter rather than the usual choice of time arose from the realization that the rate of propagation of pressure information in the working gas medium (linearly proportional to $\sqrt{R \cdot Tk}$) is more fundamental than an arbitrarily chosen time parameter (Chapter 5).
- b) In the course of the computational study, the following results were obtained:

- (i) It was postulated that two of the most important parameters defining the working gas are the gas constant R and the dynamic viscosity $\tilde{\mu}$ (Chapter 6). The speed of propagation of pressure information working gas is proportional to the square root of the gas constant R , and this defines the operating frequency at which a specific performance level can be attained. It was shown that the value of the dynamic viscosity $\tilde{\mu}$ significantly alters the form of the performance characteristic. The reasons for its importance is that both the friction factor and the heat transfer coefficient are functions of $\tilde{\mu}$. For the same values of $\tilde{\mu}$, it was shown that different working gases result in scaled performance characteristics approximately in accordance with the ratio of the square roots of the respective working gas constants.
- (ii) It was found that at least 33 cells were required for reasonable asymptotic convergence of the performance characteristics to the continuous system. It was observed, however, that the efficiency versus operating frequency characteristics were essentially parallel, independent of the number of cells used. This surprising result was valid down to the minimum feasible number of cells ($n_c = 3$), for all the various working gases evaluated. This lead to the proposal of a method whereby the performance curves at (say) $n_c = 33$ can be predicted with high accuracy even with only one experiment at $n_c = 33$, based on a set of experiments

covering the frequency range through to cutoff power using a small number of cells. A considerable amount of computing time is thus saved, allowing a large number of computer experiments to be done as required in a parameter optimisation study.

- (iii) Plots showing the intimate behaviour of the temperature, flow and pressure profiles throughout the cycle were presented, giving a further insight as to the detailed behaviour of Stirling cycle machines (Chapter 6). As far as is known, information of this nature has not been available previously.

7.3 RECOMMENDATION FOR FUTURE WORK

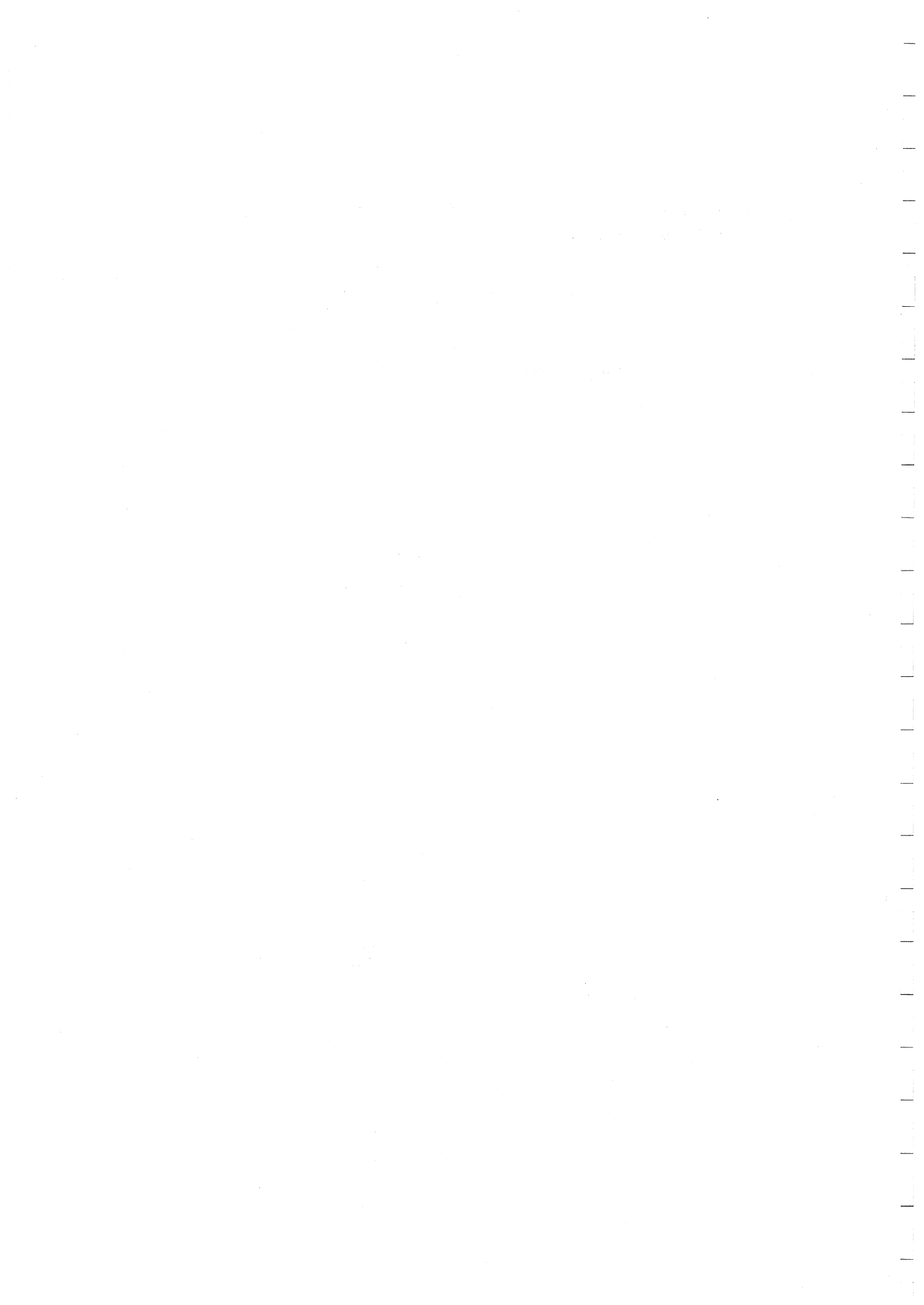
- (i) The applicability of the present model depends upon the availability of accurate relevant heat transfer and friction factor correlations for the heat exchangers -- in particular the regenerator matrix. In this context it is necessary to consider the effects of unsteady reversing flow. From Appendix F it is seen that there is a dearth of available information in this field and it is recommended that experimental studies be undertaken to fill this gap.
- (ii) It is recommended that simplifications of the model be developed and the results of their application be tested against the present comprehensive model in order to determine their range of applicability. For example at operating frequencies much less than that of peak power the instantaneous pressure drop is extre-

mely small. However, use of the comprehensive present model requires extremely small integration time intervals and correspondingly excessive computer time in order to solve the system at these low frequencies because of dynamic stability considerations. A simplified model based on the fundamental equations (D.5) and (D.19) (refer to section D.5), may result in sufficient accuracy for this case, allowing a considerable saving in computer time.

- (iii) It is suggested that the system differential equations be augmented by differential equations describing the mechanical dynamics of the machine in order to enable an overall solution to be obtained including (say) the determination of the frequency of operation. In the case of the Beale type free piston Stirling engine, this requires only four additional differential equations. For more complex mechanical systems, methods such as those due to Paul and Krajcinovik (PK70) could be employed.
- (iv) The formal dimensionless extension of the results is extremely restricted, limited to systems in which the dynamic viscosity normalizing factor, ie, $M\sqrt{R.Tk}/(Vs)^{2/3}$, is identical (Chapter 4). A dimensionless extension of results can, however, enable a considerable saving in computer time, limiting the computer experiments to those of form only. It is recommended therefore that the accuracy of extending the results to systems having different dynamic viscosity normalizing factors be examined and a range of applicability of dimensionless extension be determined.

- (v) It is recommended that the present model be validated against experiment. An experimental program is currently in progress at the University of the Witwatersrand which should, inter alia, provide the required data.

APPENDICES



A. PARAMETERS AND SYMBOLS

A.1 GENERAL

This appendix is not an exhaustive list of notation, but rather a guide to the philosophy behind the choice of the various parameters and symbols. For a complete list of symbols the reader is referred to the section entitled 'NOTATION' in the frontispiece.

The choice of symbols was governed by a number of factors:

- (i) Compatibility with current usage.
- (ii) Non-ambiguity -- prefix, suffix and subscript sets are defined with their relevant rules of usage to enable an unambiguous set of symbols to be generated. The rules of usage are such as to permit reading of the equations in the text and the computer program with a minimum of cross referencing to the list of notation.
- (iii) Readability of the computer program -- most of the computer program symbols are identical to those of the text. In some cases where this has not been possible, eg, where a *tilde* (~) has been defined in the text or where a lower case symbol has a different meaning to an upper case symbol, then a suitable suffix or prefix has been added to the computer program symbol. All Greek letters used in the text have been spelt out phonetically in the computer program.

In this appendix, the different types of parentheses have different usage. Normal curved parentheses () have either normal usage, or enclose the equivalent computer program

symbol to a text symbol. Square parentheses $[\]$ always enclose the dimensions of a parameter in SI units. Curly parentheses $\{ \}$ enclose specific sets of parameters.

A.2 NORMALIZED PARAMETERS

All parameters have been normalized with respect to the so-called base parameter set $\{M, T_k, V_s, R\}$, where:

$M[\text{kg}]$ is the nominal total mass of working gas in the machine

$T_k[\text{K}]$ is the cold sink temperature

$V_s[\text{m}^3]$ is the total power stroke volume of the machine

$R[\text{J/kg.K}]$ is the gas constant of the working gas

The nominal total mass of working gas in the machine M is determined from the charge pressure \tilde{p}_k on the assumption that the whole system is at a constant (cold sink) temperature T_k , is stationary at the total power stroke volume V_s , and that there is no leakage between the working space and the surrounding environment (bounce spaces, crankcases, etc).

The cold sink temperature T_k is usually the constant wall temperature of the cooler, however it can be the coolant temperature at the inlet to the cooler.

The total power stroke volume V_s is the swept volume of the power piston only in a piston-displacer type machine, and the sum of the swept volumes of the two pistons in a dual-piston type machine (refer to Section 1.2 for a definition of piston-displacer and dual-piston type machines). It is noted that a dual-piston type machine will have a varying effective power stroke volume depending upon the value of phase angle difference α between the volume variation in the expansion space and the volume variation in

the compression space. The above definition of V_s relates to the (hypothetical) maximum value of total power stroke volume defined when the phase angle difference α is zero. This is a hypothetical (but nevertheless unambiguous) definition of V_s since for $\alpha = 0$ the Stirling cycle engine cannot produce a net positive work output per cycle. In the piston-displacer type machine the power stroke volume V_s is unaffected by changes in phase angle difference α .

The above basic parameters form a complete unambiguous set in that they include the fundamental parameters of mass, length, time and temperature. Normalizing masses with respect to the nominal total mass of working gas in the system is convenient in that one can obtain by inspection the mass distribution of the working gas throughout the machine independent of the mean working pressure. The cold sink temperature has been chosen as a base parameter since it is approximately constant for most practical engines, being limited by the environment. Volume has been chosen as a base parameter rather than length since from thermodynamic considerations volume is the more fundamental parameter. The total power stroke volume of the machine effectively represents its physical size. The associated derived length parameter has been arbitrarily defined as the cube root of the total power stroke volume V_s . The choice of the gas constant of the working gas R as a base parameter rather than the usual choice of time arose from the realization that the rate of propagation of information in the working gas medium is more fundamental than an arbitrary time parameter chosen (say) as the inverse of the operating frequency. The rate of information propagation in the working gas is linearly proportional to $\sqrt{R.Tk}$. One thus finds that under similar conditions different working gases give

similar performance at speed ratios equal to the square root of the ratio of their respective gas constants (refer to Section 6.2).

Thus in Table A.1 the normalized and actual dimensioned parameters have been defined together with their associated normalizing factors and symbols used. For the actual parameters, the SI system of units has been adhered to throughout (NBS72). Except for the base parameters all actual parameters have been superscribed by a *tilde* (\sim). The computer symbol equivalent to all dimensioned parameters have been prefixed by the symbol E. The parameters defined in Table A.1 have been modified and extended by means of prefixes, suffixes and subscripts. The complete prefix, suffix and subscript sets have been respectively defined in Sections A.3, A.4 and A.5. Computer symbol equivalents of parameters have only been defined if they have actually found usage in the computer programs. The normalized parameters are dimensionless. In order to obtain the values of the actual parameters, given the values of the normalized parameters, the following algorithm is used:

$$\left(\begin{array}{c} \text{Actual} \\ \text{parameter} \end{array} \right) = \left(\begin{array}{c} \text{Normalizing} \\ \text{factor} \end{array} \right) \times \left(\begin{array}{c} \text{Normalized} \\ \text{parameter} \end{array} \right)$$

Table A.1 NORMALIZED AND ACTUAL PARAMETERS

BASE PARAMETERS					
PARAMETER	SI UNITS	ACTUAL PARAMETER	NORMALIZING FACTOR		NORMALIZED PARAMETER
Mass	kg	\tilde{m}	M	(EM)	m (RM)
Temperature	K	\tilde{T} (ET)	Tk	(ETK)	T (T)
Volume	m ³	\tilde{V}	Vs	(EVS)	V (V)
Specific heat capacity	J/kg.K	\tilde{c} (ECS)	R	(ER)	c (CS)
DERIVED PARAMETERS					
Heat	J	\tilde{Q}	$M.R.Tk$	(ENRGY)	Q (Q)
Work	J	\tilde{W}	$M.R.Tk$	(ENRGY)	W (W)
Area	m ²	\tilde{A}	$(Vs)^{2/3}$	(EA)	A (A)
Length	m	\tilde{x} (EX)			x (X)
		\tilde{d} (ED)	$(Vs)^{1/3}$	(EX)	d (D)
		\tilde{z}			z
Pressure	N/m ²	\tilde{p}	$M.R.Tk/Vs$	(EPK)	p (P)
Force	N	\tilde{F}	$M.R.Tk/(Vs)^{1/3}$		F (F)
Density	kg/m ³	$\tilde{\rho}$ (ERO)	M/Vs	(ERO)	ρ (RO)
Specific volume	m ³ /kg	\tilde{v}	Vs/M		v (VS)
Velocity	m/s	\tilde{U}	$\sqrt{R.Tk}$	(EU)	U
Time	s	\tilde{t}	$(Vs)^{1/3}/\sqrt{R.Tk}$	(ETIME)	t (TIME)
Frequency	Hz	\tilde{f} (EFREQ)	$\sqrt{R.Tk}/(Vs)^{1/3}$		f
Angular frequency	rad/s	$\tilde{\omega}$	$\sqrt{R.Tk}/(Vs)^{1/3}$		ω (OMEGA)
Power	W	\tilde{P}	$M(R.Tk)^{3/2}/(Vs)^{1/3}$		P
Mass flux density	kg/m ² .s	\tilde{g}	$M\sqrt{R.Tk}/Vs$		g (G)
Mass flux	kg/s	\tilde{G}	$M\sqrt{R.Tk}/(Vs)^{1/3}$		G
Dynamic viscosity	kg/m.s	$\tilde{\mu}$ (EMU)	$M\sqrt{R.Tk}/(Vs)^{2/3}$	(EMU)	μ (RMU)
Kinematic viscosity	m ² /s	$\tilde{\nu}$	$(Vs)^{1/3}\sqrt{R.Tk}$		ν
Shear stress	N/m ²	$\tilde{\sigma}$	$M.R.Tk/Vs$		σ
Thermal Conductivity	J/m.s.K	\tilde{k} (EK)	$M(R.Tk)^{3/2}/(Vs)^{2/3}Tk$		k (RK)

Table A.1 (Continued)

NORMALIZED AND ACTUAL PARAMETERS

DERIVED PARAMETERS (CONTINUED)				
PARAMETER	SI UNITS	ACTUAL PARAMETER	NORMALIZING FACTOR	NORMALIZED PARAMETER
Heat transfer coefficient	$J/m^2 \cdot s \cdot K$	h	$M(R.Tk)^{3/2}/Vs.Tk$	h (H)
Heat capacity	J/K	\tilde{c} (EC)	$M.R$	c (C)
Specific heat capacity at constant pressure	J/kg.K	\tilde{c}_p	R (ER)	c_p (CPS)
Specific heat capacity at constant volume	J/kg.K	\tilde{c}_v	R (ER)	c_v (CVS)
Ratio of specific heat capacities	-	$\gamma = c_p/c_v$	1	γ (GAMMA)
Specific internal energy	J/kg	\tilde{u}	$R.Tk$ (ERTK)	u
Specific enthalpy	J/kg	\tilde{e}	$R.Tk$ (ERTK)	e
Specific entropy	J/kg.K	\tilde{s}	R (ER)	s
Porosity	-	ψ	1	ψ
Thermal efficiency	-	η	1	η (EFF)
Energy error factor	-	ζ	1	ζ
Crank angle	-	θ	1	θ (THETA)
Volume variation phase angle difference	-	α	1	α (ALPHA)
Propagation time phase angle difference	-	δ	1	δ
Angles	-	ϕ	1	ϕ
Expansion loss Coefficient	-	β	1	β
Contraction loss Coefficient	-	Ke	1	Ke (RKE)
Convergence factor	-	Kc	1	Kc (RKC)
	-	Δ	1	Δ (DELTA)

A.3 PREFIX SET

The prefix set is used to define operators operating on a parameter or group of parameters, as well as to extend the computer program symbol set. The prefix set has been defined as follows, together with examples of usage:

(i) Operators

$D(D)$ is the total time derivative of the parameter, eg, $Dp_c(DPC)$ is the time derivative of the compression space pressure.

$\Delta(\text{DEL}, DL)$ is the difference operator. DEL denotes a spacial difference and DL (used only in the Runge-Kutta integration routine) denotes a time incremental difference, eg, $\Delta p_c(\text{DELPC})$ is the pressure drop across the entrance to the compression space due to contraction or expansion entrance effects; $DLM(I)$ is the time incremental difference of mass of working gas in the i 'th cell.

$\Sigma(S)$ is the summation operator, eg, $\Sigma Q_r(\text{SQR})$ is the algebraic sum of heat transferred to the working gas through the regenerator cell void spaces.

∇ is the divergence or gradient operator, being the vector partial differential operator with respect to the three spacial co-ordinates (refer Appendix D).

(ii) General

$B(B)$ denotes a term -- usually a combination of various constants and parameters, eg, $BOMEG = .25 * OMEGA$

R denotes a real parameter; used as a prefix to a real parameter having an integer symbol. This only applies to the computer program, where a distinction between real and integer parameters is made, eg, $mc(RMC)$ is the mass of working gas in the compression space. It is to be noted that whenever an operator prefix is added to a parameter which has a prefix R , then the prefix R is deleted eg, $Dmc(DMC)$ is the total time derivative of the mass of working gas in the compression space.

E denotes a dimensioned parameter. It is used exclusively in the computer program, eg, $ER[J/kg.K]$ is the gas constant of the working gas.

$n(N)$ denotes 'the number of'; usually referring to cells or nodes, eg, $nc(NC)$ is the number of cells in the heat exchanger section.

A.4 SUFFIX SET

The suffix set is used to define a particular parameter as to location or type. The suffix set has been defined as follows, together with examples of usage:

(i) Location

$c(C)$ denotes the compression space. The exception is $nc(NC)$, used exclusively for the total number of cells in the heat exchanger section, eg, $Tc(TC)$ is the temperatur

of the working gas in the compression space.

$k(K)$ denotes the cooler, eg, $Twk(TWK)$ is the temperature of the cooler wall.

$r(R)$ denotes the regenerator, eg, $Twr_i(TWR(I))$ is the temperature of the wall associated with the i 'th regenerator cell.

$h(H)$ denotes the heater, eg, $TwH(TWH)$ is the temperature of the heater wall.

$e(E)$ denotes the expansion space, eg, $pe(PE)$ is the pressure of the working gas in the expansion space.

$o(O)$ denotes the external environment, eg, Qro_i is the heat loss from the i 'th regenerator cell to the external environment.

$n(N)$ denotes a node (interface between adjacent cells), eg, $Tn_i(TN(I))$ is the temperature at the i 'th node (interface between cell $(i-1)$ and cell i).

$d(D)$ denotes the so-called dead space, being the heat exchanger void space and the clearance spaces associated with the compression and expansion working spaces, eg, $Vd(VD)$ is the volume of the dead space.

$p(P)$ denotes the heat exchanger pipes, eg, $xp(XP)$ is the length of the heat exchanger pipes.

(ii) Medium

$g(G)$ denotes the working gas, eg, $Awg(AWG)$ is the wetted area of the heat exchanger cell wall (ie, the area wetted

by the working gas).

$m(M)$ denotes the regenerator matrix, eg, ρ_m is the density of the regenerator matrix material.

$w(W)$ denotes the containing wall, eg, $Tw_i(TW(I))$ is the temperature of the wall containing the i 'th cell.

(iii) Special suffixes

$f(F)$ denotes frontal (used exclusively for area), eg, A_f is the frontal area of the regenerator matrix.

$s(S)$ denotes stroke (used exclusively for the total power stroke volume), eg, $V_s(EVS)$ is the total power stroke volume of the engine.

$cl(CL)$ denotes clearance (used exclusively for volume), eg, $V_{cl}(VCL)$ is the clearance volume of the compression or the expansion spaces.

$su(SU)$ denotes the Sutherland constant (refer Appendix E), eg, $T_{su}(TSU)$ denotes the Sutherland constant of the working gas.

(iv) Computer program only

I denotes the inverse of a parameter, eg, $CWI = 1./CW$ is the inverse of the total heat capacity of the cell wall.

S denotes a specific parameter (with respect to unit mass), eg, CVS is the specific heat capacity at constant volume.

In general, the suffix set is used in the following order:

Parameter $\{n\}\{w,m,g\}\{w,m,g\}\{c,k,r,h,e,d,p\}\{o\}$ {subscript set}

or in the computer program equivalent form:

Parameter $\{S\}\{N\}\{W,M,G\}\{W,M,G\}\{C,K,R,H,E,D,P\}\{O\}\{I\}$
({subscript set}).

The use of any of the suffixes is optional and only one suffix enclosed in each set of curly parentheses may be used to define a particular parameter, eg, Awg (AWG), vn_i (VSN(I)), Twr_i (TWR(I)) are valid suffixed parameters. $Pnck$ (PNCK) is not a valid suffixed parameter, since it is associated with both the compression space c and the cooler k .

The default definition of any parameter when none of the medium suffixes $\{w,n,g\}$ are used is the working gas, hence a working gas parameter does not require a suffix g , eg, Te , p_i , vn_i are working gas parameters.

Parameters which are exclusively nodal do not require a suffix n , eg, the mass flux density g_i is defined only at the i 'th node, thus does not require a suffix n .

When the medium suffix m (matrix) is used, then the location suffix r (regenerator) is superfluous, since the matrix is located exclusively in the regenerator section, eg, Tmr_i (TMR(I)) could be written Tm_i (TM(I)) without ambiguity.

A.5 SUBSCRIPT SET

In the context of the system model defined in Chapter 3, the

cooler, regenerator, and heater of the system are subdivided into cells and nodes (interfaces between adjacent cells). It is noted that for any number nc of cells there are $(nc+1)$ nodes.

The following subscript set serves to assign parameters to particular cells or nodes:

$i(I)$ denotes the running subscript. i can take on any integer value between 1 and $(nc+1)$. i is never zero or negative. It is noted that the value of a subscript is a function of the suffix used. Thus $T_{wi} \neq T_{ri}$ since even though both refer to a wall temperature, the i 'th cell in the heat exchanger system is not the i 'th regenerator cell.

$l(1)$ denotes the node interfacing the compression space and the cooler. It also denotes the cooler cell adjacent to the compression space.

$nk(NK)$ is the number of cells in the cooler section. It denotes the cooler cell adjacent to the regenerator section.

$nk1(NK1) = nk+1$ denotes the node interfacing the cooler and the regenerator. It also denotes the regenerator cell adjacent to the cooler section.

$nr(NR)$ is the number of cells in the regenerator section

$nkr(NKR) = nk+nr$ denotes the regenerator cell adjacent to the heater section.

$nkrl(NKR1) = nkr+1$ denotes the node interfacing the regenerator and the heater. It also denotes the heater cell adjacent to the regenerator section.

$nh(NH)$ is the number of heater cells.

$nc(NC) = nk+nr+nh$ is the total number of cells in the heat exchanger system. It denotes the heater cell adjacent to the expansion space.

$nc1(NC1) = nc+1$ denotes the node interfacing the heater and expansion space.

A.6 DIMENSIONLESS GROUPS

The table below defines the various dimensionless groups which have been used in this work.

Table A.2 DIMENSIONLESS GROUPS

Dimensionless Group	Symbol	Definition
Reynolds Number	Re (RE)	$g \cdot d / \nu$
Nusselt Number	Nu	$h \cdot d / k$
Stanton Number	St	$h / g \cdot c_p$ ($= h(\gamma - 1) / g \cdot \gamma$)
Fanning Friction Factor	Ff	$2\sigma \rho / g^2$ ($= 2\sigma / \rho \cdot u^2$)
Reynolds Friction Factor	Fr (FR)	$2\sigma \cdot \rho \cdot d / \mu g$ ($= Ff \cdot Re$)
Prandtl Number	Pr (PR)	$c_p \cdot \mu / k$ ($= \mu \cdot \gamma / k(\gamma - 1)$)
Relative Roughness Factor	Ro (RO)	z / d

B. SCHMIDT CYCLE ANALYSIS

The Schmidt cycle analysis is a closed form of analysis of an ideal Stirling cycle machine, based on the following assumptions:

- (i) Sinusoidal volume variations in the compression and expansion spaces
- (ii) The working gas in the compression space and cooler is at a constant temperature $T_k = 1$
- (iii) The working gas in the expansion space and heater is at a constant temperature T_h
- (iv) The regenerative process is perfect
- (v) There is no instantaneous pressure drop or leakage
- (vi) All processes are reversible
- (vii) The perfect gas equation of state applies.

In order to retain continuity with the application example test engine (Chapter 4) it has been assumed that the compression and expansion spaces have identical swept and clearance volumes. In the more complete analysis (eg Wa73) a factor κ is introduced being the ratio of the compression to the expansion space swept volumes. Normalized parameters (refer Appendix A) have been used throughout.

Volume of the compression space V_c and the expansion space V_e :

$$V_e \Delta \underline{V} e l + (1 + \cos \theta) / 4 \quad (\text{B.1})$$

$$V_e \Delta \underline{V} e l + (1 + \cos [\theta + \alpha]) / 4 \quad (\text{B.2})$$

where

θ is the crank angle

α is the angular phase advance of the expansion space volume variations with respect to the compression space volume variations.

Conservation of mass:

$$1 = m_c + m_k + m_r + m_h + m_e \quad (\text{B.3})$$

Perfect gas equation of state:

$$pV = mT \quad (\text{B.4})$$

$$(\text{B.4}) \rightarrow (\text{B.3})$$

$$1 = p(V_c + V_k + V_r / T_r + V_h / T_h + V_e / T_h) \quad (\text{B.5})$$

where T_r is the mean effective constant temperature of the regenerator space (Cr66).

(B.1), (B.2) \rightarrow (B.5):

$$1/p = [V_e l + (1 + \cos \theta) / 4 + V_k + V_r / T_r + V_h / T_h + V_e l / T_h + (1 + \cos(\theta + \alpha)) / 4 T_h]$$

$$1/p = (1+1/Th)(Vc\ell+0,25)+Vk+Vr/Tr+Vh/Th+\cos\theta/4 \\ +(\cos\theta.\cos\alpha-\sin\theta.\sin\alpha)/4.Th$$

$$1/p = B2+\cos\theta(1+\cos\alpha/Th)/4-\sin\alpha.\sin\theta/4.Th \quad (B.6)$$

where

$$B2 \triangleq (1+1/Th)(Vc\ell+0,25)+Vk+Vr/Tr+Vh/Th$$

Let

$$B1.\cos\phi \triangleq (Th+\cos\alpha)/4.Th \quad (B.7)$$

$$B1.\sin\phi \triangleq -\sin\alpha/4.Th \quad (B.8)$$

(B.8)→(B.7):

$$\tan\phi = -\sin\alpha/(Th+\cos\alpha) \quad (B.9)$$

$$B1 = \sqrt{[(Th+\cos\alpha)/4.Th]^2 + (\sin\alpha/4.Th)^2}$$

$$B1 = \sqrt{1+Th^2+2.Th.\cos\alpha}/4.Th \quad (B.10)$$

Now

$$B1.\cos(\theta-\phi) = B1.\cos\theta.\cos\phi+B1.\sin\theta.\sin\phi \quad (B.11)$$

(B.7), (B.8), (B.11)→(B.6):

$$1/p = B2+B1.\cos(\theta-\phi)$$

$$p = 1/B2[1+B.\cos(\theta-\phi)] \quad (B.12)$$

where

$$B \triangleq B1/B2$$

From the assumption of reversible operation, over a complete cycle the heat supplied to the compression (expansion) space is equal to the work done by the compression (expansion) space.

$$Q_c = W_c = \oint p dV_c$$

$$Q_e = W_e = \oint p dV_e$$

Given any function $f(\beta)$, β an angle, then by Fourier series expansion analysis (Ar70) the following is obtained:

$$f(\beta) = B_0 + \sum_{i=1}^{\infty} [B_{ci} \cos(i\beta) + B_{si} \sin(i\beta)] \quad (\text{B.15})$$

where

$$B_0 \triangleq \int_0^{2\pi} f(\beta) d\beta / 2\pi$$

$$B_{ci} \triangleq \int_0^{2\pi} f(\beta) \cos(i\beta) d\beta / \pi$$

$$B_{si} \triangleq \int_0^{2\pi} f(\beta) \sin(i\beta) d\beta / \pi$$

Let

$$\beta \triangleq \theta - \phi \quad (\text{B.16})$$

(B.16) \rightarrow (B.12):

$$p(\beta) = 1/B2(1+B \cdot \cos\beta) \quad (\text{B.17})$$

It is noted that between $\beta = 0$ and $\beta = 2\pi$, the function $p(\beta)$ is even, hence it has only a cosine expansion, thus all the $B\sin$ terms are zero. It is also noted that in the integral $\oint p dV$, dV is a fundamental sinusoidal function of β . Thus only the fundamental component of the expansion of $p(\beta)$ yields a finite value of the integral. All other components of p are orthogonal to dV and return zero integral values.

Thus only the fundamental component $Bc_1 \cos\beta$ has been evaluated:

$$Bc_1 = \int_0^{2\pi} [\cos\beta/B^2(1+B\cos\beta)]d\beta/\pi \quad (\text{B.18})$$

From Dwight (Dw61), definite integral no. 858.536 one obtains

$$\int_0^{\pi} [\cos\beta/(1+B\cos\beta)]d\beta = \pi(1-1/\sqrt{1-B^2})/B \quad (\text{B.19})$$

(B.19) \rightarrow (B.18)

$$Bc_1 = 2(1-1/\sqrt{1-B^2})/B^2 \cdot B \quad (\text{B.20})$$

Finkelstein (Fi76) has shown that equation (B.20) can be advantageously rewritten as follows:

$$Bc_1 = -2B/B^2\sqrt{1-B^2}(1+\sqrt{1-B^2}) \quad (\text{B.21})$$

Equation (B.21) does not involve the differencing of two nearly equal quantities as in equation (B.20) and is thus less sensitive to roundoff error.

Compression space: differentiating equation (B.1) one obtains

$$dV_e = -\sin\theta \cdot d\theta/4 \quad (\text{B.22})$$

(B.22), (B.21) → (B.13):

$$Q_e = [B/2 \cdot B2\sqrt{1-B^2}(1+\sqrt{1-B^2})] \int \sin\theta \cdot \cos(\theta-\phi) d\theta$$

$$Q_e = [B/4 \cdot B2\sqrt{1-B^2}(1+\sqrt{1-B^2})] \int_0^{2\pi} [\sin(2\theta-\phi) + \sin\phi] d\theta$$

$$Q_e = B\pi \sin\phi / 2 \cdot B2\sqrt{1-B^2}(1+\sqrt{1-B^2}) \quad (\text{B.23})$$

Expansion space: differentiating equation (B.2) one obtains

$$dV_e = -\sin(\theta+\alpha) d\theta/4 \quad (\text{B.24})$$

(B.24), (B.21) → (B.14):

$$Q_e = [B/2 \cdot B2\sqrt{1-B^2}(1+\sqrt{1-B^2})] \int \sin(\theta+\alpha) \cos(\theta-\phi) d\theta$$

$$Q_e = B\pi \sin(\phi+\alpha) / 2 \cdot B2\sqrt{1-B^2}(1+\sqrt{1-B^2}) \quad (\text{B.25})$$

(B.23) → (B.25)

$$Q_e/Q_c = \sin(\phi+\alpha)/\sin\phi$$

$$Q_e/Q_c = (\sin\phi \cdot \cos\alpha + \cos\phi \cdot \sin\alpha) / \sin\phi$$

$$Q_e/Q_c = \cos\alpha + \sin\alpha / \tan\phi \quad (\text{B.26})$$

(B.9) → (B.26)

$$Q_e/Q_c = \cos\alpha - (Th + \cos\alpha) \sin\alpha / \sin\alpha$$

$$Q_e/Q_c = -Th \quad (\text{B.27})$$

Thermal efficiency η :

$$\eta \triangleq W/Q_e = (Q_c + Q_e)/Q_e \quad (\text{B.28})$$

$$(\text{B.27}) \rightarrow (\text{B.28})$$

$$\eta = 1 - 1/Th \quad (\text{B.29})$$

which is the Carnot efficiency.

The application example test engine of Chapter 4 analysed by the Schmidt cycle analysis above gives the following performance:

$$\text{Efficiency } \eta = 0,65$$

Heat supplied externally to the expansion space

$$Q_e = 0,834$$

Heat supplied externally to the compression space

$$Q_c = -0,292$$

$$\text{Work done per cycle } W = Q_c + Q_e = 0,542$$

In order to assign dimensions to the above energy units they are multiplied by the energy normalizing factor (refer to Appendix A, Chapter 4):

$$MRTk = 108 \text{ Joules}$$

It is noticed from the above that the heater and cooler play no active part in the Schmidt cycle, since their net heat supplied externally over the cycle is zero.

C. BASIC IDEAL CYCLE ANALYSIS

C.1 INTRODUCTION

The Schmidt cycle analysis (Appendix B) is an ideal cycle analysis modified by the mechanical restriction of sinusoidal variations of the expansion and compression space volumes. On the thermodynamic side it is assumed that the compression and expansion processes are isothermal, and that the regenerative process is perfect. Unfortunately, if one attempts to depart from any of the idealizations imposed by Schmidt, then the closed form solutions break down, and one can only solve the system by numerical integration. However retaining Schmidt's restrictive assumptions may result in misleading conclusions, in particular with regards to optimisation studies.

An alternative approach in order to establish basic trends is to return to the simple idealized cycle analysis, but without the mechanical or thermodynamic restrictions imposed by Schmidt (RU76). In particular the effects of non-isothermal compression and expansion as well as of imperfect regeneration can be examined.

In the analyses that follow, normalized parameters (refer to Appendix A) have been used throughout. Various parameters required only in this appendix are defined in the order of their first appearance.

C.2 THE IDEAL STIRLING CYCLE

This cycle is defined by two isotherms bounded by two isochors. (Refer to the pV and Ts diagrams of figure C.1).

THE IDEAL STIRLING CYCLE

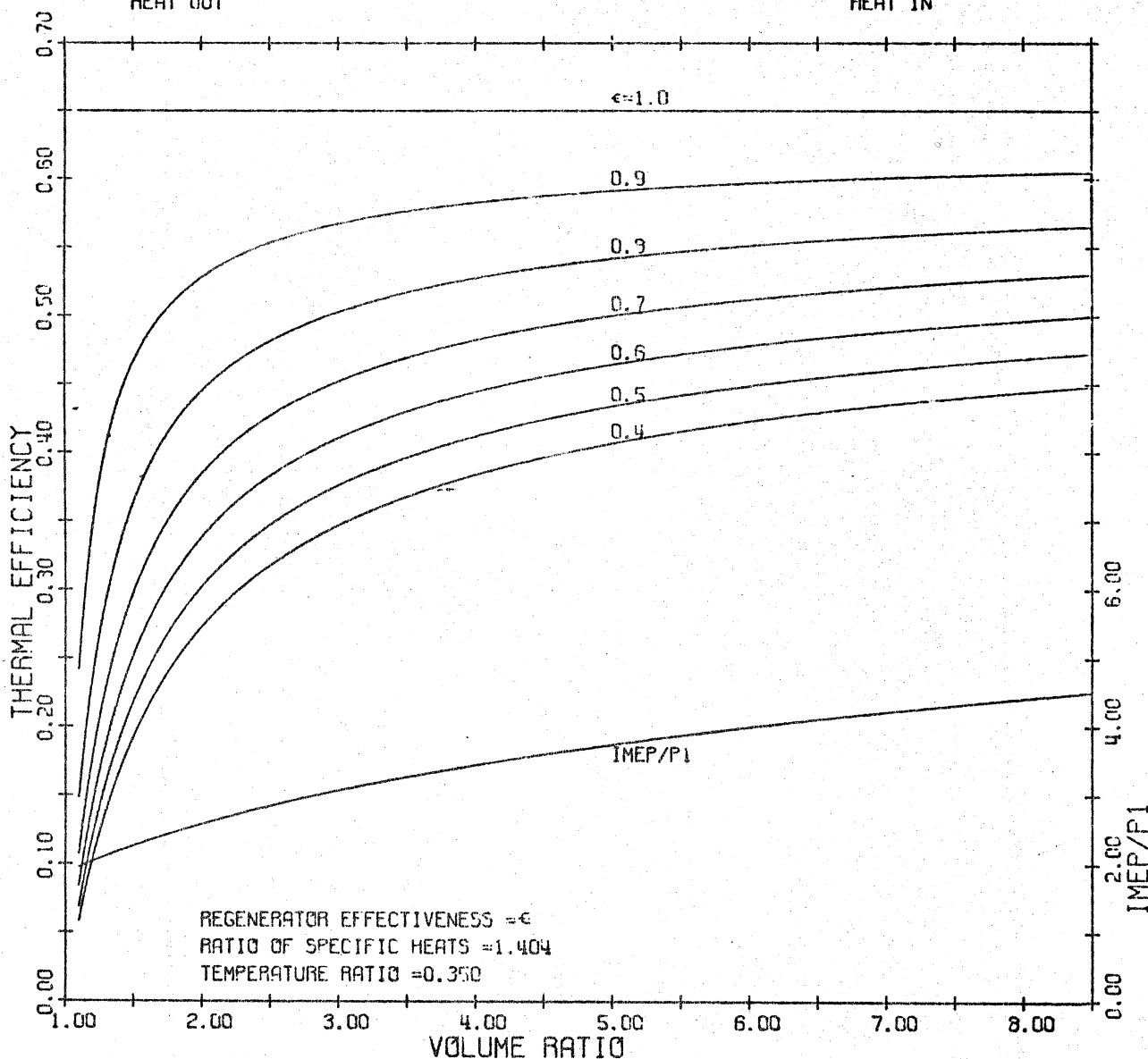
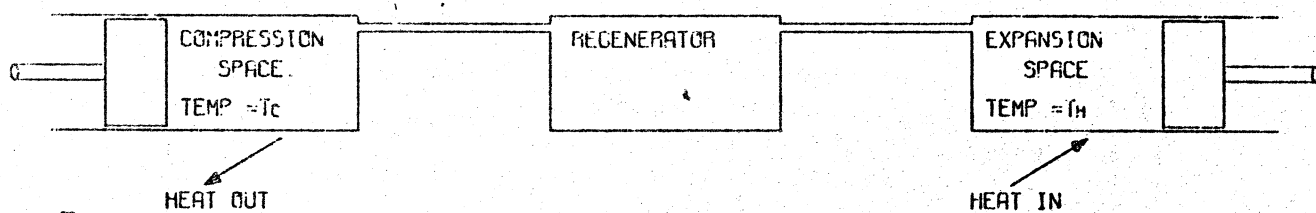
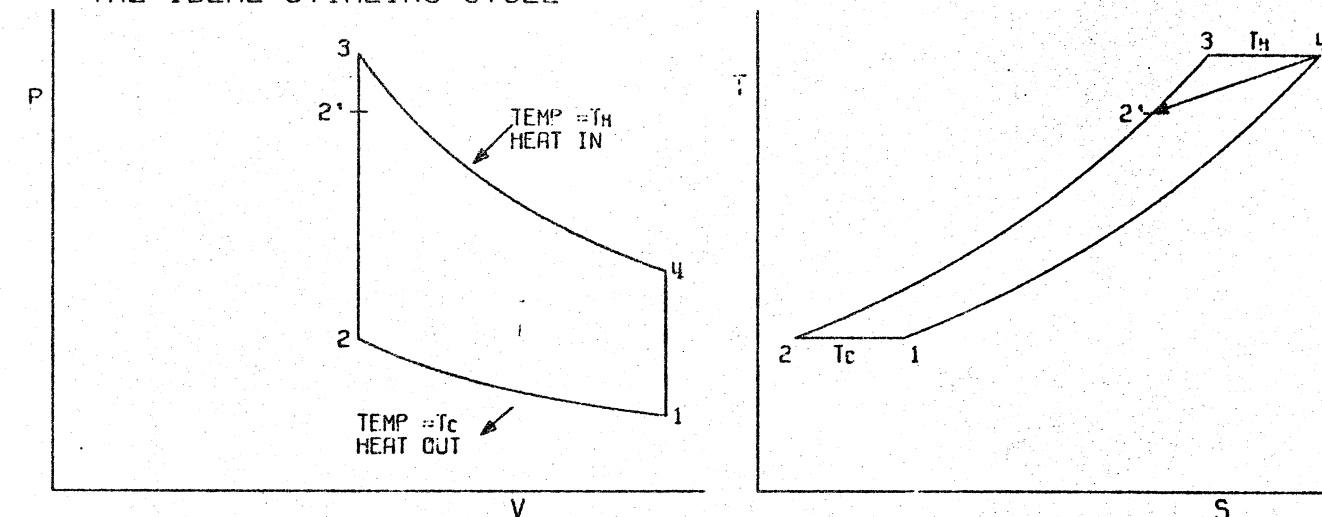


Figure C.1 THE IDEAL STIRLING CYCLE

The volume compression ratio r is defined as follows:

$$r \triangleq V_1/V_2 = V_4/V_3 \quad (\text{C.1})$$

where V_i is the volume of the working gas at state i .

The regenerator effectiveness ϵ is defined as follows:

$$\epsilon \triangleq (T_2' - T_1)/(T_3 - T_1) \quad (\text{C.2})$$

where T_i is the temperature at state i . It is noticed that T_1 is unity, being the cold sink temperature.

The thermal efficiency η is defined as follows:

$$\eta \triangleq W/Q_{ext}$$

where

W is the net external work done per cycle

Q_{ext} is the heat supplied externally per cycle

For the isothermal compression and expansion

$$W = T_3 \cdot \ln r - \ln r$$

$$W = (T_3 - 1) \ln r \quad (\text{C.4})$$

Heat is supplied externally during the processes 2'-3-4.

Thus

$$Q_{ext} = c_v(T_3 - T_2') + T_3 \cdot \ln r$$

where $c_v = 1/(\gamma-1)$ is the specific heat capacity at constant volume of the working fluid.

From equation (C.2):

$$T_2' = \epsilon T_3 + (1-\epsilon) T_1 \quad (C.6)$$

(C.6) → (C.5)

$$Q_{ext} = c_v(1-\epsilon)(T_3-1) + T_3 \ln r$$

$$Q_{ext} = (1-\epsilon)(T_3-1)/(\gamma-1) + T_3 \ln r \quad (C.7)$$

(C.7), (C.4) → (C.3):

$$\eta = \frac{(\gamma-1)(T_3-1)\ln r}{(1-\epsilon)(T_3-1) + (\gamma-1)T_3 \ln r} \quad (C.8)$$

The specific work output for this cycle may be represented by the indicated mean effective pressure, defined by

$imep \triangleq W/\text{stroke volume}$

$$imep = W/(V_1 - V_2) \quad (C.9)$$

(C.4), (C.1) → (C.9):

$$imep = (T_3-1)\ln r / V_1(1-1/r) \quad (C.10)$$

However, from the perfect gas equation of state

$$p_1 \cdot V_1 = 1 \quad (C.11)$$

(C.11)→(C.10)

$$\text{imep}/p_1 = (T_3-1)r \cdot \ln r / (r-1) \quad (\text{C.12})$$

where imep/p_1 is the normalized dimensionless indicated mean effective pressure.

Figure C.1 shows thermal efficiency η and dimensionless specific work (imep/p_1) plotted as functions of the volume compression ratio r for a range of values of regenerator effectiveness ϵ in a typical practical case where $T_3 = 2,86$ and $\gamma = 1,404$.

It is noted that for such an ideal Stirling cycle both η and imep/p_1 increase with increasing compression ratio r . Thus it would appear advantageous to operate such a cycle at as high a value of r as is practically possible. Apparently however actual machines are restricted to compression ratios not exceeding 2,5 to 1. It is noteworthy in this context that spark-ignition and compression-ignition engines -- with similar ideal η vs r characteristics -- are advantageously operated in the range of 8:1 to 20:1. Although admittedly oversimplified, such arguments inevitably suggest that there may be a discrepancy between the theoretical Stirling cycle model used in the foregoing and its practical realization.

Evidently in actual Stirling cycle machines the rapidity with which the working medium is shuttled back and forth, together with the finite heat transfer rates, give rise to a separating out of the compression, or expansion, and the heat transfer processes. It is thus not unreasonable to suppose that both compression and expansion occur polytropically and in the limit tend to adiabatic processes.

This leads to the postulation of an ideal pseudo-Stirling cycle as defined below.

C.3 THE IDEAL PSEUDO-STIRLING CYCLE

The processes 1-2-2''-2'-3-4-4'-1 in the pV and Ts diagrams of figure C.2 serve to define the so-called pseudo-Stirling cycle. This idealized cycle follows as a consequence of the in-line arrangement of the cooler, regenerator, and heater, placed between the compression and expansion spaces -- in which the working gas is said to undergo polytropic processes.

In the limiting case where both processes 3-4 and 1-2 are adiabatic

$$W = cv[(T_3 - T_4) - (T_2 - T_1)] \quad (C.13)$$

$$T_2 = r^{\gamma-1} T_1 \quad (C.14)$$

$$T_3 = r^{\gamma-1} T_4 \quad (C.15)$$

(C.14), (C.15) + (C.13):

$$W = cv[T_3(1 - 1/r^{\gamma-1}) - r^{\gamma-1} T_1 + T_1] \quad (C.16)$$

Now

$$Q_{ext} = cv(T_3 - T_2') + cv(T_4' - T_4) \quad (C.17)$$

However $T_4' = T_3$

(C.6), (C.15) + (C.17):

THE PSEUDO-STIRLING CYCLE

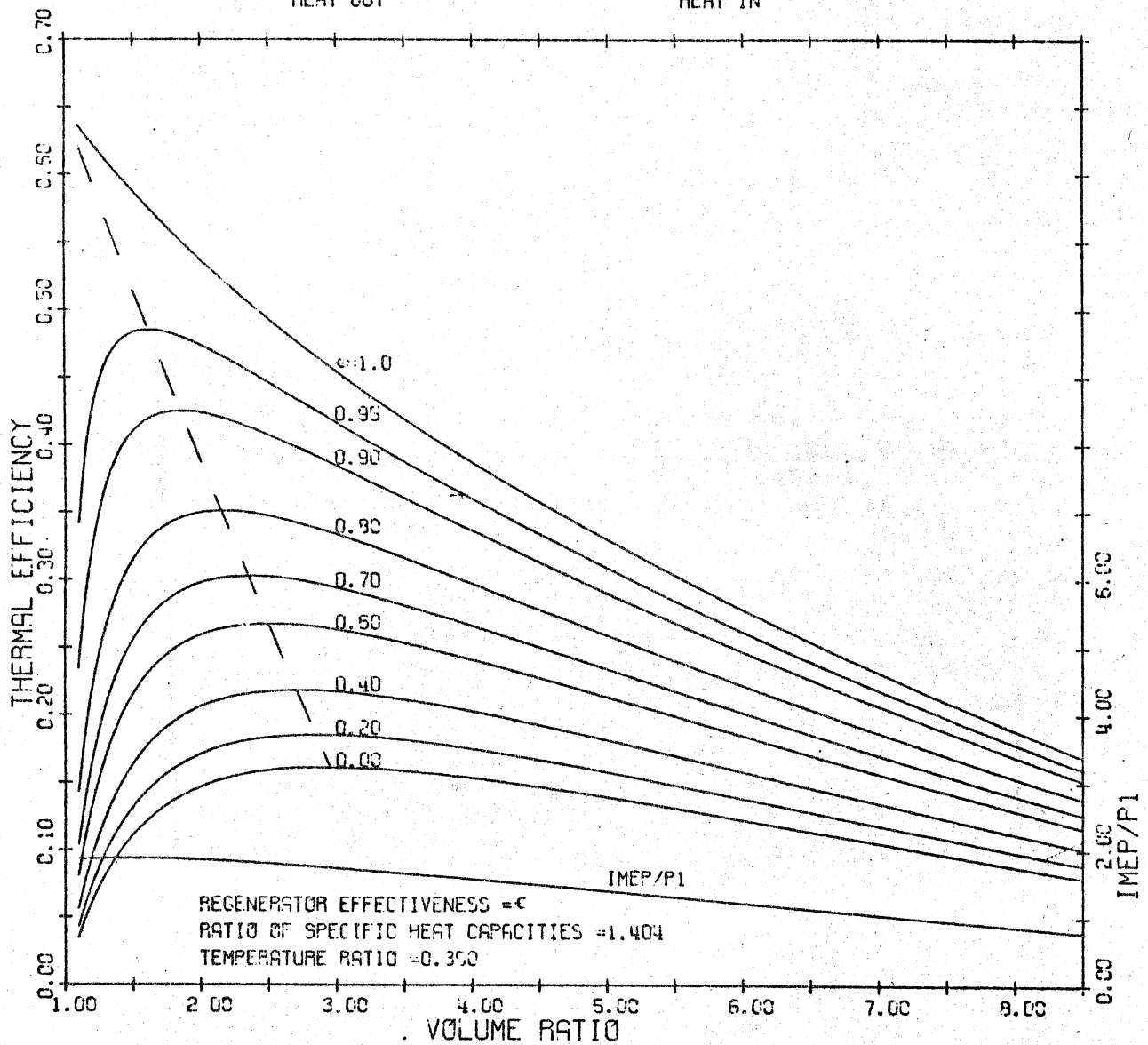
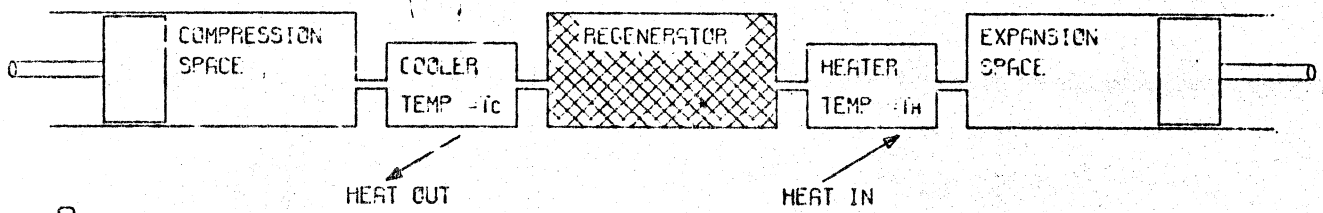
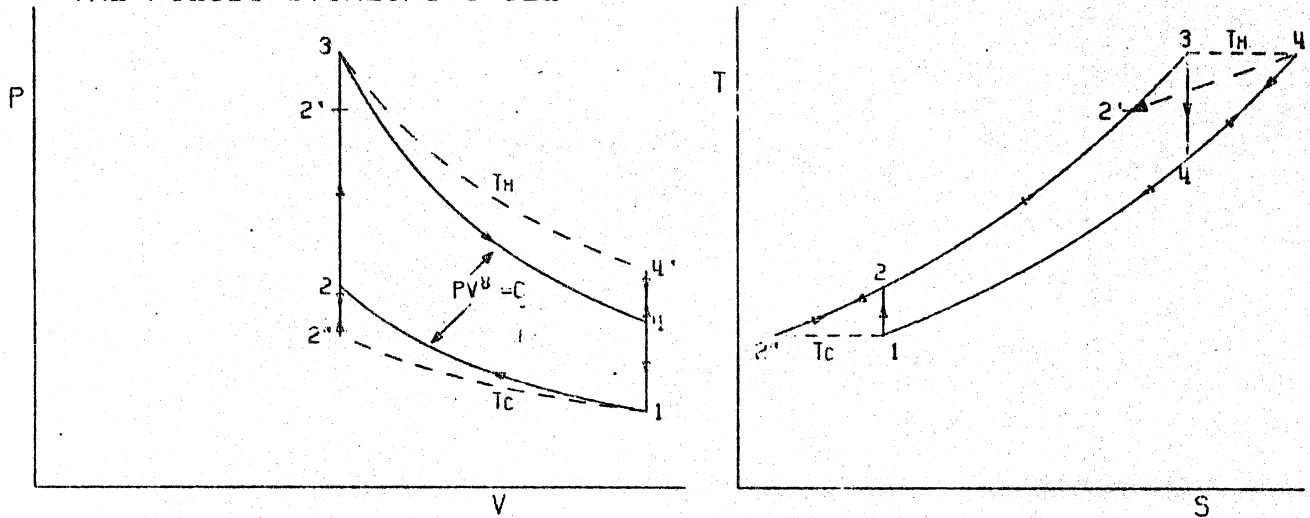


Figure C.2 THE PSEUDO-STIRLING CYCLE

$$Q_{ext} = cv[(T_3-1)(1-\epsilon)+T_3(1-1/r^{\gamma-1})] \quad (C.18)$$

(C.18), (C.16) → (C.3)

$$\eta = \frac{T_3(1-1/r^{\gamma-1})-r^{\gamma-1}+1}{(T_3-1)(1-\epsilon)+T_3(1-1/r^{\gamma-1})} \quad (C.19)$$

The indicated mean effective pressure is given by
(C.16) → (C.9):

$$imep = [T_3(1-1/r^{\gamma-1})-r^{\gamma-1}+1]/(\gamma-1)(V_1-V_2) \quad (C.20)$$

(C.1) → (C.20):

$$imep = [T_3(1-1/r^{\gamma-1})-r^{\gamma-1}+1]/V_1(\gamma-1)(1-\frac{1}{r}) \quad (C.21)$$

(C.11) → (C.21):

$$imep/p_1 = r[T_3(1-1/r^{\gamma-1})-r^{\gamma-1}+1]/(\gamma-1)(r-1) \quad (C.22)$$

Figure C.2 shows the thermal efficiency η and dimensionless specific work $imep/p_1$ plotted as functions of the compression ratio r for a range of values of regenerator effectiveness ϵ and the same typical values of $T_3 = 2,86$ and $\gamma = 1,404$ as were used in figure C.1.

Unlike the ideal Stirling cycle case, here both the thermal efficiency and the dimensionless specific work curves exhibit maxima at finite, and low, values of compression ratio r . The optimum value of r for maximum efficiency is evidently a function of regenerator effectiveness but, for all practically realizable values of ϵ , is close to about 2 to 1.

Thus, in contradistinction to the ideal Stirling cycle, it is detrimental to operate the pseudo-Stirling cycle at large compression ratios. This is one of the few cases of engine optimization in which both the specific work and thermal efficiency peak at approximately the same point, thus necessitating little compromise.

C.4 THE IDEAL PORTED REGENERATIVE CONSTANT VOLUME CYCLE

Referring to the ideal pseudo-Stirling cycle (figure C.2) it seems intuitively wasteful to cool the working gas in the cooler after heating it by compression, and similarly to heat the gas, after cooling by expansion. Thus it was decided to examine the advantages to be gained by porting the gas in order to bypass these processes. This has been heuristically discussed by Finkelstein (Fi53) who presented a design of a ported regenerative constant volume engine. However no analysis of the effect of this porting has been published.

The ideal ported regenerative constant volume cycle is defined by the processes 1-2-3-4-1 as shown by the pV and Ts diagrams in figure C.3. The work done per cycle W is identical to that of the ideal pseudo-Stirling cycle, however heat is supplied externally only during process 2'-3.

Equation (C.2) for regenerator effectiveness ϵ has to be modified, since the working fluid bypasses the heater and cooler before entering the regenerator.

Thus

$$\epsilon \triangleq (T2' - T2) / (T4 - T2)$$

$$T2' = \epsilon(T4 - T2) + T2 \tag{C.23}$$

THE PORTED REGENERATIVE CONSTANT VOLUME CYCLE

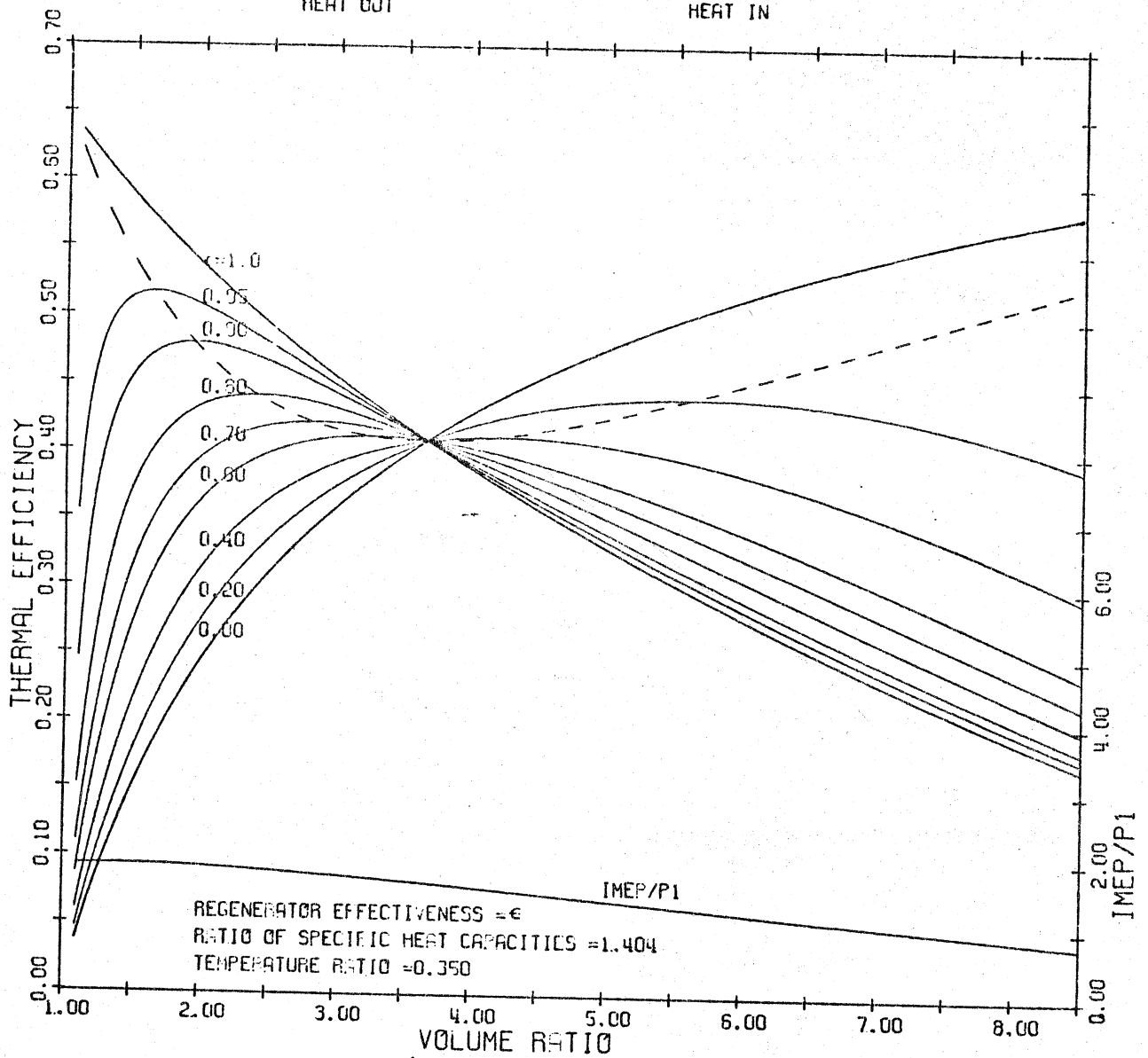
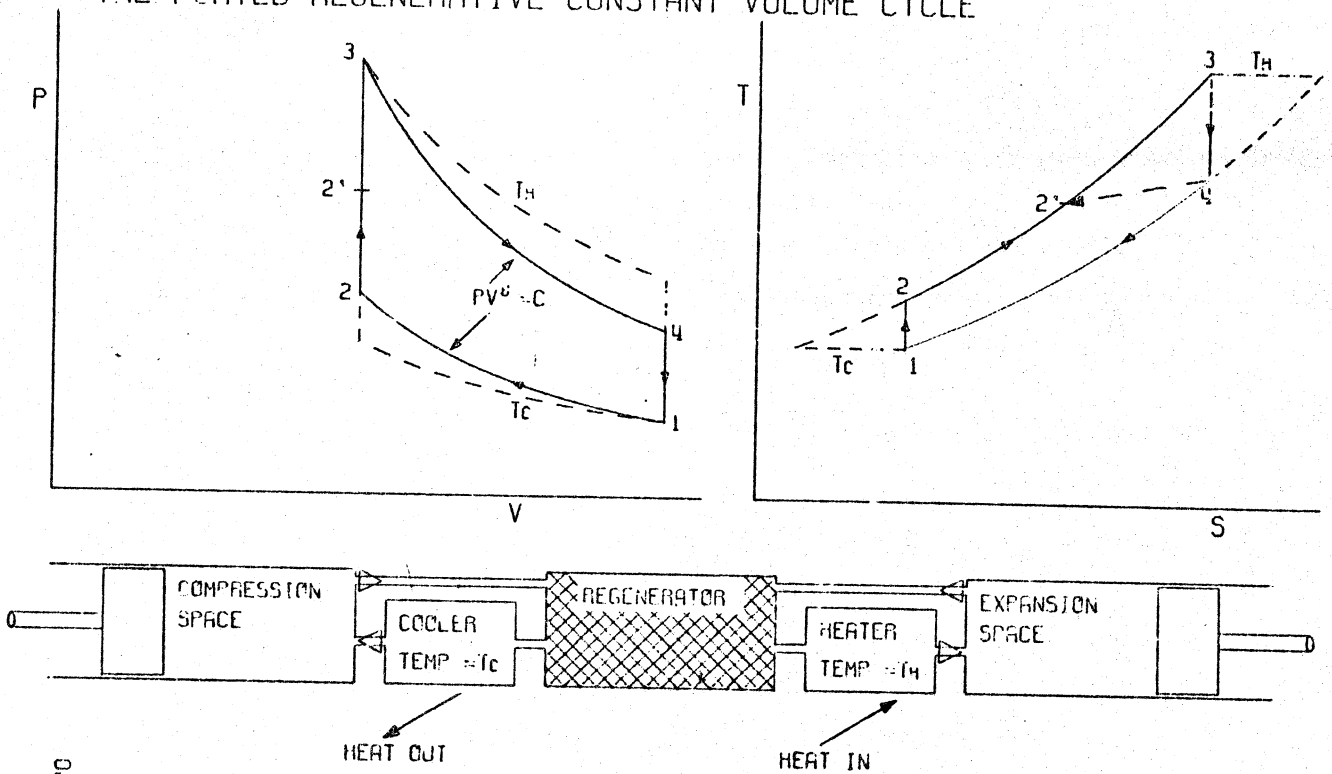


Figure C.3 THE PORTED REGENERATIVE CONSTANT VOLUME CYCLE

(C.14), (C.15) → (C.23):

$$T2' = \epsilon(T3/r^{\gamma-1} - r^{\gamma-1}) + r^{\gamma-1}$$

$$T2' = \epsilon T3/r^{\gamma-1} + r^{\gamma-1}(1 - \epsilon) \quad (C.24)$$

Now

$$Q_{ext} = cv(T3 - T2') \quad (C.25)$$

(C.24) → (C.25):

$$Q_{ext} = cv[T3(1 - \epsilon/r^{\gamma-1}) + r^{\gamma-1}(1 - \epsilon)] \quad (C.26)$$

(C.26), (C.16) → (C.3):

$$\eta = \frac{T3(1 - 1/r^{\gamma-1}) - r^{\gamma-1} + 1}{T3(1 - \epsilon/r^{\gamma-1}) + r^{\gamma-1}(1 - \epsilon)} \quad (C.27)$$

The expression for imep/p1 is identical to that of the ideal pseudo-Stirling cycle and is given by equation (C.22).

In figure C.3 the thermal efficiency η and imep/p1 are shown plotted as a function of the compression ratio r , for a range of values of regenerator effectiveness ϵ and the same typical values of $T3 = 2,86$ and $\gamma = 1,404$ as were used in figure C.2.

It is found that under all conditions the efficiency for the ideal ported regenerative constant volume cycle is higher than that of the ideal pseudo-Stirling cycle. Also it is seen that for high values of regenerator effectiveness, low compression ratios give optimum thermal efficiency.

However, it is noticed that a crossover value of compression ratio r exists, above which it is detrimental to use a regenerator. This occurs at the compression ratio at which the inlet temperature to the regenerator at the cold end T_2 is equal to the inlet temperature to the regenerator at the hot end T_4 .

It is found that in the limit when the regenerator effectiveness equals zero (ie, no regenerator) then the system has been reduced to the air standard constant volume (Otto) cycle, in which the thermal efficiency increases monotonically with increasing compression ratio.

C.5 CONCLUSION

Simplified analyses based on the ideal Stirling cycle give misleading results when applied to the component configurations generally used in practical machines. A more realistic model, based on polytropic compression and expansion of the working medium, leads to a so-called pseudo-Stirling cycle which appears to explain the apparent anomaly of the low compression ratios used in practice. It also provides a theoretical basis for choosing the optimum compression ratio for any specific system.

It is found that on modifying the ideal pseudo-Stirling cycle by the inclusion of valves or ports a distinct increase in thermal efficiency results. Also the relative reduction in thermal efficiency with reduction in regenerator effectiveness is not as pronounced as in the ideal pseudo-Stirling cycle. For high values of regenerator effectiveness the advantage of obtaining maximum thermal efficiency

together with maximum specific power output at low values of compression ratio is retained.

The introduction of check valves or ports is not a major complication since the pressure differences across the valves are slight, being due entirely to aerodynamic friction pressure drops.

D. THE FUNDAMENTAL EQUATIONS -- CONTINUITY, MOMENTUM, ENERGY

D.1 INTRODUCTION

In this appendix the fundamental equations of continuity, momentum and energy for the working gas are developed from first principles. These equations are applied to the cellular model in Appendix H in order to develop the system algorithms for solution.

An arbitrary control volume V within the flowing working gas is considered (Figure D.1).

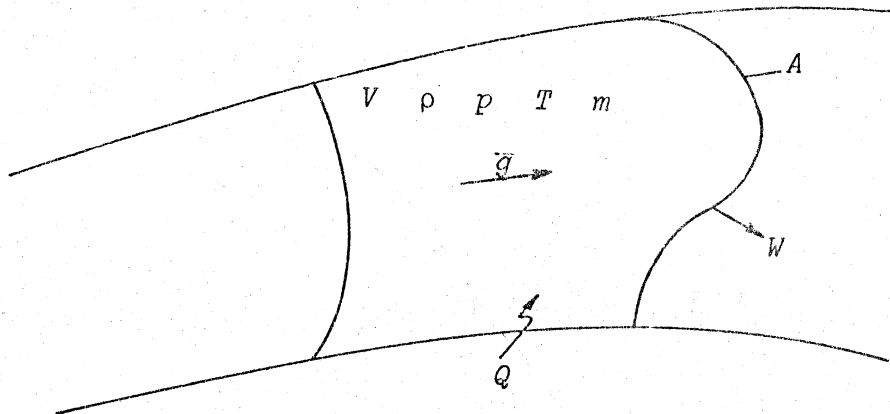


Figure D.1 CONTROL VOLUME V

Each infinitesimal element in the control volume V is represented by its density ρ (or specific volume v), pressure p , temperature T and momentum per unit volume \bar{g} (a superscripted bar indicates a vector quantity). The control volume is in an Eulerian framework in that it has

D.2 CONTINUITY

The continuity equation is based on the axiom that matter cannot be created or destroyed. Its word formulation as applied to a fluid in an Eulerian framework is as follows:

$$\left\{ \begin{array}{l} \text{rate of decrease of mass} \\ \text{in control volume } V \end{array} \right\} = \left\{ \begin{array}{l} \text{net mass flux convected} \\ \text{outwards through control} \\ \text{surface } A \end{array} \right\}$$

$$-\frac{\partial}{\partial t} \int_V \rho dV = \oint_A \rho (\bar{g} \cdot \bar{v}) \cdot \bar{N} dA \quad (\text{D.1})$$

where

ρ is the density, being the major operand

$\bar{g} \cdot \bar{v}$ is the velocity \bar{U} , being the convective factor

\bar{N} is the normal to the control surface A .

Invoking Gauss' theorem (Ar70)

$$\oint_A \bar{g} \cdot \bar{N} dA = \int_V \nabla \cdot \bar{g} dV \quad (\text{D.2})$$

where ∇ is the divergence operator when the operand is a vector, and the gradient operator when the operand is a scalar, being the vector partial differential operator in the three spacial coordinates.

(D.2) → (D.1)

$$-\frac{\partial}{\partial t} \int_V \rho dV = \int_V \nabla \cdot \bar{g} dV \quad (\text{D.3})$$

at least one point on the bounding control surface A which is in a fixed position relative to the spacial coordinate system, however it may vary in magnitude with time. Thus the momentum per unit volume \bar{g} assumes the role of a mass flux density while crossing the bounding control surface A , transporting matter, energy and momentum flux into and out of the control volume V . Energy in the form of heat Q crosses the control surface A , and mechanical work W is done by the control volume V on the surrounding environment by virtue of its volume variation with time or as shaft work.

The working gas is assumed to be Newtonian, and the nonlinear variation of its dynamic viscosity μ with temperature is considered (refer to Appendix E). It is assumed that the working gas behaves as a perfect gas and that its dynamic viscosity does not vary with pressure. This is not, however, a fundamental limitation of the method of analysis or solution, and the nonlinear behaviour of any of the parameters can be included if required.

The fundamental equations of continuity, momentum and energy are initially derived in the three spacial coordinates, however they are all subsequently reduced to the one-dimensional case. In order to account for the strictly three-dimensional effects of turbulence in the one-dimensional system, empirical correlations are invoked to determine the heat transfer and flow friction behaviour of the working gas with respect to its surroundings (refer to Appendix F).

It is assumed that the control volume is chosen such that either all the working gas properties are uniform and constant in space throughout the control volume, or that it is small enough such that all the fluid properties can be adequately represented throughout the control volume by their mean values. Thus in equation (D.3) the variables are independent of the volume integration.

$$-\frac{\partial}{\partial t}[\rho \bar{f}_V dV] = \nabla \cdot \bar{g} \bar{f}_V dV$$

$$\frac{\partial}{\partial t}[\rho V] + V \nabla \cdot \bar{g} = 0$$

$$\frac{\partial m}{\partial t} + V \nabla \cdot \bar{g} = 0$$

(D.4)

where m is the instantaneous total mass of working gas contained within the control volume V .

Reducing equation (D.4) to the one-dimensional case one obtains:

$$\frac{\partial m}{\partial t} + V \frac{\partial g}{\partial x} = 0$$

(D.5)

Equation (D.5) is the final form of the continuity equation to be used in this work.

D.3 MOMENTUM

The momentum equation is based on Newton's second law of motion -- that the rate of change of momentum of a body is proportional to the net applied force. In an Eulerian framework it is necessary to consider not only the net applied force but the momentum flux

convected through the control volume as well. Its word formulation is as follows:

$$\left\{ \begin{array}{l} \text{rate of change of} \\ \text{momentum within the} \\ \text{control volume } V \end{array} \right\} + \left\{ \begin{array}{l} \text{net momentum flux convected} \\ \text{outwards through the control} \\ \text{surface } A \end{array} \right\}$$

$$= \left\{ \begin{array}{l} \text{net force (body and surface)} \\ \text{acting on the fluid in the} \\ \text{control volume } V \end{array} \right\}$$

$$\frac{\partial}{\partial t} \int_V \bar{g} dV + \oint_A \bar{g} (\bar{g} \cdot \nu) \cdot \bar{N} dA = - \oint_A p \bar{N} dA - \bar{F} \quad (\text{D.6})$$

where

\bar{g} is the momentum/unit volume, being the major operand

$\bar{g} \cdot \nu$ is the velocity \bar{U} , being the convective factor

\bar{F} is the frictional drag force.

It is noted in equation (D.6) that the only forces that have been considered are surface forces -- being the normal pressure force and the shear frictional drag. Body forces such as gravitational, centripetal, magnetic and electrical forces have been neglected as irrelevant to the class of problems that are treated. The frictional drag force can be determined analytically only for laminar flow in a known simple geometry (KL64). In general empirical correlations are used for its evaluation (refer to Appendix F).

Invoking Gauss' theorem on equation (D.6)

$$\frac{\partial}{\partial t} \int_V \bar{g} dV + \int_V \nabla(\bar{g}^2 v) dV + \int_V \nabla p dV + \bar{F} = 0 \quad (\text{D.7})$$

It has been noted previously that the fluid parameters are considered to be either constant or represented by their mean values throughout the control volume V .

$$\frac{\partial}{\partial t} (\bar{g} \cdot V) + V \nabla(\bar{g}^2 v) + V \nabla p + \bar{F} = 0 \quad (\text{D.8})$$

Reducing equation (D.8) to the one dimensional case

$$\frac{\partial}{\partial t} (g \cdot V) + V \frac{\partial}{\partial x} (g^2 v) + V \frac{\partial p}{\partial x} + F = 0 \quad (\text{D.9})$$

Equation (D.9) represents the final form of the momentum equation of the working gas to be used in this work.

D.4 ENERGY

The energy equation is based upon the first law of thermodynamics -- that energy cannot be created or destroyed. In the Eulerian framework the formulation of the energy equation is as follows:

$$\left. \begin{array}{l} \text{rate of heat transferred} \\ \text{to the working gas from} \\ \text{the environment through} \\ \text{control surface } A \end{array} \right\} = \left. \begin{array}{l} \text{rate of energy} \\ \text{accumulation} \\ \text{within the control} \\ \text{volume } V \end{array} \right\}$$

$$+ \left. \begin{array}{l} \text{net energy flux} \\ \text{convected outwards by} \\ \text{the working gas crossing} \\ \text{the control surface } A \end{array} \right\} + \left. \begin{array}{l} \text{net rate of flow} \\ \text{work in pushing the} \\ \text{mass of working gas through} \\ \text{the control surface } A \end{array} \right\}$$

+ $\left\{ \begin{array}{l} \text{net rate of mechanical work done by} \\ \text{the working gas on the environment by} \\ \text{virtue of the rate of change of the} \\ \text{magnitude of the control volume } V \end{array} \right\}$

+ $\left\{ \begin{array}{l} \text{net rate of shaft work done by the} \\ \text{working gas on the environment by} \\ \text{virtue of the rotation of a shaft} \\ \text{crossing the control surface } A \end{array} \right\}$

The shaft work term is neglected as irrelevant to the class of systems that are to be treated.

$$\frac{dQ}{dt} = \frac{\partial}{\partial t} \int_V [u + (\bar{g} \cdot v)^2 / 2] \rho dV + \oint_A [u + (\bar{g} \cdot v)^2 / 2] \rho (\bar{g} \cdot v) \cdot \bar{N} dA + \oint_A p (\bar{g} \cdot v) \cdot \bar{N} dA + \frac{dW}{dt} \quad (\text{D.10})$$

where

u is the specific internal energy of the working gas.

$(\bar{g} \cdot v)$ is the velocity \bar{u} , being the convective factor.

$(\bar{g} \cdot v)^2 / 2$ is the specific kinetic energy of the working gas.

$[u + (\bar{g} \cdot v)^2 / 2] \rho$ is the energy per unit volume of the working gas, being the major operand.

It is noted that the working gas energy is assumed to consist of internal energy and kinetic energy only. Potential, chemical, nuclear, and all other possible forms of fluid energy have been considered as being irrelevant to

the class of systems that are treated. It is also noted that the total time derivative is taken of the heat transferred Q and the mechanical work done W . This is because Q and W are path functions and not properties of the working gas, and only their global values crossing the control surface A from the external environment are considered.

Collecting terms in equation (D.10)

$$\frac{dQ}{dt} = \frac{\partial}{\partial t} \int_V [u + (\bar{g} \cdot v)^2 / 2] \rho dV + \oint_A [(u + p \cdot v) + (\bar{g} \cdot v)^2 / 2] \bar{g} \cdot \bar{N} dA + \frac{dW}{dt} \quad (D.11)$$

Invoking Gauss' theorem on equation (D.11)

$$\frac{dQ}{dt} = \frac{\partial}{\partial t} \int_V [u + (\bar{g} \cdot v)^2 / 2] \rho dV + \int_V \nabla \cdot [e + (\bar{g} \cdot v)^2 / 2] \bar{g} dV + \frac{dW}{dt} \quad (D.12)$$

where $e \triangleq u + p \cdot v$ is the specific enthalpy of the working gas.

The fluid parameters are considered to be either constant or represented by their mean values throughout the control volume V .

$$\frac{dQ}{dt} = \frac{\partial}{\partial t} [u \rho V + \rho V (\bar{g} \cdot v)^2 / 2] + V \nabla \cdot [e + (\bar{g} \cdot v)^2 / 2] \bar{g} + \frac{dW}{dt}$$

$$\frac{dQ}{dt} = \frac{\partial}{\partial t} [m \cdot u + m (\bar{g} \cdot v)^2 / 2] + V \nabla \cdot [e + (\bar{g} \cdot v)^2 / 2] \bar{g} + \frac{dW}{dt} \quad (D.13)$$

For a perfect gas

$$u = T / (\gamma - 1) \quad (D.14)$$

$$e = \gamma T / (\gamma - 1) \quad (D.15)$$

where

$1/(\gamma-1)$ is the normalized specific heat capacity of the working gas at constant volume

$\gamma/(\gamma-1)$ is the normalized specific heat capacity of the working gas at constant pressure

(D.14), (D.15) \rightarrow (D.13)

$$\frac{dQ}{dt} = \frac{\partial}{\partial t} \left[\frac{m \cdot T}{(\gamma-1)} + m(\bar{g} \cdot v)^2 / 2 \right] + V \nabla \cdot \left[\frac{\gamma T \cdot \bar{g}}{(\gamma-1)} + \bar{g}(\bar{g} \cdot v)^2 / 2 \right] + \frac{dW}{dt} \quad (D.16)$$

Reducing equation (D.16) to the one-dimensional case and expanding

$$\frac{dQ}{dt} = \frac{\partial}{\partial t} \left[\frac{m \cdot T}{(\gamma-1)} + m(g \cdot v)^2 / 2 \right] + V \frac{\partial}{\partial x} \left[\frac{\gamma T \cdot g}{(\gamma-1)} + g(g \cdot v)^2 / 2 \right] + \frac{dW}{dt}$$

$$\frac{dQ}{dt} = \frac{\partial}{\partial t} \left(\frac{m \cdot T}{\gamma-1} \right) + V \frac{\partial}{\partial x} \left(\frac{\gamma T \cdot g}{\gamma-1} \right) + \frac{\partial}{\partial t} [m(g \cdot v)^2 / 2] + V \frac{\partial}{\partial x} [g(g \cdot v)^2 / 2] + \frac{dW}{dt}$$

$$\frac{dQ}{dt} = \frac{\partial}{\partial t} \left(\frac{m \cdot T}{\gamma-1} \right) + V \frac{\partial}{\partial x} \left(\frac{\gamma T \cdot g}{\gamma-1} \right) + \frac{\partial}{\partial t} [(g \cdot v)^2 / 2m] + V \frac{\partial}{\partial x} [g(g \cdot v)^2 / 2] + \frac{dW}{dt}$$

$$\frac{dQ}{dt} = \frac{\partial}{\partial t} \left(\frac{m \cdot T}{\gamma-1} \right) + V \frac{\partial}{\partial x} \left(\frac{\gamma T \cdot g}{\gamma-1} \right) + g \cdot v \frac{\partial}{\partial t} (g \cdot v) - \frac{(g \cdot v)^2}{2} \frac{\partial m}{\partial t}$$

$$+ V \frac{\partial}{\partial x} [g(g \cdot v)^2 / 2] + \frac{dW}{dt} \quad (D.17)$$

Substituting for the momentum equation (D.9) and the continuity equation (D.5) into the energy equation (D.17) and simplifying

$$\begin{aligned} \frac{dQ}{dt} = & \frac{\partial}{\partial t} \left(\frac{m \cdot T}{\gamma-1} \right) + V \frac{\partial}{\partial x} \left(\frac{\gamma T \cdot g}{\gamma-1} \right) - g \cdot m \cdot v^2 \left[\frac{\partial}{\partial x} (g^2 v) + \frac{\partial p}{\partial x} \right] - g \cdot v \cdot F \\ & + \frac{(g \cdot v)^2}{2} V \frac{\partial g}{\partial x} + V \frac{\partial}{\partial x} [g(g \cdot v)^2 / 2] + \frac{dW}{dt} \end{aligned}$$

$$\frac{dQ}{dt} = \frac{\partial}{\partial t} \left(\frac{m \cdot T}{\gamma - 1} \right) + V \frac{\partial}{\partial x} \left(\frac{\gamma T \cdot g}{\gamma - 1} \right) - g \cdot v \left(V \frac{\partial p}{\partial x} + F \right) + \frac{dW}{dt} - g \cdot m \cdot v^2 \frac{\partial}{\partial x} (g^2 v) \\ + \frac{g^2 m \cdot v^3}{2} \frac{\partial g}{\partial x} + \frac{m \cdot v}{2} \frac{\partial}{\partial x} (g^3 v^2)$$

$$\frac{dQ}{dt} = \frac{\partial}{\partial t} \left(\frac{m \cdot T}{\gamma - 1} \right) + V \frac{\partial}{\partial x} \left(\frac{\gamma T \cdot g}{\gamma - 1} \right) - g \cdot v \left(V \frac{\partial p}{\partial x} + F \right) + \frac{dW}{dt} - g^3 m \cdot v^2 \frac{\partial v}{\partial x} \\ - 2g^2 m \cdot v^3 \frac{\partial g}{\partial x} + \frac{g^2 m \cdot v^3}{2} \frac{\partial g}{\partial x} + m \cdot v^2 g^3 \frac{\partial v}{\partial x} + \frac{3m \cdot v^3 g^2}{2} \frac{\partial g}{\partial x}$$

$$\frac{dQ}{dt} = \frac{\partial}{\partial t} \left(\frac{m \cdot T}{\gamma - 1} \right) + V \frac{\partial}{\partial x} \left(\frac{\gamma T \cdot g}{\gamma - 1} \right) - g \cdot v \left(V \frac{\partial p}{\partial x} + F \right) + \frac{dW}{dt} \quad (\text{D.18})$$

Equation (D.18) represents the final form of the energy equation of the working gas to be used in this work.

If the kinetic energy of the working gas is ignored in the initial formulation of the energy equation (D.10) then equation (D.18) reduces to

$$\frac{dQ}{dt} = \frac{\partial}{\partial t} \left(\frac{m \cdot T}{\gamma - 1} \right) + V \frac{\partial}{\partial x} \left(\frac{\gamma T \cdot g}{\gamma - 1} \right) + \frac{dW}{dt} \quad (\text{D.19})$$

Thus the only manifestation of the kinetic energy term in the energy equation is in the term $g \cdot v (V \partial p / \partial x + F)$. However on examining the momentum equation (D.9) it is seen that the term $(V \partial p / \partial x + F)$ represents the net applied force to the working gas in the control volume, $V \partial p / \partial x$ being the normal pressure force and F being the frictional drag. One thus comes to the important conclusion that ignoring the kinetic energy of the fluid is consistent with reducing the system to a quasi-steady state, in which the momentum equation (D.9) is reduced to

$$V \frac{dp}{dx} + F = 0 \quad (\text{D.20})$$

D.5 THE FUNDAMENTAL SYSTEMS OF EQUATIONS

From the above arguments three systems of fundamental equations governing the working gas in the control volume V are obtained:

- (i) The kinetic energy of the working gas is not negligible as compared with the internal energy of the working gas:

$$\frac{\partial m}{\partial t} + V \frac{\partial g}{\partial x} = 0 \quad (\text{D.5})$$

$$\frac{\partial}{\partial t}(g \cdot V) + V \frac{\partial}{\partial x}(g^2 v) + V \frac{\partial p}{\partial x} + F = 0 \quad (\text{D.9})$$

$$\frac{dQ}{dt} = \frac{\partial}{\partial t} \left(\frac{m \cdot T}{\gamma - 1} \right) + V \frac{\partial}{\partial x} \left(\frac{\gamma T \cdot g}{\gamma - 1} \right) + \frac{dW}{dt} - g \cdot v \left(V \frac{\partial p}{\partial x} + F \right) \quad (\text{D.18})$$

- (ii) The kinetic energy of the working gas can be ignored with respect to the internal energy of the working gas:

$$\frac{\partial m}{\partial t} + V \frac{\partial g}{\partial x} = 0 \quad (\text{D.5})$$

$$V \frac{dp}{dx} + F = 0 \quad (\text{D.20})$$

$$\frac{dQ}{dt} = \frac{\partial}{\partial t} \left(\frac{m \cdot T}{\gamma - 1} \right) + V \frac{\partial}{\partial x} \left(\frac{\gamma T \cdot g}{\gamma - 1} \right) + \frac{dW}{dt} \quad (\text{D.19})$$

(iii) The working gas motion is so slow that there is a negligible pressure drop throughout the system. In this case the momentum equation drops out altogether:

$$\frac{\partial m}{\partial t} + v \frac{\partial g}{\partial x} = 0 \quad (\text{D.5})$$

$$\frac{dQ}{dt} = \frac{\partial}{\partial t} \left(\frac{m \cdot T}{\gamma - 1} \right) + v \frac{\partial}{\partial x} \left(\frac{\gamma T \cdot g}{\gamma - 1} \right) + \frac{dW}{dt} \quad (\text{D.19})$$

E. TRANSPORT PROPERTIES - VISCOSITY, THERMAL CONDUCTIVITY

E.1 INTRODUCTION

The most important contributing factors to the non-ideal performance of Stirling cycle machines are the working gas pressure drop due to flow friction and the limited finite heat exchange with the external environment. Both of these phenomena have their roots in the transport properties of the fluid, specifically its internal friction (or viscosity) and thermal conductivity. Basically each molecule of the working gas, being in random motion and colliding with other molecules, transfers its momentum (the phenomenon of viscosity) and its kinetic energy (the phenomenon of heat conduction).

E.2 DYNAMIC VISCOSITY

Throughout this work it has been exclusively assumed that the working gas is Newtonian, ie, the shear stress between adjacent layers of working gas is proportional to the velocity gradient in these layers normal to flow direction. This leads to the definition of the dynamic viscosity μ given by the so-called Newton's law of viscosity (Br71):

$$\sigma = -\mu \frac{dU}{dz}$$

where

σ is the shear stress

μ is the dynamic viscosity

du/dz is the velocity gradient normal to the direction of flow

The kinetic theory of gases predicts that the dynamic viscosity is independent of pressure. This rather surprising result is borne out by experiment over a large pressure range. In this pressure range the dependence of the dynamic viscosity on temperature is found to be

$$\mu = K(T)^{3/2} / (T + T_{su}) \quad (E.2)$$

where

μ is the dynamic viscosity at temperature T

K, T_{su} are constants, characteristic of a given gas

If the value of the viscosity μ_0 is known at a given temperature T_0 , then K can be eliminated as follows:

$$\mu_0 = K(T_0)^{3/2} / (T_0 + T_{su}) \quad (E.3)$$

$$(E.3) \rightarrow (E.2)$$

$$\mu = \mu_0 \left(\frac{T_0 + T_{su}}{T + T_{su}} \right) \left(\frac{T}{T_0} \right)^{3/2} \quad (E.4)$$

T_{su} is the so-called Sutherland constant (Br71) and is found to be approximately constant at temperatures far exceeding the critical temperature of the gas.

In the application example test engine of Chapter 4, three working gases have been considered -- air, helium and hydrogen.

Table E.1 gives the actual dynamic viscosity μ_0 at a temperature T_0 of 273 K as well as the associated Sutherland constant \tilde{T}_{su} for these three gases (a superscribed *tilde* (\sim) refers to a dimensioned or actual parameter -- refer to Appendix A for definitions of actual and normalized parameters). It is noted that \tilde{T}_{su} has the dimensions of temperature and is thus normalized with respect to the cold sink temperature T_k before it can be incorporated into the normalized system equations.

Table E.1 VALUES OF THE VISCOSITIES OF GASES (Br71)

Gas	Dynamic Viscosity at 273 K $\mu_0 \times 10^{-6}$ [kg/m.s]	Sutherland constant \tilde{T}_{su} [K]
Air	17,08	112
Helium	18,85	80
Hydrogen	8,35	84,4

E.3 THERMAL CONDUCTIVITY

The kinetic theory of gases predicts that the thermal conductivity of a gas is independent of pressure and this, too, is born out by experiment. The ratio of thermal conductivity of a gas to its dynamic viscosity is approximately a constant, and is determined most conveniently via the Prandtl number.

The definition of the Prandtl number Pr is as follows (KL64):

$$Pr = c_p \cdot \mu / k \quad (E.5)$$

where

c_p is the constant pressure specific heat capacity of the gas

k is the thermal conductivity of the gas

$$c_p = \gamma / (\gamma - 1) \quad (E.6)$$

(E.6) → (E.5):

$$Pr = \gamma \cdot \mu / k (\gamma - 1) \quad (E.7)$$

The Prandtl number is approximately constant for all gases, varying between 0,65 and 1 (RM67). A value of $Pr = 0,71$ has been chosen in the application example test engine of Chapter 4 to represent air, helium and hydrogen. The ratio of specific heat capacities γ is approximately 1,4 for the diatomic gases (air and hydrogen), and 1,67 for the monatomic gases (helium).

F. FRICION FACTOR AND HEAT TRANSFER COEFFICIENT

F.1 INTRODUCTION

The basic system model considered in this work is one-dimensional. However the fundamental concepts of fluid friction paradoxically break down under one-dimensional flow. From Newton's law of viscosity (equation D.1) it is seen that a Newtonian fluid cannot sustain a shear stress unless the flow is two-dimensional. This paradox is bypassed by stating that the flow is not strictly one-dimensional, but rather represented by its mean bulk mass flow rate. Empirical correlations are thus invoked in order to determine the friction (and related heat transfer) behaviour of the working gas with respect to its surroundings.

In this appendix the conventional Fanning friction factor is considered and found to be unsuitable for use in the reversing flow situation. A new friction factor, the so-called Reynolds friction factor is introduced in order to overcome this problem. Circular pipes are treated in detail and the Reynolds simple analogy is used to determine the related heat transfer coefficient. Porous matrices suitable for use in the regenerator are also considered.

Normalized parameters are used throughout (refer to Appendix A).

F.2 THE REYNOLDS FRICTION FACTOR

The quasi-steady state momentum equation (D.20) is now considered:

$$Vdp/dx + F = 0 \quad (D.20)$$

For a finite length of heat exchanger section (or regenerator matrix)

$$V\Delta p/\Delta x + F = 0 \quad (F.1)$$

By definition, the drag force F is related to the shear stress σ as follows:

$$F \triangleq \sigma \cdot A_{wg} \quad (F.2)$$

where A_{wg} is the wetted area of the elemental length Δx of heat exchanger section.

The hydraulic diameter of the flow passage d is defined as follows (KL64):

$$d/\Delta x \triangleq 4A/A_{wg} \quad (F.3)$$

where $A = V/\Delta x$ is the free flow area.

It is noted that for flow in a circular pipe d reduces to the internal diameter of the pipe and A to its internal cross sectional area.

(F.3) \rightarrow (F.2):

$$F = 4\sigma \cdot V/d \quad (F.4)$$

The conventional Fanning friction factor is defined by the shear stress divided by the dynamic head (KL64).

$$Ff \triangleq 2\sigma/g^2 v \quad (\text{F.5})$$

(F.5)→(F.4):

$$F = 2Ff \cdot g^2 V \cdot v/d \quad (\text{F.6})$$

(F.6)→(F.1):

$$\Delta p + 2Ff \cdot g^2 v \Delta x/d = 0. \quad (\text{F.7})$$

For the case of steady flow in the positive direction ($g > 0$), Δp is negative since there is a pressure drop in the positive direction and equation (F.7) is satisfied. However, for the case of steady flow in the reverse direction ($g < 0$) then Δp must be positive, and equation (F.7) is thus violated since the second term is always positive!

A more suitable definition of friction factor is thus proposed which relates the shear stress to the mass flux density and properties of the fluid, rather than to the dynamic head. The Reynolds number is first defined (KL64):

$$Re \triangleq |g \cdot d/\mu|$$

The so-called 'Reynolds' friction factor Fr is thus defined as follows:

$$Fr \triangleq Ff \cdot Re \quad (\text{F.9})$$

(F.8), (F.9)→(F.6):

$$F = 2Fr \cdot \mu \cdot g \cdot V \cdot v/d^2 \quad (\text{F.10})$$

(F.10)→(F.1):

$$\Delta p + 2Fr \cdot \mu \cdot g \cdot v \Delta x / d^2 = 0 \quad (F.11)$$

Equation (F.11) is satisfied for both positive and reversed flow, since the sign of Δp is always correctly related to the sign of g .

Since all current empirical data on the Fanning friction factor is given as a function of Reynolds number, it will be a simple matter to convert that data to the required Reynolds friction factor.

F.3 FRICTION FACTOR FOR CIRCULAR PIPES

Both the heater and cooler heat exchanger sections of a Stirling cycle engine are usually constructed from groups of parallel circular pipes. In the application example test engine (Chapter 4) the regenerator has been considered to be constructed from parallel circular pipes as well, the reasons for which have been amplified in Chapter 4.

The Fanning friction factor versus Reynolds number curves for various relative roughness factors has been widely documented and in widespread use for some decades (Mo48, Sc55) (Figure F.1).

Referring to figure F.1, the so-called Moody diagram or friction factor chart, it is noticed that the flow can be separated into three regimes; a laminar flow regime ($Re < 2000$), a critical flow regime ($2000 < Re < 4000$) and a turbulent flow regime ($Re > 4000$).

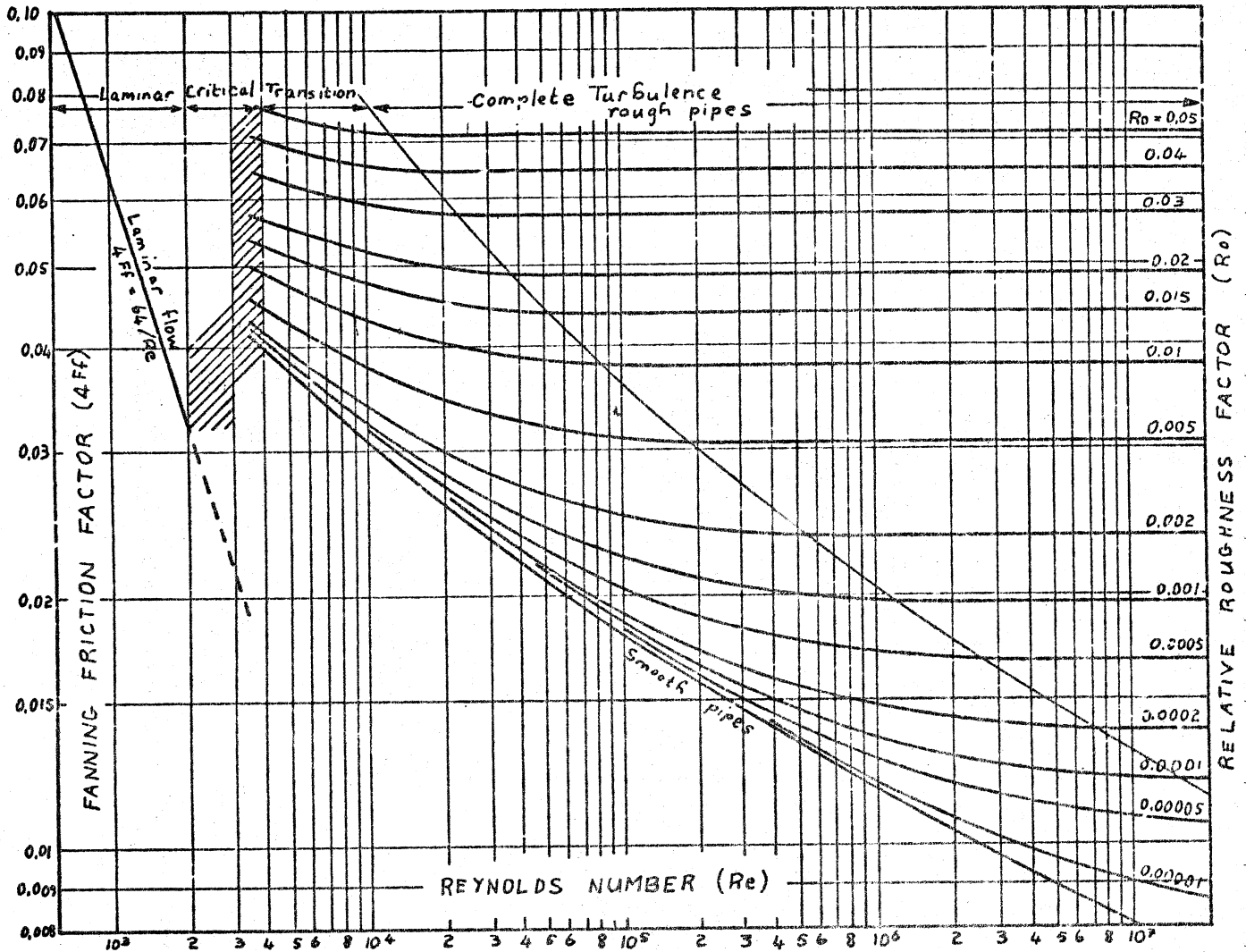


Figure F.1 FANNING FRICTION FACTOR DIAGRAM
 (After Pipe Friction Manual, 3rd Edition,
 Hydraulic Institute, 1961).

The turbulent flow regimes can be subdivided into the 'transition' zone and the 'complete turbulence rough pipes' zone, where the friction factor is constant with Reynolds number. The turbulent flow regime shows a

number of curves for different values of relative roughness factor Ro .

$$Ro \triangleq z/d \quad (F.12)$$

where z is the height of the protrusions.

For computation purposes it was decided to represent the Moody diagram by three equations conditional on the Reynolds number Re and the relative roughness factor Ro .

$$0 < Re < 2000, Ro \geq 0 \Rightarrow Ff \leftarrow 16/Re \quad (F.13)$$

$$Re \geq 2000, Ro = 0 \Rightarrow Ff \leftarrow 0,0791/(Re)^{0,25} \quad (F.14)$$

$$Re \geq 2000, Ro > 0 \Rightarrow \begin{cases} Ff1 \leftarrow 0,0791/(Re)^{0,25} \\ Ff2 \leftarrow 1/(4[1,14-0,8686 \ln(Ro)]^2) \\ Ff1 > Ff2 \Rightarrow Ff \leftarrow Ff1 \\ Ff1 < Ff2 \Rightarrow Ff \leftarrow Ff2 \end{cases} \quad (F.15)$$

Equation (F.13) is based on the Hagen-Poiseuille equation of laminar flow through a pipe, which can be derived from first principles (Sc55).

Equation (F.14) cannot be deduced theoretically; it is an experimentally determined relation, the so-called 'friction law of Blasius' and it holds reasonably well for turbulent flow in smooth pipes up to Reynolds numbers of about 200 000 (RM67).

In equation (F.15), F_{f1} is the 'friction law of Blasius' and F_{f2} is a relationship due to von Kármán based upon extensive experimental results due to Nikuradse for fully developed turbulent flow in rough pipes (Sc55). The friction factor F_f is thus chosen to be the greater of F_{f1} and F_{f2} .

The friction factor diagram which results from the use of equations (F.13), (F.14) and (F.15) is shown in figure F.2.

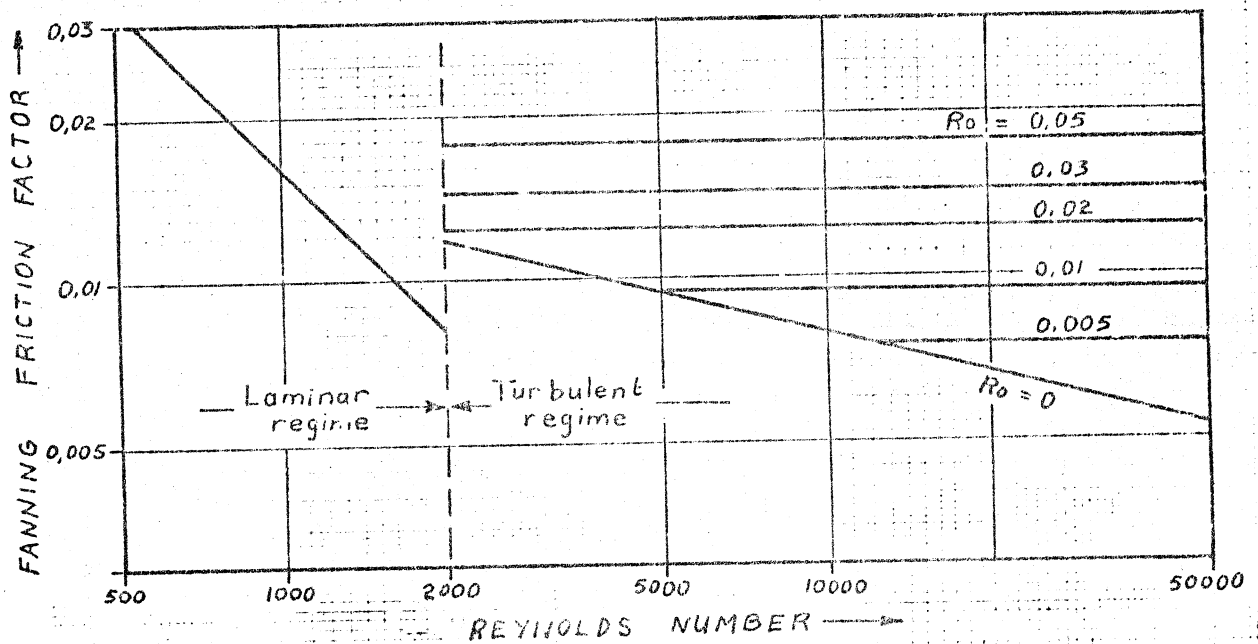


Figure F.2 APPROXIMATE FRICTION FACTOR DIAGRAM

It is noticed from figure F.2 that the critical flow regime and transition zone have been eliminated, it being assumed that the flow is fully turbulent for all Reynolds numbers greater than or equal to 2000.

In section F.2 it was shown that the Reynolds friction factor is more suitable for use with reversing flow situations, than is the conventional Fanning friction factor. The friction factor equations (F.13), (F.14) and (F.15) are transformed as follows:

(F.9) → (F.13), (F.14), (F.15):

$$0 \leq Re < 2000, Ro \geq 0 \Rightarrow Fr = 16 \quad (F.16)$$

$$Re \geq 2000, Ro = 0 \Rightarrow Fr = 0,0791(Re)^{0,75} \quad (F.17)$$

$$Re \geq 2000, Ro > 0 \Rightarrow \begin{cases} Fr1 = 0,0791(Re)^{0,75} \\ Fr2 = Re / (4 [1,14 - 0,8686 \ln(Ro)]^2) \\ Fr1 > Fr2 \Rightarrow Fr = Fr1 \\ Fr2 < Fr1 \Rightarrow Fr = Fr2 \end{cases} \quad (F.18)$$

The friction factor diagram which results from the use of equations (F.16), (F.17) and (F.18) is shown in figure F.3.

The Reynolds friction factor diagram (figure F.3) appears more intuitively logical to appreciate than the equivalent Fanning friction factor diagram (figure F.2). One can see directly on figure F.3 that in the laminar flow region the frictional drag force is proportional to the mass flow rate (Fr constant), and that in the fully developed Nikuradse turbulent regime to the square of the mass flow rate (Fr has slope 1).

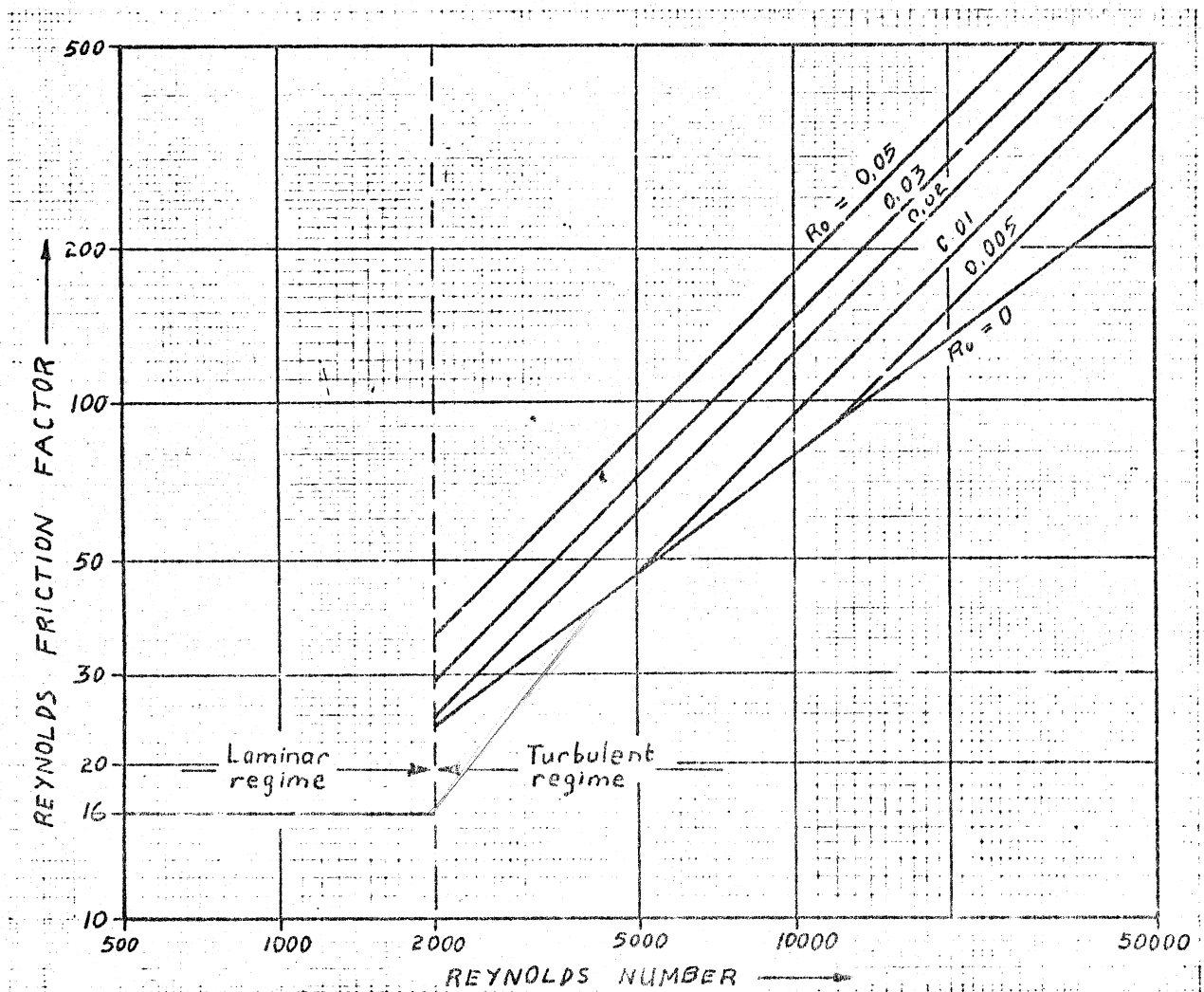


Figure F.3 APPROXIMATE REYNOLDS FRICTION FACTOR DIAGRAM

F.4 HEAT TRANSFER COEFFICIENT FOR CIRCULAR PIPES

Heat transfer by convection is related to bulk mass flow rate in a similar way to friction. For fully developed laminar flow in circular pipes one can theoretically determine the heat transfer coefficient (RM67). It is found that the Nusselt number Nu becomes a constant, its

value being a function of the type of heat exchange with the surrounding wall. The Nusselt number is defined as follows:

$$Nu \triangleq h \cdot d/k \quad (F.19)$$

where

h is the heat transfer coefficient

k is the working gas thermal conductivity.

Significantly it is noted from equation (F.16) that under laminar flow conditions the Reynolds friction factor is also constant.

It is not possible to produce a complete analytical solution for heat transfer by convection when the flow is turbulent. It was suggested by Reynolds that there exists a similarity between forced convection heat transfer and fluid friction (RM67).

Thus the so-called Reynolds simple analogy has been derived based upon the assumption that the Prandtl number is unity:

$$Nu = Ff \cdot Re/2 \quad (F.20)$$

In terms of the Reynolds friction factor, the Reynolds simple analogy can be written.

$$(F.9) \rightarrow (F.20)$$

$$Nu = Fr/2 \quad (F.21)$$

For the Prandtl number different from unity Prandtl and Taylor suggested a modification to the Reynolds simple analogy (RM67):

$$Nu = Fr/2 [1 + 1.99 Re^{-1/8} (Pr-1)] \quad (F.22)$$

However, for the range of Reynolds number and Prandtl number encountered in this work it has not been considered that the use of equation (F.22) can significantly increase the accuracy.

The Reynolds simple analogy, equation (F.21), has been derived for the turbulent flow regime. When used in the laminar flow regime it predicts values of Nusselt number that are about twice as large as the theoretical values for fully developed laminar flow. However, for the application example test engine (Chapter 4) it was found that laminar flow occurs only during a small fraction of the cycle, forming the transition between turbulent flow in the one direction, and turbulent flow in the opposite direction. From Kays and London (KL64) it is found that when the laminar flow is not fully developed then the Nusselt number can be very much greater than that for fully developed flow. Based on the above considerations it was decided to use the Reynolds simple analogy throughout, covering both the laminar and turbulent regimes.

F.5 REGENERATOR MATRICES

In the case of porous regenerator matrices, the equivalent hydraulic diameter, wetted area and free flow area are required to be evaluated. These are related to the concept of the porosity of the matrix ψ .

$$\psi \triangleq V/(V+V_m) \quad (\text{F.23})$$

where

V is the void volume of the matrix

V_m is the volume of the matrix material

$(V+V_m)$ is thus the total volume of the matrix.

Dividing the numerator and denominator of equation (F.23) by the matrix length, the effective free flow area of the matrix is obtained:

$$A = \psi A_f \quad (\text{F.24})$$

where

A is the free flow area.

A_f is the frontal area of the matrix.

In order to calculate the equivalent hydraulic diameter of the matrix, the wetted area A_{wg} must first be evaluated.

A common form of regenerator matrix used is a stacked wire mesh, either in the form of stacked woven wire gauze, crossed rods or wire wool. The total wetted area A_{wg} for the wire mesh matrix is given by

$$A_{wg} = \pi \cdot d_m \cdot x_m \quad (\text{F.25})$$

where

d_m is the mesh wire diameter

x_m is the total effective length of the wire in the matrix (number of wires times the length of each wire).

The total volume of wire mesh is given by

$$V_m = \pi \cdot x_m (d_m)^2 / 4 \quad (\text{F.26})$$

The total mass of matrix m_m is

$$m_m = V_m \cdot \rho_m \quad (\text{F.27})$$

where ρ_m is the density of the matrix material

(F.26), (F.27) → (F.25):

$$A_{wg} = 4m_m / \rho_m \cdot d_m \quad (\text{F.28})$$

Thus given the matrix mass, density, wire diameter, porosity and frontal area, the wetted area, free flow area and hydraulic diameter can be evaluated.

Little experimental work has been published on friction factors or heat transfer coefficients of matrices suitable for use in Stirling cycle machines. There has been quite an extensive experimental investigation of the friction and heat transfer behaviour of stacked sphere matrices under steady flow conditions. These have been correlated by Kays and London (KL64) who presented graphical data for the Fanning friction factor and the so-called Colburn j -factor (Ki70) versus Reynolds number (figure F.4).

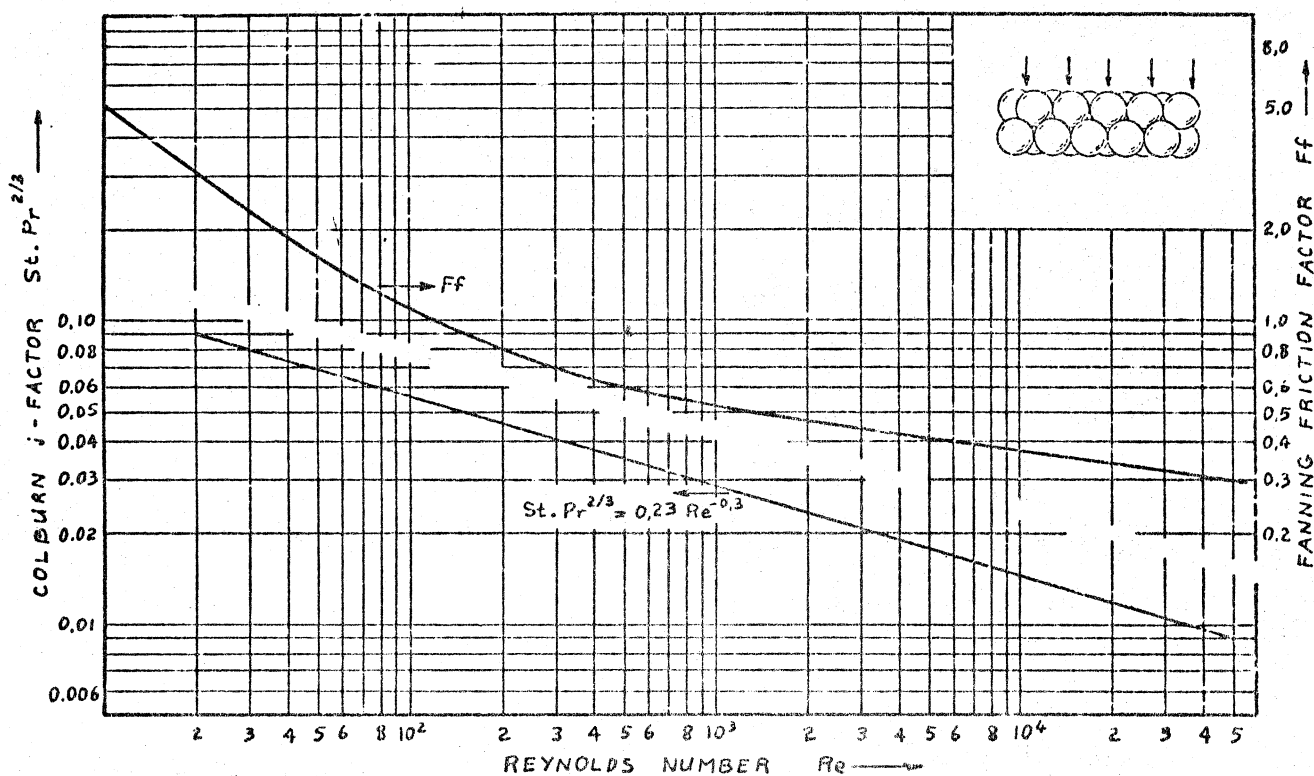


Figure F.4 FLOW FRICTION AND HEAT TRANSFER CHARACTERISTICS FOR FLOW THROUGH STACKED SPHERE MATRICES (After Kays and London KL64)

The Colburn j -factor is defined as $St. Pr^{2/3}$. Kim (Ki70) determined experimental correlations for cyclic operation of stacked sphere matrices. He found that due to the cyclic operation (which is more realistically related to Stirling cycle machine operation) he obtained both friction factor and heat transfer coefficients which were about 20% higher than the steady flow values given by Kays and London. Kim's correlations are given as follows:

$$Ff = 488/Re + 1,92 \quad (F.29)$$

$$St. (Pr)^{2/3} = 0,144Re^{-0,2} \quad (F.30)$$

The range of Reynolds numbers tested by Kim was 390 to 1183. Stacked sphere matrices are more usually used in cryogenic refrigerators than in engines. This is because the various materials which have a reasonably high thermal capacity at cryogenic temperatures (eg, lead) are more easily available in the form of spheres. Unfortunately no equivalent extension of Kim's experimental work has been done on stacked wire mesh matrices.

Kays and London (KL64) present curves of Fanning friction factor and heat transfer characteristics for both randomly stacked woven screen matrices and crossed rod matrices. The data for the woven screen matrices has been based on steady flow experiments using mesh sizes ranging from 5x5 mesh per inch through 60x60 mesh per inch. Since this data is presented in graphical form only it has been reproduced here for convenience (figure F.5). The data for crossed rod matrices has been based on steady flow experiments using rod diameters of 0,375 inch only, hence it is not of interest.

Vasishta and Walker (VW70, Va69) conducted steady flow experimental investigations of the friction factor and heat transfer characteristics of dense mesh wire screens (200x200 and 400x400 mesh per inch). Since the data has not been reduced to the same format as that of Kays and London (KL64), and the original unreduced data is not available in either of the publications, it is extremely

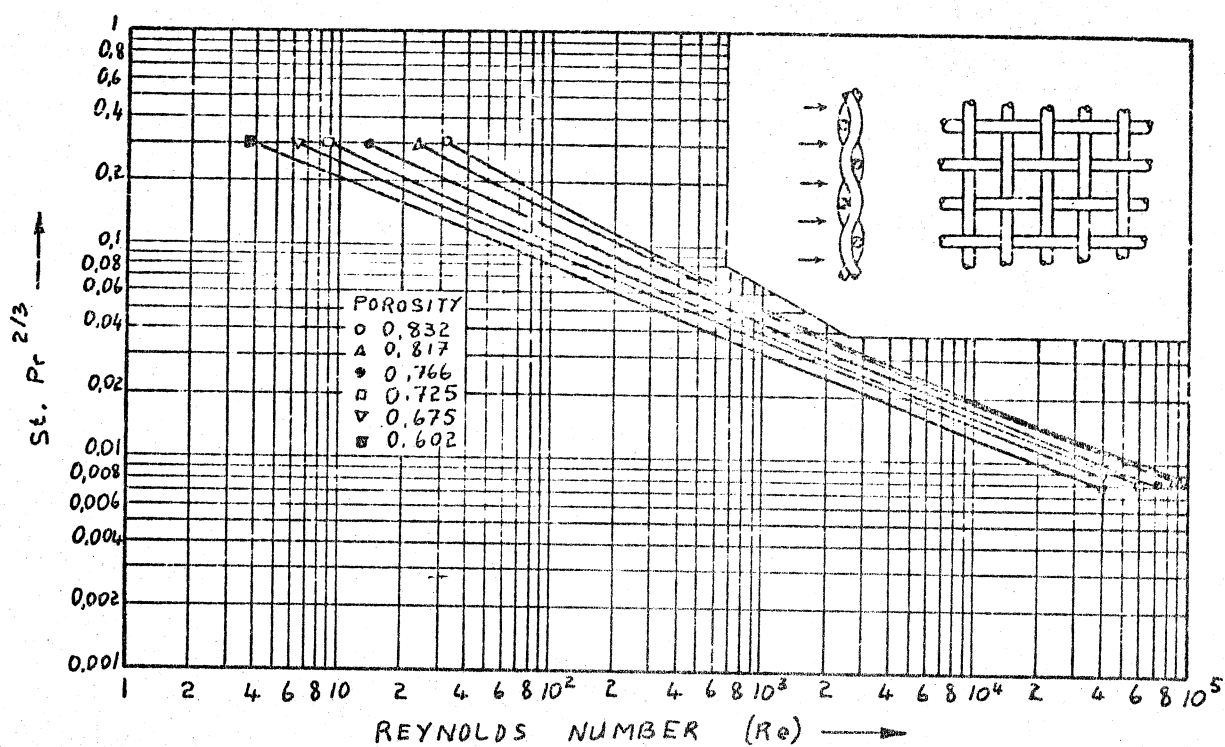
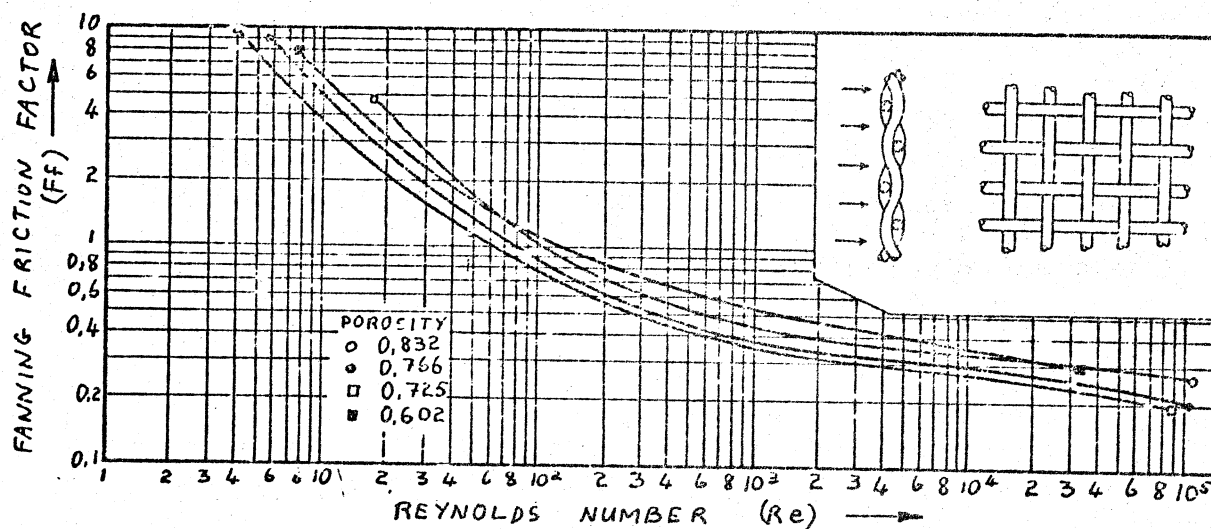


Figure F.5 FLOW FRICTION AND HEAT TRANSFER CHARACTERISTICS
 THROUGH INFINITE RANDOMLY STACKED WOVEN SCREEN
 MATRIX (After Kays and London KL64)

difficult to determine if it can be used as an extension to the results given in figure F.5. Unless this reduction is done its use will be limited to systems having the identical dense mesh dimensions.

F.6 CONCLUSIONS

It is seen from the above discussion that there is a grave lack of experimental correlation data available for matrices suitable for use in Stirling cycle regenerators. Even where this data is available, eg, stacked sphere matrices, then the work by Kim (Ki70) has indicated that under cyclic conditions of operation the friction factor and heat transfer coefficient are much higher than those predicted by steady flow experiments. Much experimental and theoretical investigation needs to be done in this field. In defining the system model and solution technique, the method of approach adopted in this work has been to develop a method of analysis which will be able to accept new correlation data as it becomes available.

G. METHOD OF SOLUTION

G.1 THE METHOD OF LINES

The fundamental nonlinear partial differential equations in space and time have been developed in Appendix D. In this appendix the method of applying these equations to the model defined in Chapter 4, as well as of their solution, is outlined. The usual method of solving partial differential equations on a digital computer consists of approximating the partial derivatives with respect to all the independent variables by finite difference expressions. The resulting algebraic relationships are then solved at the grid points of the discretized region of interest. Kim (Ki70) used this technique to solve a system of equations similar to equations (D.5), (D.20), and (D.19) as applied to the regenerator of a Stirling cycle machine. Another approach is to convert the partial differential equations to a system of ordinary differential equations by discretizing all but one of the independent variables, which is left continuous. This method has been called 'the method of lines' (FW60). Hicks and Wei (HW67) enumerated a number of computational advantages of the method and demonstrated its applicability to linear and nonlinear partial differential equations. Fehlberg (Fe69) demonstrated the high accuracy of the method by integrating highly nonlinear partial differential equations by Runge-Kutta methods of various orders. The major advantage is that once the problem has been converted to an initial value problem, involving a system of simultaneous ordinary differential equations, several powerful numerical techniques are available for use in solving these equations.

G.2 APPROACH TO SOLUTION

The Stirling cycle machine is not an initial value problem, but rather a boundary value problem. However, because of its cyclic nature it can be formulated as an initial value problem using arbitrary (but consistent) initial conditions, and integrating the equations through several complete cycles until cyclic steady state has been reached. This is the equivalent of the 'warm up' operation of the actual machine in which the machine will start from (say) the stationary state and go through successive transient cycles until the values of all the variables at the end of each cycle are equal to their values at the beginning of that cycle. The time needed until cyclic steady state has been attained is dependent mainly upon the thermal capacitance of the system -- in particular that of the regenerator matrix -- and can require as much as several hundred crankshaft revolutions (Fi75). Since a typical computation cycle takes two minutes computing time on an IBM 370-158 machine, accelerating convergence techniques had to be developed.

There are a number of gross performance indices available in order to determine whether or not cyclic steady state has been attained, ie, thermal efficiency, net regenerator heat transferred per cycle, and the overall cyclic energy balance. Of these, only the net regenerator heat transferred per cycle can be used in the form of a feedback loop in order to accelerate convergence. The convergence technique that was developed is based on the principle that when cyclic steady state has been attained, then through each cycle the net transfer of heat between the working fluid and the regenerator matrix is zero. Now since the

regenerator section is divided up into a finite number of cells, the previous statement can be extended to read: through each steady state cycle the net transfer of heat between the working fluid and each individual regenerator cell matrix is zero. Furthermore, if it is found a posteriori that the residual regenerator cell heat transfer is positive, then its respective matrix temperature is higher than its cyclic steady state value; and if negative, then it is lower than its cyclic steady state value. This allows convergence to be accelerated by means of altering all the regenerator cell matrix temperatures individually at the end of each cycle in accordance with the following algorithm:

$$T_{m_i} \leftarrow T_{m_i} - Q_{r_i} \Delta \quad (\text{G.1})$$

where

T_{m_i} is the temperature of the i 'th regenerator cell matrix at the end of the cycle

Q_{r_i} is the a posteriori residual i 'th regenerator cell heat transferred at the end of the cycle

Δ is an arbitrary convergence factor.

The choice of convergence factor Δ is critical to both the rate of convergence, and the stability of convergence. It is a complex function of the system parameters, the number of cells and the closeness that the system is to steady state, and can only be determined empirically by trial and error. The correct choice of the convergence factor can, however, reduce the number of cycles required for convergence by some orders of magnitude.

G.3 THE ALGORITHM OF SOLUTION

The reduction of the system partial differential equations to the set of simultaneous first order differential equations is presented in Appendix H. The fourth order Runge-kutta integration technique using Runge's coefficients was chosen in order to solve the differential equations. It is the most widely used of the vast number of numerical methods available, mainly because of its programming simplicity (Ku65). The algorithm of solution is given in the flow chart diagram (figure G.1). The system configuration, size, charge pressure, operating frequency, matrix properties, working gas properties, etc, are first defined. If this is the first cycle being run for this particular system, then a consistent set of initial conditions are calculated based upon the system being stationary and in temperature equilibrium. If not, then the most updated initial conditions which have been evaluated from previous runs of this particular system are introduced, thus allowing continuation after limited time runs. The cyclic initial conditions mainly take the form of setting all the energy (heat and work) terms to zero. The Runge-Kutta integration routine integrates the equations over a single differential time increment. In doing so it calls a subroutine called DERIV four times. DERIV is simply the set of ordinary differential equations of the system. Thus given the system parameters, each time DERIV is called it will return the corresponding set of derivatives, which are nonlinear functions of those parameters. Once the integration has been completed over a full cycle of crankshaft rotation, then the convergence algorithm (equation G.1) is applied before beginning the next cycle.

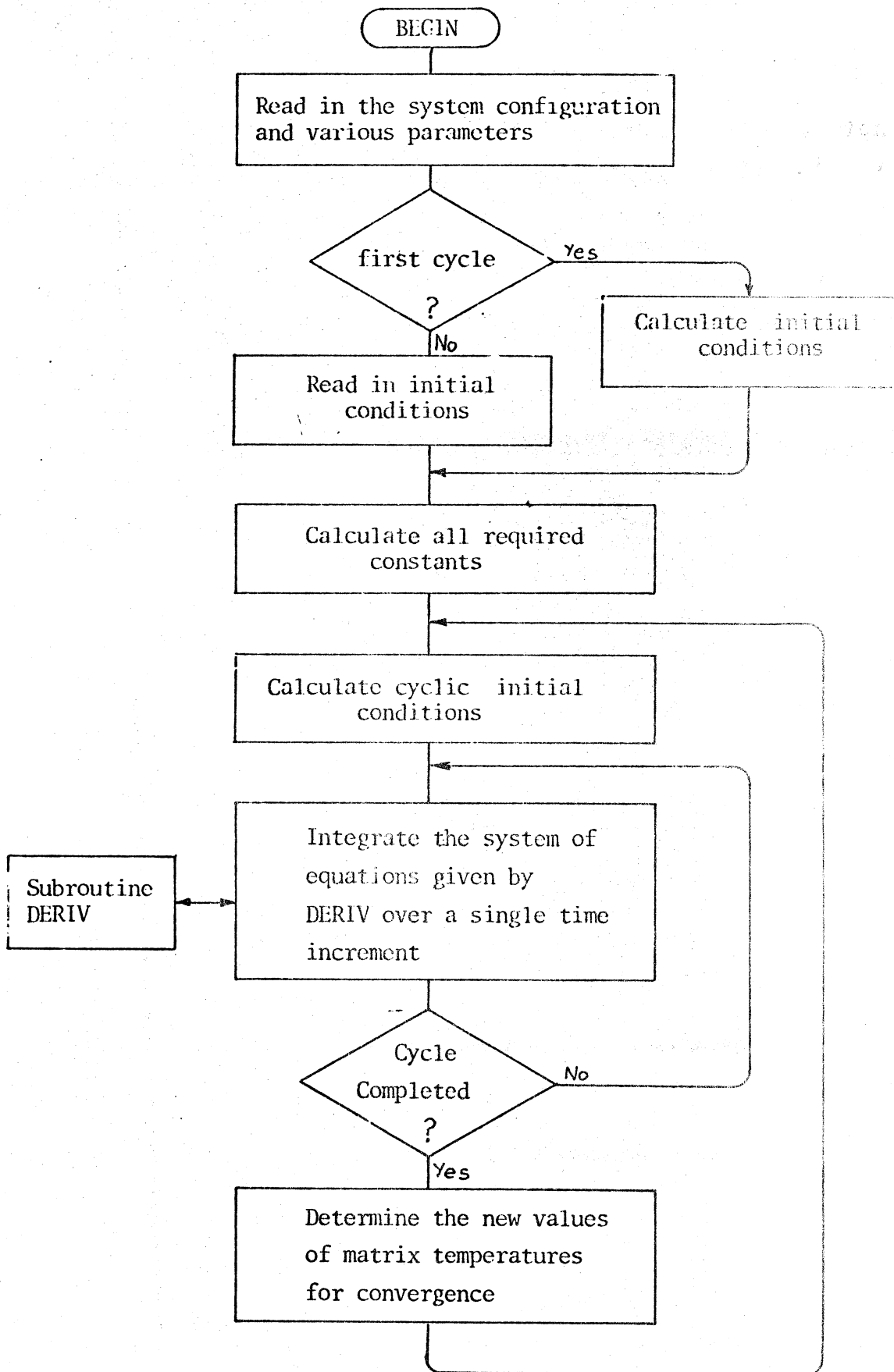


Figure G.1 THE ALGORITHM OF SOLUTION

It is noticed from figure G.1 that the solution never ends, relying upon a predetermined time limit to stop the computation.

Information printout of any of the parameters can be obtained at any stage of the computation.

H. SYSTEM ALGORITHMS

H.1 GENERAL

In this appendix the fundamental system of equations developed in Appendix D is applied to the system model defined in Chapter 3, in order to evolve suitable algorithms for solution. From Chapter 3 it is seen that the model is composed of an interconnection of two different types of component; variable volume cylinders, and constant volume cells. The most general form of cell that has been considered is given in figure H.1.

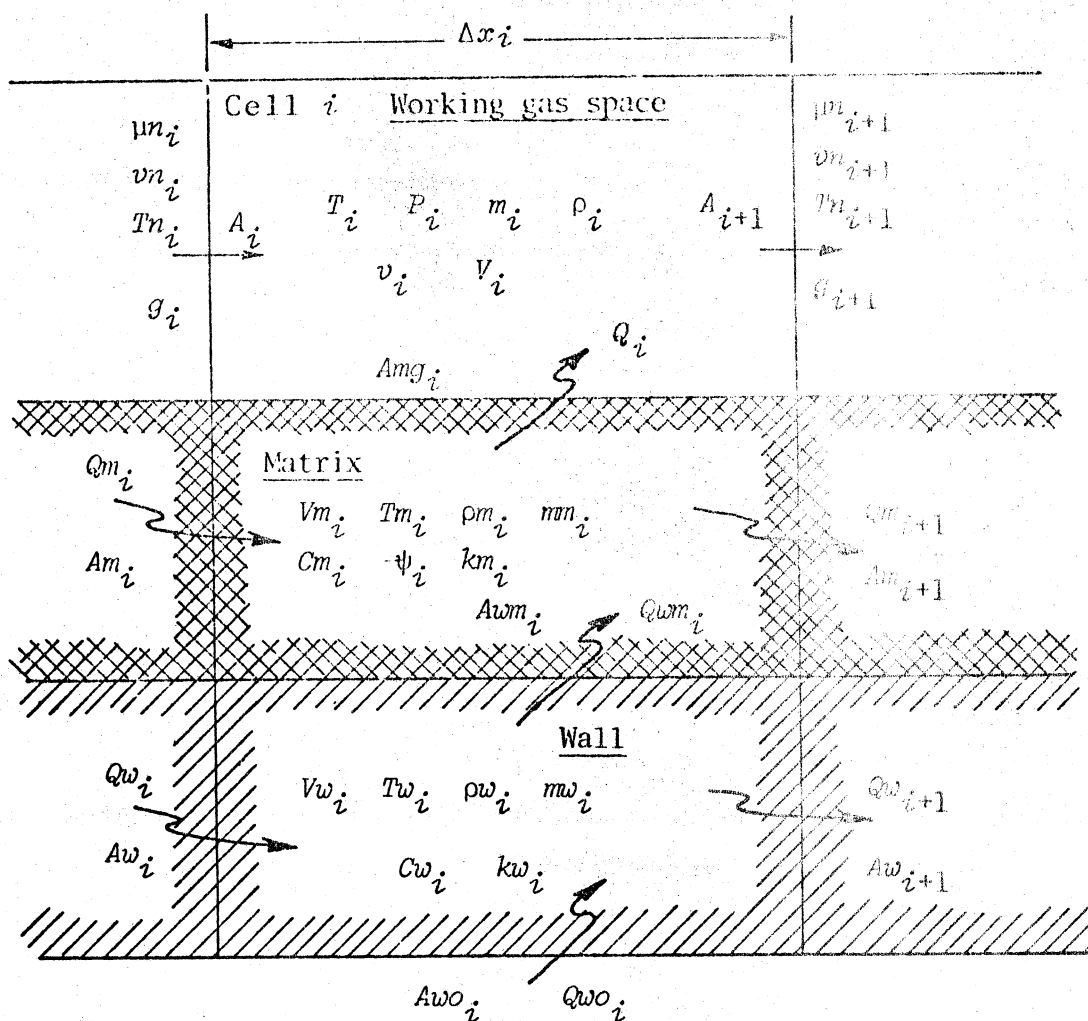


Figure H.1 THE GENERALIZED i 'TH ELEMENTAL CELL

The direction of the arrows give the arbitrarily defined positive direction of flow (heat q and mass flux density g) which has been adhered to throughout.

The most general form of variable volume cylinder that has been considered is shown in figure H.2, which shows specifically the compression space. The expansion space is similar in form.

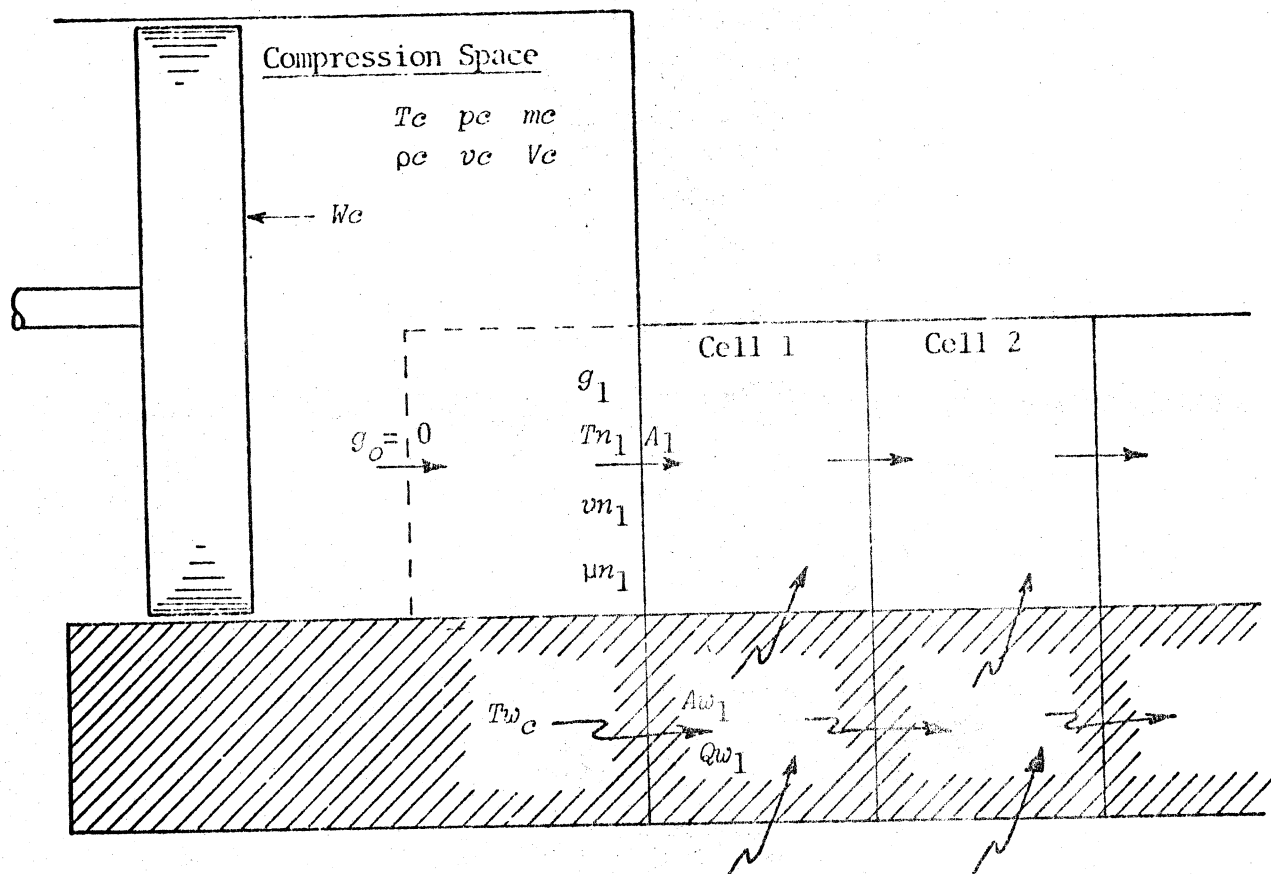


Figure H.2 THE GENERALIZED COMPRESSION SPACE

In what follows, subsets of the above generalized components are considered, in accordance with the specific algorithm being developed.

H.2 CONTINUITY

From Appendix D the continuity equation is given as follows:

$$\frac{\partial m}{\partial t} + v \frac{\partial g}{\partial x} = 0 \quad (\text{D.5})$$

The working gas in the void space of the i 'th cell is considered (figure H.3).

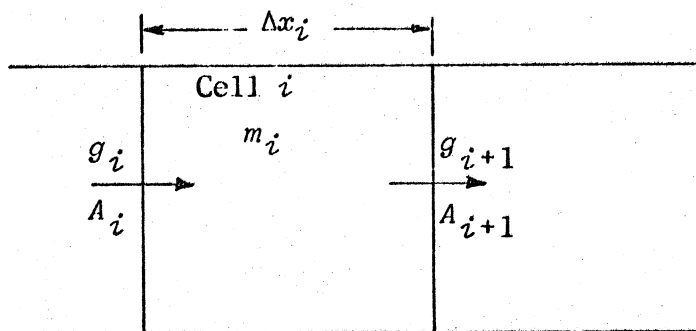


Figure H.3 THE i 'TH CELL

Equation (D.5) is discretized in the spacial coordinate and applied to the i 'th cell:

$$Dm_i \leftarrow A_i g_i - A_{i+1} g_{i+1} \quad (\text{H.1})$$

where

D is the total time differential operator d/dt , and \leftarrow is the algorithmic operator 'is replaced by'. It is

noted that equation (H.1) is in fact an algorithm for obtaining the derivative Dm_i given the relevant parameters.

In the case of node i being the interface between cells of different dimensions, eg, node 1 being the interface between the compression space and cell 1, then A_i will always be the minimum free flow area between the adjacent cells.

The FORTRAN equivalent statement of equation H.1 is given by

$$DM(I)=A(I)*G(I)-A(I+1)*G(I+1) \quad (H.2)$$

The working gas in the compression space is now considered (figure H.4).

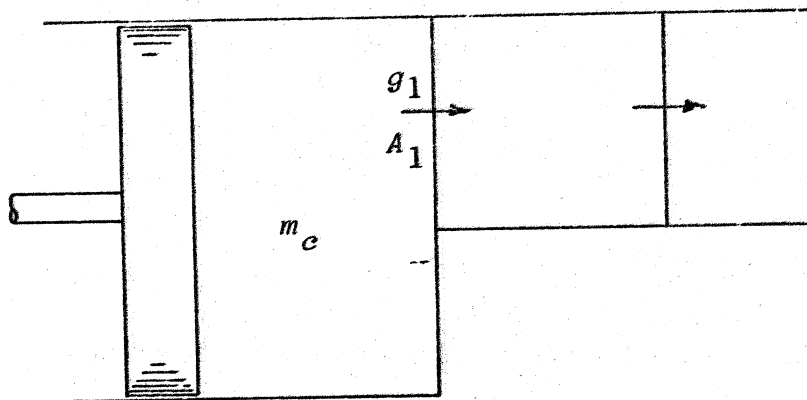


Figure H.4 THE COMPRESSION SPACE

Equation (D.5) is discretized in the spacial coordinate and applied to the compression space:

$$Dm_c \leftarrow -A_1 g_1 \quad (H.3)$$

It is noted that equation (H.3) precludes any leakage of working fluid past the piston. This is not a fundamental limitation of the model, however, and a leakage term can always be added to equation (H.3) if necessary.

A similar algorithm for the mass accumulation in the expansion space is obtained:

$$Dm_e \leftarrow A_{nc1} g_{nc1} \quad (H.4)$$

The FORTRAN equivalent statements of equations (H.3) and (H.4) are respectively

$$\begin{aligned} DMC &= -A(1)*G(1) \\ DME &= A(NC1)*G(NC1) \end{aligned} \quad (H.5)$$

On summing equations (H.1), (H.3) and (H.4) over the complete machine, it is found that the total mass of working fluid in the system is conserved.

$$Dmc + Dme + \sum_{i=1}^{nc} Dm_i = -A_1 g_1 + A_{nc1} g_{nc1} + \sum_{i=1}^{nc} (A_i g_i - A_{i+1} g_{i+1}) = 0$$

Thus at any instant of time there is no net accumulation of working gas mass in the machine.

H.3 MOMENTUM

From Appendix D the momentum equation is given as follows:

$$\frac{\partial}{\partial t}(g \cdot V) + v \frac{\partial}{\partial x}(g^2 v) + v \frac{\partial p}{\partial x} + F = 0 \quad (D.9)$$

The i 'th node interface between the adjacent cell working gas spaces ($i-1$) and i is considered (figure H.5).

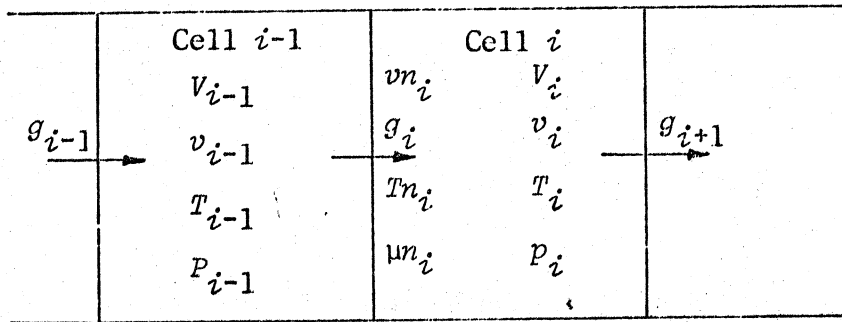


Figure H.5 THE i 'TH NODE

In equation (D.9), the volume V is considered to be the mean of the volumes of the cells adjacent to node i and located about node i . It will always be a constant volume and its time derivative is therefore zero. On expanding equation (D.9) one obtains:

$$\frac{\partial g}{\partial t} + 2g \cdot v \frac{\partial g}{\partial x} + g^2 \frac{\partial v}{\partial x} + \frac{\partial p}{\partial x} + \frac{F}{V} = 0 \tag{H.6}$$

The drag force term F has been evaluated in terms of the Reynolds friction factor in Appendix F.

$$F = 2Fr \cdot \mu \cdot g \cdot V \cdot v / d^2 \tag{F.10}$$

(F.10) → (H.6):

$$\frac{\partial g}{\partial t} + 2g \cdot v \frac{\partial g}{\partial x} + g^2 \frac{\partial v}{\partial x} + \frac{\partial p}{\partial x} + 2Fr \cdot \mu \cdot g \cdot v / d^2 = 0 \tag{H.7}$$

In the context of the system model the mass flux density g is only defined at, and continuous across, the cell nodes, thus equation (H.7) is applied only at the nodes. However the specific volume and temperature are defined as being constant within the cells and discontinuous at the nodes. At all nodes, therefore, vn and Tn are considered to be conditional convective parameters (conditional on the sign of g at that node) taking on the value of the adjacent upstream cell values of specific volume v and temperature T respectively.

In order to avoid numerical instability the 'upstream difference' technique of evaluating $\partial g/\partial x$ has been used, always in terms of upstream and local values of g (Ro72).

The case of the i 'th node having adjacent cells of identical dimensions is considered first. Thus discretizing equation (H-7) in the spacial coordinate and applying it to the i 'th node:

$$Dg_i + [2g_i vn_i \Delta g_i + g_i^2 (v_{i-1} - v_i)] / \Delta x_i + \Sigma F_i \quad (\text{H.8})$$

where

$$\Sigma F_i + (p_{i-1} - p_i) / \Delta x_i - 2Fr \cdot \mu \cdot g_i vn_i / d_i^2$$

$$g_i \geq 0 \Rightarrow vn_i + v_{i-1}, Tn_i + T_{i-1}, \Delta g_i + (g_{i-1} - g_i)$$

$$g_i < 0 \Rightarrow vn_i + v_i, Tn_i + T_i, \Delta g_i + (g_i - g_{i+1})$$

μ is the dynamic viscosity at node i and is evaluated as a function of Tn_i in accordance with equation (E.4)

d_i is the hydraulic diameter at node i

Fr is the Reynolds friction factor evaluated at node i .

The FORTRAN equivalent statements of equation (H.8) are:

```

      IF(G(I))25,30,30
25  DELG(I)=G(I)-G(I+1)
      TN(I)=T(I)
      VSN(I)=VS(I)
      GO TO 35
30  DELG(I)=G(I-1)-G(I)
      TN(I)=T(I-1)
      VSN(I)=VS(I-1)
35  DELP(I)=P(I-1)-P(I)
      DELVS(I)=VS(I-1)-VS(I)

```

(H.9)

↓
Algorithm for calculating μ (RMU) and Fr (FR) at node i .

↓

```

BFRIC(I)=2./(D(I)*D(I))
SF=DELP(I)*DELXI(I)-BFRIC(I)*FR*RMU*G(I)*VSN(I)
DG(I)=G(I)*DELXI(I)*(2.*VSN(I)*DELG(I)+G(I)*DELVS(I))+SF

```

The case of the i 'th node having adjacent cells of unequal dimensions (as for example at the cooler/regenerator interface) is now considered (figure H.6).

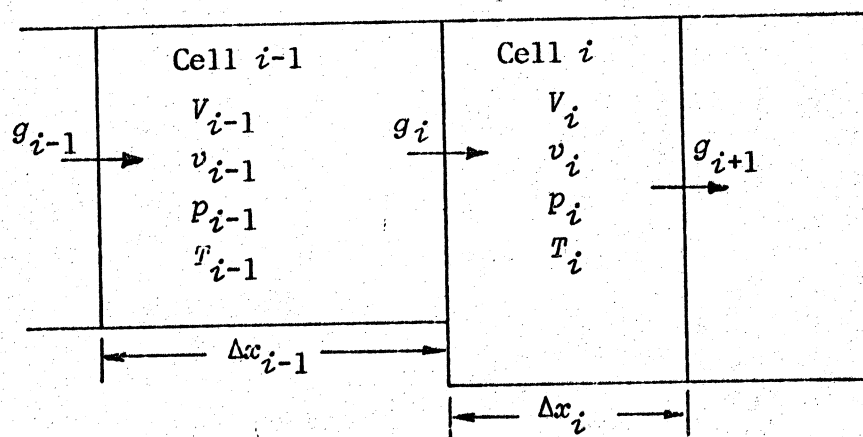


Figure H.6 THE i 'TH NODE - UNEQUAL ADJACENT CELLS

Discretizing equation (H.7) and applying it to the i 'th node of figure H.6:

$$Dg_i + 2g_i v n_i (\Delta g / \Delta x)_i + 2g_i^2 (v_{i-1} - v_i) / (\Delta x_{i-1} + \Delta x_i) + \Sigma F_i \quad (\text{H.10})$$

where

$$\Sigma F_i + 2(p_{i-1} - p_i) / (\Delta x_{i-1} + \Delta x_i) - 2Fr \cdot \mu \cdot g_i v n_i / d_i^2$$

$$g_i \geq 0 \Rightarrow v n_i + v_{i-1}, T n_i + T_{i-1}, (\Delta g / \Delta x)_i + (g_{i-1} - g_i) / \Delta x_{i-1}$$

$$g_i < 0 \Rightarrow v n_i + v_i, T n_i + T_i, (\Delta g / \Delta x)_i + (g_i - g_{i+1}) / \Delta x_i$$

d_i is the minimum hydraulic diameter of the two adjacent cells

Fr is the friction factor evaluated at node i using the hydraulic diameter d_i .

The FORTRAN equivalent statements of equation (H.10) are as follows:

```

IF(G(I))25,30,30
25 DELGX(I)=(G(I)-G(I+1))*DELXI(I)
   TN(I)=T(I)
   VSN(I)=VS(I)
   GO TO 35
30 DELGX(I)=(G(I-1)-G(I))*DELXI(I-1)
   TN(I)=T(I-1)
   VSN(I)=VS(I-1)
35 DELP(I)=P(I-1)-P(I)
   DELVS(I)=VS(I-1)-VS(I)

```

(H.11)

↓

Algorithm for calculating μ (RMU) and F_r (FR) at node i

↓

```

BDLXI(I)=2./(DELX(I-1)+DELX(I))
BFRIC(I)=2./(D(I)*D(I))
SF=DELP(I)*BDLXI(I)-BFRIC(I)*FR*RMU*G(I)*VSN(I)
DG(I)=G(I)*(2.*VSN(I)*DELGX(I)+G(I)*DELVS(I)*BDLXI(I))+SF

```

The case of the two end nodes, being the interfaces between the compression space and cell 1, and the expansion space and cell n_c respectively (figure H.7) are now considered. In these cases it is assumed that an extra cell has been projected into the working space, the gas in that cell having the same properties as those of its respective working space. It is also assumed that the gas in the working space is stationary, and has uniform mixed mean properties throughout.

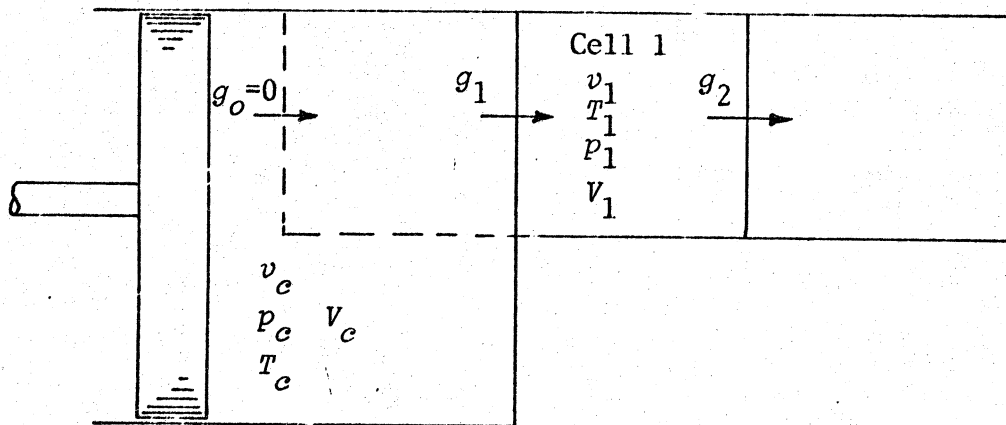


Figure H.7 NODE 1

Discretizing equation (H.7) and applying it to node 1:

$$Dg_1 \leftarrow [2g_1 v n_1 \Delta g_1 + g_1^2 (v_c - v_1)] / \Delta x_1 + \Sigma F_1 \quad (\text{H.12})$$

where

$$\Sigma F_1 \leftarrow (p_c - p_1 + \Delta p_c) / \Delta x_1 - 2Fr \cdot \mu \cdot g_1 v n_1 / d_1^2$$

$$g_1 \geq 0 \Rightarrow v n_1 \leftarrow v_c, T n_1 \leftarrow T_c, \Delta g_1 \leftarrow -g_1$$

$$g_1 < 0 \Rightarrow v n_1 \leftarrow v_1, T n_1 \leftarrow T_1, \Delta g_1 \leftarrow g_1 - g_2$$

d is the hydraulic diameter of cell 1

Fr is the friction factor at node 1 evaluated using hydraulic diameter d_1

Δp_c is the irrecoverable pressure drop due to the expansion (contraction).

The irrecoverable pressure drop is given in Kays and

London (KL64) for the two cases when the flow is entering the heat exchanger (contraction loss) and leaving the heat exchanger (expansion loss).

$$\Delta p_c = -K_c \cdot g_1^2 v n_1 / 2 \quad (\text{contraction}) \quad (\text{H.13})$$

where K_c is the contraction loss coefficient.

$$\Delta p_e = -K_e \cdot g_1^2 v n_1 / 2 \quad (\text{expansion}) \quad (\text{H.14})$$

where K_e is the expansion loss coefficient

The determination of K_c and K_e has been done both analytically and experimentally by Kays for multiple circular pipe heat exchangers with abrupt contraction and expansion (KL64). The results have been reproduced in figure H.8 for convenience.

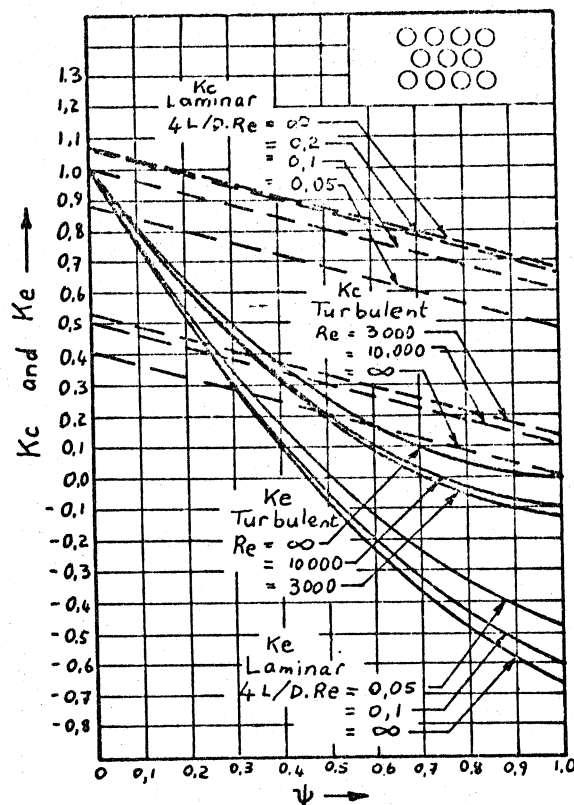


Figure H.8 ABRUPT EXPANSION AND CONTRACTION PRESSURE
COEFFICIENTS (After Kays and London KL64)

The ordinate of the graphs in figure H.8 has been loosely defined as ψ or 'porosity', being the ratio of the free flow area to the total frontal area. In the case of the application example test engine (Chapter 4) the free flow area is the internal cross sectional area of the bank of heat exchanger pipes, whereas the frontal area is the area of the piston face. For most practical purposes, ψ is almost zero hence it is seen from figure H.8 that K_e is always unity and K_c can vary between 0,4 and 1,1 as a function of the Reynolds number in the heat exchanger pipes. In this work K_e and K_c have been defined both unity in order to denote the worst case of abrupt expansion and contraction (typical) and zero to denote well rounded and tapered expansion and contraction.

It is noted that for the case of a node interfacing the cooler and the regenerator, or the regenerator and the heater (equation H.10) the concept of a pressure loss coefficient is ignored. This is because for flow into matrix surfaces the entrance and exit behaviour has already been taken into consideration in the matrix friction factors (KL64).

Rewriting equation (H.12) to include the above arguments:

$$Dg_1 \leftarrow [2g_1 v n_1 \Delta g_1 + g_1^2 (v_c - v_1)] / \Delta x_1 + \Sigma F_1 \quad (\text{H.15})$$

where

$$\Sigma F_1 \leftarrow (p_c - p_1 + \Delta p_c) / \Delta x_1 - 2Fr \cdot \mu \cdot g_1 v n_1 / d_1^2$$

$$g_1 \geq 0 \Rightarrow v_{n1} \leftarrow v_c, T_{n1} \leftarrow T_{c1}, \Delta g_1 \leftarrow -g_1,$$

$$\Delta p_c \leftarrow -K_c \cdot g_1^2 v_{n1} / 2$$

$$g_1 < 0 \Rightarrow v_{n1} \leftarrow v_1, T_{n1} \leftarrow T_1, \Delta g_1 \leftarrow g_1 - g_2,$$

$$\Delta p_c \leftarrow K_e \cdot g_1^2 v_{n1} / 2$$

d_1 is the hydraulic diameter of cell 1

Fr is the friction factor at node 1 evaluated using hydraulic diameter d_1

K_c is the contraction pressure loss coefficient

K_e is the expansion pressure loss coefficient.

The FORTRAN equivalent statements of equation (H.15) are given as follows:

```

      IF(G(1))10,15,15
10  DELG(1)=G(1)-G(2)
      TN(1)=T(1)
      VSN(1)=VS(1)
      DELPC=.5*RKE*VSN(1)*G(1)*G(1)
      GO TO 20
15  DELG(1)=-G(1)
      TN(1)=TC
      VSN(1)=VSC
      DELPC=-.5*RKC*VSN(1)*G(1)*G(1)
20  DELP(1)=PC-P(1)+DELP
      DELVS(1)=VSC-VS(1)

```

Algorithm for calculating μ (RMU) and Fr (FR) at node 1

```

BFRIC(1)=2./(D(1)*D(1))
SF=DELP(1)*DELXI(1)-BFRIC(1)*FR*RMU*G(1)*VSN(1)
DG(1)=G(1)*DELXI(1)*(2.*VSN(1)*DELG(1)+G(1)*DELVS(1))+SF

```

For the node interfacing the expansion space and cell nc a similar algorithm applies:

$$Dg_{nc1} \leftarrow [2g_{nc1}v_{nc1}\Delta g_{nc1} + g_{nc1}^2(v_{nc} - v_e)] / \Delta x_{nc} + \Sigma F_{nc1} \quad (H.17)$$

where

$$\Sigma F_{nc1} \leftarrow (p_{nc} - p_e + \Delta p_e) / \Delta x_{nc} - 2Fr \cdot \mu \cdot g_{nc1} v_{nc1} / d_{nc1}^2$$

$$g_{nc1} \geq 0 \Rightarrow v_{nc1} \leftarrow v_{nc}, T_{nc1} \leftarrow T_{nc}, \Delta g_{nc1} \leftarrow (g_{nc} - g_{nc1}),$$

$$\Delta p_e \leftarrow -K_e \cdot g_{nc1}^2 v_{nc1}^2 / 2$$

$$g_{nc1} < 0 \Rightarrow v_{nc1} \leftarrow v_e, T_{nc1} \leftarrow T_e, \Delta g_{nc1} \leftarrow g_{nc1},$$

$$\Delta p_e \leftarrow K_c \cdot g_{nc1}^2 v_{nc1}^2 / 2$$

d_{nc1} is the hydraulic diameter of cell nc

Fr is the friction factor at node $nc1$ evaluated using hydraulic diameter d_{nc1}

K_c is the contraction pressure loss coefficient

K_e is the expansion pressure loss coefficient

The FORTRAN equivalent statements of equation (H.17) are given as follows:

```

IF(G(NC1))45,50,50
45 DELG(NC1)=G(NC1)
   TN(NC1)=TE
   VSN(NC1)=VSE
   DELPE=.5*RKC*VSN(NC1)*G(NC1)*G(NC1)
   GO TO 55
50 DELG(NC1)=G(NC)-G(NC1)
   TN(NC1)=T(NC)
   VSN(NC1)=VS(NC)
   DELPE=-.5*RKE*VSN(NC1)*G(NC1)*G(NC1)
55 DELP(NC1)=P(NC)-PE+DELPE
   DELVS(NC1)=VS(NC)-VSE

```

↓

Algorithm for calculating μ (RMU) and Fr (FR) at node $nc1$.

↓

```

BFRIC(NC1)=2./(D(NC1)*D(NC1))
SF=DELP(NC1)*DELXI(NC)-BFRIC(NC1)*FR*RMU*G(NC1)*VSN(NC1)
DG(NC1)=G(NC1)*DELXI(NC)*(2.*VSN(NC1)*DELG(NC1)+
+G(NC1)*DELVS(NC1))+SF

```

H.4 ENERGY BALANCE OF THE WORKING GAS

From Appendix D the energy equation for the working gas is given as follows:

$$\frac{dQ}{dt} = \frac{\partial}{\partial t} \left(\frac{m \cdot T}{\gamma - 1} \right) + v \frac{\partial}{\partial x} \left(\frac{\gamma T \cdot g}{\gamma - 1} \right) - g \cdot v \left(v \frac{\partial p}{\partial x} + F \right) + \frac{dW}{dt} \quad (D.18)$$

The term dW/dt in equation (D.18) is now considered.

Mechanical work can be classified into indicated mechanical work or brake mechanical work. Brake mechanical work is available at the output of an engine and includes the mechanical friction losses of the bearings, pistons, etc. In this work the emphasis has been placed on the internal gas dynamic and heat transfer behaviour of the engine, hence only indicated mechanical work has been considered. It has been assumed that the mechanical work is done reversibly.

$$dW/dt = p dV/dt \quad (H.19)$$

It is assumed that the working gas behaves as a perfect gas. The perfect gas normalized equation of state is:

$$p \cdot V = m \cdot T \quad (H.20)$$

(H.19), (H.20) + (D.18):

$$\frac{dQ}{dt} = \frac{\partial}{\partial t} \left(\frac{p \cdot V}{\gamma - 1} \right) + V \frac{\partial}{\partial x} \left(\frac{\gamma T \cdot g}{\gamma - 1} \right) - g \cdot v \left(V \frac{\partial p}{\partial x} + F \right) + p \frac{dV}{dt} \quad (H.21)$$

Equation (H.21) is applied separately to the heat exchanger cells and to the working spaces. For the heat exchanger cells the volume is constant with time, and equation (H.21) reduces to:

$$\frac{dQ}{dt} = \frac{V}{\gamma - 1} \frac{\partial p}{\partial t} + \frac{V \gamma}{\gamma - 1} \frac{\partial}{\partial x} (T \cdot g) - g \cdot v \left(V \frac{\partial p}{\partial x} + F \right) \quad (H.22)$$

The term $[V\gamma/(\gamma-1)] \partial(T \cdot g)/\partial x$ in equation (H.22) is now considered. This term represents the net enthalpy

transport to the cell. It has been previously noted that in the context of the system model the temperature is constant throughout the cell and is discontinuous at the cell nodes. Thus the node temperatures are conditional convective parameters (conditional on the sign of g at that node) taking on the adjacent upstream cell values of temperature. The cell temperatures return a zero spacial derivative.

The term $g.v(V\partial p/\partial x+F)$ in equation (H.22) is now considered. It is noticed from the momentum equation algorithms (equations (H.8) through (H.18)) that the term $(\partial p/\partial x+F/V)$ has been evaluated at all the nodes. In order to utilize these values in the cell energy equations, the weighted arithmetic mean of these adjacent nodal terms (weighted by the local values of g and vn) will be used.

It is noticed from equation (H.22) that there are two time derivative terms, dQ/dt and $\partial p/\partial t$. However, dQ/dt can be evaluated independantly from convective heat transfer considerations, hence equation (H.22) is solved for $\partial p/\partial t$.

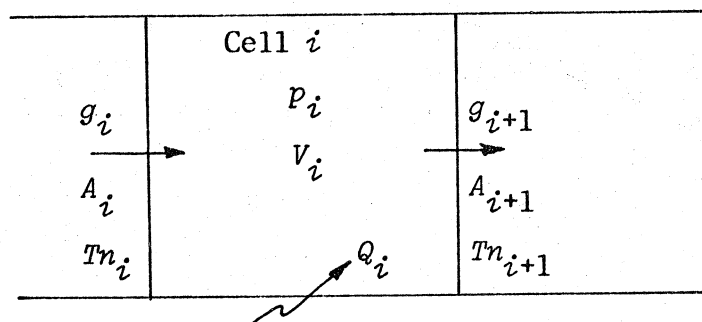


Figure H.9 THE i 'TH CELL

Discretizing equation (H.22) and applying it to the i 'th cell (figure H.9):

$$Dp_i + (\gamma-1) [DQ_i + (A_i g_i Tn_i - A_{i+1} g_{i+1} Tn_{i+1}) \gamma / (\gamma-1)] / v_i - (\gamma-1) (g_i v n_i \Sigma F_i + g_{i+1} v n_{i+1} \Sigma F_{i+1}) / 2 \quad (\text{H.23})$$

where vn_i , Tn_i , ΣF_i are given in equations (H.8), (H.10).

The FORTRAN equivalent statements of equation (H.23) are given as follows:

$$\begin{aligned} &\downarrow \\ >NA(I) = G(I) * TN(I) * A(I) \\ &BF(I) = G(I) * VSN(I) * SF \\ &\downarrow \\ &DP(I) = CVS I * (((DQ(I) + CPS * (GTNA(I) - GTNA(I+1))) / V(I) - \\ &\quad - .5 * (BF(I) + BF(I+1)))) \end{aligned} \quad (\text{H.24})$$

In the case of the working spaces the volume is varying with time. Expanding equation (H.21):

$$\frac{dQ}{dt} = \frac{V}{(\gamma-1)} \frac{\partial p}{\partial t} + \frac{\gamma p}{(\gamma-1)} \frac{\partial V}{\partial t} + \frac{\gamma V}{(\gamma-1)} \frac{\partial}{\partial x} (T \cdot g) - g \cdot v \cdot V \left(\frac{\partial p}{\partial x} + \frac{F}{V} \right) \quad (\text{H.25})$$

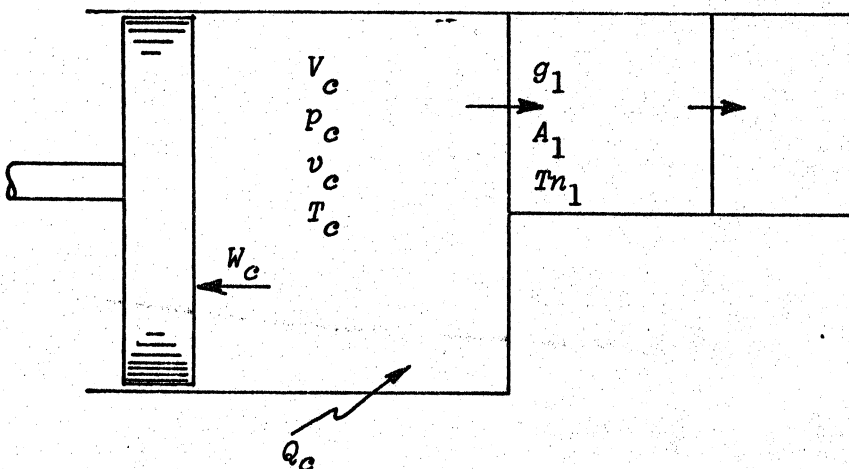


Figure H.10 THE COMPRESSION SPACE

Discretizing equations (H.19), (H.25), and applying them to the compression space (figure H.10):

$$Dwc + pc \cdot Dvc \quad (H.26)$$

$$Dpc + [(\gamma-1)DQc - \gamma(Dwc + A_1 g_1 Tn_1) - (g_1 v n_1 \Sigma F_1)(\gamma-1)V_1/2] / Vc \quad (H.27)$$

where Tn_1 , vn_1 , ΣF_1 are given in equation (H.12)

The generalized system model has been defined for adiabatic working spaces hence the heat transfer term DQc falls away. This is not a fundamental limitation of the model or analysis, however, and a heat transfer term can be added if required. One specific example is when heat transfer by conduction is allowed to take place between the wall of the compression space and the wall of the first cell. It can be assumed in this case that some of this heat comes from the compression space working fluid, thus DQc in equation (H.27) will be finite.

For DQc zero equation (H.27) becomes

$$Dpc + -[\gamma(Dwc + A_1 g_1 Tn_1) + (g_1 v n_1 \Sigma F_1)(\gamma-1)V_1/2] / Vc \quad (H.28)$$

The FORTRAN equivalent statements of equations (H.26), (H.28) are given by the following:

```

↓
GTNA(1)=G(1)*TN(1)*A(1)
BF(1)=G(1)*VSN(1)*SF
BGV1=.5*CVSI*V(1)
↓
DWC=PC*DVC
DPC=- (GAMMA*(DWC+GTNA(1))+BGV1*BF(1))/VC

```

(H.29)

For the expansion space a similar set of equations apply:

$$DWe \leftarrow pe \cdot DVe \quad (H.30)$$

$$Dpe \leftarrow -[\gamma(DWe - A_{nc1} g_{nc1}) + (g_{nc1} v_{nc1} \Sigma F_{nc1}) (\gamma - 1) v_{nc1} / 2] / ve \quad (H.31)$$

where Tn_{nc1} , Vn_{nc1} , ΣF_{nc1} are given in equation (H.17)

The FORTRAN equivalent statements of equations (H.30), (H.31) are given as follows:

$$\begin{array}{l} \downarrow \\ GTNA(NC1) = G(NC1) * TN(NC1) * A(NC1) \\ BF(NC1) = G(NC1) * VSN(NC1) * SF \\ BGVNC = .5 * CVS1 * V(NC) \\ \downarrow \\ DWE = PE * DVE \\ DPC = - (GAMMA * (DWE - GTNA(NC1)) + BGVNC * BF(NC1)) / VE \end{array} \quad (H.32)$$

The total indicated mechanical work W is given by the sum of the compression space work and the expansion space work

$$DW = DWE + DWC \quad (H.33)$$

H.5 ENERGY BALANCE OF THE COOLER (HEATER) WALL

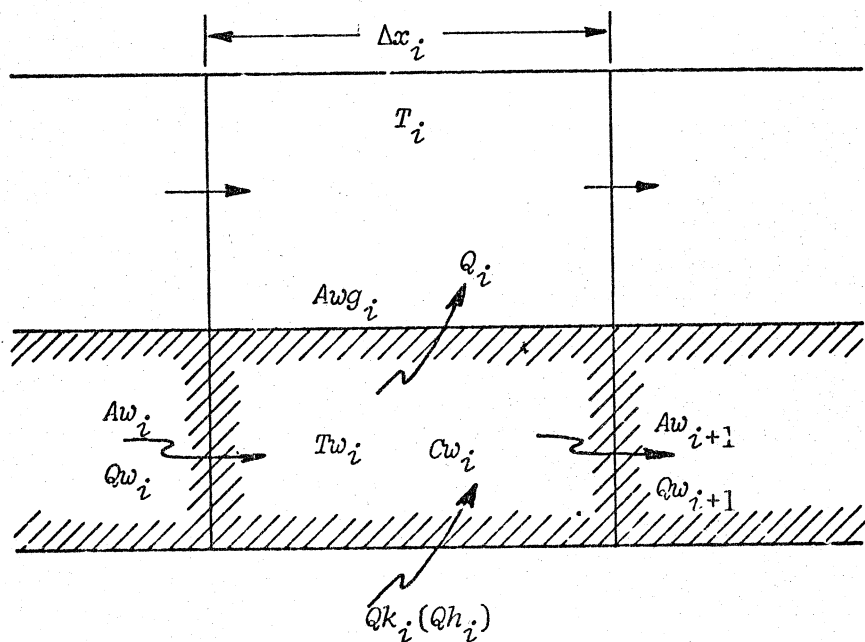


Figure H.11 THE COOLER (HEATER) WALL.

The only form of energy that can pass through the heat exchanger wall is heat. Energy is stored in the heat exchanger wall in terms of its heat capacity and temperature. Thus referring to figure H.11 the energy balance for the i 'th (cooler) cell wall is given by:

$$Cw_i DTw_i + DQw_i + DQk_i - DQ_i - DQw_{i+1} \quad (H.34)$$

where

Q_{w_i} , $Q_{w_{i+1}}$ are longitudinal conductive heat flows in the wall

Q_i is the convective heat transfer between the wall and the working fluid

Qk_i is the convective heat transfer between the external coolant and the wall.

The various heat flows in equation (H.34) are respectively:

$$DQw_i \leftarrow 2kw \cdot Aw_i (Tw_{i-1} - Tw_i) / (\Delta x_{i-1} + \Delta x_i) \quad (\text{H.35})$$

where

kw is the wall material thermal conductivity

Aw_i is the smaller of the wall cross sectional areas of the two adjacent cells ($i-1$) and i .

$$DQ_i \leftarrow (h_i + h_{i+1}) Aw_i (Tw_i - T_i) / 2 \quad (\text{H.36})$$

where

h_i is the convective heat transfer coefficient between the wall and the working fluid, calculated at node i in accordance with the methods given in Appendix F.

$$DQk_i \leftarrow hk_i Aw_{o_i} (To_i - Tw_i) \quad (\text{H.37})$$

where

hk_i is the convective heat transfer coefficient between the wall and the external coolant adjacent to cell i

To_i is the temperature of the coolant adjacent to cell i .

Usually it is assumed that T_{w_i} is a constant for all the cooler cells and that DQ_{k_i} is exactly metered in order to maintain T_{w_i} at that constant value T_{wk} . In this case all the DQ_{w_i} in the cooler section are zero excepting for the end values. Thus since T_{wk} is generally different from the temperature of the first regenerator cell wall there is non-zero conductive heat flow DQ_{wr_1} . Similarly since the cylinder wall of the compression space has in general a different temperature to T_{wk} there is a non-zero conductive heat flow DQ_{w_1} . The actual value of cylinder wall temperature T_{wc} is dependant on the particular configuration and ambient conditions and can only be accounted for from experimental measurement of an actual machine. It may also be necessary to subtract some of the heat flow DQ_{w_1} from the working gas energy in the compression space. In the application example test engine of Chapter 4, DQ_{w_1} has been considered to be zero, which would be normal practice until experimental values of T_{wc} could be obtained.

It is not specifically of interest to obtain the heat transfer to the working fluid from each individual cell wall, but rather the bulk behaviour of the cooler.

Thus applying the above arguments to equations (H.34) through (H.37):

$$DQ_{wr_1} \leftarrow 2kw \cdot Aw_{nk1} (T_{wk} - T_{wr_1}) / (\Delta x_{nk} + \Delta x_{nk1}) \quad (\text{H.38})$$

$$DQ_i \leftarrow (h_i + h_{i+1}) Aw_{g_i} (T_{w_i} - T_i) / 2 \quad (\text{H.39})$$

$$DQ_k \leftarrow DQ_{wr_1} + \sum_{i=1}^{nk} DQ_i \quad (\text{H.40})$$

where DQ_k is the total heat transferred to the cooler wall from the external coolant.

The FORTRAN equivalent statements of equations (H.38) through (H.40) are given by the following:

```

↓
BAWG(I) = .5*AWG(I)
BCONK = RKW*AW(NK1)*2./(DELX(NK)+DELX(NK1))
↓
DQWR(1) = BCONK*(TWK-TWR(1))
DQ(I) = BAWG(I)*(H(I)+H(I+1))*(TW(I)-T(I))
DQK = DQWR(1)
DO 125 I=1,NK
125 DQK = DQK + DQ(I)

```

(H.41)

A similar set of arguments and equations apply to the heater, as follows:

$$DQ_{wr_{nr1}} \leftarrow 2kw \cdot Aw_{nkr1} (T_{wr_{nr1}} - T_{wh}) / (\Delta x_{nkr} + \Delta x_{nkr1}) \quad (\text{H.42})$$

$$DQ_h \leftarrow -DQ_{wr_{nr1}} + \sum_{i=nkr1}^{nc} DQ_i \quad (\text{H.43})$$

where

DQ_i is given in equation (H.39)

DQ_h is the total heat transferred to the heater wall from the external heat source.

The FORTRAN equivalent statements of equation (H.42), (H.43) are given by the following:

```

↓
BCONH=RKW*AW(NKR1)*2./(DELX(NKR)+DELX(NKR1))
↓
DQWR(NR1)=BCONH*(TWR(NKR)-TWH)
DQH=-DQWR(NR1)
DO 130 I=1,NH
NKRI=NKR+I
130 DQH=DQH+DQ(NKRI)

```

(H.44)

H.6 ENERGY BALANCE OF THE REGENERATOR MATRIX

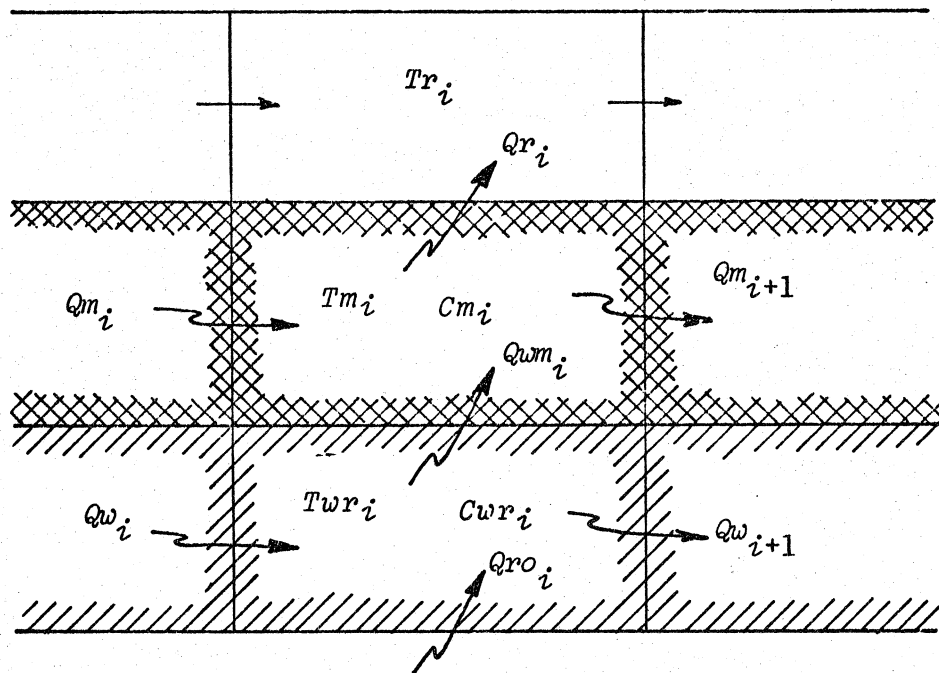


Figure H.12 THE REGENERATOR MATRIX AND ENCLOSING WALL

The same considerations apply here as in section H.5. Energy balance in the regenerator matrix involves heat flow and storage only. Referring to figure H.12 the energy balance in the i 'th regenerator cell matrix is given by:

$$Cm_i DTm_i + DQm_i + DQwm_i - DQr_i - DQm_{i+1} \quad (H.45)$$

where

Qm_i , Qm_{i+1} are longitudinal conductive heat flows in the matrix

Qr_i is the convective heat transfer between the matrix and the working fluid

Qwm_i is the conductive heat transfer between the regenerator enclosing wall and the matrix.

The energy balance for the i 'th regenerator cell wall is given by:

$$Cwr_i DTwr_i + DQwr_i + DQro_i - DQwm_i - DQwr_{i+1} \quad (H.46)$$

where

Qwr_i , Qwr_{i+1} are longitudinal heat flows by conduction

Qro_i is the heat loss from the regenerator to the external environment.

It is noted from equation (H.46) that within the context of the model, if there is a regenerator matrix

in the machine then all the heat is transferred to the working gas from the matrix in the regenerator section, and not from the adjacent enclosing wall.

In equations (H.45) and (H.46), DQm_i , $DQwm_i$ and $DQro_i$ are normally ignored as being negligible in comparison to the other terms.

$$Cm_i DTm_i \leftarrow -DQr_i \quad (\text{H.47})$$

$$Cwr_i DTwr_i \leftarrow DQwr_i - DQwr_{i+1} \quad (\text{H.48})$$

Thus heat transfer takes place in the matrix by convection only and in the wall by conduction only.

The various heat flows are given by:

$$DQr_i \leftarrow (h_{nki} + h_{nki+1}) Amg_i (Tm_i - T_{nki}) / 2 \quad (\text{H.49})$$

$$DQwr_i \leftarrow 2kw \cdot Awr_i (Twr_{i-1} - Twr_i) / (\Delta x_{nki-1} + \Delta x_{nki}) \quad (\text{H.50})$$

where

$$nki = nk+i$$

h_{nki} is the convective heat transfer coefficient between the matrix and the working gas at node nki

Awr_i is the smaller of the wall cross sectional areas of the adjacent two regenerator cells ($i-1$) and i .

The FORTRAN equivalent statements of equations (H.47) through (H.50) are given by the following:

```

NKI=NK+I
BCONR(I)=RKW*AWR(I)*2./(DELX(NKI-1)+DELX(NKI))
DQWR(I)=BCONR(I)*(TWR(I-1)-TWR(I))
BAMG(I)=.5*AMG(I)
DQR(I)=(H(NKI)+H(NKI+1))*BAMG(I)*(TM(I)-T(NKI))
DTM(I)=-CMI(I)*DQR(I)
DTWR(I)=CWRI(I)*(DQWR(I)-DQWR(I+1))

```

(H.51)

In the application example test engine (Chapter 4) the system chosen does not have a regenerator matrix. The regenerator is the continuation of the bundle of heat exchanger pipes, regenerative action taking place in the walls of these pipes. In this case heat transfer Dq_{r_i} takes place between the regenerator wall and the working fluid, and equations (H.47) and (H.48) merge.

$$Cwr_i DTwr_i + Dqwr_i - Dqwr_{i+1} - Dqr_i \quad (H.52)$$

The FORTRAN equivalent statement of equation (H.52) is

```

CWRI(I)=1./CWR(I)
DTWR(I)=CWRI(I)*(DQWR(I)-DQWR(I+1)-DQR(I))

```

(H.53)

H.7 VISCOSITY

In Appendix E, the dynamic viscosity as a function of temperature is given by equation (E.4).

$$\mu = \mu_0 \left(\frac{T_0 + Tsu}{T + Tsu} \right) \left(\frac{T}{T_0} \right)^{3/2} \quad (\text{E.4})$$

If the base temperature used is $T_0 = 1$ then (E.4) becomes

$$\mu = \mu_k (T)^{3/2} (1 + Tsu) / (T + Tsu) \quad (\text{H.54})$$

From equation (H.8) it is seen that the dynamic viscosity is always evaluated at the nodes. The algorithm for obtaining the dynamic viscosity at node i is thus

$$\mu = \mu_k (Tn_i)^{3/2} (1 + Tsu) / (Tn_i + Tsu) \quad (\text{H.55})$$

The FORTRAN equivalent statement of equation (H.55) is given by:

$$\text{RMU} = (1 + \text{TSU}) * \text{TN}(I) ** 1.5 * \text{RMUK} / (\text{TN}(I) + \text{TSU}) \quad (\text{H.56})$$

H.8 REYNOLDS FRICTION FACTOR AND FLOW TAG

In Appendix F the Reynolds friction factor is defined. The evaluation of friction as a function of Reynolds number is based on empirical observations, and is dependent upon the type of geometry used. In what follows, the geometry used has been restricted to that of a bundle of circular pipe heat exchangers, as in the application example test engine given in Chapter 4.

From Appendix F, the Reynolds friction factor for a circular pipe (or a bundle of circular pipes) is given by equations (F.16), (F.17) and (F.18)

$$0 \leq Re < 2000, Ro \geq 0 \Rightarrow Fr \leftarrow 16 \quad (\text{F.16})$$

$$Re \geq 2000, Ro = 0 \Rightarrow Fr \leftarrow 0,0791(Re)^{0,75} \quad (\text{F.17})$$

$$Re \geq 2000, Ro > 0 \Rightarrow \begin{cases} Fr1 \leftarrow 0,0791(Re)^{0,75} \\ Fr2 \leftarrow Re / (4 [1,14 - 0,86861 \ln(Ro)]^2) \\ Fr1 > Fr2 \Rightarrow Fr \leftarrow Fr1 \\ Fr1 < Fr2 \Rightarrow Fr \leftarrow Fr2 \end{cases} \quad (\text{F.18})$$

where

$$Re \triangleq |g \cdot d / \nu| \quad (\text{F.8})$$

The various flow regimes are denoted by a so-called 'flow tag' $Iflo$ as follows:

Laminar flow regime

$$Fr \leftarrow 16 \Rightarrow Iflo \leftarrow 1 \quad (\text{H.57})$$

Blasius turbulent flow regime

$$Fr \leftarrow 0,0791(Re)^{0,75} \Rightarrow Iflo \leftarrow 2 \quad (\text{H.58})$$

Nikuradse turbulent flow regime

$$Fr \leftarrow Re / (4 [1,14 - 0,86861 \ln(Ro)]^2) \Rightarrow Iflo \leftarrow 3 \quad (\text{H.59})$$

The flow tag $Iflo$ also takes on a sign, indicating the direction of flow:

$$g_i > 0 \Rightarrow Iflo_i \text{ positive}$$

$$g_i = 0 \Rightarrow Iflo_i = 0 \quad (H.60)$$

$$g_i < 0 \Rightarrow Iflo_i \text{ negative}$$

In addition a check is made to determine if sonic velocity is ever attained across any of the nodes. Sonic velocity is attained at the i 'th node whenever:

$$g_i v n_i = \sqrt{\gamma T n_i} \quad (H.61)$$

If sonic velocity is attained, then the flow tag $Iflo$ is assigned a value 4.

$$|g_i| v n_i \geq \sqrt{\gamma T n_i} \Rightarrow Iflo_i = 4 \quad (H.62)$$

The FORTRAN equivalent statements of the above arguments and equations are given as follows:

```

      IF(RO)50,50,55
50  BRUF=0.
      GO TO 60
55  BRUFF=1.14-.8686*ALOG(RO)
      BRUF=1./(4.*BRUFF*BRUFF)
60  CONTINUE

```



```

      RE=ABS(G(I))*D/RMU
      FR=16.
      IFLO(I)=1
      IF(RE-2000.)80,65,65
65  FR1=.0791*RE**.75
      FR2=BRUF*RE
      IF(FR1-FR2)70,75,75
70  FR=FR1
      IFLO(I)=2
      GO TO 80
75  FR=FR2
      IFLO(I)=3
80  IF(ABS(G(I))*VSN(I))-SQRT(GAMMA*TN(I))90,85,85
85  IFLO(I)=4
90  IF(G(I))95,100,105
95  IFLO(I)=-IFLO(I)
      GO TO 105
100 IFLO(I)=0
105 CONTINUE

```

(H.63)

H.9 THE HEAT TRANSFER COEFFICIENT

In Appendix F, the Reynolds simple analogy is given by equation (F.21).

$$Nu = Fr/2 \quad (F.21)$$

where

$$Nu \triangleq h.d/k \quad (F.19)$$

In Appendix E, the thermal conductivity k is given in terms of the Prandtl number by equation (E.5).

$$Pr \Delta \mu \cdot \gamma / (\gamma - 1) \cdot k \quad (E.5)$$

(E 5), (F.19) → (F.21):

$$h = Fr \cdot \mu \cdot \gamma / (\gamma - 1) \cdot 2 \cdot d \cdot Pr \quad (H.64)$$

The FORTRAN equivalent statements of equation (H.64) for the heat transfer coefficient at the i 'th node is given by the following:

$$\begin{array}{l} BPR = .5 * CPS / (D * PR) \\ \downarrow \\ FRMU = FR * RMU \\ H(I) = BPR * FRMU \end{array} \quad (H.65)$$

H.10 VOLUME VARIATION

The volume variation of the compression and expansion spaces and their time derivatives must be defined. Any arbitrary volume variation may be used, and it has been decided for convenience to define sinusoidal volume variation, as in the Schmidt cycle (Appendix B).

$$\theta = \omega t \quad (H.66)$$

where

ω is the angular speed of crankshaft rotation

θ is the crank angle

$$V_e = V_{c1} + (1 + \cos \theta) / 4 \quad (B.1)$$

$$V_e = V_{c1} + [1 + \cos(\theta + \alpha)] / 4 \quad (B.2)$$

where

V_{cl} is the clearance volume

α is the (constant) angular phase lead of the volume variation of the expansion space to that of the compression space.

Differentiating equations (B.1), (B.2) with respect to time

$$DVe \leftarrow -\omega \sin \theta / 4 \quad (H.67)$$

$$DVe \leftarrow -\omega \sin(\theta + \alpha) / 4 \quad (H.68)$$

The FORTRAN equivalent statements of the above equations are as follows:

```

BOMEG=.25*OMEGA
↓
THETA=OMEGA*TIME
VC=VCL+.25*(1.+COS(THETA))
VE=VCL+.25*(1.+COS(THETA+ALPHA))
DVC=-BOMEG*SIN(THETA)
DVE=-BOMEG*SIN(THETA+ALPHA)

```

(H.69)

I. COMPUTER PROGRAM

I.1 GENERAL

This appendix presents a complete FORTRAN listing of the computer program for the application example test engine of Chapter 4. The complete program comprises a main or driving program and the differential equation subroutine DERIV. The main program follows the lines of the method of solution given in Appendix G. Subroutine DERIV has been based on the system algorithms given in Appendix H. No attempt has been made to produce a completely generalized program. Because of the considerable computer solution times involved the approach has been to tailor both the main program and the subroutine DERIV to each specific system configuration.

I.2 SUBROUTINE DERIV

```

SUBROUTINE DERIV
DIMENSION TN(46),DELG(46),GTN(46),DQ(45),VS(45),VSN(46),DQWR(16),
-DELP(46),H(46),BF(46),DELVS(46)
COMMON RMC,PC,PE,W,QK,QH,QR(15),TWR(16),RM(45),P(45),G(46)
COMMON DMC,DPC,DPE,DW,DQK,DQH,DQR(15),DTWR(16),DM(45),DP(45)
COMMON DG(46),TW(45),T(45),TC,TE,VC,VE,RME,TIME,DELPC,DELPE
COMMON IFLO(46),NK,NR,NR1,NKR,NH,NC,NC1
COMMON VCL,V,VI,A,BAWG,DELXI,D
COMMON OMEGA,ALPHA,BOMEG,GAMMA,BGV,CPS,CVSI,BCON,CWI
COMMON TSU,RMUK,BFRIC,BRUF,BPR,TWH,TWK
THETA=OMEGA*TIME
VC=VCL+.25*(1.+COS(THETA))
VE=VCL+.25*(1.+COS(THETA+ALPHA))
DVC=-BOMEG*SIN(THETA)
DVE=-BOMEG*SIN(THETA+ALPHA)
VSC=VC/RMC
TC=PC*VSC
DMC=-A*G(1)
SM=RMC
DO 5 I=1,NC
VS(I)=V/RM(I)
T(I)=P(I)*VS(I)
DM(I)=A*(G(I)-G(I+1))
5 SM=SM+RM(I)
RME=1.-SM
VSE=VE/RME
TE=PE*VSE
IF(G(1))10,15,15
10 DELG(1)=G(1)-G(2)
TN(1)=T(1)
VSN(1)=VS(1)
DELPC=.5*VSN(1)*G(1)*G(1)
GO TO 20
15 DELG(1)=-G(1)
TN(1)=TC
VSN(1)=VSC
DELPC=-.5*VSN(1)*G(1)*G(1)
20 DELP(1)=PC-P(1)+DELPC
DELVS(1)=VSC-VS(1)
GTN(1)=G(1)*TN(1)
DO 40 I=2,NC
IF(G(I))25,30,30
25 DELG(I)=G(I)-G(I+1)
TN(I)=T(I)
VSN(I)=VS(I)
GO TO 35
30 DELG(I)=G(I-1)-G(I)
TN(I)=T(I-1)

```

```

VSN(I)=VS(I-1)
35 DELP(I)=P(I-1)-P(I)
   DELVS(I)=VS(I-1)-VS(I)
40 GTN(I)=G(I)*TN(I)
   IF(G(NC1))45,50,50
45 DELG(NC1)=G(NC1)
   TN(NC1)=TE
   VSN(NC1)=VSE
   DELPE=.5*VSN(NC1)*G(NC1)*G(NC1)
   GO TO 55
50 DELG(NC1)=G(NC)-G(NC1)
   TN(NC1)=T(NC)
   VSN(NC1)=VS(NC)
   DELPE=-.5*VSN(NC1)*G(NC1)*G(NC1)
55 DELP(NC1)=P(NC)-PE+DELPE
   DELVS(NC1)=VS(NC)-VSE
   GTN(NC1)=G(NC1)*TN(NC1)
   DO 60 I=1,NR
   NKI=NK+I
60 TW(NKI)=TWR(I)
   DO 110 I=1,NC1
   RMU=(1.0+TSU)*TN(I)**1.5*RMUK/(TN(I)+TSU)
   RE=ABS(G(I)*D/RMU)
   FR=16.
   IFLO(I)=1
   IF(RE-2000.)80,65,65
65 FR1=.0791*RE**.75
   FR2=BRUF*RE
   IF(FR2-FR1)70,75,75
70 FR=FR1
   IFLO(I)=2
   GO TO 80
75 FR=FR2
   IFLO(I)=3
80 IF(ABS(G(I)*VSN(I))-SQRT(GAMMA*TN(I)))90,85,85
85 IFLO(I)=4
90 IF(G(I))95,100,105
95 IFLO(I)=-IFLO(I)
   GO TO 105
100 IFLO(I)=0
105 FRMU=FR*RMU
   H(I)=BPR*FRMU
   SF=DELP(I)*DELXI-BFRIC*FRMU*G(I)*VSN(I)
   BF(I)=G(I)*SF*VSN(I)
110 DG(I)=G(I)*DELXI*(2.*VSN(I)*DELG(I)+G(I)*DELVS(I))+SF
   DWC=PC*DVC
   DPC=- (GAMMA*(DWC+A*GTN(1))+BGV*BF(1))/VC
   DO 115 I=1,NC
   DQ(I)=BAWG*(H(I)+H(I+1))*(TW(I)-T(I))
115 DP(I)=CVSI*(DQ(I)*VI+CPS*(GTN(I)-GTN(I+1))*DELXI-
   -.5*(BF(I)+BF(I+1)))
   DQWR(1)=BCON*(TWK-TWR(1))
   DO 120 I=1,NR
   NKI=NK+I
   DQR(I)=DQ(NKI)
   DQWR(I+1)=BCON*(TWR(I)-TWR(I+1))
120 DTWR(I)=CWI*(DQWR(I)-DQWR(I+1)-DQR(I))
   DQK=DQWR(1)
   DO 125 I=1,NK

```

PAGE 3

```
125 DQK=DQK+DQ(I)
    DQH=-DQWR(NR1)
    DO 130 I=1,NH
    NKR!=NKR+I
130 DQH=DQH+DQ(NKRI)
    DWE=PE*DVE
    DPE=- (GAMMA*(DWE-A*GTN(NC1))+BGV*BF(NC1))/VE
    DW=DWC+DWE
    RETURN
    END
```

I.3 MAIN PROGRAM

```

DIMENSION Y(6),DY(6),YY(6),DLY(6),PP(45),DLP(45),RMM(45),
-DLM(45),GG(46),DLG(46),TTWR(15),DLTWR(15),QQR(15),DLQR(15)
COMMON RMC,PC,PE,W,QK,QH,QR(15),TWR(16),RM(45),P(45),G(46)
COMMON DMC,DPC,DPE,DW,DQK,DQH,DQR(15),DTWR(16),DM(45),DP(45)
COMMON DG(46),TW(45),T(45),TC,TE,VC,VE,RME,TIME,DELPC,DELPE
COMMON IFLO(46),NK,NR,NR1,NKR,NH,NC,NC1
COMMON VCL,V,VI,A,BAWG,DELXI,D
COMMON OMEGA,ALPHA,BOMEG,GAMMA,BGV,CPS,CVSI,BCON,CWI
COMMON TSU,RMUK,BFRIC,BRUF,BPR,TWH,TWK
EQUIVALENCE (DY(1),DMC),(DY(2),DPC),(DY(3),DPE),(DY(4),DW)
EQUIVALENCE (DY(5),DQK),(DY(6),DQH)
EQUIVALENCE (Y(1),RMC),(Y(2),PC),(Y(3),PE),(Y(4),W),(Y(5),QK)
EQUIVALENCE (Y(6),QH)
READ(5,5) EVS,VD,VCL,EXP,DIA,RO,NP
5 FORMAT(6F10.6,I10)
WRITE(6,10)EVS,VD,VCL,EXP,DIA,RO,NP
10 FORMAT(' TOTAL STROKE VOL=',F10.6,' CUBIC M',10X,' FRACTIONAL DEAD V
-OL=',F6.3,10X,' FRACTIONAL CLEARANCE VOL=',F6.3/' H.E.LENGTH=',
-F8.5,' M',10X,' H.E.PIPE DIAM RATIO=',F6.3,10X,' ROUGHNESS=',F6.3,
-10X,' NO OF PIPES=',I5)
READ(5,15)GAMMA,ER,PR,ETSU,ETO,EMUO
15 FORMAT(5F10.3,E12.5)
WRITE(6,20)GAMMA,ER,PR,EMUO,ETO,ETSU
20 FORMAT(' GAMMA=',F6.3,10X,' R=',F9.3,10X,' PR=',F6.3/
-' DYNAMIC VISCOSITY=',E12.5,' KG/M.S AT TEMP',F8.3,' K',10X,
-' SUTHERLAND CONSTANT=',F9.3,' K')
READ(5,25)ECSW,EROW,EKW
25 FORMAT(3F10.3)
WRITE(6,30)ECSW,EROW,EKW
30 FORMAT(' WALL SPECIFIC HEAT=',F10.3,' J/KG.K',10X,
-' DENSITY=',F10.3,' KG/CU.M',10X,' THERMAL COND=',F10.3,' W/M.K')
READ(5,35)ETK,ETH,EFREQ,EPK,ALPHA
35 FORMAT(3F10.3,E12.5,F12.9)
WRITE(6,40)ETK,ETH,EFREQ,EPK,ALPHA
40 FORMAT(' TK=',F10.3,' K',5X,' TH=',F10.3,' K',10X,' FREQ=',F10.3,
-' HZ',10X,' CHARGE PRESS=',E12.5,' PA'/' ALPHA=',F12.9,' RADIANS')
READ(5,45)NK,NR,NH,NINC,NPRNT,JCYCL,JPRNT
45 FORMAT(7I5)
WRITE(6,50)NK,NR,NH,NINC,NPRNT,JCYCL,JPRNT
50 FORMAT(I5,' COOLER CELLS,',I5,' REGEN CELLS,',I5,' HEATER CELLS,',
-I10,' INCS/CYCLE,',I5,' INCS/PRINTOUT'/' CYCLE',I2,' OUTPUT',I2)
READ(5,55)(TWR(I),I=1,NR)
55 FORMAT(8F10.5)
WRITE(6,60)(TWR(I),I=1,NR)
60 FORMAT(' TWR',10F7.4)
READ(5,65)DELTA
65 FORMAT(F10.5)
WRITE(6,70)DELTA

```

```

70 FORMAT(' REGEN WALL TEMP CORRECTION FACTOR=',F10.5)
C NORMALIZING FACTORS-
  ERTK=ER*ETK
  EM=EPK*EVS/ERTK
  EX=EVS**0.3333333
  EA=EX*EX
  EU=SQRT(ERTK)
  ETIME=EX/EU
  EMU=EM*EU/EA
  EK=EM*ERTK**1.5/(EA*ETK)
  ENRGY=EM*ERTK
  ERO=EM/EVS
C NORMALIZED DYNAMIC VISCOSITY AT TK-
  RMUK=(ETK/ETO)**1.5*(ETO+ETSU)*EMUO/(EMU*(ETK+ETSU))
  TSU=ETSU/ETK
C NORMALIZED FIXED PARAMETERS AND CONSTANTS
  NK1=NK+1
  NKR=NK+NR
  NKR1=NKR+1
  NR1=NR+1
  NC=NK+NR+NH
  NC1=NC+1
  RNK=NK
  RNH=NH
  RNC=NC
C CELL VOLUME-
  V=(VD-2.*VCL)/RNC
  VI=1./V
C HEAT EXCHANGER PIPE LENGTH-
  XP=EXP/EX
C CELL LENGTH-
  DELX=XP/RNC
  DELXI=RNC/XP
C HEAT EXCHANGER FREE FLOW AREA-
  A=V*DELXI
C HEAT EXCHANGER PIPE INTERNAL DIAMETER (HYDRAULIC DIAMETER)-
  RNP=NP
  PI=3.141592624
  D=2.*SQRT(A/(RNP*PI))
C HEAT EXCHANGER WETTED AREA/CELL
  AWG=RNP*PI*D*DELX
  BAWG=.5*AWG
C DIMENSIONED HEAT EXCHANGER PIPE INTERNAL AND EXTERNAL DIAMETERS-
  DO=DIA*D
  ED=D*EX
  EDO=DO*EX
  WRITE(6,75)ED,EDO
75 FORMAT(' H.E.PIPE I.DIAM=',E12.5,'M',10X,'O.DIAM=',E12.5,'M')
C RELATIVE ROUGHNESS FACTOR-
  IF(RO)80,80,85
80 BRUF=0.
  GO TO 90
85 BRUFF=1.14-0.8686*ALOG(RO)
  BRUF=1./(4.*BRUFF*BRUFF)
90 CONTINUE
C HEAT EXCHANGER WALL PARAMETERS-
C WALL CROSS SECTIONAL AREA-
  AW=.25*PI*(DO*DO-D*D)*RNP
C WALL VOLUME/CELL-

```

```

      VW=AW*DELX
C   WALL DENSITY-
      ROW=EROW/ERO
C   SPECIFIC HEAT CAPACITY-
      CSW=ECSW/ER
C   TOTAL HEAT CAPACITY/CELL-
      CW=CSW*ROW*VW
      CWI=1./CW
C   WALL THERMAL CONDUCTIVITY-
      RKW=EKW/EK
      BCON=RKW*AW*DELXI
C   HEATER AND COOLER WALL TEMPERATURES-
      TWK=1.
      TWH=ETH/ETK
      DO 95 I=1,NK
    95  TW(I)=TWK
      DO 100 I=1,NK
      NKRI=NKR+I
    100  TW(NKRI)=TWH
      TWR(NR1)=TWH
C   GAS PARAMETERS-
C   CONSTANT VOLUME SPECIFIC HEAT CAPACITY-
      CVS=1./(GAMMA-1.)
      CVSI=GAMMA-1.
C   CONSTANT PRESSURE SPECIFIC HEAT CAPACITY-
      CPS=GAMMA*CVS
C   VARIOUS OTHER CONSTANTS-
      BGV=.5*CVSI*V
      BPR=.5*CPS/(PR*D)
      BFRIC=2./(D*D)
C   ANGULAR FREQUENCY-
      OMEGA=EFREQ*ETIME*2.*PI
      BOMEG=.25*OMEGA
C   INTEGRATION TIME INCREMENT-
      RNINC=NINC
      DTIME=2.*PI/(RNINC*OMEGA)
      GO TO (145,105),JCYCL
C   PRIMARY INITIAL CONDITIONS (CONTINUATION CYCLE)-
    105  READ(5,110)RMC,PC,PE
    110  FORMAT(3F10.6)
      WRITE(6,115)RMC,PC,PE
    115  FORMAT(' RMC=',F10.6,10X,'PC=',F10.6,10X,'PE=',F10.6)
      READ(5,120)(TWR(I),I=1,NR)
    120  FORMAT(8F10.6)
      WRITE(6,125)(TWR(I),I=1,NR)
    125  FORMAT(' TWR',10F10.6)
      READ(5,120)(RM(I),I=1,NC)
      WRITE(6,130)(RM(I),I=1,NC)
    130  FORMAT('  M',10F10.6)
      READ(5,120)(P(I),I=1,NC)
      WRITE(6,135)(P(I),I=1,NC)
    135  FORMAT('  P',10F10.6)
      READ(5,120)(G(I),I=1,NC1)
      WRITE(6,140)(G(I),I=1,NC1)
    140  FORMAT('  G',10F10.6)
      GO TO 170
C   PRIMARY INITIAL CONDITIONS (STARTUP ONLY)-
C   GAS TEMPERATURES-
    145  STI=0.

```

```

DO 150 I=1,NK
150 T(I)=TWK
STI=STI+RNK/TWK
DO 155 I=1,NR
NKI=NK+I
T(NKI)=TWR(I)
155 STI=STI+1./T(NKI)
DO 160 I=1,NH
NKRI=NKR+I
160 T(NKRI)=TWH
STI=STI+RNH/TWH
C WORKING SPACE VOLUMES AND TEMPERATURES-
VC=VCL+.5
VE=VCL+.25
TC=TWK
TE=TWH
C GAS PRESSURES AND MASS DISTRIBUTION-
PC=1./((VC/TC+VE/TE+V*STI))
RMC=PC*VC/TC
PE=PC
RME=PE*VE/TE
PV=PC*V
DO 165 I=1,NC
P(I)=PC
RM(I)=PV/T(I)
165 G(I)=0.
G(NC1)=0.
C BEGIN CYCLE-
170 CONTINUE
TIME=0.
JPRNT=0
W=0.
QK=0.
QH=0.
DO 175 I=1,NR
175 QR(I)=0.
SQR=0.
VC=VCL+.5
VE=VCL+.25
VT=VC+VE+VD-2.*VCL
WRITE(6,180)EVS,EPK,ENRGY
180 FORMAT(' VOL FACTOR=',E12.5,' CU M',10X,' PRESS FACTOR=',E12.5,
-' PASCALS',10X,' ENERGY FACTOR=',E12.5,' JOULES')
WRITE(6,185)
185 FORMAT(' VOLUME          PCOM          PEXP          QKOL          QREG          QHOT
- WORK')
WRITE(6,190)VT,PC,PE,QK,SQR,QH,W
190 FORMAT(7F10.5)
C RUNGE-KUTTA 4TH ORDER INTEGRATION ROUTINE-
DO 320 INC=1,NINC
DO 195 I=1,6
195 YY(I)=Y(I)
DO 200 I=1,NC
PP(I)=P(I)
RMM(I)=RM(I)
200 GG(I)=G(I)
GG(NC1)=G(NC1)
DO 205 I=1,NR
TTWR(I)=TWR(I)

```



```
205 QQR(I)=QR(I)
    TTIME=TIME
    CALL DERIV
    DO 210 I=1,6
    DYDT=DY(I)*DTIME
    DLY(I)=DYDT
210 Y(I)=YY(I)+.5*DYDT
    DO 215 I=1,NC
    DYDT=DP(I)*DTIME
    DLP(I)=DYDT
    P(I)=PP(I)+.5*DYDT
    DYDT=DM(I)*DTIME
    DLM(I)=DYDT
215 RM(I)=RMM(I)+.5*DYDT
    DO 220 I=1,NC1
    DYDT=DG(I)*DTIME
    DLG(I)=DYDT
220 G(I)=GC(I)+.5*DYDT
    DO 225 I=1,NR
    DYDT=DTWR(I)*DTIME
    DLTWR(I)=DYDT
    TWR(I)=TTWR(I)+.5*DYDT
    DYDT=DQR(I)*DTIME
    DLQR(I)=DYDT
225 QR(I)=QQR(I)+.5*DYDT
    TIME=TTIME+.5*DTIME
    CALL DERIV
    DO 230 I=1,6
    DYDT=DY(I)*DTIME
    DLY(I)=DLY(I)+2.*DYDT
230 Y(I)=YY(I)+.5*DYDT
    DO 235 I=1,NC
    DYDT=DP(I)*DTIME
    DLP(I)=DLP(I)+2.*DYDT
    P(I)=PP(I)+.5*DYDT
    DYDT=DM(I)*DTIME
    DLM(I)=DLM(I)+2.*DYDT
235 RM(I)=RMM(I)+.5*DYDT
    DO 240 I=1,NC1
    DYDT=DG(I)*DTIME
    DLG(I)=DLG(I)+2.*DYDT
240 G(I)=GG(I)+.5*DYDT
    DO 245 I=1,NR
    DYDT=DTWR(I)*DTIME
    DLTWR(I)=DLTWR(I)+2.*DYDT
    TWR(I)=TTWR(I)+.5*DYDT
    DYDT=DQR(I)*DTIME
    DLQR(I)=DLQR(I)+2.*DYDT
245 QR(I)=QQR(I)+.5*DYDT
    CALL DERIV
    DO 250 I=1,6
    DYDT=DY(I)*DTIME
    DLY(I)=DLY(I)+2.*DYDT
250 Y(I)=YY(I)+DYDT
    DO 255 I=1,NC
    DYDT=DP(I)*DTIME
    DLP(I)=DLP(I)+2.*DYDT
    P(I)=PP(I)+DYDT
    DYDT=DM(I)*DTIME
```

```

DLM(I)=DLM(I)+2.*DYDT
255 RM(I)=RMM(I)+DYDT
DO 260 I=1,NC1
DYDT=DG(I)*DTIME
DLG(I)=DLG(I)+2.*DYDT
260 G(I)=GG(I)+DYDT
DO 265 I=1,NR
DYDT=DTWR(I)*DTIME
DLTWR(I)=DLTWR(I)+2.*DYDT
TWR(I)=TTWR(I)+DYDT
DYDT=DQR(I)*DTIME
DLQR(I)=DLQR(I)+2.*DYDT
265 QR(I)=QQR(I)+DYDT
TIME=TIME+DTIME
CALL DERIV
DO 270 I=1,6
DYDT=DY(I)*DTIME
DLY(I)=DLY(I)+DYDT
270 Y(I)=YY(I)+DLY(I)*.166667
DO 275 I=1,NC
DYDT=DP(I)*DTIME
DLP(I)=DLP(I)+DYDT
P(I)=P(I)+DLP(I)*.166667
DYDT=DM(I)*DTIME
DLM(I)=DLM(I)+DYDT
275 RM(I)=RMM(I)+DLM(I)*.166667
DO 280 I=1,NC1
DYDT=DG(I)*DTIME
DLG(I)=DLG(I)+DYDT
280 G(I)=GG(I)+DLG(I)*.166667
DO 285 I=1,NR
DYDT=DTWR(I)*DTIME
DLTWR(I)=DLTWR(I)+DYDT
TWR(I)=TTWR(I)+DLTWR(I)*.166667
DYDT=DQR(I)*DTIME
DLQR(I)=DLQR(I)+DYDT
285 QR(I)=QQR(I)+DLQR(I)*.166667
C CHECK FOR PRINTOUT
J=J+1
IF(J-NPRNT)320,290,290
290 J=0
SQR=0.
DO 295 I=1,NR
295 SQR=SQR+QR(I)
VT=VC+VE+VD-2.*VCL
WRITE(6,190)VT,PC,PE,QK,SQR,QH,W
IF(JPRNT)320,320,300
300 WRITE(6,135)(P(I),I=1,NC)
WRITE(6,305)TC,TE
305 FORMAT(' TC',F10.6,10X,'TE=',F10.6)
WRITE(6,310)(T(I),I=1,NC)
310 FORMAT(' T',10F10.6)
WRITE(6,125)(TWR(I),I=1,NR)
WRITE(6,312)RMC,RME
312 FORMAT(' MC=',F10.6,10X,'ME=',F10.6)
WRITE(6,130)(RM(I),I=1,NC)
WRITE(6,140)(G(I),I=1,NC1)
WRITE(6,315)(IFLO(I),I=1,NC1)
315 FORMAT(' FLOW',46I2)

```

```
320 CONTINUE
C CYCLE COMPLETED.
  WRITE(6,125)(TWR(I),I=1,NR)
  WRITE(6,325)(QR(I),I=1,NR)
325 FORMAT(' QR',10F10.6)
  SQQR=0.
  DO 330 I=1,NR
330 SQQR=SQQR+QR(I)*QR(I)
  RMSQR=SQRT(SQQR)
  WRITE(6,335)RMSQR
335 FORMAT(' RMS REGEN HEAT=',E12.5)
  EFF=W/QH
  WRITE(6,340)EFF
340 FORMAT(' EFFICIENCY='F7.3)
C ALTER TWR FOR CONVERGENCE-
  DO 345 I=1,NR
345 TWR(I)=TWR(I)-DELTA*QR(I)
C PRINT OUT ALL VARIABLES-
  WRITE(6,115)RMC,PC,PE
  WRITE(7,110)RMC,PC,PE
  WRITE(6,125)(TWR(I),I=1,NR)
  WRITE(7,120)(TWR(I),I=1,NR)
  WRITE(6,130)(RM(I),I=1,NC)
  WRITE(7,120)(RM(I),I=1,NC)
  WRITE(6,135)(P(I),I=1,NC)
  WRITE(7,120)(P(I),I=1,NC)
  WRITE(6,140)(G(I),I=1,NC1)
  WRITE(7,120)(G(I),I=1,NC1)
  GO TO 170
END
```

J. SELECTED COMPUTER OUTPUT AND RESULTS

J.1 GENERAL

It is not feasible to present all the computational results in this work. They are available on file as a data supplement (Ur77). The gross output results of thermal efficiency η , power output \tilde{P} and energy error factor (Chapter 6), as well as the number of increments per cycle used are given in table J.1 through to table J.7 below for all the computer experiments run. In Chapter 4, a description of the application example test engine configuration and operational parameters used is given. A typical computer output follows table J.7 in both partial printout and full printout form. The output chosen is for air as the working gas operating at 20 Hz cycle frequency. The partial printout gives the pressures in the working spaces and energy variables at every 10° over the cycle, whereas the full printout gives the heat exchanger variables as well.

Table J.1 POWER AND EFFICIENCY FOR AIR

Frequency \tilde{f} [Hz]	Number of cells n_c	3	9	15	21	27	33	39	45
2,5	η	-	0,238	0,260	-	-	-	-	-
	\tilde{P} [W]	-	125,6	127,9	-	-	-	-	-
5,0	η	0,146	0,217	0,238	0,243	0,251	-	-	-
	\tilde{P} [W]	177,3	231,0	239,0	240,1	242,6	-	-	-
10,0	η	0,122	0,193	0,213	0,221	0,227	0,229	-	-
	\tilde{P} [W]	288,2	404,3	424,2	429,1	434,1	434,8	-	-
15,0	η	0,098	0,170	0,190	0,200	0,204	0,208	0,209	-
	\tilde{P} [W]	340,3	525,6	556,9	568,9	573,9	577,9	579,3	-
20,0	η	0,068	0,142	0,162	0,170	0,176	0,178	0,180	0,181
	\tilde{P} [W]	309,8	576,8	621,7	636,4	647,1	651,9	654,7	655,0
25,0	η	0,030	0,107	0,126	0,134	0,140	0,143	0,145	0,147
	\tilde{P} [W]	170,9	533,9	596,4	616,6	632,3	639,7	644,4	647,8
30,0	η	-	0,064	0,082	0,091	0,095	0,098	0,100	0,101
	\tilde{P} [W]	-105,8	373,0	456,3	488,8	505,2	515,2	521,1	526,2
35,0	η	-	0,011	0,028	0,036	0,041	0,043	0,045	0,046
	\tilde{P} [W]	-	73,5	181,2	223,7	245,8	259,4	268,2	274,2

Table J.2 POWER AND EFFICIENCY FOR AIR

Frequency \tilde{f} [Hz]	Diameter ratio \tilde{d}_{ia}	1,5	3	4
1,0	η \tilde{P} [W]	0,189 48,3	0,161 48,3	0,120 48,3
2,0	η \tilde{P} [W]	0,174 87,5	0,160 87,5	0,135 87,5
3,0	η \tilde{P} [W]	0,160 119,5	0,151 119,5	0,134 119,5
5,0	η \tilde{P} [W]	0,146 177,3	0,141 177,4	0,130 177,4
10,0	η \tilde{P} [W]	0,122 288,2	0,120 288,4	0,115 288,4

Table J.3 ENERGY ERROR FACTOR AND NUMBER OF INCREMENTS PER CYCLE FOR AIR

Frequency f [Hz]	Number of cells nc	3	9	15	21	27	33	39	45
1	ζ <i>nine</i>	0,0044 5400	-	-	-	-	-	-	-
2	ζ <i>nine</i>	0,0013 2880	-	-	-	-	-	-	-
2,5	ζ <i>nine</i>	-	0,0034 5400	0,0003 5400	-	-	-	-	-
3	ζ <i>nine</i>	0,0018 1800	-	-	-	-	-	-	-
5	ζ <i>nine</i>	0,0019 1440	0,0037 3600	0,0036 2880	0,0071 3600	0,0071 4680	-	-	-
10	ζ <i>nine</i>	0,0035 720	0,0040 900	0,0059 1440	0,0078 1800	0,0098 2340	0,0090 2880	-	-
15	ζ <i>nine</i>	0,0069 540	0,0081 720	0,0090 1080	0,0096 1260	0,0099 1620	0,0109 1980	0,0115 2340	-
20	ζ <i>nine</i>	0,0119 360	0,0132 540	0,0141 720	0,0164 900	0,0154 1440	0,0161 1620	0,0166 1800	0,0184 1980
25	ζ <i>nine</i>	0,0186 360	0,0203 360	0,0215 540	0,0237 720	0,0232 1080	0,0236 1440	0,0245 1620	0,0251 1800
30	ζ <i>nine</i>	0,0268 360	0,0292 360	0,0308 540	0,0320 720	0,0327 900	0,0334 1080	0,0340 1620	0,0349 1800
35	ζ <i>nine</i>	-	0,0402 360	0,0437 540	0,0455 540	0,0443 720	0,0452 900	0,0460 1440	0,0465 1440

Table J.4 POWER AND EFFICIENCY FOR HELIUM

Frequency \tilde{f} [Hz]	Number of cells nc	15	33
10	η \tilde{P} [W]	0,289 449,5	-
15	η \tilde{P} [W]	0,274 661,3	-
20	η \tilde{P} [W]	0,257 843,8	-
25	η \tilde{P} [W]	0,243 1004,7	-
30	η \tilde{P} [W]	0,229 1135,7	0,251 1175,7
35	η \tilde{P} [W]	0,215 1248,5	-
40	η \tilde{P} [W]	0,201 1336,0	0,221 1391,6
45	η \tilde{P} [W]	0,187 1390,5	-
50	η \tilde{P} [W]	0,172 1421,7	0,191 1498,5
55	η \tilde{P} [W]	0,157 1415,2	-
60	η \tilde{P} [W]	0,140 1371,1	0,158 1481,6
65	η \tilde{P} [W]	0,122 1279,3	-
70	η \tilde{P} [W]	0,100 1114,0	0,118 1259,3
75	η \tilde{P} [W]	0,077 905,3	-

Table J.4 (Continued)

Frequency f [Hz]	Number of cells nc	15	33
80	η \tilde{P} [W]	0,052 653,1	0,070 828,5
85	η \tilde{P} [W]	0,027 354,3	-
90	η \tilde{P} [W]	-	0,017 218,7

Table J.5 ENERGY ERROR FACTOR AND NUMBER OF INCREMENTS
PER CYCLE FOR HELIUM

Frequency f [Hz]	Number of cells n_c	15	33
10	ζ <i>ninc</i>	0,0019 5400	-
15	ζ <i>ninc</i>	0,0020 2880	-
20	ζ <i>ninc</i>	0,0019 2340	-
25	ζ <i>ninc</i>	0,0045 1800	-
30	ζ <i>ninc</i>	0,0056 1440	0,0067 2880
35	ζ <i>ninc</i>	0,0068 1260	-
40	ζ <i>ninc</i>	0,0089 1080	0,0097 2160
45	ζ <i>ninc</i>	0,0108 1080	-
50	ζ <i>ninc</i>	0,0131 900	0,0142 1800
55	ζ <i>ninc</i>	0,0159 900	-
60	ζ <i>ninc</i>	0,0184 720	0,0202 1440
65	ζ <i>ninc</i>	0,0227 720	-
70	ζ <i>ninc</i>	0,0265 540	0,0281 1260
75	ζ <i>ninc</i>	0,0307 540	-

Table J.5 (Continued)

Frequency f [Hz]	Number of cells nc	15	33
80	ζ <i>nine</i>	0,0353 540	0,0370 1080
85	ζ <i>nine</i>	0,0401 540	-
90	ζ <i>nine</i>	-	0,0477 1080

Table J.6 POWER AND EFFICIENCY FOR HYDROGEN

Frequency \tilde{f} [Hz]	Number of cells nc	15	33
10	η \tilde{P} [W]	0,211 410,0	-
15	η \tilde{P} [W]	0,211 611,2	-
20	η \tilde{P} [W]	0,210 808,1	-
25	η \tilde{P} [W]	0,208 994,5	-
30	η \tilde{P} [W]	0,205 1178,2	-
40	η \tilde{P} [W]	0,199 1518,0	-
50	η \tilde{P} [W]	0,189 1797,6	0,209 1873,1
60	η \tilde{P} [W]	0,178 2023,8	0,196 2101,7
70	η \tilde{P} [W]	0,165 2168,7	0,182 2264,9
80	η \tilde{P} [W]	0,149 2227,8	0,166 2345,0
90	η \tilde{P} [W]	0,131 2183,5	0,148 2328,0
100	η \tilde{P} [W]	0,110 2025,0	0,124 2156,5
110	η \tilde{P} [W]	0,087 1740,2	0,103 1941,3

Table J.6 (Continued)

Frequency f [Hz]	Number of cells nc	15	33
120	η \tilde{P} [W]	0,061 1319,2	0,076 1553,0
130	η \tilde{P} [W]	0,032 753,5	0,047 1026,3
140	η \tilde{P} [W]	0,001 32,5	0,015 344,1

Table J.7 ENERGY ERROR FACTOR AND NUMBER OF INCREMENTS
PER CYCLE FOR HYDROGEN

Frequency \tilde{f} [Hz]	Number of cells nc	15	33
10	ζ <i>ninc</i>	0,0062 5040	-
15	ζ <i>ninc</i>	0,0062 5400	-
20	ζ <i>ninc</i>	0,0058 3600	-
25	ζ <i>ninc</i>	0,0036 2520	-
30	ζ <i>ninc</i>	0,0044 1980	-
40	ζ <i>ninc</i>	0,0066 1620	-
50	ζ <i>ninc</i>	0,0068 1260	0,0107 2700
60	ζ <i>ninc</i>	0,0095 1080	0,0108 2160
70	ζ <i>ninc</i>	0,0121 900	0,0135 1980
80	ζ <i>ninc</i>	0,0156 720	0,0170 1620
90	ζ <i>ninc</i>	0,0195 720	0,0210 1440
100	ζ <i>ninc</i>	0,0240 540	0,0309 1080
110	ζ <i>ninc</i>	0,0290 540	0,0310 1080
120	ζ <i>ninc</i>	0,0345 540	0,0368 1080

Table J.7 (Continued)

Frequency f [Hz]	Number of cells n_c	15	33
130	ζ <i>nine</i>	0,0405 540	0,0469 900
140	ζ <i>nine</i>	0,0471 540	0,0502 900

TOTAL STROKE VOL= 0.000216CUBIC M FRACTIONAL DEAD VOL= 0.320 FRACTIONAL CLEARANCE VOL= 0.010
 H.E.PIPE LENGTH= 0.50000M H.E.PIPE DIAM RATIO= 1.500 ROUGHNESS= 0.010 NC OF PIPES= 100
 GAMMA= 1.400 R= 287.000 PR= 0.710
 DYNAMIC VISCOSITY= 0.20660E-04KG/M.S AT TEMP 350.000K SUTHERLAND CONSTANT= 112.000
 MATRIX SPECIFIC HEAT CAPACITY= 461.000J/KG.K DENSITY= 7690.000 THERMAL COND= 25.000W/M.K
 TK= 350.000K TH= 1000.000K FREQ= 20.000HZ CHARGE PRESS= 0.50000E+06PA
 ALPHA= 1.57079601 RADIAN
 IICOOLER CELLS, 11REGEN CELLS, 11HEATER CELLS, 1620INCS/CYCLE, 45INCS/PRINTOUT
 CYCLE 2. OUTPUT 0
 TM 1.1500 1.9100 1.4600 1.6200 1.7700 1.9300 2.0800 2.2400 2.3900 2.5500
 TM 2.7000
 TMAP CORRECTION FACTOR= 1.00000 O.DIAM= 0.19269E-02M
 H.E.PIPE I.DIAM= 0.12846E-02M PC= 1.159328 PE= 1.259032
 RMC= 0.650753
 TM 1.367209 1.467516 1.569431 1.673232 1.778440 1.884529 1.991698 2.099864 2.208946 2.318514
 TM 2.428513
 M 0.010002 0.009870 0.009702 0.009489 0.009223 0.008966 0.008499 0.008030 0.007487
 M 0.006878 0.006216 0.005871 0.005562 0.005282 0.005030 0.004801 0.004593 0.004232
 M 0.004076 0.003935 0.003809 0.003635 0.003467 0.003305 0.003153 0.003002 0.002851
 M 0.004334 0.004325 0.004294
 P 1.160874 1.161167 1.161507 1.161886 1.162312 1.162778 1.163285 1.163829 1.164407 1.165014
 P 1.165649 1.166305 1.167405 1.168664 1.170059 1.171681 1.173449 1.175391 1.177516 1.179824
 P 1.182320 1.185005 1.187881 1.191377 1.194900 1.198453 1.202033 1.205640 1.209271 1.212928
 P 1.216603 1.220297 1.224005
 G -0.061675 -0.062928 -0.064157 -0.065362 -0.066540 -0.067685 -0.068793 -0.069859 -0.070878 -0.071843
 G -0.072751 -0.073597 -0.074380 -0.075130 -0.075839 -0.076507 -0.077138 -0.077734 -0.078293 -0.078834
 G -0.079344 -0.079827 -0.080288 -0.080727 -0.081161 -0.081594 -0.082024 -0.082452 -0.082879 -0.083305
 G -0.083731 -0.084158 -0.084585 -0.085010
 VOL FACTOR= 0.21600E-03CU M PRESS FACTOR= 0.50000E+06PASCALS ENERGY FACTOR= 0.10800E+03JOULES
 VOLUME PCOM PEXE GKOL GREG GHOT WORK
 1.07000 1.15933 1.23903 0.0 0.0 0.0 0.0
 1.02279 1.21471 1.30018 -0.04449 -0.08323 0.04971 -0.06003
 0.96942 1.28841 1.35649 -0.08529 -0.16314 0.09571 -0.13002
 0.91151 1.38243 1.43129 -0.12114 -0.23777 0.13661 -0.20960
 0.85082 1.50055 1.52960 -0.14914 -0.30468 0.17104 -0.29837
 0.78920 1.64804 1.66180 -0.16789 -0.35758 0.13750 -0.39585
 0.72851 1.82797 1.81531 -0.18748 -0.39757 0.21609 -0.50123
 0.67060 2.02909 1.98148 -0.21585 -0.43709 0.22716 -0.61225
 0.61723 2.24078 2.16016 -0.25847 -0.47213 0.23003 -0.72534
 0.57002 2.46922 2.34526 -0.30398 -0.49840 0.23840 -0.83597
 0.53040 2.71130 2.55262 -0.35069 -0.49324 0.22335 -0.93895
 0.49958 2.97187 2.78327 -0.40318 -0.42632 0.21988 -1.02822
 0.47850 3.24394 3.02122 -0.46550 -0.30563 0.23964 -1.09730
 0.46780 3.48984 3.24160 -0.53760 -0.14923 0.29570 -1.13910
 0.46779 3.66332 3.41758 -0.61368 0.03143 0.38433 -1.14665
 0.47848 3.73112 3.52328 -0.68370 0.22399 0.43549 -1.11511
 0.49955 3.68542 3.54148 -0.73762 0.41185 0.61795 -1.04378
 0.53036 3.54055 3.46764 -0.76595 0.57710 0.73950 -0.93690
 0.56996 3.32178 3.30969 -0.78186 0.70434 0.84790 -0.80274
 0.61716 3.03516 3.08057 -0.78580 0.78157 0.93193 -0.65189
 0.67053 2.74578 2.79347 3.08057 -0.78731 0.81593 -0.49572
 0.72843 2.47712 2.53368 -0.77842 0.85092 1.01876 -0.34266
 0.78912 2.22779 2.31696 -0.76466 0.88885 1.05104 -0.19737
 0.85074 2.02783 2.12435 -0.75929 0.92259 1.08121 -0.06369
 0.91143 1.84249 1.94858 -0.77156 0.93186 1.10947 0.05624
 0.96935 1.67465 1.78822 1.78822 -0.80103 0.90339 1.14288 0.16008
 1.02272 1.52599 1.64511 -0.84229 0.84421 1.18083 0.24679
 1.06994 1.40037 1.52362 -0.89019 0.76833 1.22206 0.31631
 1.10956 1.29379 1.42525 -0.94149 0.68534 1.26719 0.36931
 1.14039 1.21999 1.34837 -0.99428 0.59958 1.31554 0.40670

M 0.022012 0.020078 0.018333 0.016755 0.015336 0.014078 0.012981 0.012036 0.011222 0.010517
M 0.009903 0.008606 0.008189 0.008141 0.007903 0.007812 0.007795 0.007811 0.007843 0.007891
M 0.007959 0.008054 0.008189 0.008141 0.007903 0.007812 0.007795 0.007811 0.007843 0.007891
G 0.252449 0.246837 0.240761 0.234299 0.227435 0.220129 0.212401 0.204268 0.195638 0.186337
G 0.176212 0.165104 0.154149 0.143138 0.131949 0.120727 0.109816 0.099555 0.090125 0.081558
G 0.073785 0.066701 0.060212 0.054374 0.049424 0.045565 0.042453 0.039957 0.037749 0.035566
G 0.033537 0.031720 0.030133 0.028797 0.027612 0.026532 0.025541 0.024628 0.023774 0.022966
FLOW 3 3 3 3 3 3 3 3 3 3 2 2 2 2 2 2 2 2 2 2 1 1 1 1 1 1 1
0.49958 2.97187 2.78327 2.60318 2.44232 2.29989 2.18282
P 2.866826 2.881541 2.876546 2.871845 2.867443 2.863335 2.859511 2.855967 2.852695 2.849689
P 2.846947 2.839911 2.833087 2.826481 2.820279 2.814493 2.809166 2.804263 2.799749 2.795193
P 2.814460 2.811703 2.809372 2.807066 2.804824 2.802649 2.800535 2.798476 2.796469 2.794499
P 2.790483 2.788598 2.786780 2.785027 2.783384 2.781845 2.780312 2.778784 2.777261 2.775744
TC= 1.196514 TE= 2.823384
T 1.149779 1.116431 1.092814 1.075719 1.063512 1.055007 1.049375 1.046074 1.044814 1.045529
T 1.048382 1.139215 1.235079 1.335702 1.441136 1.551359 1.666166 1.785102 1.907520 2.032643
T 2.159054 2.297944 2.490372 2.650511 2.774478 2.864243 2.922416 2.954663 2.968630 2.970995
T 2.965931 2.953647 2.934099 2.908627 2.874478 2.833087 2.826493 2.823339 2.820267 2.817313
TM 1.367577 1.468177 1.570252 1.674191 1.779520 1.885772 1.993049 2.101903 2.210460 2.320084
TM 2.420240

MC= 0.433458 ME= 0.024622
M 0.022845 0.022464 0.022929 0.024270 0.024511 0.024673 0.024772 0.024820 0.024821 0.024778
M 0.024687 0.022690 0.020903 0.019305 0.017872 0.016582 0.015422 0.014378 0.013441 0.012600
M 0.011947 0.011172 0.010253 0.009624 0.009186 0.008890 0.008706 0.008604 0.008558 0.008545
M 0.008554 0.008583 0.008634 0.008694 0.008744 0.008787 0.008824 0.008852 0.008872 0.008886
G 0.277744 0.271633 0.264974 0.257871 0.250406 0.242644 0.234640 0.226422 0.217986 0.209298
G 0.200286 0.190835 0.181474 0.172976 0.164483 0.156189 0.148036 0.140012 0.132139 0.124455
G 0.117046 0.109928 0.103134 0.096902 0.091046 0.085620 0.080742 0.076470 0.072752 0.069460
G 0.066477 0.063743 0.061260 0.059082 0.057152 0.055361 0.053601 0.051977 0.050477 0.049089
FLOW 3 3 3 3 3 3 3 3 3 3 3 3 2 2 2 2 2 2 2 2 2 2 2 2 2 2
0.47850 3.24394 3.02122 2.80650 2.60553 2.41964 2.24730 2.09730
P 3.152452 3.147089 3.141956 3.137151 3.132583 3.128283 3.124246 3.120467 3.116938 3.113646
P 3.110584 3.106492 3.102386 3.098274 3.094166 3.090063 3.085974 3.081906 3.077867 3.073860
P 3.068243 3.064970 3.061629 3.058212 3.054749 3.051249 3.047819 3.044461 3.041174 3.037967
P 3.033738 3.030906 3.028159 3.025486 3.022894 3.020382 3.017951 3.015601 3.013324 3.011124
TC= 1.225142 TE= 2.933646
T 1.171329 1.133571 1.105800 1.078628 1.052951 1.027824 1.003196 0.979024 0.955251 0.931824
T 1.042936 1.130177 1.221644 1.316888 1.415428 1.517118 1.621608 1.728710 1.838264 1.950096
T 2.069910 2.179421 2.301900 2.438561 2.589570 2.754956 2.935740 3.132918 3.347470 3.580598
TM 1.367075 1.467580 1.579777 1.673728 1.779078 1.885251 1.992653 2.100934 2.210117 2.319772
TM 2.423968

MC= 0.357218 ME= 0.044737
M 0.024467 0.023239 0.023831 0.024673 0.025594 0.026521 0.026974 0.027069 0.027120 0.027133
M 0.021114 0.024888 0.023086 0.021389 0.019873 0.018516 0.017300 0.016237 0.015221 0.014330
M 0.015322 0.012789 0.011743 0.011038 0.010541 0.010177 0.009906 0.009703 0.009556 0.009454
G 0.298164 0.292119 0.285482 0.278351 0.270821 0.262871 0.254870 0.246571 0.238111 0.229509
G 0.230765 0.221453 0.211453 0.200992 0.195225 0.189203 0.183170 0.177447 0.171998 0.166950
G 0.150195 0.144420 0.139218 0.134422 0.129458 0.124855 0.120334 0.115909 0.111629 0.107564
G 0.103761 0.100241 0.096973 0.093928 0.091092 0.088428 0.085919 0.083544 0.081303 0.079186
FLOW 3 3 3 3 3 3 3 3 3 3 3 3 3 3 3 3 2 2 2 2 2 2 2 2 2 2
0.46780 3.48984 3.24160 2.99230 2.74300 2.49370 2.24440 1.99510 1.74580 1.49650
P 3.599554 3.594729 3.590085 3.585530 3.581068 3.576701 3.572425 3.568241 3.564149 3.560148
P 3.559776 3.554938 3.550190 3.545448 3.540710 3.536081 3.531562 3.527154 3.522856 3.518568
P 3.520574 3.515839 3.511173 3.506574 3.502039 3.497564 3.493149 3.488784 3.484469 3.480204
P 3.480214 3.475954 3.471744 3.467584 3.463474 3.459414 3.455404 3.451444 3.447534 3.443674
TC= 1.251124 TE= 2.580099
T 1.120491 1.116801 1.113201 1.109646 1.106182 1.102851 1.099581 1.096381 1.093241 1.090161
T 1.040325 1.128204 1.216114 1.304064 1.392064 1.480114 1.568214 1.656364 1.744564 1.832814
T 2.030597 2.114162 2.202581 2.295064 2.392614 2.495244 2.602964 2.715784 2.833714 2.956764
TM 1.367075 1.467580 1.579777 1.673728 1.779078 1.885251 1.992653 2.100934 2.210117 2.319772
TM 2.423968

REFERENCES

- Ar70 ARFKEN G. *Mathematical Methods for Physicists*. Academic Press, Second Edition, 1970.
- ASD63 Potential capabilities of the Stirling engine for space power. *Aeronautical Systems Division, Air Force Systems Command, Technical Documentary Report No. ASD-TDR-62-1099*, Jan 1963.
- Ba1885 BABCOCK G H. Substitutes for steam. *Trans ASME* 1885, pp 680-741.
- Be69 BEALE W T. Free piston Stirling engines - some model tests and simulations. *SAE Paper No. 690230*, Jan 1969.
- Br71 BRETSZNAJDER S. *Prediction of the transport and other physical properties of fluids*. International series of Monographs in Chemical Engineering, Vol Pergamon Press, 1971.
- BR77 BERCHOWITZ D M, RALLIS C J, URIELI I. A new mathematical model for Stirling cycle machines. *School of Mechanical Engineering, University of Witwatersrand*. In preparation.
- CF74 COOKE-YARBOROUGH E H, FRANKLIN E, GEISOW T, HOWLETT R, WEST C D. Thermomechanical generator; an efficient means of converting heat to electric at low power levels. *Proc IEE*, Vol 121, No. 7, Jul 1974, pp 749-751.

- CL75 CARLQVIST S G, LIA T, LUNDHOLM G S K.
Stirling engines: their potential use in commercial vehicles and their impact on fuel utilization. *Inst Mech Eng*, Paper C4/75, 1975, pp 35-46.
- Co74 COOKE - YARBOROUGH E H. Simplified expressions for the power output of a lossless Stirling engine. *UK Atomic Energy Authority Harwell*, AERE - M2437 (revised), Mar 1974.
- Cr66 CRESWICK F A. Thermal design of Stirling-cycle machines. *SAE Trans*, Paper No. 560079, 1966.
- De53 DENHAM F R. *A study of the reciprocating hot air engine*. PhD Thesis, University of Durham, England, Sept 1953.
- Dw61 DWIGHT H B. *Tables of integrals and other mathematical data*. The Macmillan Co, Fourth Edition, 1961.
- Eng 1875 Editorial. Air engines. *Engineering*, Vol 19, Part 1 - Mar 12, 1875, pp 200-201, Part 2 - Mar 26, 1875, pp 241-242, Part 3 - Apr 9, 1875, pp 287-289, Part 4 - Apr 30, 1875, pp 355-356, Part 5 - May 21, 1875, pp 417-418, Part 6 - Jun 18, 1875, pp 504-505.
- Fe69 FEHLBERG E. Low order classical Runge-Kutta formulas with stepsize control and their application to some heat transfer problems. *NASA TR R-315*, July 1969.

- Fi53 FINKELSTEIN T. *Theory of air cycles with special reference to the Stirling cycle.* PhD Thesis, Imperial College, London, Jan 1953.
- Fi59 FINKELSTEIN T. Air Engines. *The Engineer*, Vol 207, Part 1 - Mar 27, 1959, pp 492-497, Part 2 - Apr 3, 1959, pp 522-527, Part 3 - Apr 10, 1959, pp 568-571, Part 4 - May 8, 1959, pp 720-723.
- Fi60.1 FINKELSTEIN T. Optimum phase angle and volume ratio for Stirling cycle engines. *SAE Paper No. 118C*, Jan 1960.
- Fi60.2 FINKELSTEIN T. Generalized thermodynamic analysis of Stirling engines. *SAE Paper No. 118B*, Jan 1960.
- Fi62 FINKELSTEIN T. Cyclic processes in closed regenerative gas machines analysed by a digital computer simulating a differential analyser. *Trans ASME, Jnl Eng for Industry*, Feb 1962 pp 165-179.
- Fi64 FINKELSTEIN T. Analysis of practical reversible thermodynamic cycles. *ASME Paper No. 64-HT-37* 1964.
- Fi67.1 FINKELSTEIN T. Thermophysics of regenerative energy conversion. *AIAA 5'th Aerospace Science Meeting*, Paper No. 67-216, Jan 1967.

- Fi67.2 FINKELSTEIN T. Thermodynamic analysis of Stirling engines. *Jnl of Spacecraft and Rockets*, Vol 4, No. 9, Sept 1967, pp 1184-1189.
- Fi75 FINKELSTEIN T. Computer analysis of Stirling engines. *Proc 10th IECEC*, Paper No. 759140, 1975, pp 933-941.
- Fi76 FINKELSTEIN T. *UCLA Short Course 'Stirling Engines'*, Sep 1976.
- Fp60 FLYNN G Jnr, PERCIVAL W H, HEFFNER F E. GMR Stirling thermal engine, part of the Stirling engine story, 1960 chapter. *SAE Trans*, Vol 68, 1960, pp 665-684.
- FW60 FORSYTHE G E, WAGSON W R. *Finite difference methods for partial differential equations*. Wiley, 1960.
- HW67 HICKS J S, WEI J. Numerical solution of parabolic partial differential equations with two-point boundary conditions by use of the method of lines. *Jnl Ass Comp Mach*, Vol 14, No. 3, Jul 1967, pp 549-562.
- Ki62 KIRKLEY D W. Determination of the optimum configuration for a Stirling engine. *Jnl Mech Eng Science*, Vol 4, No. 3, 1962, pp 204-212.
- Ki63 KIRKLEY D W. *An investigation of the losses occurring in reciprocating hot air engines*. PhD Thesis, University of Durham, England, Oct 1963.

- Ki66 KIRKLEY D W. A Thermodynamic analysis of the Stirling cycle and a comparison with experimer
SAE Trans, Paper No. 650078, 1966.
- Ki70 KIM J C. *An analytical and experimental study of heat transfer and flow friction characteristics for periodically reversing flow through the pc matrix of thermal regenerators.* PhD Thesis, Purdue University, USA, June 1970.
- KJ54 KOHLER J W L, JONKERS C O. Fundamentals of th gas refrigerating machine. *Philips Technical Review*, Vol 16, No. 3, Sep 1954, pp 69-104.
- KL64 KAYS W M, LONDON A L. *Compact heat exchangers* McGraw-Hill, Second Edition, 1964.
- KM59 KARAVANSKI I I, MELTZER L Z. Thermodynamic investigations of the working cycle of the Philips machine. *Proc 10'th International Congress on Refrigeration*, Paper No. 3-29, 195 pp 209-215.
- Kö60 KOHLER J W L. The gas refrigerating machine a its position in cryogenic technique. *Progress in Cryogenics*, Vol 2, Editor Mendelssohn K, He wool and Co, London, 1960, pp 41-67.
- Ko68 KOLIN I. The Stirling cycle with nuclear fuel
Nuclear Engineering International, Vol 13, No. 1, Dec 1968, pp 1027-1034.
- Ku65 KUO S S. *Numerical methods and computers.* Addison - Wesley, 1965.

- LF68 LEACH C E, FRYER B C. A 7.3kW(e) radioisotope energized undersea Stirling engine. *Proc 3'rd IECEC*, Paper No. 689115, 1968, pp 830-844.
- Me59 MEIJER R J. The Philips hot-gas engine with rhombic drive mechanism. *Philips Technical Review*, Vol 20, No. 9, May 1959, pp 245-276.
- Me61 MEIJER R J. The Philips Stirling thermal engine. *Philips Research Reports*, Supplement 1, 1961.
- Me68 MEIJER R J. Der Philips-Stirling motor. *Motor Technische Zeitschrift*, Vol 29, No. 7, 1968, pp 284-298.
- Me70 MEIJER R J. Prospects of the Stirling engine for vehicular propulsion. *Philips Technical Review*, Vol 31, No. 5/6, 1970, pp 168-185.
- MJ68 MARTINI W R, JOHNSTON R P, GORANSON R B, WHITE M A. Development of a simplified Stirling engine to power circulatory assist devices. *Proc 3'rd IECEC*, Paper No. 689102, 1968, pp 733-749.
- Mo48 MOODY L F. Friction factors for pipe flow. *Trans ASME*, Vol 66, 1948, pp 671-
- MW74 MARTINI W R, WHITE M A. How unconventional Stirling engines can help conserve energy. *Proc 9'th IECEC*, Paper No. 749151, Aug 1974, pp 1092-1099.

- NBS72 The international system of units (SI).
Editors Page C H, Vigourex p, *National
Bureau of Standards*, Special Publication
330, 1972 Edition, US Department of Commerce.
- Or75 ORGAN A J. The concept of 'critical length
ratio' in heat exchangers for Stirling
cycle machines. *Proc 10'th IECEC*, Paper
No. 759151, 1975, pp 1012-1019.
- Or76 ORGAN A J. Fluid particle trajectories in
Stirling cycle machines. Research Report,
Dept of Mechanical Engineering, King's College,
London, Jan 1976.
- PK70 PAUL B, KRAJCINOVIC D. Computer analysis of
machines with planar motion. *Trans ASME, Jnl
Applied Mechanics*, Sep 1970, pp 697-712.
- QS68 QVALE E B, SMITH J L Jnr. A mathematical model
for steady operation of Stirling-type engines.
Trans ASME, Jnl Eng for Power, Jan 1968 pp 45-5
- QS69 QVALE E B, SMITH J L Jnr. An approximate
solution for the thermal performance of a Stirl
engine generator. *Trans ASME, Jnl Eng for Powe*
Vol 91 (Ser A, No. 2), Apr 1969, pp 109-112.
- RD46 RINIA H, du PRÉ F K. Air engines. *Philips
Technical Review*, Vol 8, No. 5, May 1946, pp
129-160.
- RM67 ROGERS G F C, MAHEW Y R. *Engineering thermo-
dynamics work and heat transfer*. Longman,

Second Edition (SI units), 1967.

- Ro72 ROACHE P J. *Computational fluid dynamics*.
Hermosa publishers, New Mexico, 1972.
- RS70 RIOS P A, SMITH J L Jnr. An analytical and
experimental evaluation of the pressure-drop
losses in the Stirling cycle. *Trans ASME, Jnl
Eng for Power*, Apr 1970, pp 182-188.
- RU76 RALLIS CJ, URIELI I. Optimum compression ratios
of Stirling cycle machines. Research report No.
68, *School of Mechanical Engineering, University
of the Witwatersrand*, June 1976.
- Sc1871 SCHMIDT G. Theorie der Lehmann'schen calorischen
Machine. *Zeitschrift des Verlines deutscher
Ingenieure*, Vol 15, Part 1 - No. 1, Jan 1871,
pp 1-12, Part 2 - No. 2, Feb 1871, pp 98-112.
- Sc55 SCHLICHTING H. *Boundary layer theory*. Pergamon
Press, 1955.
- UR76 URIELI I, RALLIS C J. A new regenerator model
for Stirling cycle machines. Research report
No. 67, *School of Mechanical Engineering, Univers
of the Witwatersrand*, May 1976.
- Ur77 URIELI I. Data supplement to PhD thesis, 1977.
On file, *School of Mechanical Engineering,
University of the Witwatersrand*.

- Va69 VASISHTA V. *The heat transfer and flow friction characteristics of regenerator matrices of Stirling cycle machines.* MSc Thesis, University of Calgary, Canada, Feb 1969.
- VW70 VASISHTA V, WALKER G. The heat transfer and flow friction characteristics of dense mesh wire screens of Stirling cycle regenerative matrices. Prepared for presentation at the *Fourth International Heat Transfer Conference*, Paris, France, Sep 1970.
- Wa62.1 WALKER G. *Some aspects of the design of Stirling cycle machines.* PhD Thesis, University of Durham, England 1962.
- Wa62.2 WALKER G. An optimization of the principal design parameters of Stirling cycle machines. *Jnl Mech Eng Science*, Vol 4, No. 3, 1962, pp 226-240.
- Wa73 WALKER G. *Stirling-cycle machines.* Oxford University Press, 1973.
- WA73 WALKER G, AGBI B. Thermodynamic aspects of Stirling engines with two-phase, two-component working fluids. *Trans Canadian Society for Mechanical Engineers*, Vol 2, No.1, 1973-74, pp 1-8.
- We47 van WEENEN F L. The construction of the Philips air engine. *Philips Technical Review*, Vol 9, No.5, 1947, pp 125-160.

- WK65 WALKER G, KHAN M I. Theoretical performance of Stirling cycle engines. *SAE Paper No.* 949A, Jan 1965.
- Za73 ZACHARIAS F A. Unique requirements for the cooperation of computation and design in the development of Stirling engines. *von Karman Institute for Fluid Dynamics*, Lecture series 53, Stirling engines, Feb 1973.
- Zi71 ZIMMERMAN M D. A piston power plant fights back: the Stirling engine. *Machine Design*, May 27, 1971, pp 21-25.